UNIVERSITÉ DU QUÉBEC

MÉMOIRE
PRÉSENTÉ À
UNIVERSITÉ DU QUÉBEC À CHICOUTIMI
COMME EXIGENCE PARTIELLE
DU GRADE DE MAÎTRISE EN SCIENCES DE LA TERRE

PAR
KATHERINE BOGGS

RETROGRADE CATION EXCHANGE IN GARNETS DURING SLOW COOLING OF MID CRUSTAL GRANULITES AND THE P-T-t TRAJECTORIES FROM THE MONT LAURIER REGION, GRENVILLE PROVINCE, QUEBEC

APRIL 1996

Bibliothèque
Paul-Émile-Boulet

UQAC
Université du Québec
à Chicoutimi

Mise en garde/Advice

Afin de rendre accessible au plus grand nombre le résultat des travaux de recherche menés par ses étudiants gradués et dans l'esprit des règles qui régissent le dépôt et la diffusion des mémoires et thèses produits dans cette Institution, **l'Université du Québec à Chicoutimi (UQAC)** est fière de rendre accessible une version complète et gratuite de cette œuvre.

Motivated by a desire to make the results of its graduate students' research accessible to all, and in accordance with the rules governing the acceptation and diffusion of dissertations and theses in this Institution, the **Université du Québec à Chicoutimi (UQAC)** is proud to make a complete version of this work available at no cost to the reader.

L'auteur conserve néanmoins la propriété du droit d'auteur qui protège ce mémoire ou cette thèse. Ni le mémoire ou la thèse ni des extraits substantiels de ceux-ci ne peuvent être imprimés ou autrement reproduits sans son autorisation.

The author retains ownership of the copyright of this dissertation or thesis. Neither the dissertation or thesis, nor substantial extracts from it, may be printed or otherwise reproduced without the author's permission.

RETROGRADE CATION EXCHANGE IN GARNETS DURING SLOW COOLING OF MID CRUSTAL GRANULITES AND THE P-T-t TRAJECTORIES FROM THE MONT LAURIER REGION, GRENVILLE PROVINCE, QUEBEC

PAR KATHERINE BOGGS

Mai, 1996

RÉSUMÉ

Les études de pression et température en pétrologie métamorphique peuvent être faussées par la diffusion rétrograde. Par exemple, Spear (1991) a démontré que le thermomètre grenat-biotite, basé sur la partition des ions de Fe-Mg, est capable de sous-estimer les températures jusqu'à 200°C parce qu'il se produit de la diffusion rétrograde entre le grenat et le biotite. Holdaway et Mukhopadhyay (1993) ont dit que les géothermomètres d'échange sont facilement rééquilibrés aux températures des granulites. Ainsi, tous les géothermobaromètres ont enregistré des pressions et températures trop basses à cause de la diffusion; et ceux qui, comme le thermomètre biotite-grenat, font intervenir un échange Fe-Mg sont spécialement sensibles à l'échange rétrograde des cations. Un des objectifs de cette thèse est d'étudier l'importance et les effets de rééquilibration en fonction de la taille des grains des minéraux.

Le deuxième objectif principal de cette thèse est de développer l'évolution et la trajectoire de pression-température-temps pour le complexe gneissique de Bondy (CGB) et pour la zone de déformation de Nominingue-Chénéville (NCDZ). Cela inclut l'analyse des zircons, des monazites, des titanites, des rutiles et des biotites pour trouver la date du maximum de température métamorphique, et le calcul des taux de refroidissement et de soulèvement.

La Ceinture Métasédimentaire Centrale (CMC) représente une croûte jeune dans la Province Grenville. Le terrain d'étude est situé dans la Réserve Faunique de Papineau-Labelle à 100 km au nord de la rivière Ottawa entre Ottawa et Montréal. Il contient le plus grand terrain granulitique de la CMC appelé "complexe gneissique de Bondy". Ce complexe qui est un dôme granulitique domine les deux-tiers ouest de la carte. Il contient principalement des orthogneiss avec quartzites, un pluton tonalitique et des metapelites. La zone de déformation de Nominingue-Chénéville, orientée nord-sud, coupe les structures du CGB à l'est de la carte. Des complexes monzonitique-dioritiques se sont mis en place syntectoniquement dans la ZDNC entre 1167 et 1164 Ma.

Les textures et les caractéristiques de la migmatisation varient beaucoup à partir i) de leucosomes granitiques entourés par des niveaux riches en grenats et des mélanosomes

riches en biotite, ii) à des minces (<1mm) traînées de leucosomes discontinus, iii) à des couronnes felsiques qui enveloppent les grenats, iv) jusqu'à des leucosomes continus d'épaisseur supérieure à 1 cm. Plusieurs lames minces contiennent des porphyroblastes de feldspath-K et de plagioclase avec des renfoncements et des inclusions de biotite et de quartz qui indiquent que ces porphyroblastes ont grandi pendant une réaction qui a produit un fondu.

L'assemblage biotite - plagioclase - quartz se trouve dans chaque lame mince et chaque affleurement. Le travail de Vielzeuf et Montel (1994), sur la réaction biotite + plagioclase + quartz = orthopyroxène + grenat + feldspath-K + Fondu, donne une limite de température maximum inférieure à 980°C. Un affleurement contient des grenats avec des inclusions de spinel dans les bordures, qui suggèrent la réaction spinel + quartz = grenat + aluminosilicate; ce qui implique donc températures maximales supérieures à 850°C. L'absence de kyanite limite la pression à moins que 95 à 110 MPa entre 850 et 970°C. L'absence d'osumilite suggère une pression supérieure à 85 MPa.

L'assemblage de kornerupine - orthopyroxène - tourmaline - cordiérite - plagioclase s'est développé dans le CGB. Il y a des inclusions d'orthopyroxène et de tourmaline dans les cristaux de kornerupine; cela implique la réaction tourmaline + orthopyroxène + cordiérite = kornerupine + plagioclase pour la production de kornerupine. Des assemblages biotite - grenat et grenat - orthopyroxène ont été utilisés comme géothermomètres, et des assemblages grenat - orthopyroxène, grenat - aluminosilicate - silice - plagioclase (GASP), grenat - aluminosilicate - spinel - quartz, et cordiérite - grenat - aluminosilicate - quartz comme géobaromètres.

Corriveau et al. (1995) ont proposé que le complexe gneissique de Bondy est le produit d'une altération hydrothermale. Les plagioclases du CGB ont des compositions très diverses (entre An_{25} et An_{88}), possiblement à cause de cette altération hydrothermale. Les analyses de spinel (CGB) sont similaires à celles de la littérature qui proviennent d'autres parties de l'orogène grenvillien tel que reconstruit à 0.8 Ga par Dalziel 1991; Hoffman 1991; Moores 1991; Young 1992. La cordiérite, l'orthopyroxène et le spinel ont été observés dans la CGB, mais pas dans la ZDNC; la calcite a été observée seulement dans le ZDNC. Ces différences minéralogiques entre le CGB et la ZDNC sont probablement dues à l'écoulement d'un fluide dans le ZDNC pendant la déformation qui a introduit le carbonate et le Ca. Des projections AFM démontrent aussi cette diversité entre ces deux domaines tectonostratigraphiques. Les grenats du CGB sont jusqu'à 20% plus riches en Mg que ceux de la ZDNC, et les biotites du CGB sont aussi jusqu'à 30% plus riches en Mg que celles de la ZDNC.

Les grenats sont les seuls minéraux où on trouve des profils de zonation réguliers. Dans le coeur d'un grenat qui n'a pas d'inclusions, le pourcentage molaire du grossulaire augmente vers le centre alors que celui du pyrope reste constant. Indares et Martignole (1990a) ont proposé que cette forme est due à une décompression isothermique; ce qui s'accorde avec les évidences structurales d'extension dans la ZDNC.

Typiquement, le pourcentages molaires de l'almandin augmentent vers le coeur des grenats, avec une diminution correspondante des valeurs du pyrope. Spear (1991) a développé un modèle d'évolution de la zonation des minéraux. Pendant la première étape de croissance, les minéraux développent un profil en cloche. Si les conditions métamorphiques maximales sont supérieures à 650°C, le grenat devient homogène et le profil s'aplatit (deuxième étape). Avec des taux refroidissement faibles (<10°C/Ma), les

profils redeviennent en cloche (troisième étape). Dans cette étape, si les taux de refroidissement sont rapides (>100°C/Ma), les profils formeront des cloches peu marquées. Pendant la dernière étape, les grenats développent un profil plat; si ces minéraux sont assez petits, ils deviennent homogènes. Dans notre étude, les températures maximales sont supérieures à 650°C, avec un taux de refroidissement plus lent que 10°C/Ma en bas de 650°C, alors les profils de zonation des grenats qui ont la forme d'une cloche suggèrent que ces grenats ont subi un échange rétrograde des cations (étape 3). Les grenats plus petits que 3.5 mm^2 seraient rehomogénéïsés (étape 4).

Pour examiner les effets de ces échanges rétrogrades de cations sur les géothermomètres, les résultats du thermomètre biotite-grenat ont été placés en fonction de la taille des grenats. Une tendance générale est visible: les plus petits grenats enregistrent des températures plus basses que les plus grands grenats. Les grenats plus petits que 15 mm^2 enregistrent des températures entre 100 et 550°C plus basses que la température de 950°C proposée comme température maximale. De façon inattendue, les températures les plus élevées sont obtenues par des grenats de taille moyenne sans inclusions. Les plus gros grenats sont pleins d'inclusions de biotite, de spinel et d'ilmenite qui ont créé des domaines de diffusion plus petits, et qui ont ainsi augmenté les effets d'échange rétrograde des cations. La température maximale de 950°C est supportée par les résultats du géothermomètre orthopyroxène-grenat. Le travail de Vielzeuf et Montel (1994) limite l'activité de l'eau à moins de 0.2 à 950°C.

La pression maximale de métamorphisme a été atteinte à $\geq 1186 \pm 4$ Ma en même temps que le température maximale de métamorphisme parce que le diagramme pression - température indique une décompression isothermique, confirmée par l'extension tectonique et les profils des grenats. Ainsi, la pression de 100 à 105 MPa à 950°C, obtenue des baromètres de l'Al dans l'orthopyroxène et de grenat - aluminosilicate - silice - plagioclase, est proposée comme la pression maximale pour la région. Des résultats du baromètre spinel - grenat ont donné une pression de 84 MPa à 950°C. La position des inclusions de spinel sur les profils des grenats suggèrent que cette réaction avait lieu vers la fin de la décompression isothermique, en conséquence, cette pression de 84 MPa fournit une limite inférieure de pression pour la décompression isothermique.

Durant sa trajectoire rétrograde, le CGB s'est soulevé à un taux de 25 mm/an par rapport à la ZDNC (5 mm/an), qui, étant donné la compétence plus grande du CGB, a concentré l'épisode de déformation et de plutonisme (1167 à 1157 Ma). En conséquence, après la décompression isothermique et l'extension, les histoires de refroidissement du CGB et de la ZDNC ont divergé. Initialement, la ZDNC a refroidi plus lentement de 14.7 à 9.5°C/Ma que le CGB de 25 à 5°C/Ma, probablement à cause de la chaleur ajoutée par l'injection de magma. Cela se reflète dans les trajectoires de pression - température; la trajectoire rétrograde de la ZDNC est systématiquement 5 à 10 MPa plus élevée en pression que celle du CGB. Les courbes de refroidissement montrent cette divergence dans l'histoire de le CGB et de la ZDNC, les titanites de la ZDNC sont déplacées à des ages plus jeunes (i.e., refroidissement plus lent) que celles du CGB. Après l'injection de magma dans la ZDNC, le taux de soulèvement dans le CGB et la ZDNC était de 0.03 mm/an.

Un modèle tectonique a été développé pour la région de Mont Laurier. Avant 1186 Ma, il y avait une compression créée par la collision entre les terrains Elzevir, Frontenac et Laurentia. Les contraintes et les chevauchements ont bâti les conditions nécessaires pour établir des pressions de 100 à 105 MPa et des températures de 950°C. Après 1186 Ma,

avec la poursuite des chevauchements, des conditions d'extension ont commencé à se développer dans les parties distales des nappes crustales et l'emplacement syntectonique des complexes de monzonite - diorite dans la ZDNC s'est produit entre 1167 et 1164 Ma.

Bohlen (1987) a proposé un champ de pression et de température pour une "granulite générale". Mais, comme le montrent Harley et Hensen (1990), il y a beaucoup de terrains granulitiques qui ne tombent pas dans ce champ. La région de Mont Laurier est un de ces terrains, la température maximum de 950°C et la pression maximum de 100 à 105 MPa place cette région dans des conditions de très haute température et de pression moyenne.

Il y a beaucoup de ressemblances dans les conditions de pression et de température, dans les trajectoires de pression et température, dans les lithologies, dans la chimie, dans la chronologie, et dans la tectonique entre la région de Mont Laurier de la province de Grenville et des régions d'Antarctique, de Madagascar, de l'est de l'Inde, et d'Australie, qui étaient réunies dans le même continent à 0.8 Ga (Dalziel 1991; Hoffman 1991; Moores 1991; Young 1992). Entre les Himalayas et le Grenville, il y a aussi beaucoup de ressemblances (Dewey and Burke 1973; Baer 1976; Davidson et al. 1982; Windley 1986; Hanmer 1988; van der Pluijm and Carlson 1989). Leurs coupes transverses sont très similaires, avec des tectoniques convergentes. L'arc Kohistan et le CMC sont des arcs insulaires qui ont été serrés entre deux continents.

Tel que discuté par Harley et Hensen (1990), c'est dangereux d'essayer de trop simplifier, mais il est possible que toutes ces régions aient connu des taux de refroidissement et de soulèvement qui ressemblent à ceux calculés ici. Aussi, le Grenville, l'Araku du Ghats en Inde (Sengupta et al. 1991), le Series Highland au Sri Lanka (Schümacher et al. 1990), Madagascar (Nicollet 1988), et les Himalayas ont tous eu une croûte surépaissie. La méthode d'analyse des résultats d'un thermomètre en fonction de la taille des minéraux pour établir les températures maximales dans les conditions de haut grade métamorphique, développée ici, est peut-être applicable dans ces autres terrains granulitiques.

La température et la pression maximale de cette région est de 950°C, et de 100 à 105 MPa respectivement. Ces conditions élevées ont soumis les grenats à des effets de diffusion rétrograde des cations. Ces changements ont influencé les résultats des géothermomètres, les petits grenats (<3.5mm^2) ont enregistré des températures jusqu'au 550°C plus basses que la température maximale. Les grenats entre 3.5 et 15 mm^2 ont enregistré des températures entre 100 et 550°C plus basses que la température maximale. Les grenats moyens (entre 15 et 50 mm^2), sans inclusions, ont enregistré les températures les plus élevées. Les taux de refroidissement sont inférieurs à 10°C/Ma pour des températures inférieures à 700°C. Ces faibles taux de refroidissment ont augmenté les effets de diffusion rétrograde des cations.

ABSTRACT

During the past decade, there have been many advances in the domain of metamorphic geology that have rendered previous P-T results questionable. For example, Spear (1991) demonstrated that the widely used garnet-biotite Fe-Mg ion-exchange thermometer can underestimate temperatures by as much as 200°C due to retrograde diffusion between the garnet and biotite. Holdaway and Mukhopadhyay (1993) noted that exchange geothermometers are easily reset at granulite-grade metamorphism. Thus, all geothermobarometers would record lower diffusion-based post-peak metamorphic pressures and temperatures, particularly those such as the biotite-garnet Fe-Mg exchange geothermometer which are expecially sensitive to retrograde cation exchange. One objective of this thesis is to quantify this effect of resetting as a function of mineral grain size.

The field area is located 100 km north of the Ottawa River between Ottawa and Montreal in the Central Metasedimentary Belt (CMB) of the Grenville Province. It contains the largest granulite terrane within the CMB. The western two thirds of the field area is dominated by the Bondy Gneiss Complex (BGC), a granulitic dome, consisting principally of orthogneisses with quartzites, a tonalitic pluton and metapelites. The north-south trending Nominingue-Chénéville Deformation Zone (NCDZ), cuts through the structural trend of the BGC and dominates the eastern third of the field area.

The morphology and textures of migmatites in the area vary greatly from layers of leucosomes with granitic composition flanked by garnet-rich layers, and biotite-rich melanosomes through thin (1mm) wispy-discontinuous leucosomes and felsic moats surrounding garnets to continuous leucosomes greater than 1cm thick. Many thin sections contain embayed K-feldspar or plagioclase grains with inclusions of biotite that formed from a melt-producing reaction. Biotite is present throughout the field area, which limits the peak temperature to below 980°C. One outcrop contains garnets with spinel inclusions, suggesting the reaction Als + Grt = Spl + Qtz, which implies peak temperatures above 850°C. The Krn-Opx-Tur-Crd-Pl assemblage occurs in the BGC implying the kornerupine-forming reaction Tur + Opx + Crd = Krn + Pl.

It has been proposed that the Bondy Gneiss Complex was hydrothermally altered. The plagioclase composition from the BGC are unusually diverse (between An_{25} and An_{88}), possibly due to this hydrothermal alteration. Cordierite, orthopyroxene, and spinel were only observed in the NCDZ. The spinel analyses were similar to literature values from the reconstructed Grenville Orogen at 0.8 Ga. Calcite was only observed in metapelites from the NCDZ, possibly due to fluid flow along this deformation zone during deformation. AFM projections also demonstrate this diversity between these two tectonostratigraphic domains. Garnets in the BGC are up to 20% more Mg-rich than those in the NCDZ, and the BGC biotites are also up to 30% more Mg-rich than the NCDZ biotites.

Garnets were the only mineral found to exhibit regular zoning patterns. Typically, the X_{Alm} values decreased inwards from the rim to the cores, with a corresponding increase in the X_{Pyp} values. In one inclusion-free core, the X_{Grs} value increased towards the centre while the X_{Pyp} value remained constant. This pattern was proposed to be due to isothermal decompression, which agrees with the observed structural evidence for extension in the NCDZ.

To examine the effects of this observed retrograde cation exchange, on the geotheromobarometers, the results from the bioite-garnet Fe-Mg exchange thermometer were plotted versus the size of the garnet. A general trend was observed, where the smaller garnets recorded lower temperatures than the larger garnets. Garnets under 15 mm^2 recorded temperatures between 100 and 550°C below the proposed peak temperature of 950°C. Unexpectedly, the peak temperatures were recorded by the medium-sized garnets, which did not contain inclusions in their cores. The larger garnets were filled with biotite-spinel-ilmenite inclusions which created smaller diffusion domains, thus increasing the effect of retrograde cation exchange. The peak temperature of 950°C was supported by the results from the orthopyroxene-garnet thermometer.

The inferred isothermal decompression and extension imply that the peak metamorphic pressure would have been obtained at $\geq 1186 \pm 4$ Ma, the same time as the peak metamorphic temperature. Thus, a pressure of 100 to 105 MPa at 950°C obtained from the Al in orthopyroxene and garnet-aluminosilicate-silica-plagioclase barometers is proposed to be the maximum pressure. The spinel-garnet barometer resulted in a pressure of 84 MPa at 950°C. The locations of the spinel inclusions, on the garnet zonation profile, suggest that this reaction occurred towards the end of the isothermal decompression, therefore, this pressure of 84 MPa provides a lower pressure limit for the phase of isothermal decompression.

During retrogression, the BGC was uplifted (at 2.3 mm/year) with respect to the NCDZ (0.6mm/year), which along with the comparative competence of the BGC, focussed the 1175 to 1155 Ma episode of deformation and plutonism into the less competent NCDZ. Consequently, it was only after this isothermal decompression, that the cooling histories of the BGC and NCDZ diverged. Initially, the NCDZ cooled more slowly (between14.7 and 9.5°C/Ma), probably because of heat added to it by magma injection, than the BGC (between 25 and 5°C/Ma). This was reflected in the corresponding P-T-t trajectories with the BGC retrograde path following a curve between 5 and 10 MPa lower than that of the NCDZ.

These granulites have similar conditions, P-T trajectories, very high temperature, and isothermal decompression to many other granulite terranes. There are also similarities in P-T conditions, P-T-t trajectories, lithologies, chemistry, chronology and tectonics between the Mont Laurier Region of the Grenville Province and portions of Antarctica, Madagascar, eastern India and Australia which are believed to have been once all linked together at 0.8 Ga (Dalziel 1991; Hoffman 1991; Moores 1991; Young 1992). It is possible that all of these areas experienced similar cooling and uplift histories. The proposed method of plotting recorded temperatures from the biotite-garnet Fe-Mg exchange thermometer versus garnet size to obtain more accurate estimates of peak metamorphic temperatures in high grade terranes may be applicable to these other granulites terranes.

ACKNOWLEDGEMENTS

To start with, the best, my advisor Ed Sawyer. You have been a rock, thank-you for being there! Thank-you for the freedom to learn from my own mistakes and then the guidance when I was getting 'bogged down'. The conferences in Edmonton, Boston and Edinburgh were very appreciated, learning experiences! And then there is the committee. Thank-you Ned Chown for taking over when Ed was on sabbatical. I also like the nickname 'Admiral Boggs'. Thank-you Denis Roy for having faith in me! Regardless of the outcome, your opinion has helped me gain a lot of much-needed self-confidence.

Thank-you Otto van Breemen for the use of the picking lab in Ottawa, and the guidance. Those dates gave my thesis excellent versatility! Louise Corriveau, thank-you for the wonderful field area, and the summer job. Without you, this project wouldn't exist. Thank-you for helping me to discover UQAC! A great crew.... Guillaume, Nahlini, Louis, Michèle, you guys were superb! The staff at the Réserve Faunique de Papineau-Labelle; Alain, thank-you for introducing me to the fox family! I will never forget you... Max, and the rest, thank-you for taking care of me when I sprained my ankle. Your hospitality was greatly appreciated!

Thank-you Arlene Beisswenger for actually wearing a dress to present me and figuring out the toast of the day. On the sappy side, without you and Patricia Corcoran, life would have been pretty dull! I can not forget the French language service in the Departement des Sciences Appliquées! Thank-you Ehouman, Mustapha, Isabel, Martin, Damien, Marianne, Hassan, Macoura, Daniel, Clement, Christine, and everyone else for your much-needed assistance. Thank-you Marc, for the drives when I was a pathetic 'sicky'. Yvonne, the prompt, reliable service for thin sections was greatly appreciated. Claude, thank-you very much for the fitting in the scans, and the help with Illustrator!

One can't forget the all-important family! Thanks Mom, Dad, John, Aunt Jean and cuz Paul. Thanks Mom for being Mom, Dad for the support, John? well you know! Thank-you Aunt Jean for being an intellectual model! Paul? The word is sublimation!

This last one is bizarre... thank-you to the Canadian Armed Forces, for providing some exotic back-drops for working on the 'brick'... Thank-you also for introducing me to Jake, who is a rock in my life! Thank-you NCSM Champlain for the support! LCdr Otis, J.C., and Josée Paris, your presence at my presentation was greatly appreciated. Josée Deschenes, thank-you for the pen and pencil set that I used to write down the last words of the 'brick'. Finally, thank-you CFB Bagotville for providing me with a not-always-quiet, but interesting, place to live!

Financial support from the Eric Dimroth Bursary, and the NSERC grant to EWS for operating funds on the microprobe were also greatly appreciated.

TABLE OF CONTENTS

LIST OF FIGURES

LIST OF PLATES

LIST OF TABLES

CHAPTER 1

INTRODUCTION

1.1 The Problem

1.1a Geothermobarometry and Petrography

During the past decade, there have been many advances in the domain of metamorphic geology that have rendered previous P-T results questionable. For example, Spear (1991) demonstrated that the widely used garnet-biotite Fe-Mg ion-exchange thermometer can underestimate temperatures by as much as 200°C due to retrograde diffusion between the garnet and biotite (Figure 1-I). Many earlier studies have also ignored the effect of grain size on the extent to which diffusion between garnet and biotite occurs (Figure 1-II). For example, the smaller the grain size, the shorter the diffusion path length from the centre of the grain, and thus the higher probability that the P-T estimates may be incorrect (i.e. reset) due to the effects of diffusion. Ductile deformation of most rocks will decrease the grain size and thus facilitate rapid re-equilibration due to diffusion (Brodie and Rutter 1985; Spear 1991). The Nominingue-Chénéville Deformation Zone has affected much of the eastern half of the study area (Chapter 2) and reduced grain size there compared with the coarser-grained rocks in the core of the Bondy Gneiss Complex.

Holdaway and Mukhopadhyay (1993) noted that exchange geothermometers are easily reset at granulite-grade metamorphism (e.g. this study area, Chapter 5). Retrograde diffusion has significantly altered the zoning profiles of the garnets in this study (Chapter 4). Thus, all geothermobarometers would record lower diffusion-based post-peak metamorphic pressures and temperatures, particularly those such as the biotite-garnet Fe-Mg exchange

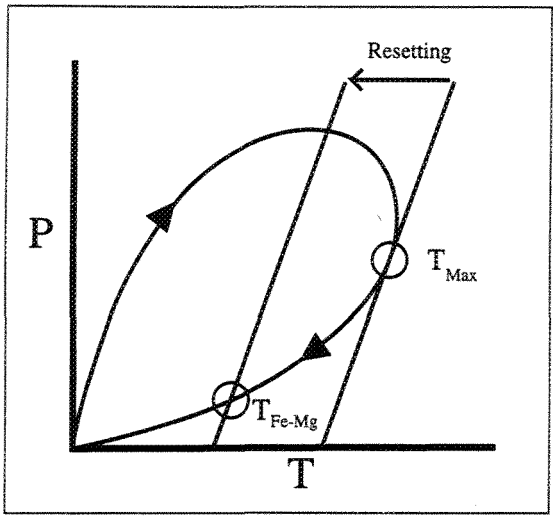

FIGURE 1-I: Sketch to demonstrate effect of resetting due to diffusion on Fe-Mg exchange geothermometers. A clockwise P-T loop is chosen for simplicity in all three of these Figures; although other P-T trajectories may occur, or indeed be the norm in nature, the main conclusion generally still holds.

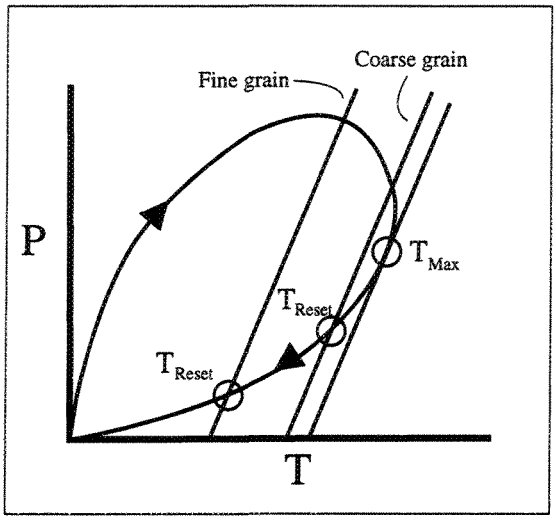

FIGURE 1-II: Sketch to demonstrate the effect of deformation on Fe-Mg exchange geothermometers.

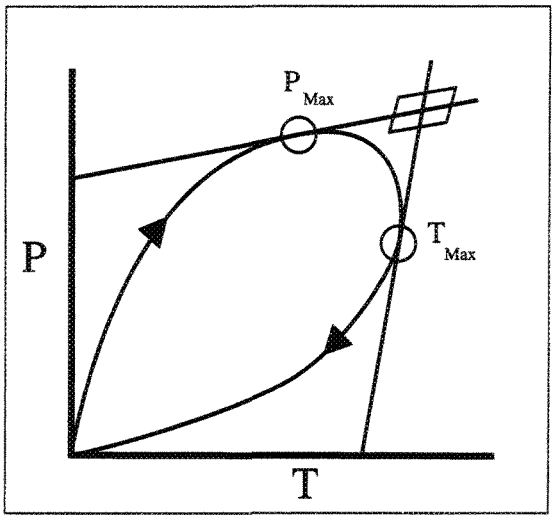

FIGURE 1-III: Sketch to illustrate the potential error in assuming that P_{max} (or T_{max}) can be used to constrain T_{max} (or P_{max}). This assumption also requires T_{max} and P_{max} to have been reached at the same time

geothermometer which is especially sensitive to retrograde cation exchange. Also, it is likely that the Fe-Mg exchange thermometers have closure temperatures for cation exchange below those of granulite facies metamorphism (O'Hara 1977; O'Hara and Yarwood 1978; Lasaga 1983). Straightforward insertion of the stoichiometric data into a thermodynamic database would not allow a close examination of either the effects of the low closure temperatures for cation exchange or retrograde cation exchange. This would have dire consequences on the reliability of the resultant calculated P-T values as stated by Frost and Chacko (1989), Harley (1989), Spear (1991 1992) and Spear and Florence (1992).

Cooling rates have not been calculated by many authors (e.g. Indares and Martignole 1990a, 1990b). The faster the cooling rate, the lower the chance of mineral pairs reaching complete re-equilibration, and the greater chance that P-T estimates might record conditions near the full metamorphic peak. The slower the cooling rate, the greater the chance that mineral pairs have been affected by retrograde diffusion, possibly causing complications when interpreting geothermobarometer results (Spear 1991). The cooling rates determined in this study are slow (Chapter 6).

Many previous studies use estimated temperatures to calculate pressures or vice versa. Such an approach implies that the maximum temperature occurs at the same time as the maximum pressure, which is not necessarily the case (Figure 1-III; England and Richardson 1977). Using the variation in closure temperatures between different minerals, it is possible to determine when the peak metamorphic temperatures occurred; however, it is more complicated to determine when the peak metamorphic pressures occurred (Dodson 1973).

1.1b Field Location

The field area for this study (Figure 1-IV) is contained within two 1:50,000 map sheets (31J03 and 31J06) from the eastern part of the CMB-Q, 100 km north of the Ottawa

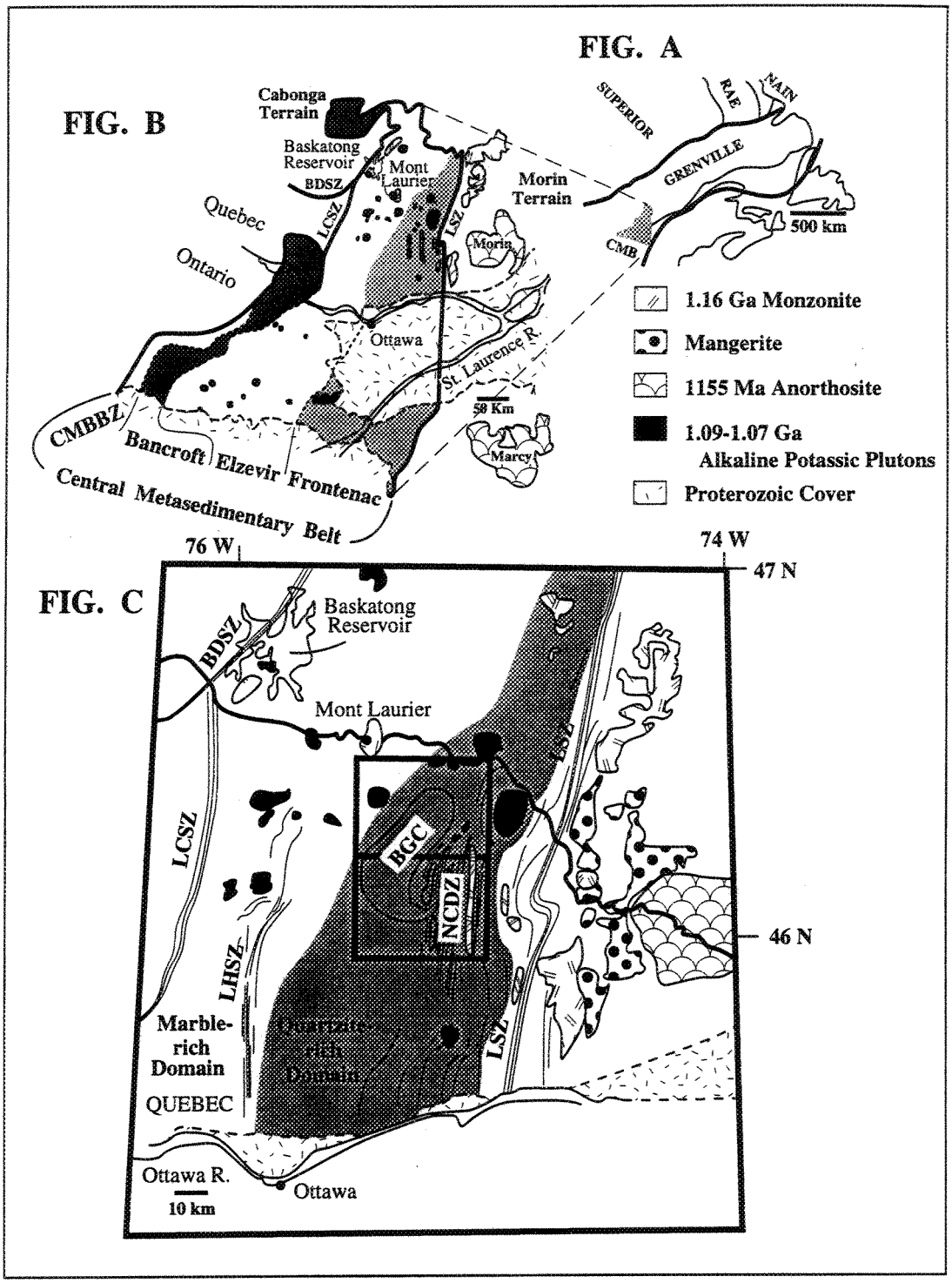

FIGURE 1-IV: The location of the field area. 'A' shows the Grenville Province, and the location of the CMB, 'B' illustrates the divisions of the CMB (note the difference between the divisions of the CMB in Quebec and those in Figure 2-VIII); 'C' outlines the field area (after Corriveau et al., 1995).

River in the Grenville Province. Field work was undertaken as a part of a Geological Survey of Canada regional mapping project led by Corriveau of the Centre Géoscientifique de Québec.

1.1c Previous Work

Indares and Martignole (1990a; 1990b) completed a metamorphic study along highway 117 which traverses the Mont Laurier area and the northeastern corner of the present field area (Figure 1-V). Within this terrane, they also examined a region south of Maniwaki and the shores of the Baskatong Reservoir. They observed garnet zoning patterns in most metapelites and garnet amphibolites which imply P-T paths suggestive of cooling and decompression following the peak temperatures obtained during Grenville orogenic thrusting. Two P-T fields were suggested due to the distribution of determined maximum P-T conditions in metapelites and garnet amphibolites: P-T field "A" at 725-875 MPa, 725-800°C; and P-T field "C" at 425-600 MPa, 625-725°C. Indares and Martignole (1990a, 1990b) suggested that these two clusters of P-T conditions were best explained by the existence of two different crustal levels in the Mont Laurier "Region".

There have also been several structural studies completed 100 km to the west in the vicinity of Otter Lake (Sharma et al. 1995; 1994; 1993a; 1993b; Lévesque and Sharma 1990; Madore et al.1993a; 1993b; 1994; Madore and Sawyer 1991). With SEASAT-RADAR and Airborne-RADAR images, and field work, the Cayament Lineament was defined as the western limit of the Central Metasedimentary Belt and the eastern limit of the Central Metasedimentary Belt Boundary Zone (Sharma et al. 1995; 1994; 1993a; 1993b; Lévesque and Sharma 1990; Madore et al.1993a; 1993b; 1994). Madore and Sawyer (1991) studied the structural features of the Otter Lake-Danford Lake area gneisses observing dominant compression shear zones (W-NW oriented) with parallel and cross-cutting discrete extensional shear zones. This geometric relationship between the compressive and

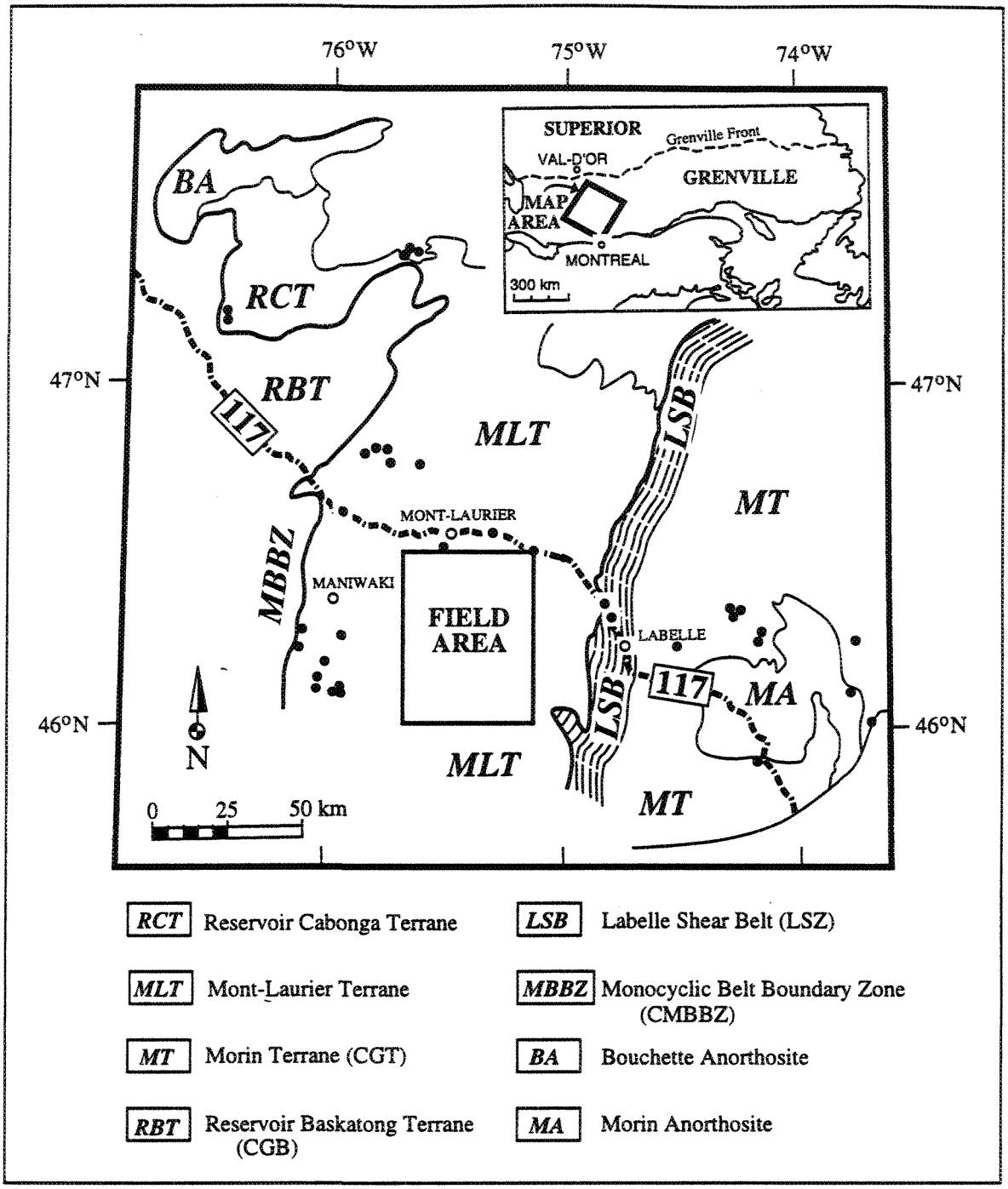

FIGURE 1-V: Sample site locations from Indares and Martignole's (1990) study area (• designates their sample locations) Note, that Indares and Martignole used the terminology of Rivers et al. (1989); the terminology on the legend shown in brackets is that of Wynne-Edwards (1972).

extensional features suggests that the extensional tectonics began early and continued until the post-metamorphic denudation of the Grenville Orogeny (Madore and Sawyer 1991). The thrusting orientation noted by Sharma et al. (1993b); Madore et al. (1993a; 1993b; 1994); and Madore and Sawyer 1991) supports the general west-to-northwest thrusting orientation proposed for the Central Metasedimentary Belt and the Central Gneiss Belt (Hanmer and Ciesielski 1984; Davidson 1986; Easton 1986; Hanmer 1988; Hanmer and McEachern 1992).

Perkins et al., (1982); Kretz, (1959; 1964; 1977; 1978; 1980); and Kretz et al. (1989) have completed several metamorphic analyses of the Otter Lake area. Kretz (1959; 1964) determined that the minerals were in equilibrium. Kretz (1980), in his study of carbonates, suggested peak metamorphic temperatures of 650°C for the Otter Lake area. Perkins et al. (1982) determined maximum metamorphic conditions of 600-650°C and 550-700 MPa for the Otter Lake area, and then noted that the pressures and temperatures increased to the east. Kretz et al. (1989), in his study of the metagabbros in the Otter Lake area, detected chemical zoning in plagioclase (frequent), Ca pyroxene (occasional), hornblende (rare), but not in garnets. With five geothermometers, Kretz et al. (1989), proposed that the peak metamorphic temperatures were up to 700°C in the vicinity of the metagabbros.

McEachern and van Breemen (1993) determined an age of 1190 Ma for the initiation of deformation along the Central Metasedimentary Belt Boundary Zone, which they proposed corresponded to the closure of the marginal basin as the Elzevir Terrane was thrust northwestwards over Laurentia. Throughout the Grenville Province, ages between 1180 and 1150 Ma, have been proposed for the peak metamorphic temperatures (Davidson 1995; Mezger et al. 1991; 1993; van Breemen et al.1986; Hanmer and McEachern 1992; Nadeau and Hanmer 1992; McEachern and van Breemen 1993; Wodicka 1994; Jamieson et al. 1992). Cooling rates from the peak metamorphic temperature through 500 to 150°C for the

CMB of Ontario have been calculated at 1-4°C/Ma (Cosca et al.1991; 1992) which corresponds to regional uplift/erosional rates of 0.03-0.14 km/Ma. Mezger et al. (1993) proposed average cooling rates of 3±1°C/Ma with denudation rates of 120±40 m/Ma for the Grenville Province in their study of the CGB and CMB in Ontario and New York. However, they noted that cooling rates as high as 16°C/Ma were appropriate for the western Elzevir Terrane near the Bancroft Shear Zone due to extensional tectonics. Cooling rates up to 10°C/Ma were measured in the Frontenac Terrane of Ontario. Rates of erosion of 100 m/Ma were calculated for the deepest portions of the CGB, and 30 m/Ma for the shallowest portions of the CMB (Mezger et al. 1993). Cooling rates and uplift/denudation rates have not been published for the CMB of Quebec.

1.2 Objectives for this Thesis

The detailed mapping for this project was designed to note the relevant metamorphic mineral assemblages and textures in order to unravel the metamorphic history of the Central Metasedimentary Belt of Quebec (CMB-Q). The results of this study will then be combined with other current geochronological, geochemical and structural studies in the same field area. Thus, this co-operative effort using modern concepts and detailed observations will lead to a more advanced understanding of the regional geological processes in this poorly understood region of the Canadian Shield.

This thesis will consider four main questions with the goal of better understanding the metamorphic history of the CMB-Q rocks:

i) What were the P-T conditions?

ii) What is the age of metamorphism?

iii) What is the P-T-t path?

iv) What is the cooling/uplift history in each of the main structural blocks in the CMB of Quebec.

The effects of retrograde diffusion on the geothermobarometers must be carefully examined in order to determine accurately what the P-T conditions were for this field area. Thus, to obtain the P-T conditions for this field area, several further question must be considered:

i) Is there retrograde cation exchange?

ii) How can the effects of retrograde cation exchange be determined?

iii) Does the retrograde cation exchange affect the results of the geothermobarometers?

iv) How can reliable temperatures and pressures be obtained from geothermobarometers once there has been retrograde cation exchange?

v) Does grain size influence the effects of retrograde cation exchange?

vi) Is it possible to use the different grain sizes to obtain accurate temperatures and pressures?

vii) Has retrograde cation exchange effected previous studies in this field area, and other granulite terranes?

The answers to the four questions concerning the P-T conditions, age of metamorphism, P-T-t path and the cooling/uplift history for the CMB-Q will then be used to develop a tectono-chronological model similar to that of van Breemen et al. (1986), van Breemen and Davidson (1990), and Cosca et al. (1991; 1992) for the Parry Sound Region of Ontario and that of Mezger et al. (1988; 1992; 1993) for the Adirondacks of New York.

1.3 Methods

1.3a Geothermobarometry and Petrography

This study will determine P-T conditions from samples across the study area. In order to improve the reliability of the Fe-Mg geothermobarometers, it is necessary to plot the reactions and mineral assemblages in P-T space on experimentally based petrogenetic grids. These plots will provide an accurate check for the geothermobarometers. It is also advisable

to apply as many well calibrated geothermobarometers as possible to the individual samples to provide cross checks.

A detailed study of relict inclusions within porphyroblasts is necessary in order to develop an accurate metamorphic history of mineral reactions and mineral assemblages (e.g. Brown and Earle 1983; St. Onge 1987; Jones and Brown 1990). These reactions and assemblages may then be plotted on metamorphic grids in order to provide a more accurate approximation of P-T trajectories and estimated pressures or temperatures. Such a plot may also be used as a check against the P-T estimates from the Fe-Mg exchange geothermobarometers.

To test for the effects of grain size and deformation on P-T estimates, it is advisable to compare the results between fine-grained and coarse-grained phases; and to check for differences between the core and the rim of individual grains (Figure 1-III). To improve the reliability of geothermobarometric studies, it is necessary to choose samples with the largest grain size possible so as to reduce the effect of diffusion of ions out of small grains. For example, it would be wiser to choose a sample from within a coarse-grained boudin than from the fine grained surrounding matrix. In the case of garnet and biotite, it is advisable to choose samples with a garnet to biotite ratio of one to thirty to minimise the effects of diffusion on K_d (Spear 1991).

This study will use petrography to determine equilibrium mineral assemblages, textural evidence of disequilibrium and to determine relict assemblages necessary for determination of the form of the P-T trajectory (e.g. Brown and Earle 1983; St-Onge 1987; Jones and Brown 1990). Pressures and temperatures were estimated using mineral compositions analysed with the electron microprobe at the Université du Québec à Chicoutimi. Fifteen spots of each mineral were analysed to test for zoning. The results from fine- and coarse-grained samples are compared to test for the grain size effects.

The following geothermobarometers will be used individually:

i) Biotite-Garnet

ii) Garnet-Aluminosilicate-Silica-Plagioclase (GASP)

iii) Spinel-Garnet

iv) Al in Orthopyroxene

v) Orthopyroxene-Garnet

vi) Cordierite-Garnet

ix) Melting Reactions and P-T grids (e. g. Vielzeuf and Holloway 1988).

1.3b Geochronology

Fifteen samples were chosen for U-Pb dating of both monazite and titanite to establish metamorphic ages. Three other samples were chosen because rounded metamorphic zircons were observed during a routine petrographic examination of thin sections. These metamorphic zircons were selected in order to date the peak of metamorphism. Biotite was separated from the same three samples for ^{40}Ar-^{39}Ar analysis. In addition one rutile was analysed.

It is necessary to date this many minerals in order to calculate the post-peak metamorphism cooling rates. A cooling rate is calculated by a comparison between the closure temperature (T_c) and the determined date for the individual minerals. Dodson (1973) defined the closure temperature as "the temperature the mineral experienced at the time given by its age". A comparison of the maximum temperatures obtained by geothermometers with the T_c for specific minerals can determine whether the resultant ages correspond to prograde metamorphism (mineral growth) or to retrograde metamorphism (cooling ages; Mezger 1990).

Closure temperatures must be determined empirically because it is not possible at present to predict the diffusion behaviour for a given ion in a specific mineral accurately

enough from first principles. T-t conditions in contact aureoles (Hart 1964; Hanson and Gast 1967; Hanson et al.1971) and regional metamorphic terranes (Purdy and Jäger 1976; Mezger et al.1989a; 1989b) where the thermal history can be evaluated as well as in experiments (Harrison 1981; Harrison et al.1985) can be used to determine closure temperatures empirically (Mezger 1990).

A specific T_c is characteristic of both the individual minerals and the elemental ions used in the analysis (Table 1-I), for example, it is >900°C for the U-Pb system in zircons (Mezger 1990). To obtain an accurate cooling rate, it is necessary to choose minerals forming a series with a wide range of T_c. Here the represented range is from >900°C for zircon down to 350°C for biotite (Purdy and Jäger 1976; Dodson and McClelland-Brown 1985; Harrison et al.1985). Rutile and monazite provide closure temperatures intermediate to those for zircon and biotite; 650-750°C for monazite (Copeland et al.1988; Parrish 1988; 1990; Mezger et al.1988; 1991) and 420-380°C for rutile (Mezger et al.1989b). The closure temperature for titanite is also intermediate, 500-670°C (Cliff and Cohen 1980; Gascoyne 1986). Uplift rates may then be calculated using the resultant cooling rates and the pressures calculated from the geothermobarometric studies.

1.4 Outline

The regional geology of the Grenville Province, Central Metasedimentary Belt, and the study area is outlined in Chapter 2. An intimate understanding of the regional geology is necessary in order to comprehend the local and regional geological processes. This knowledge is a fundamental base to the development of a tectono-chronological model for the Central Metasedimentary Belt of Quebec. Also, for the rest of this study the Bondy Gneiss Complex (BGC) and the Nominingue-Chénéville Deformation Zone (NCDZ) were considered separately because of their separate geological histories.

Table 1-I: Mineral Closure Temperatures (in °C)

MINERAL	TEMPERATURE	GRAIN SIZE	REFERENCES
	(C)	(um)	
	U-PB System		
Zircon	>900 (950)		Mezger, 1990; this study
Garnet	>800	>1000	Mezger et al., 1988
Monazite	650-750	40-2000	Parrish 1988, Copeland et al., 1988
Titanite	500-670	500-30000	Cliff and Cohen 1980, Gascoyne 1986
Rutile	420-380	430-130	Mezger et al. 1989
Apatite	350-550?	200-1000	Mattinson 1978, Cliff and Cohen 1980,
			Watson et al., 1985
	K/Ar and Ar/Ar System		
Hornblende	500-450	160	Harrison 1981
Muscovite	350-400		Hanson and Gast 1967, Purdy and Jager
			1976, Cliff and Cohen 1980
Biotite	300-350		Purdy and Jager 1976, Harrison et al.,
			1985, Dodson and McClelland-Brown 1985
Microcline	150-250	125-250	Harrison and McDougall 1982
	Rb/Sr System		
Muscovite	450-500		Hanson and Gast 1967, Jager et al., 1967
			Purdy and Jager 1976, Wagner et al., 1977
Biotite	350		Jager et al. 1967, Purdy and Jager 1976
			Wagner et al. 1977, Dodson 1979
			Harrison and McDougall 1983
Orthoclase	320	1000	Dodson 1979

Chapter 3 contains a description of the observed assemblages and textures. These observations were plotted in P-T space on petrogenetic grids, which provide a general form of the P-T trajectory and guidelines for the results from the geothermobarometers (Chapter 5). The results from the microprobe analyses are discussed in Chapter 4. Compositional profiles were carefully documented for the effects of retrograde cation diffusion, which would effect the results from the geothermobarometers. And differences in the chemical composition of the minerals between the BGC and the NCDZ were carefully noted.

The geothermobarometers and their results are considered in Chapter 5. The results were compared with the P-T trajectories developed from the assemblages and textures. Any discrepancies were carefully examined. In order to observe the effect of grain size on retrograde cation diffusion, the temperatures from the biotite-garnet Fe-Mg exchange thermometer were plotted against the size of the garnets. These plots were also used to justify the proposed peak temperature. The proposed peak pressures were necessary to calculate the uplift rates in Chapter 6. The results from the geothermobarometers, assemblages and structural observations were then used to develop P-T trajectories for the BGC and the NCDZ.

The results from the geochronological analyses are contained in Chapter 6. U-Pb analyses of metamorphic zircons and monazites were used to propose a minimum age for peak metamorphic conditions. The variation in closure temperatures between zircon, monazite, titanite, rutile and biotite was used to determine cooling rates. Uplift rates were calculated from the cooling rates and the calculated pressures. The results from the BGC and the NCDZ were compared to note any variation that may have occurred due to their differing retrograde histories.

A tectono-chronological model is proposed in Chapter 7 from information contained within Chapters 2 through 6. The Mont Laurier Region of the CMB was compared with

regions from Antarctica, India, Madagascar and Australia which were all linked together with the Grenville Province at ~0.8 Ga (Hoffman 1991; Dalziel 1991; Young 1992; Moores 1991). The tectonic processes of the CMB were compared with those of the Kohistan Arc Complex of the Himalayas. The P-T conditions and the P-T-t trajectories from the study area were also compared with other granulites from the work of Harley (1989) and Harley and Hensen (1990). The significance of these comparisons are then discussed in the final section.

CHAPTER 2

GEOLOGICAL SETTING

2.1 Purpose and Outline

To develop a tectono-chronological model for the present field area, the complete regional geology must be studied, including tectonics, chronology, metamorphism, cooling and uplift rates. In order to put this study in context with other work, it is necessary to place the field area with respect to the geology in previously studied areas. Also, in order to comprehend some trends in the chemistry of various minerals (Chapter 4), and the different configurations of the P-T-t trajectories (Chapters 3, 5 and 6), it is necessary to understand the division between the two main geological features within this study area; the Bondy Gneiss Complex (BGC) and the Nominingue-Chénéville Deformation Zone (Figure 2-I, NCDZ).

The Grenville Province is exposed in the southeastern Canadian Shield (Gill 1948), and extends from the Atlantic shore of Labrador southwestwards to Lake Huron (Figure 2-II; Moore 1982; Woussen et al. 1986). The southern extent of the Grenville Province is covered by the Phanerozoic platform sediments of the Michigan Basin (Davidson 1995). There are two well-accepted schemes for subdividing the Grenville Province:

a) Parautochthonous Polycyclic Belt, Allochthonous Polycyclic Belt and the Allochthonous Monocyclic Belt (Figure 2-III; Rivers et al.1989).

b) Grenville Front Tectonic Zone (GFTZ), Central Gneiss Belt (CGB), Central Metasedimentary Belt (CMB) and the Central Granulite Terrane (CGT) (Figure 2-IV; Wynne-Edwards 1972)

These are described in detail, with the applicable metamorphic, tectonic and geochronological studies.

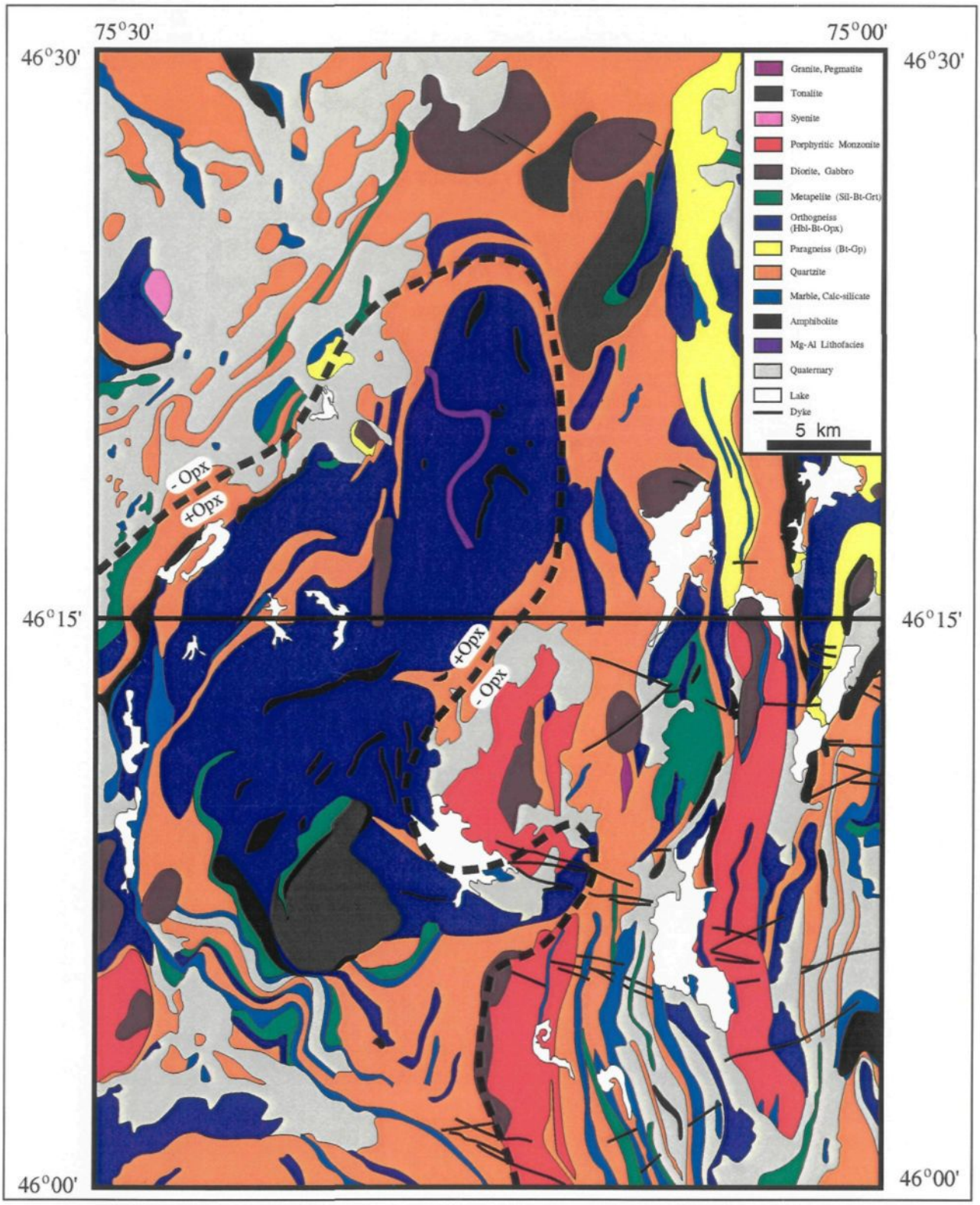

Figure 2-I: Geological map of field area. Note the Bondy Gneiss Complex (orthogneiss complex that dominates the western half of the map sheet), and the syntectonically emplaced monzonite-diorite complexes oriented north-south along the eastern half of the map sheet (in the Nominingue-Chénéville Deformation Zone). Note also, the orthopyroxene-in isograd that closely follows the outlines of the Bondy Gneiss Complex (simplified after Corriveau et al., 1994).

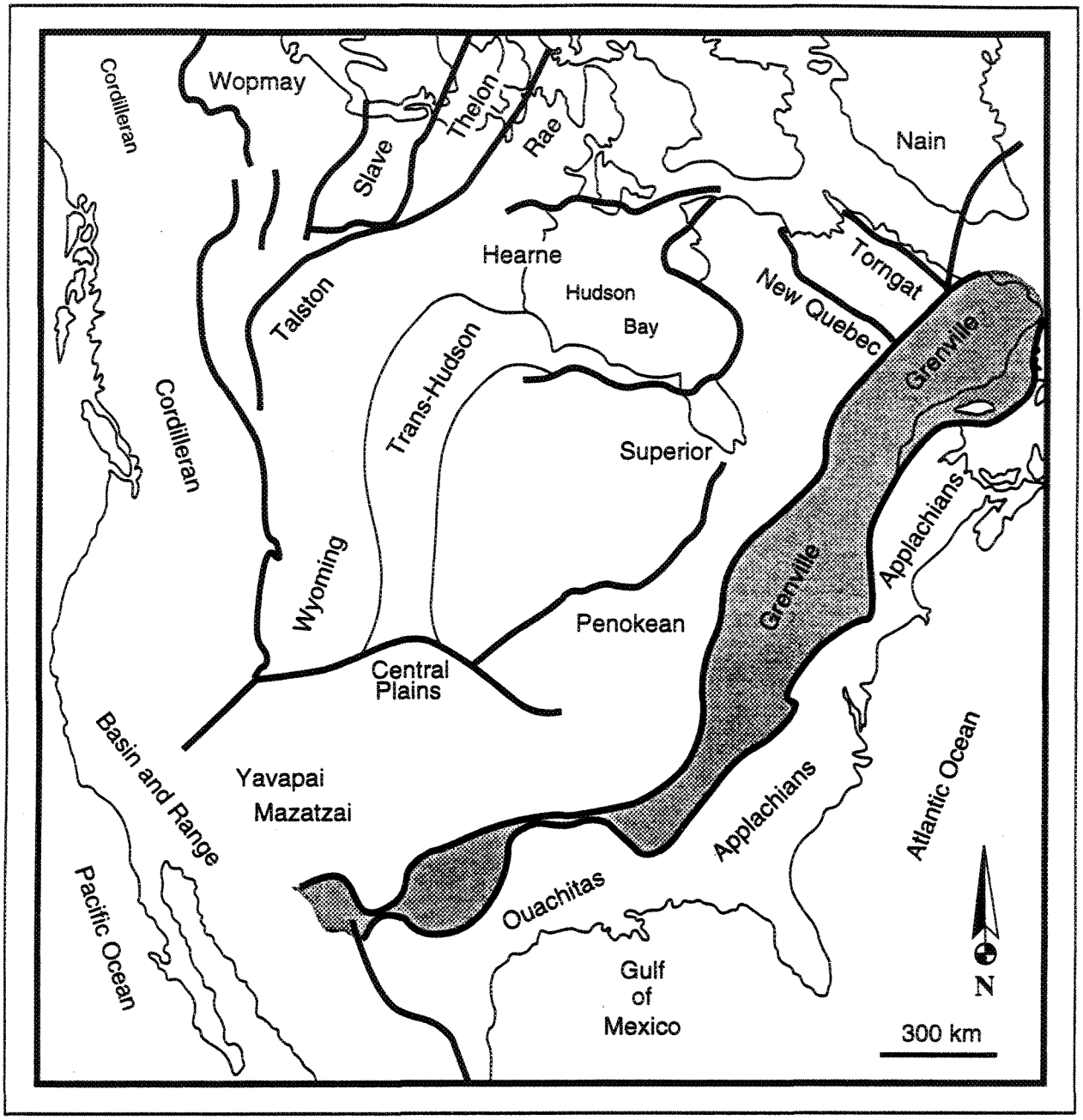

FIGURE 2-II: The extent of the Grenville Orogenic Province with the principal subdivisions of the Precambrian of North America (terminology of Hoffman 1989; after Easton, 1992).

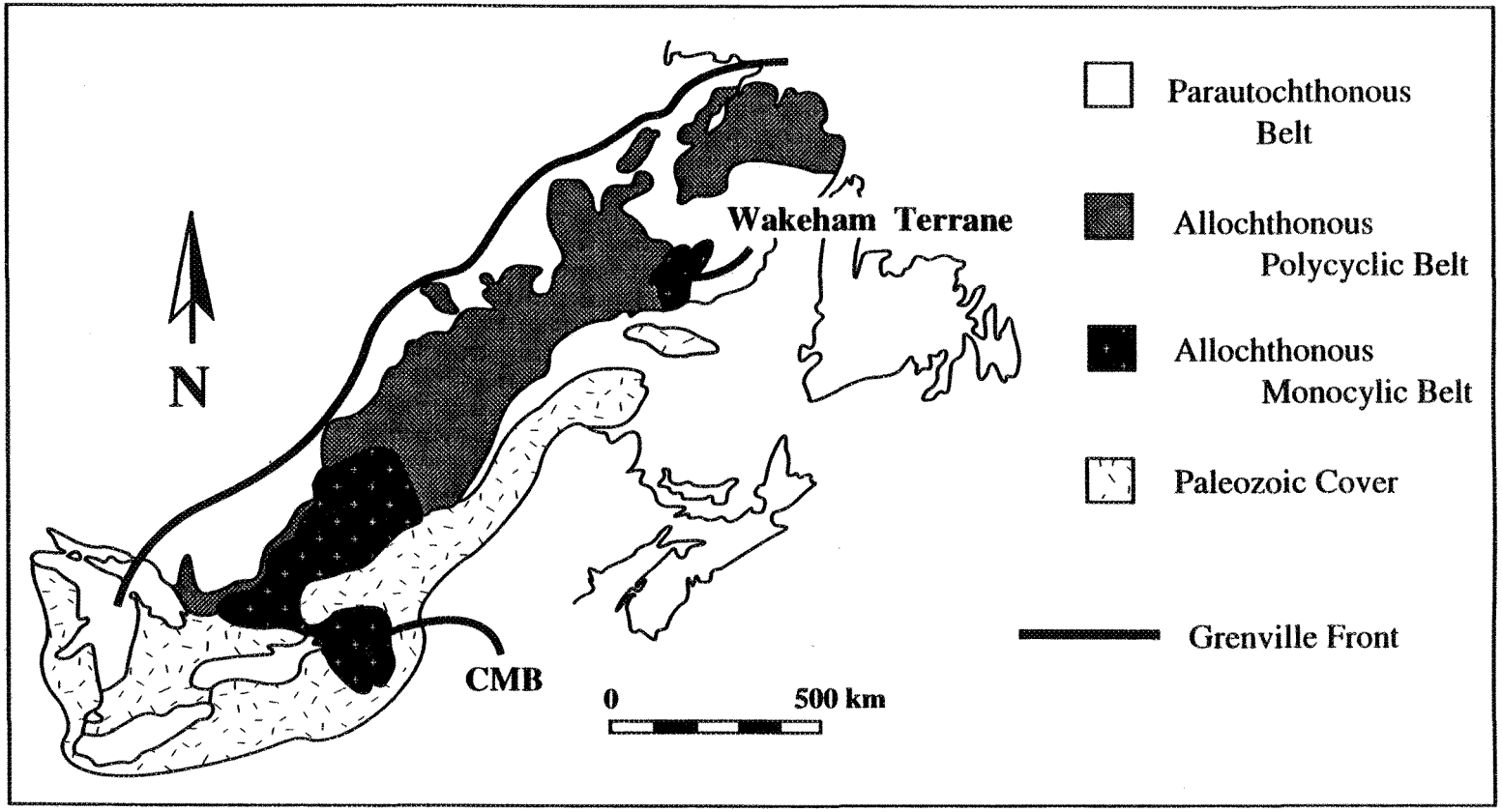

FIGURE 2-III: Rivers et al (1989) tectonostratigraphic divisions of the Grenville Province.

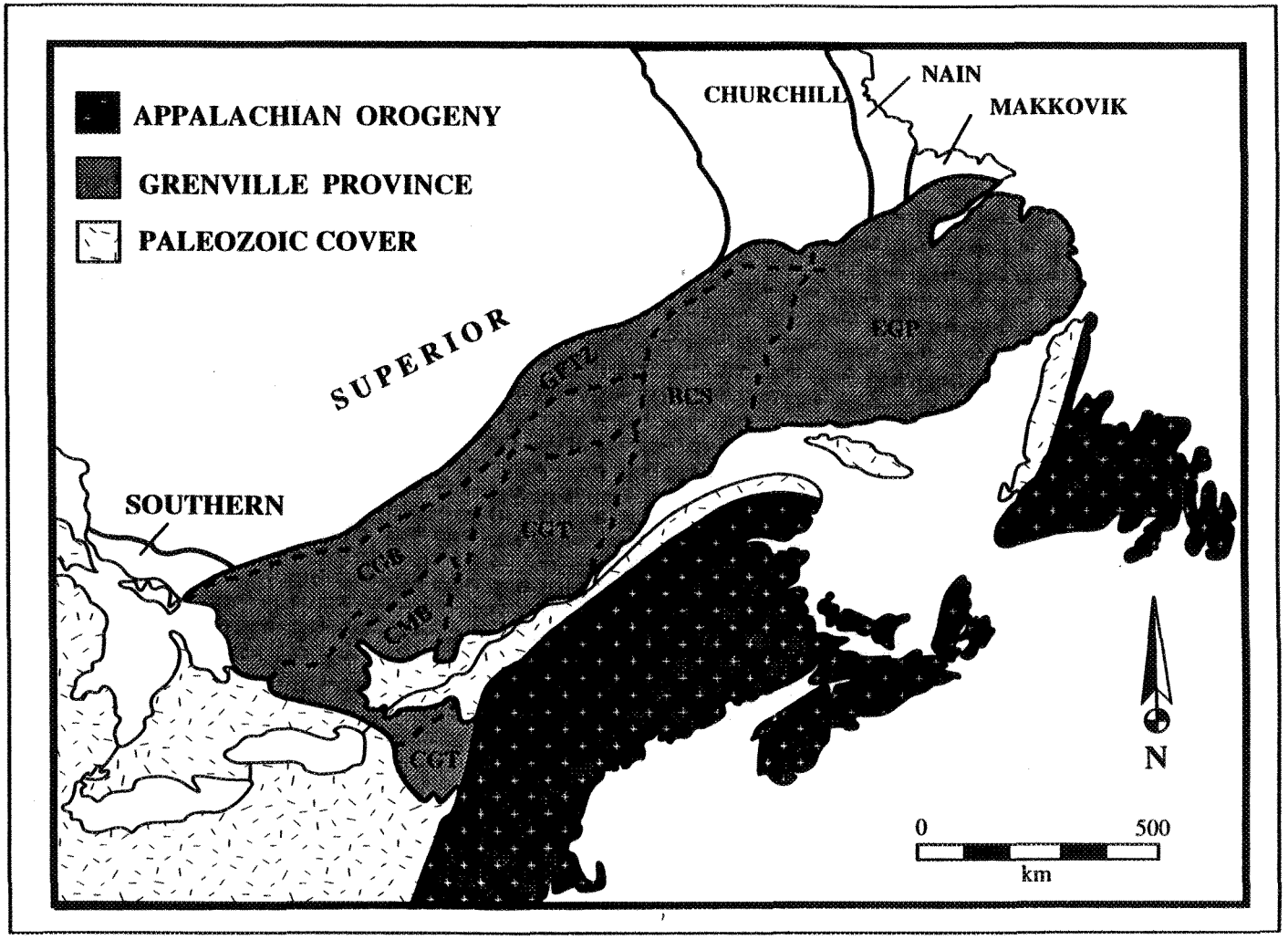

Figure 2-IV: Relationship of Grenville Province with surrounding provinces of the Canadian Shield. Subdivisions of Wynne-Edwards (1972); EGP - Eastern Grenville Province; BCS - Baie Comeau Segment; CGB - Central Gneiss Belt; GFTZ - Grenville Front Tectonic Zone; CGT - Central GranuliteTerrane; CMB - Central Metasedimentary Belt (after Moore 1986).

The study area (Figure 1-IV) comprising of two map sheets (31J06, 31J03) is located within the Central Metasedimentary Belt of Wynne-Edwards (1972) and the Allochthonous Monocyclic Belt of Rivers et al. (1989). The Bondy Gneiss Complex (BGC) is a core to the field area which consists of a 30 x 15km dome structure that exposes a proposed Proterozoic hydrothermal system surrounded by quartzo-feldspathic gneisses of possible volcanic origin (Corriveau et al. 1995). The north-south oriented Nominingue-Chénéville Deformation Zone (NCDZ) is adjacent to the BGC and cuts through the eastern third of the field area (Corriveau et al. 1995). It contains syntectonically emplaced monzonite and diorite plutons. Both the BGC and the NCDZ will be discussed in further detail in Chapters 2, 3, 4, 5, 6, and 7.

2.2 The Grenville Orogen

The Grenville Orogen is exposed in several places, in North America (Figure 2-II), extending southwestwards from the Canadian Shield to Texas and Mexico (Rankin et al. 1993; Ruiz et al. 1988). In southwestern Scandinavia, the Sveconorwegian Province, is the trans-Atlantic counterpart of the Grenville Orogen (Gower 1985, 1990). Remnants of the Grenville orogeny also occur in Scotland and northern Ireland (Davidson 1995). In continental plate configurations for ~0.8 Ga (Figure 2-V; Hoffman 1991) Madagascar, eastern India, the Musgrave Block and the Albany-Fraser Belt of southwestern Australia and portions of Antarctica are connected to the Grenvillian orogenic system (Davidson 1995; Young 1992; Dalziel 1991; Hoffman 1991).

The Grenville Orogen developed between ~1.5 and 0.6 Ga during a relatively inactive period of Earth history (Davidson 1995). Perhaps the first expression of the Grenvillian orogeny was the closure of the Grenvillian Ocean which terminated with an episode of volcanism in the Elzevir superterrane at ~1.25 Ga, and plutonism extending to ~1.23 Ga (Windley 1989, 1993). The Frontenac block may have collided with Laurentia during the

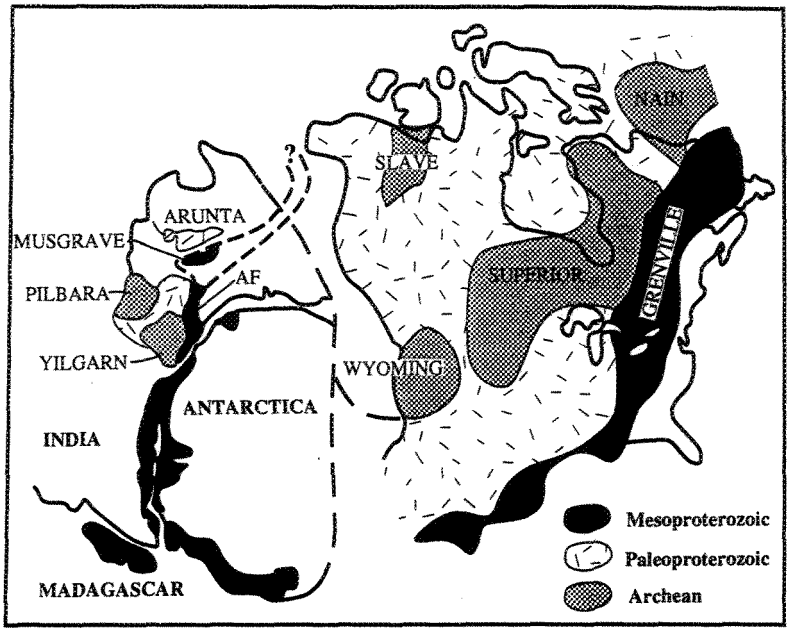

FIGURE 2-V: Moores (1991) reconstruction of post-Grenvillian supercontinent. AF is Albany-Fraser belt. Reworked Archaean blocks are included in palaeo-proterozoic in North America.

closure of the Grenville Ocean at ~1.2 Ga, and then experienced continuing northwest-directed compression until ≤1.16 Ga (Davidson 1995). The Frontenac terrane was then uplifted and cooled (Mezger et al. 1993; Cosca et al. 1992), with detritus shedding northwestward onto the exhumed arc rocks of the Elzevir superterrane (Flinton Group; Moore and Thompson 1980; Sager-Kinsman and Parrish 1993). Small potassic syenite and granite plutons between 1.09 and 1.06 Ga appear to have 'stitched' together the different terranes of the Central Metasedimentary Belt (Davidson 1995). Uplift, erosion, and the final cooling occurred between 1.0 and 0.9 Ga. The Grenville Province appears to have remained inactive until ~600 Ma when the Iapetus Ocean started to form, breaking up the Grenville Orogen, allowing the southeastern continental mass to rift away (Davidson 1995).

2.3 The Grenville Province

The width of the Grenville Province (Figure 2-II) is unknown. The southeast margin is mostly buried under a narrow strip of Early Palaeozoic sediments. Grenvillian rocks occur in tectonic windows and thrust slices throughout the Appalachians and suggest considerably wider extent than the presently exposed conterminous Grenvillian age rocks (Davidson 1995). The Grenville Front, is its northwestern margin and is a sharp tectonic lineament that appears on aeromagnetic maps and cross cuts several tectonic provinces (Rivers et al. 1989).

Metamorphism in the Grenville Province is diverse, ranging from the 40 MPa, 400°C greenschist facies rocks of the Hastings Low through to the 110 MPa, 800°C granulite facies rocks of the Central Metasedimentary Belt of Quebec (CMB-Q; Anovitz and Essene 1990; Cosca et al. 1992). The rate of cooling from ~ 500°C down to ~ 150°C; determined from coexisting minerals with differing Ar closure temperatures, appears to be relatively consistent throughout Ontario (1°-4°C/Ma). The rate of unroofing of the Grenville Orogen, inferred from the retrograde P-T paths, and the measured cooling rates, was calculated to be 0.03 to

0.14 km/Ma (Cosca et al. 1991). Evidence for earlier i.e. pre-Grenvillian deformation and metamorphic events has been overprinted by Grenvillian remobilisation (Davidson 1995).

2.4 Divisions of Rivers et al.

Rivers et al. (1989) divided the Grenville Province into three longitudinal belts - Allochthonous Monocyclic Belt (AMB), Allochthonous Polycyclic Belt (APB) and Parautochthonous Belt (PB) - based on geochronological, geophysical and geological data (Figure 2-III). Their term "monocyclic" refers to those rocks metamorphosed only during the Grenville Orogeny. Three tectonic boundaries (Monocyclic Belt Boundary Zone (MBBZ), Allochthon Boundary Thrust (ABT) and Grenville Front (GF)) delineate these three belts. Recent information from between 1989 (Rivers et al.) and 1972 (Wynne-Edwards) was used to precisely determine the boundaries of the terraines proposed by Wynne-Edwards.

2.4a Allochthonous Monocyclic Belt

The MBBZ represents the decollement between overlying monocyclic rocks (AMB) and the lower polycyclic rocks (APB). The AMB contains two Supergroups, the Wakeham Supergroup comprising terrestrial rift sediments in northeastern Quebec, and the Grenville supergroup consisting of marine platform and/or continental margin sequences in Ontario-Quebec (Figure 2-III). The Wakeham and Grenville Supergroups are both younger than 1300 Ma, and are monocyclic in that they were metamorphosed only during the Grenville Orogeny. The boundaries of the AMB are uncertain (Rivers et al. 1989).

2.4ai The Wakeham Terrane

The Wakeham Terrane (Figure 2-III) consists of a thick pile of volcanic and sedimentary rocks. Martignole et al. (1994) proposed two rift sequences, the basal Aguanus Group and the upper Davy Group. Two stages of rifting, one at 1280 Ma and the later at

1180 Ma, were suggested because only one of the two deformation stages found in the Aguanus Group is present in the Davy Group (Martignole et al. 1994).

2.4b Allochthonous Polycyclic Belt

The APB (Figure 2-III) contains terranes of high-grade paragneisses and orthogneisses locally intruded by anorthosites, gabbros and granites. Several of these terranes at the western margins of the APB tectonically overly the PB. Pre-Grenvillian orogenies have affected some of the supracrustal rocks within these terranes, which defines the polycyclic nature of this division. Due to the limited nature of the geological mapping completed within the APB, it is possible that the underlying PB may appear south of the ABT in tectonic windows (Rivers et al. 1989).

2.4c Allochthon Boundary Thrust

The boundary between the allochthonous and parautochthonous terranes is the ABT (Figure 2-III). Geochronology, metamorphism and structures have established the location of this thrust. A pronounced aeromagnetic signature was used to map it in eastern Quebec. The aeromagnetic signature in Ontario and western Quebec is less clear, and thus its location there is tentative. This boundary is interpreted to be a locus for major thrust displacements because it is characterized by subhorizontal mylonitic rocks that typically mark a break in isotopic dates and/or an inversion in metamorphic grade (Rivers et al. 1989).

2.4d Parautochthonous Belt

The PB (Figure 2-III) is up to 150 km wide and located between the ABT and the Grenville Front. In several places, it is the lithological continuation of foreland rocks further north of the Grenville Province. Typically, much of the northwestern part of the PB is characterised by isoclinal folds that are overturned to the northwest and by northeast trending shear zones. The grade of metamorphism increases in an approximate southeasterly direction away from the Grenville Front (Rivers et al. 1989).

2.4e Grenville Front

The northeast trending Grenville Front is exposed for some 2000 km; it represents the northwestern limit of the Grenville Province (Figure 2-III). It dips approximately 30° southeastwards possibly as deep as the lower crust (Rivers et al. 1989). A northwest directed thrusting along the Front is suggested by moderately to steeply dipping foliation and strong down-dip lineations (Jamieson et al. 1995). The GF is the surface expression of a crustal discontinuity that overprints structural trends in the neighbouring provinces to the northwest, and delimits the northweastern extent of penetrative Grenvillian metamorphism and deformation (Rivers et al. 1989). The Grenville Front, of Ontario, lacks the extensional features of the adjacent Britt Domain in the parauchthonous belt, however, it does preserve evidence for two episodes of thrusting, one ≥1035 Ma and a second at ≥980 Ma (Jamieson et al. 1995).

2.5 Divisions of Wynne-Edwards

Wynne-Edwards (1972) proposed a division scheme for the Grenville Province by considering the rock units and structural divisions.

2.5a The Central Gneiss Belt

Tectonically layered amphibolites and gneisses that have been metamorphosed to upper amphibolite or granulite facies conditions are typical of the CGB (Figures 2-IV, 2-VI). A network of ductile shear zones (up to tens of kilometers long) separate lithotectonically distinctive domains and subdomains (Davidson 1984). This pattern has been interpreted to depict a series of imbricate crustal slices assembled during orogenesis (Culshaw et al. 1983; Davidson 1984). Stretching lineations combined with rotated porphyroblasts indicate thrusting towards the north-east (Davidson 1984).

U/Pb zircon ages from syntectonic pegmatites intruded into the shear zones, have been used to estimate the timing of the thrusting events within the CGB. These ages range

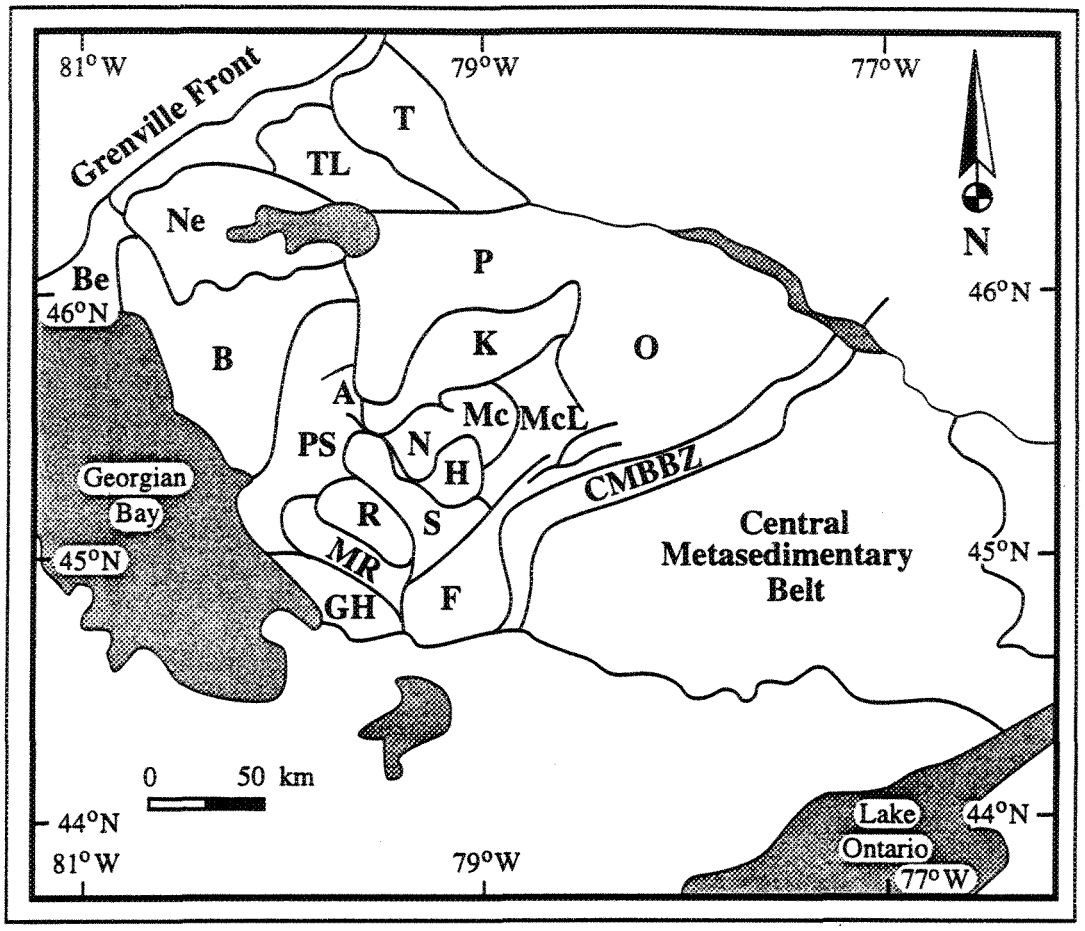

Figure 2-VI: Domains of the Central Gneiss Belt of Ontario. A-Ahmic, B-Britt, Be-Beaverstone Bay, F-Fishog, GH-Go Home, H-Huntsville, Mc-McCraney, McL-McLintock, MR-Moon River, N-Novar, NE-Nepawassi, O-Opeongo, P-Powassan, PS-Parry Sound, R-Rosseau, S-Seguin, T-Tomiko, TL-Tilden Lake (after Easton, 1992; Tuccillo, 1995).

from; (a) 1159 to 1121 Ma for two shear zones within the most deeply buried Parry Sound domain (Figure 2-VI) in Ontario (van Breemen et al. 1986) to, (b) 1103 Ma from a syntectonic pegmatite that cuts the deformation fabric of rocks that overlie the Parry Sound domain structurally (van Breemen and Davidson 1990). There is no significant detectable (> ±10 MPa (Moecher et al. 1988; Anovitz and Essene 1990)) variation in metamorphic pressures observed across most of the shear zones mapped by Davidson (1984) in the CGB.

There is a discordance of about 25 Ma in hornblende and muscovite/K-feldspar $^{40}Ar/^{39}Ar$ ages between the Grenville Front and the adjacent Britt Domain (Figure 2-VI). These were interpreted by Reynolds et al. (1995) to reflect variations in crustal thickness and geothermal gradients between the flank and the interior of the Grenville Orogen. Reynolds et al. (1995) inferred a cooling rate of 2°C/Ma between 500 and 350°C for exhumation controlled by post-orogenic erosion.

Calcium zoning profiles in garnets, which cross-cut those for iron and magnesium, were used by Tucillo et al. (1990) to suggest a drop in pressure of 80 MPa at 700 ±50°C for the Britt Domain. Barometry from other garnet-bearing samples, was consistent with the zoning patterns, giving pressures of 12.9 at 700°C and 4.7 at 700°C. An interval of 300 to 400 Ma between the U-Pb ages of allanites, garnets, monazites and titanites was used as evidence for two episodes of metamorphism. Peak conditions at 1450 Ma were followed by thrusting of the Parry Sound Domain over the Britt Domain at 1160 Ma culminating in a second period of metamorphism at 1060 Ma (Tucillo et al. 1992).

2.5b The Central Metasedimentary Belt

Sir William Logan started mapping the Central Metasedimentary Belt (Figures 2-III, 2-IV) over a century and a half ago. He initially described the "Grenville Series" from an area just west of Montreal in the vicinity of the village Grenville after which the rock Series was named. In three papers, Wilson (1918, 1925, 1939) referred to the general area of the

TABLE 2-I: Terrane Terminology

(after Easton and Davidson, 1994)

Terrane: a package of strata bounded by faults with a geologic history distinct form the conterminous geologic units

Terranes may be (after Howell, 1989):

Metamorphic (e.g., Mazinaw Terrane?)

Disrupted (e.g., Bancroft Terrane)

Stratigraphic
i. fragments of ocean basins
ii. fragments of volcanic arcs (e.g., Elzevir or Mazinaw Terranes)
iii. representing fragments of continental margins (e.g., Frontenac Terrane)
iv. representing fragments of continents

A combination (e.g., Mazinaw Terrane)

Other genetic terminology includes:

Exotic, suspect or accreted - terrane transported to its current position (e.g. an island arc sliver accreted to a craton)

Pericratonic - formed on attenuated continental crust and contains cratonal detritus

Tectonic assemblage - rock-stratigraphic units formed in tectonic settings (e.g., island arcs or ocean floors)

Domain: a volume of rock with structural homogenity, bounded by structural or compositional discontinuitites. These may be termed subterranes, and may contain minor stratigraphic distinctions.

Superterrane: a compound terrane, containing more than one terrane that were amalgamated before the subsequent orogenesis.

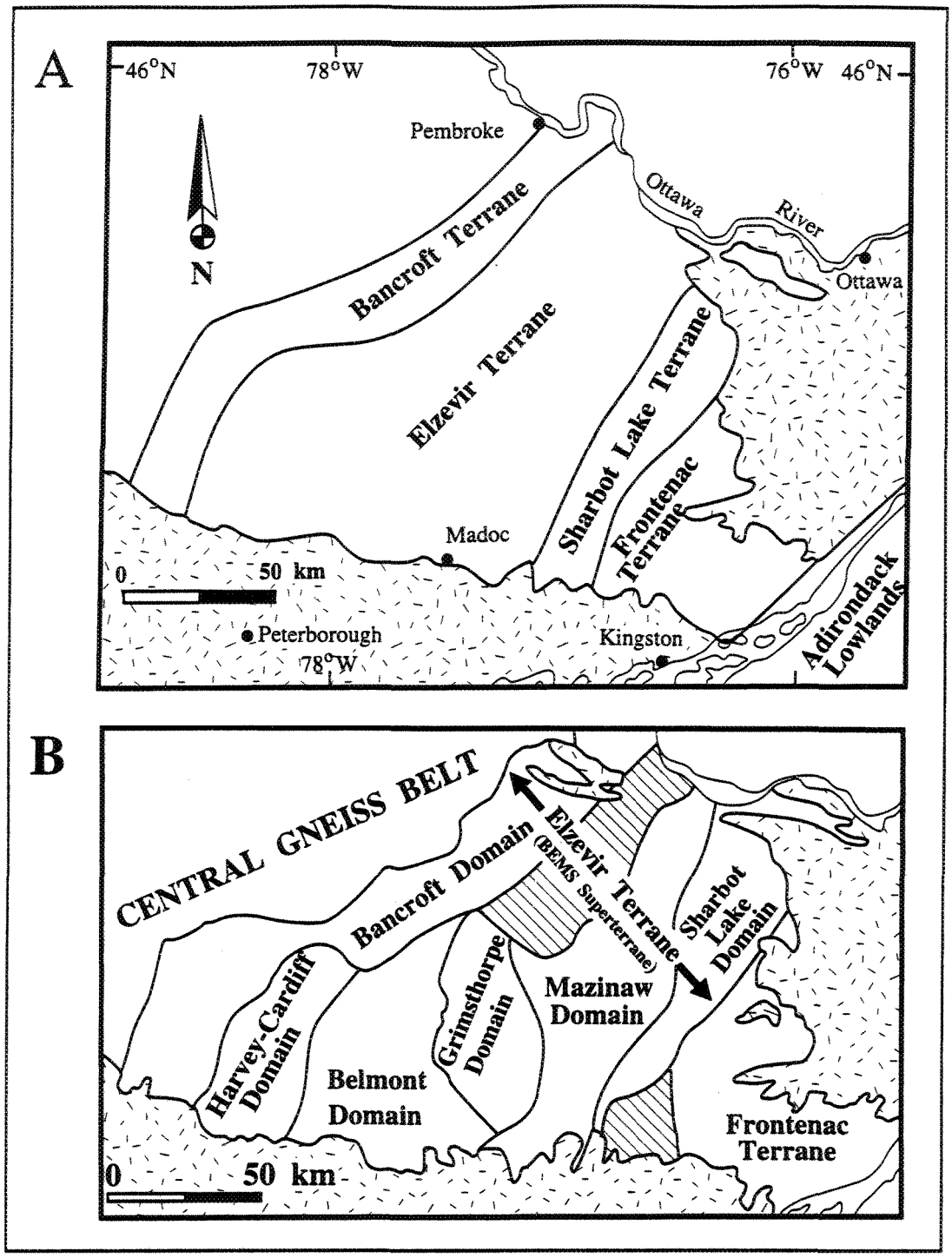

FIGURE 2-VII: Terrane subdivision of the Central Metasedimentary Belt; A as proposed by Moore (1982); B as proposed by Easton (1992). The dash marks are paleozoic cover, and the diagonal lines are regions that are not easily assigned to the existing domains. BEMS stands for Bancroft-Elzevire-Mazinaw-Sharbot Lake (after Easton and Davidson, 1995).

CMB as the Grenville subprovince. Finally, Wynne-Edwards (1972) coined the term Central Metasedimentary Belt for the rocks of the region including Logan's Grenville Series.

The CMB is composed of sediments, felsic and mafic intrusives, and volcanics metamorphosed from upper greenschist through to granulite facies (Carmichael et al. 1978; Anovitz and Essene 1990). It has been divided by Moore (Figure 2-VII; 1982) into the Bancroft, Elzevir, Sharbot Lake, and Frontenac Terranes. Easton (Figure 2-VII; 1992) proposed joining the Bancroft, Elzevir and Sharbot Lake terranes as the Elzevir Terrane or the BEMS (Bancroft-Elzevir-Mazinaw-Sharbot Lake) Superterrane. He then further divided the Elzevir Terrane into the Harvey-Cardiff, Belmont, Grimsthorpe and Mazinaw Domains. The definitions of domain and terrane, and the logic behind the formation of these domains/terranes, is contained in TABLE 2-I from Easton and Davidson (1994).

The "Hastings metamorphic low" near Madoc contains the lowest metamorphic grade rocks (Carmichael et al. 1978). The metamorphic grade increases from this low, through amphibolite to granulite facies, northwest towards Bancroft, northeast towards Quebec, and southeast towards the St. Lawrence River. U/Pb ages of titanites, garnets and monazites inferred to have grown during metamorphism have been used to suggest that the peak of metamorphism occurred between 1170 to 1020 Ma (Mezger et al. 1993). Because of geochemical evidence, it has been suggested that parts of the CMB were assembled into their present positions by terrane accretion, whereas others evolved in an island arc environment (e.g. Davidson 1986; Corriveau 1990).

Hornblende $^{40}Ar/^{39}Ar$ cooling ages vary by over 200 Ma between the Elzevir and Frontenac terranes (Cosca et al. 1992). Most of this age variation occurs across the shear zones that separate the two terranes. However, there is also a second variation in these hornblende ages associated with the Hastings metamorphic low. To the east, outside of this low, the ages are ~ 935 Ma; inside the metamorphic low, the ages are ~ 1010 Ma. These

combined $^{40}Ar/^{39}Ar$ ages possibly suggest that these terranes experienced separate metamorphic histories before they were assembled after having cooled below the argon closure temperature for hornblende. It is also possible that these variations in hornblende dates were a consequence of differential uplift resulting from extensional deformation during the later stages of cooling after the Grenville Orogeny. If the CMB had been unroofed as a single rigid block during the period of cooling, the $^{40}Ar/^{39}Ar$ cooling ages for each mineral should be approximately the same. This is not the case, therefore, the CMB was not unroofed as a single domain, but rather in stages or as smaller subdomains (Cosca et al. 1992).

2.5c The Central Metasedimentary Belt Boundary Zone

The CMBBZ (Figure 2-IV, 2-VII) is at least 200 km long and represents a 10 km thick stack of crystalline thrust sheets enclosed by an anatomosing network of ductile thrust zones. It is a crustal-scale shear zone with the CMB as the hanging wall and the CGB as the footwall (Hanmer and McEachern 1992; McEachern and van Breemen 1993).

The CMBBZ has long been recognized as a zone of intense tectonism (Hanmer and McEachern 1992). The rocks of the CMBBZ were originally named the Radcliffe Hybrid Gneiss. Lumbers et al. (1990) proposed that this zone was a deferred unconformity where late Precambrian rocks of the Grenville Supergroup overlie plutonic rocks. He also proposed that these rocks were tectonically modified by the diapiric rise of the underlying Algonquin Batholith during the Grenville Orogeny. As evidence for this theory, Lumbers et al. (1990) mentioned that the Radcliffe Hybrid Gneiss contains clasts of the same rock type as the underlying metaplutonic rocks.

In 1986, Davidson demonstrated that the gneissic rocks along the CMBBZ are highly strained, and that the layering is not necessarily sedimentary bedding. He also mentioned that some of the conglomerates are tectonic with "clasts" that are tectonic inclusions. There

are also lenses of exotic anorthosite and pyroxenite that are not typical of bordering terranes, nor of the rocks within this zone. Finally the metasediments (marbles and quartzites) within the CMBBZ occur as discrete lenses, they are not traceable beds. The northwest directed kinematic indicators noted by Davidson (1986) also negate diapiric rise for the Algonquin batholith.

Kinematic indicators such as mineral augen, rotated boudins, C and S fabrics and shear bands indicate a northwest transport of the CMB over the CGB (Davidson 1986; van der Pluijm and Carlson 1989; Hanmer and Cielsielski 1984; Hanmer et al. 1985; Hanmer 1988). Thrusting within the CMBBZ appears to have commenced at about 1140 Ma in accordance with field observations and U/Pb zircon ages (McEachern and van Breemen 1993). U/Pb zircon ages from syntectonic pegmatites and granites (van Breemen and Hanmer 1986), and titanites from nearby marbles appear to indicate re-activation of the CMBBZ until 1030 Ma (van Breemen and Hanmer 1986).

2.5d Shear Zones of the CMB

Changes in metamorphic grade, or zones of high strain, often mark the boundaries of terranes within the CMB (e.g.,. Davidson 1986; Easton 1988). Within the terranes, there are also highly strained zones associated with regional and local shearing (e.g., Ayres et al. 1971; Carmichael et al. 1978; Easton 1988, NCDZ). Field relationships suggest that the Sharbot Lake mylonite has a southeast dip of 60 to 70° (Easton 1988), the Roberston Lake Mylonite a southeast dip of close to 30° (Easton 1988), and the Bancroft shear zone a southeast dip of 30° (Carlson et al. 1990). The stretching lineations are towards the southeast. The sense of motion is difficult to determine, and often complicated. For example in the Bancroft Terrane, numerous northwest-directed shear sense indicators have been observed (Easton and Bartlett 1984; Davidson 1986), but there are also southeast directed extensional shear sense indicators (Carlson et al. 1990). In many cases, the kinematic

indicators have been obscured by the high strain deformation that formed ultramylonitic zones within these shear zones (Cosca et al. 1992).

The Bancroft Shear Zone was suggested to be the result of orogenic collapse after most terranes were emplaced into their present position (van der Pluijm and Carlson 1990). Cosca et al. (1995) suggested that this extensional event lasted from 1040 to 893 Ma with a displacement rate of 0.06 to 0.13 km/Ma.

Corriveau et al. (1994) and Culshaw et al. (1994) proposed that some terrane boundaries may be cryptic especially those that are a result of early terrane accretion as opposed to the boundaries due to later thrusting relationships. Hildebrand and Easton (1995) suggested that the top of a marble unit within the Frontenac Terrane was an ~1161 Ma northwest directed fault. This was proposed to be a regional scale thrust that placed hot pluton-ridden (1179-1162 Ma) metamorphic rocks over cool platform carbonates. It is possible that this is a fundamental contact between upper and lower plates during collision suggesting that the Adirondacks represent the upper hinterland and the lower plate basement is towards the northwest in the Frontenac Terrane. Hildebrand and Easton (1995) pointed out the similarities between this proposed thrust and the Parry Island Thrust Sheet, suggesting that these two thrust sheets were part of the same plate thrust over the southwest margin of Laurentia at ~1160 Ma.

2.5e The Bancroft Terrane

The long axis of the Bancroft Terrane (Figures 2-IV, 2-VII; Wynne-Edwards 1972) is roughly parallel to the CMBBZ. This terrane principally contains marble breccias and marble with nepheline-bearing gneisses and other silica-undersaturated plutonic rocks present as clasts or sheets within the marble (Davidson 1986; Hanmer 1988). The metamorphic grade ranges from middle to upper amphibolite facies (Anovitz and Essene 1990). The Bancroft Terrane has been interpreted to be part of the same northwest-directed thrust-nappe

complex as the CGB (Easton and Bartlett 1984; Davidson 1986). The Bancroft Shear Zone is the boundary between the Bancroft and Elzevir terranes and represents a late extensional shear zone with an inferred vertical offset of 5-6 km (van der Pluijm and Carlson 1989; Carlson et al. 1990). Cosca et al. (1992) used $^{40}Ar/^{39}Ar$ hornblende dates to suggest a vertical offset of 7 km for this shear zone.

2.5f The Elzevir Terrane

The Elzevir Terrane (Figure 2-IV, 2-VII; Wynne-Edwards 1972) consists of a supracrustal sequence containing marbles, interlayered with, and underlain by metavolcanics dated at 1287-1248 Ma (Davidson 1986; Davis and Bartlett 1988). These were intruded, contact metamorphosed and deformed by calc-alkaline, tonalitic plutons during the Elzevirian Orogeny (Moore and Thompson 1980). A second period of plutonism is represented there by smaller, discrete plutons ranging in composition through gabbro, monzonite and syenite to granite (Davidson 1986). Detritus from the erosion of these plutons formed the Flinton Group (Moore and Thompson 1980). The post-Flinton Group Ottawan metamorphism produced greenschist to granulite facies assemblages (Davidson 1986). Whole rock Rb/Sr ages and discordant U/Pb zircon and titanite ages suggest that thrusting within the ~1250 Ma Elzevir terrane predates the regional peak metamorphism dated at between 1102 and 1088 Ma (Silver and Lumbers 1966; Bell and Blenkinsop 1980; Heaman et al. 1986; Davis and Bartlett 1988; Corriveau 1990; Mezger et al. 1991).

Some primary structures are preserved in "metamorphic lows" where the rocks are in greenschist or lower amphibolite facies. These are the only locations within the CMB where primary sedimentary features are preserved. Even with these features, correlation between units outside of, and units inside the Elzevir Terrane, is impossible. In most areas within the CMB, the overall stratigraphic relationships and correlations have been lost due to metamorphic recrystallization and transposition (Davidson 1986).

2.5fi The Mazinaw Domain

The Mazinaw terrane (Figure 2-VII) was proposed as a separate domain, even though it resembles the Elzevir Terrane lithologically, because it is covered by the Flinton Group (at ≥1150 Ma), and records a structural history similar to that of the Frontenac Terrane (Easton 1992; Easton and Ford 1990;1991). The Mazinaw Terrane consists of plutonic, volcanic and sedimentary rocks which were intensely faulted and folded and metamorphosed up to upper amphibolite facies (Corfu and Easton 1995). An early period of magmatism and sedimentation (1280-1240 Ma), in a probable marginal basin setting, and a multistage metamorphic evolution (1100-980 Ma) likely related to crustal thickening by imbrication during compression of the Mazinaw Terrane, were established by U-Pb geochronology (Corfu and Easton 1995).

2.5f.ii The Sharbot Lake Terrane

The Sharbot Lake terrane (Figure 2-VII; Easton 1988) consists of volcanic and sedimentary rocks metamorphosed to amphibolite facies conditions. The narrow Robertson Lake Mylonite Zone, dips 30° to the southeast and, marks the boundary between the amphibolite facies Sharbot Lake Terrane and the greenschist facies Elzevir Terrane. The 250-300 m wide Sharbot Lake mylonite zone, defines the boundary between the Sharbot Lake terrane (amphibolite facies) and the Frontenac terrane (granulite facies; Easton 1988).

2.5g The Frontenac Terrane/New York Lowlands

Upper amphibolite to granulite facies marbles with associated orthogneisses, amphibolites, quartzites and metapelites comprise the Frontenac Terrane/New York Lowlands (Figure 2-VII; Carmichael et al. 1978; Lonker 1980; Davidson 1986; Anovitz and Essene 1990). The metamorphic grade increases to the southeast, reaching low pressure, upper granulite facies in the Frontenac terrane. The high grade metamorphism in the

Frontenac Terrane was achieved prior to 1170 Ma, followed by a second metamorphism, along with the Elzevir Terrane, at ~1100 Ma (Sager-Kinsman and Parrish 1993).

In the New York Lowlands, the metamorphic grade decreases to amphibolite facies (Davidson 1986) and then increases to granulite facies towards the Carthage Colton Mylonite Zone which defines the boundary between the New York Lowlands and Highlands (Geraghty et al. 1980). Metamorphic temperatures increase from 650 to 760°C in the northeast, with a corresponding increase in pressure from 54 to 80 MPa. The a_{H2O} ranges from 0.08 to 0.5, does not correlate with the metamorphic grade (Edwards and Essene 1988).

Before 1160 Ma (McLelland et al. 1988), the Lowlands and Highlands had similar histories. The subsequent high-grade metamorphism is restricted to the Highlands, while the Lowlands domain had cooled to the U-Pb closure temperature of rutile. This is supported by the U-Pb garnet, titanite, monazite and rutile ages of Mezger et al. (1991). These rutile and monazite ages were used to deduce cooling rates of ~1.5°C/Ma for the 150 Ma following the last episode of high grade metamorphism. The Lowlands had cooled to ~400°C by ~1000 Ma (Mezger et al. 1991).

Mezger et al. (1992) suggested that the Carthage Colton Mylonite Zone does not separate two completely unrelated terranes as proposed by Windley (1986), instead that it represents a boundary between two terranes that were joined up to ~1098 Ma, separated and then rejoined after 1000 Ma. They proposed that the CCMZ be considered as the remnant of a complete Wilson cycle (opening and closing of an ocean; Mezger et al. 1992).

Northwest-directed shearing is suggested to have occurred along the mylonite zones developed within the Frontenac terrane and along the boundary between the Frontenac and the Sharbot Lake terranes. Later southeast directed shearing was suggested due to

superimposed structural indicators, although few, or no, kinematic indicators are contained within most of the mylonite zones (Easton 1992).

2.5h The Mont Laurier "Terrane"

The Mont Laurier "Terrane" (Figure 2-VIII) consists predominantly of pelitic gneisses and quartzites, with up to 80% marbles in its western portions. The metamorphic grade ranges between amphibolite and granulite facies; granulites are more widespread in the northern portions. Structural trends are steeply dipping (Davidson 1986). The original southern boundary for this terrane (Wynne-Edwards 1972) was the Ottawa River.

The Labelle shear zone (LSZ) separates the eastern margin of this terrane from the Morin Terrane of the CGT (Brock and Moore 1983). The 1 to 3 km long N-NE trending subvertical LSZ forms part of the Gatineau-Chibougamau Lineament (Baer 1976) and is possibly the northern extension of the Carthage Colton Mylonite Zone (CCMZ, Forsyth et al. 1988), which would then have a length of over 1700 km (Mezger et al. 1992). Lamb (1993) suggested crystallization temperatures of ~900°C with dynamic recrystallization at 470 to 550°C for porphyroclasts from the Diana metasyenite located within the CCMZ. The LSZ tectonites are derived from the charnockites of the Morin Terrane and the metasediments of the Mont Laurier 'Terrane'. Rotated porphyroclasts in the straight gneisses of the LSZ suggest a sinistral sense of shear (Indares and Martignole 1990a).

Lithologically, the Mont Laurier Terrane appears to represent the northward extension of the Frontenac, Elzevir and Bancroft Terranes (Figures 1-IV, 2-VIII). The eastern portions of the Mont Laurier "Terrane" contain the K-rich stocks, mafic metavolcanic rocks and has the flat aeromagnetic signature typical of the Elzevir Terrane (Corriveau 1990, Forsyth et al. 1992). Corriveau (1990) has suggested the name Gatineau Domain for this northern extension of the Elzevir terrane. A supracrustal sequence with abundant granulite facies quartzite and metapelite located within the southeastern part of the Mont Laurier "Terrane"

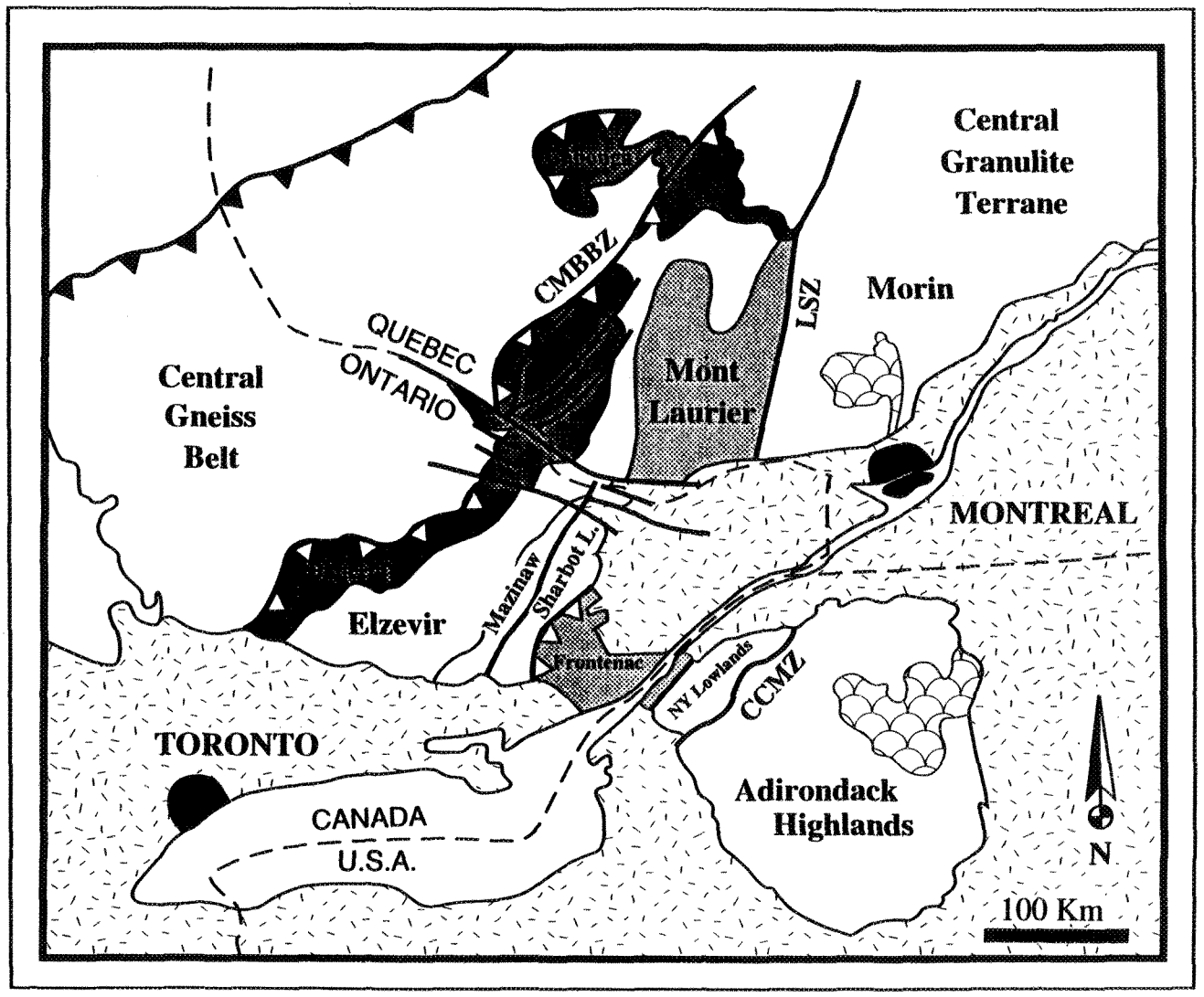

FIGURE 2-VIII: Divisions of the Central Metasedimentary Belt (after Davidson, 1995). Note the division of the Elzevir Terrane (into Mazinaw and Sharbot Lake). This division scheme is different than that in Figure 1-IV for the "Mont Laurier Terrane" of Quebec.

was suggested by Davidson (1986) to correlate well with the Frontenac terrane. Due to these lithological similarities which suggest that the well established terranes of Ontario extend further north, Corriveau (1990) has suggested that the term Mont Laurier 'Terrane' be eliminated altogether.

There is some discrepancy between the proposed extensions of the Ontario CMB terranes into Quebec. A comparison between Figures 2-VIII and 1-IV demonstrates that Davidson (1995) proposes a much thicker extension of the Frontenac terrane into Quebec than does Corriveau et al. (1995). Davison (1995) also extends the equivalent to the Bancroft terrane completely across the northern portions of the CMB in Quebec. For the purposes of this thesis, the scheme developed by Corriveau et al. (1995) is used.

The syenitic plutons present throughout the "Elzevir Terrane" were previously thought to be products of anorogenic intraplate magmatism in an extensional environment (Baragar 1977; Lumbers et al. 1990), or crustal thickening (Windley 1986). However recent petrological and geochronological studies south of Mont-Laurier, indicate that these now appear to belong to a 1089-1076 Ma, 400 km-long, northeast-trending, K-rich alkaline and shoshonitic plutonic belt that includes ultrapotassic rocks (Corriveau 1990). These plutons appear to have been emplaced before the formation of the major ductile shear zones, but after the regional metamorphism, because of their preserved igneous textures, deflection of the country-rock gneissic layering into concordance with plutonic contacts and the local amphibolite-grade deformation of the plutons near the CMBBZ and the Labelle shear zone (Corriveau 1990).

Windley (1986) suggested that these potassic plutons were not the products of crustal thickening during the final stages of an arc-continental collision between the CGB and the CMB, and that the regional metamorphism was not associated with the Ottawan Orogeny. Corriveau (1990) proposed that this 1089-1076 Ma episode of potassic magmatism was

initiated by a previously unrecognized subduction event that represented the initial stages of the Ottawan Orogeny. The next stage was the joining of the Frontenac Terrane with the Elzevir Terrane. During the final episode of the Ottawan Orogeny, the CMB was accreted to the Central Granulite Terrane. The suggested northwest-directed thrusting of the CMB over the CGT at 1060 Ma and the hypothesis that the CMBBZ is a suture (Windley 1986) are consistent with this model (Corriveau 1990).

2.5i Cabonga Reservoir Terrane

The Cabonga Reservoir Terrane (CRT) overlies the parautochthonous Dozois Reservoir Terrane (DRT; Figure 1-V). The NE trending Baskatong Reservoir Terrane separates the CRT from the DRT, other than in the northern end where a narrow belt of deformed sediments connects the CRT with the Mont Laurier 'Terrane'. High strain gneisses with NE plunging lineations mark the boundaries with the underlying terranes (Indares and Martignole 1990a).

The CRT is composed principally of marbles, metagabbros and garnet amphibolites structurally overlain by garnetiferous metapelites and quartzites (Laurin 1960; 1961). The elongate SE-dipping, highly deformed Bouchette anorthosite-gabbro igneous complex forms the northwestern boundary to the metasediments (Ottan 1978). A spoon-shaped structure is suggested by the moderately dipping convergent foliations in the CRT (Indares and Martignole 1990a).

A mylonite zone located within gently dipping Archean migmatites which underlie the CRT forms the base of a large thrust sheet consisting of a migmatitic sole and the CRT. Contrasting garnet zoning profiles between the migmatites and the western CRT metasediments were used by Martignole and Pouget (1993) to propose that the CRT metasediments were metamorphosed under relatively high pressures before being thrust upon the Archean migmatites and then both were subjected to a lower pressure metamorphism.

Rotated porphyroblasts and CS fabrics in shear zones within the Bouchette anorthosite, the location of the CRT and the lithologies within the CRT suggest a northwest directed transport of the CMB lithologies over the parautochthon (Indares and Martignole 1990a).

2.6 Present Field Area

The field area (Figures 1-IV, 2-I) for this thesis consists of 2 map sheets and is located south of Mont Laurier. The boundary between the proposed northern extensions of the Elzevir and Frontenac Terranes cuts through the northeastern corner of the study area. Marble dominates to the northeast of this boundary, but quartzites are omnipresent throughout the entire field area (Corriveau and Jourdain 1992, Corriveau et al. 1994).

The Bondy Gneiss Complex (Corriveau et al. 1995) forms an elongate dome with steep flanks which dominates the core of the study area (Figure 2-I). In the southwestern part of the study area a basin complex consisting of monzonites, mangerite and diorite is enclosed by orthogneisses and quartzites. Graphite-rich paragneisses and serpentine bearing dolomitic marbles border the Bondy Gneiss Complex to the west. At the eastern margin of these two map sheets there is the Nominingue-Chénéville Deformation Zone (NCDZ), an amphibolite-facies ductile shear zone with syntectonically emplaced lit-par-lit injections of diorite, monzonite and dykes of microdiorite, syenite and granite (Corriveau and Jourdain 1992; Corriveau et al. 1994).

The important first order structural elements in the field area consist of a synform in the southwestern corner of 31J03, an antiform in the central-western portion of 31J06, a shear zone (NCDZ) along the eastern margin of both map sheets and a granulitic dome (BGC) in the southwestern corner of 31J06 and the northwestern portion of 31J03. The orthopyroxene-in isograd (Figure 2-I) follows both flanks in the northern portion of the granulite dome, then bends eastwards, it then leaves the southern portion of the dome and runs southwards to the bottom of map sheet 31J03. The folded form of this isograd

demonstrates that peak regional metamorphism occurred before the development of the large scale regional fold (Corriveau and Jourdain 1992; Corriveau et al. 1994).

2.6a The Paragneisses

The paragneisses in these two map sheets (Figures 2-I, 2-IX) are composed of quartzites and siliceous gneisses intercalated with metapelites, biotite-bearing quartzo-feldspathic gneisses and local graphite and iron sulphide-bearing marbles and calc-silicates. The gneissosity, compositional layering and the preferential orientation of the tabular and acicular minerals marks the regional foliation. The orientation of sillimanite in metapelites, quartz in granitic veins, and various other mineral aggregates defines the regional mineral lineation. The mineral lineations are not consistently oriented except along the Nomininguе-Chénéville Deformation Zone, where they are oriented towards the south. Foliation is strongly aligned east-west (Corriveau et al. 1994).

2.6b Bondy Gneiss Complex

The main components of this 30 x 15 km granulitic dome-complex (crystallization age 1240 Ma, metamorphic age 1190 Ma) are granitic and tonalitic migmatitic orthogneisses intercalated with <4m thick horizons of metabasite (Figures 2-I, 2-IX). These fine-grained leucocratic orthogneisses contain hornblende, biotite, garnet and/or orthopyroxene as accessory minerals. The foliation defined by orthopyroxene and biotite is parallel to the gneissosity. The well-developed orthopyroxene-containing granitic leucosomes are medium-grained, parallel to the local foliation and massive to slightly foliated (Corriveau et al. 1994).

At the southern end of this dome, there is a 30 km^2 tonalitic pluton with gneissic borders. This mass is leucocratic, granoblastic to slightly foliated and relatively homogenous; with biotite and hornblende ± orthopyroxene. Leucosomes within this mass are medium grained, massive and granitic to tonalitic. It is possible that this body represents the protolith for the orthogneiss, because the presence of the leucosomes suggest that it has

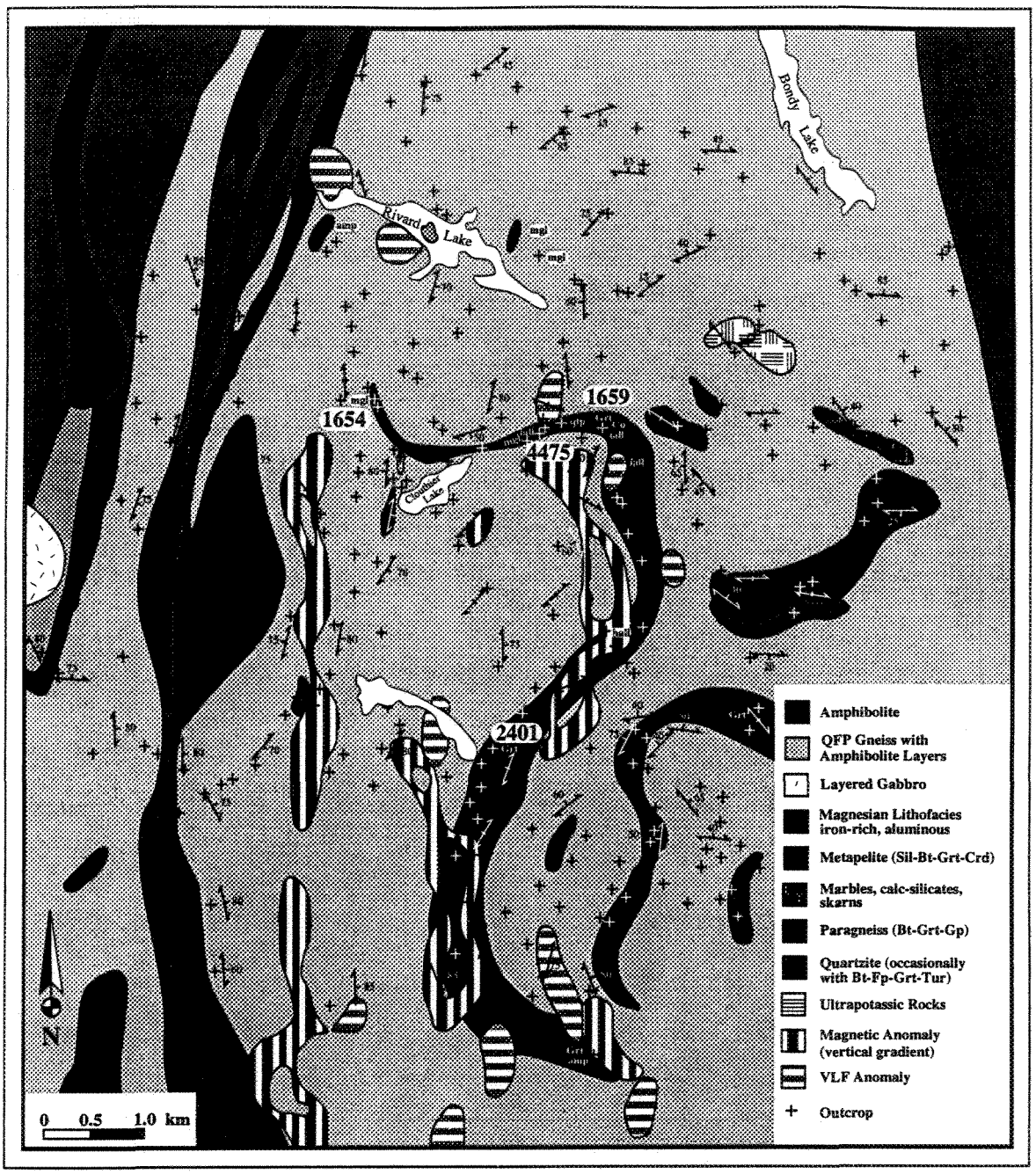

FIGURE 2-IX : Geological Map of northern portions of Bondy Gneiss Complex. Four important outcrops discussed in the thesis are from this region; 2401D2 (spinel inclusions in garnet); 1654 (kornerupine-bearing outcrop); 1659 (garnet-orthopyroxene-cordierite-sillimanite); and 4475D3 (large garnets with ilmenite inclusions). This figure demonstrates the complex lithological and structural relationships within the BGC (simplified after Corriveau et al. 1995). amp- amphibolite; Cu- copper showing; Grt- garnetite; qfp- quartzo-feldspathic gneiss; iall- iron and aluminum lithofacies; hall- hyperaluminous lithofacies; mgl- magnesian lithofacies.

been subjected to some considerable metamorphism, but the lack of penetrative gneissosity suggests that it has not yet been subjected to the same extent of deformation as the orthogneiss. It is also possible that it was a pluton whereas the gneisses were not (Corriveau et al. 1994).

This tonalite, and the orthogneiss were both injected by net-veined lamprophyric dykes that contain phenocrysts of pyroxene, amphibole and locally biotite. In places rounded centimeter to decimeter masses of lamprophyre are contained within granitic lenses which are locally separated by magma mingling zones. In order to develop the irregular lobed contacts observed between the lamprophyre and the granite, the mafic component was most likely injected into the core of pegmatites and then disrupted by flow before solidification occurred (Corriveau et al. 1994).

The northwest portion of the dome (Figure 2-IX) contains scattered outcrops of granitic gneisses and garnetiferous amphibolites of possible volcanic origin. These gneisses are crosscut by the Rivard ultrapotassic breccia dyke. The magnesian and hyperaluminous lithofacies are also present in these outcrops. Granitic leucosomes occur commonly within this dome, and there are numerous local ductile shear zones (Corriveau et al. 1994).

A sequence of graphite-rich metasediments with minor dolomitic marbles and olivine-bearing marbles lines the western margin of this dome. A regional synform plunging towards the south is defined by these paragneiss layers in the southwest of map sheet 31J03 (Corriveau et al. 1994).

Corriveau et al. (1995) proposed that a volcanic-plutonic suite with deep-level felsic intrusives, such as a 1240 Ma tonalitic pluton and shallow-level volcanogenic rocks containing exhalative Cu-bearing hydrothermal systems, formed the protolith for the BGC.

2.6b.i Magnesian and Hyperaluminous Facies

A folded 10 km x 100m wide band of distinctive rocks in the northern BGC contains:

i) a laminated quartzo-feldspathic gneiss,

ii) layered garnetiferous amphibolite, chalcopyrite-bearing metabasite and metabasite,

iii) Boron-rich units consisting of tourmaline-bearing quartz-rich rocks and tourmalinite,

iv) Al-rich units, comprising sillimanite-quartz-pyrrhotite gneiss, sillimanite-biotite-garnet gneiss and cordierite-garnet-orthopyroxene gneiss,

v) Mg-rich, Ca-poor white gneiss unit with kornerupine, tourmaline, Mg-cordierite, bronzite, quartz and plagioclase (Figure 2-IX; Corriveau et al. 1995).

A white quartzo-feldspathic gneiss with cm-thick magnesium-rich bands (MgO: 10%) containing bronzite, Mg-cordierite, kornerupine, Mg-tourmaline and accessory pyrrhotite, pyrite, magnetite, and zircon is the principal component of this lithofacies. This quartzo-feldspathic gneiss is interlayered with a) a laminated granitic gneiss, b) a sillimanite-garnet-cordierite-biotite gneiss with pyrrhotite and zircon, c) a gneiss with cordierite, hypersthene and garnet, and rich in zircon, and d) a garnetiferous rock with magnetite and pyrite, pyrrhotite and chalcopyrite masses. Further south, this quartzo-feldspathic gneiss becomes hyperaluminous, being composed almost entirely of sillimanite and quartz with accessory biotite and pyrrhotite, and traces of pyrite and chalcopyrite. This extremely rusty weathering zone is isoclinally folded and cut by abundant granitic veins (Corriveau et al. 1994).

2.6c Rivard Breccia

This north-south oriented ultrapotassic minette dyke is 200m long and contains 40 to 70% xenoliths. The lamprophyre magma was emplaced at 1080 Ma (Corriveau et al.1995). This unaltered dyke intrudes garnet-rich amphibolites, orthogneisses, pegmatitic veins and crosscuts the regional foliation. The grain size, composition and abundance of the xenoliths

vary along and across the dyke, and has been interpreted as due to six episodes of magma injection into this dyke (Corriveau et al. 1995).

The Rivard breccia is correlated with the 1.09 to 1.07 Ga Kensington-Skootamata K-rich alkaline plutonic suite which are all spatially associated with marble (Corriveau et al. 1995). These magmas had very low viscosities ($1x10^{02}$ Pa·s; Corriveau and Leblanc 1995), and would thus propagate via dyke propagation according to rock and magma rheological models. Marble, which is ductile at deep crustal levels, would favour magma pooling (Lister and Kerr 1991; Clemens and Mawer 1992). Rigid gneiss bodies would fracture, allowing lamprophyre dykes, such as this one, to be formed (Corriveau et al. 1995).

The xenoliths have an extremely wide range of composition and form. Thirty percent of the 1500 described xenoliths are ultramafic; peridotites, websterites, orthopyroxenites and clinopyroxenites (with garnet, spinel and micas). Approximately 30% are mafic to intermediate; calc-silicates, metabasites, anorthosites, norites, and gabbros. The remaining 40% are felsic ortho- or paragneiss with garnet, grey quartzites and granitoids. Xenoliths range in form from rounded to angular, and in size from 1 mm to 70 cm (Corriveau et al. 1994).

The lamprophyric matrix contains 20% millimetric biotite and clinopyroxene phenocrysts. Clinopyroxene, biotite, K-feldspar, plagioclase, amphibole and apatite with minor sulfides, zircon, titanite and quartz make up the remaining 80%. Local magmatic foliations around certain xenoliths are defined by the phenocrysts, which demonstrate an upwards flow direction (Corriveau et al. 1994).

2.6d Nominingue-Chénéville Deformation Zone

Amphibolite grade protomylonitic to mylonitic paragneisses dominate the eastern part of the study area (Figure 2-I). Diorite and monzonites were syntectonically emplaced as sheet-like intrusions into these porphyroclastic paragneisses. Most of the shearing was

completed by 1156 Ma (U-Pb monazite age from late-tectonic pegmatite), less than 10 Ma after the emplacement of the plutons (1165 Ma; Corriveau et al. 1994; 1995). Vertically-layered monzonite plutons and mafic intrusions were the result of this coeval magmatism. Pegmatites that crosscut these plutons are commonly thoroughly mylonitised. Textures and layering in the gabbros are preserved except locally along the margins of some intrusions and in some minor shear zones. The host to the gneiss complexes behaved as a rigid body during regional shearing allowing diorite and composite net-veined lamprophyre dykes to preserve intricate magma-mixing textures (Corriveau et al. 1994; 1995).

The strongly layered and foliated nature, together with the transition from monzonite to gneiss observed in the eastern region suggests that it constitutes a regional scale shear zone that trends 183°/60° extending from Chénéville to Lac Nominingue (Dimroth 1966). The presence of muscovite in the biotite gneisses suggests that metamorphic retrogression down to amphibolite facies occurred during shearing. The intensity of deformation increases across the shear zone from west to east. In the east, the microdioritic and pegmatitic dykes have all been mylonitized; whereas most of these dykes in the west still preserve their original magmatic foliation (Corriveau et al. 1994).

CHAPTER 3

ASSEMBLAGES, PETROLOGY AND PETROGENETIC GRIDS

3.1 Purpose and Outline

The mineral assemblages and textures of the samples collected during the field study are described in this chapter. A detailed study of the assemblages, inclusions, and textures from individual samples can determine the reaction sequence experienced during the P-T history (e.g. Jones and Brown 1990). The reaction sequence can be used to deduce an approximate P-T trajectory on established petrogenetic grids (e.g. Vielzeuf and Holloway 1988). The P-T trajectories suggested from the assemblages and textures can be used to constrain the results from the geothermobarometers in Chapter 5. The geochronological analyses of these samples (Chapter 6) can then be used to provide an approximate age for peak metamorphic temperatures for the P-T-t trajectories developed from these petrological observations and the geothermobarometry results.

The samples were chosen from aluminous gneisses containing assemblages useful for geothermobarometric and geochronological studies. Figures 3-I and 3-II show the sample locations. Appendix A contains a brief petrographic description of each thin section; the evidence for melt-producing reactions is in Appendix B. A list of assemblages is displayed in Table 3-I. Section 3.7 summarizes the P-T trajectories implied by the assemblages and textures observed in this chapter.

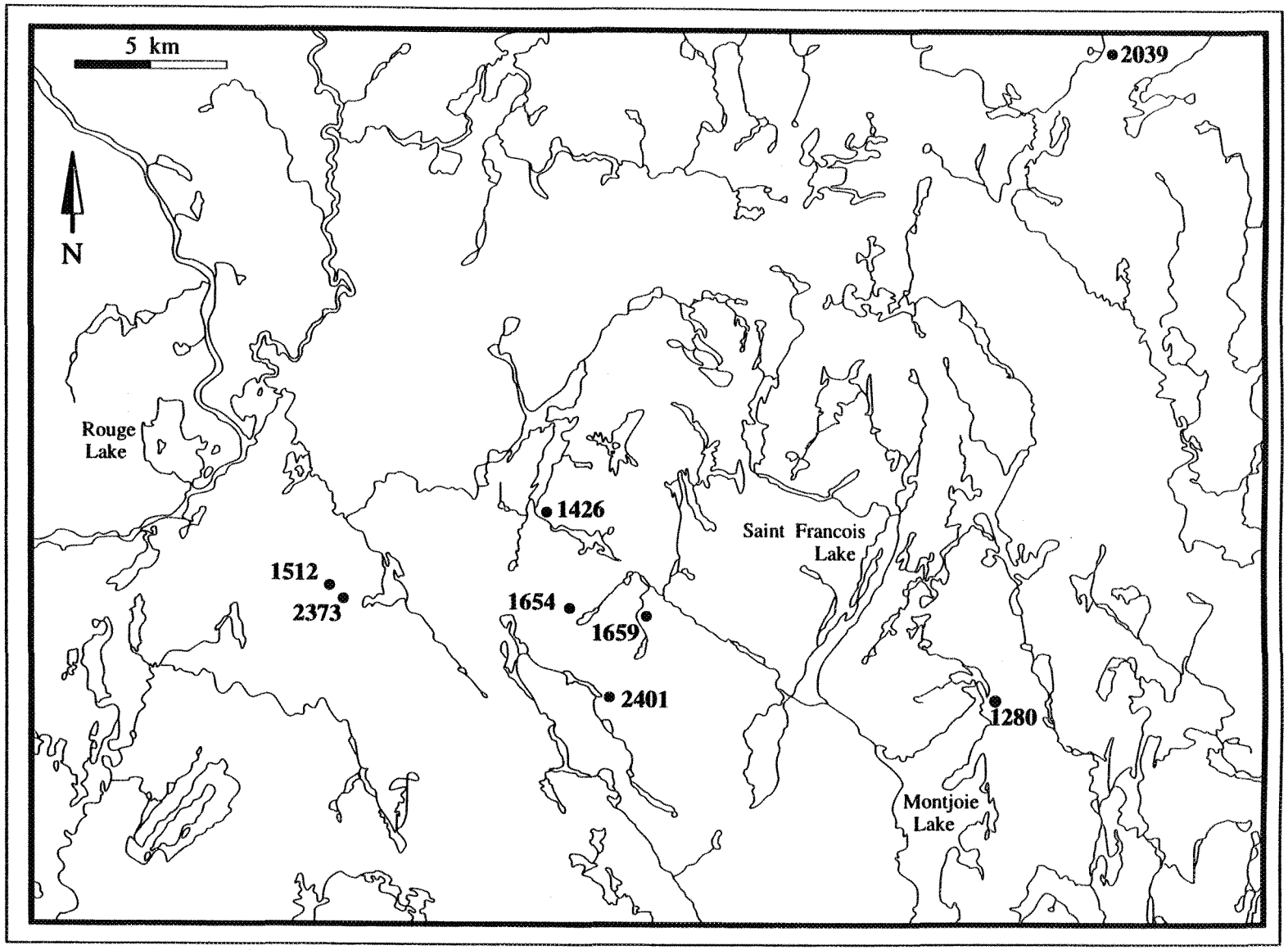

Figure 3-I: Sample locations in Nomininguе, 31J06 map sheet. Sample numbers 2373, 1512, 1426, 1654, 1659 and 2401 are in the Bondy Gneiss Complex. Samples 1280 and 2039 are in the Nomininguе-Cheneville Deformation Zone (Figures 2-I, 2-X).

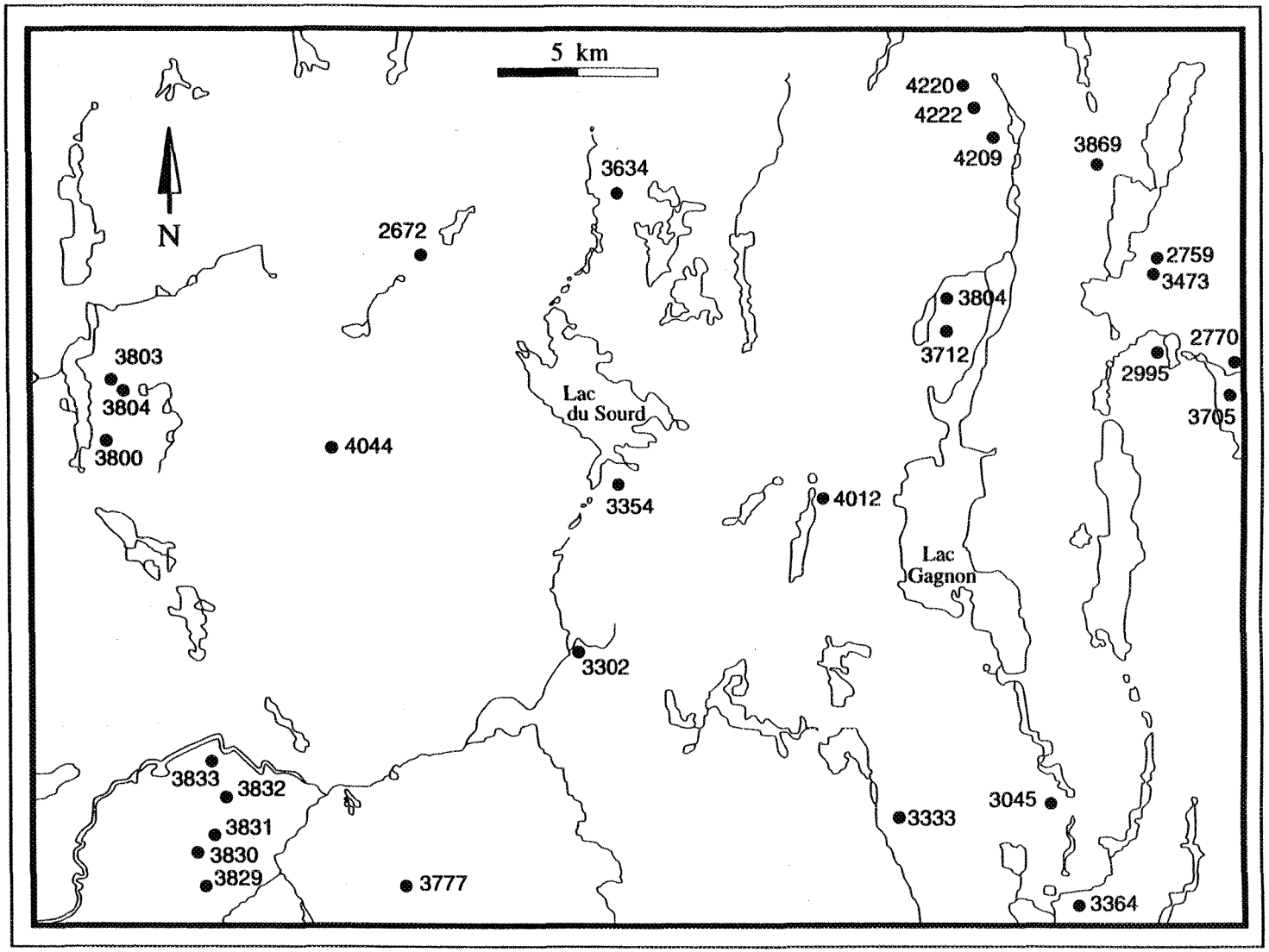

Figure 3-II: Locations of samples from 31J03, Duhamel map sheet. The Bondy Gneiss Complex (samples 3302, 3354, 3634, 4044, 2672, 3803, 3804, and 3800) cuts through the western half of the map sheet, the Nominingue-Cheneville Deformation Zone (samples 4220,4222, 4209, 3804, 3712, 4012, 3333, 3045, 3869, 2759, 3473, 2995, 2770, and 3705) cuts through the eastern half of the map sheet from north to south (Figure 2-I).

Table 3-I: List of Assemblages (abbreviations after Kretz, 1983; see Appendix C)

SAMPLE	Qtz	Pl	Kfs	Bt	Phl	Grt	Crd	Krn	Tur	Sil	Rt	Ilm	Opq	Spl	Ser	Opx	Hbl	MELT	Others
1280-2	X	X	X	X								X							Ap
	X	X		X		X												MG	
1475A1	X	X		X		X						X					X	MG	Ap
1475A3	X	X	X	X		X						X				X	X		Ap
1475B1	X	X		X		X						X					X	MG	
1512	X	X		X		X				X			X						
1654A1	X	X			X			X	X							X			
1654C1	X	X						X	X							X			
1654C2	X	X			X			X	X				X			X			
	X	X	X		X		X									X			Ttn, Zrn
1654D	X	X			X		X	X	X				X			X			
1654D2	X				X			X	X	X			X						
1654-E	X	X	X					?		?									
1654F2	X	X					X		X				X			X			
1654F2	X				X			X	X				X			X			
1654H	X	X			X											X			Ttn
1654I3	X				X		X			X			X						
1654K	X								X	X									
			X												X				
1654L		X			X											X			
1659H1						X	X			X						X		MG	
				X		X	X			X								MG	
2039A	X	X		X		X							X						Ms, Ap
2039B	X	X		X		X							X						
	X			X													X		Ap
2373	X	X		X		X				X			X						
2401U	X	X	X		X	X				X			X			X			
					X	X				X			X	X				MG	
2401D1	X	X			X	X							X			X			

Table 3-I: List of Assemblages - continued

						X				X			X	X				MG
2401D2	X	X	X		X	X				X			X			X			Ap
		X				X				X			X	X				MG	
2401E	X	X	X		X	X													
		X			X	X				X				X				MG	
2401F2	X	X			X	X							X			X			
					X	X							X	X		X		MG	
		X													X				
2401F3	X				X	X							X			X		MG	
2401G1	X	X	X	X									X			X			
	X	X		X		X							X			X		MG	
		X	X												X				
2401G2	X	X	X	X		X							X					MG	
2672	X	X		X		X	?			X			X						
2672		X		X		X				X			X						
2770	X	X		X		X			X	X			X		X				
2995	X			X									X						Ms
3028B	X			X		X				X									Ttn
	X	X		X		X				X			X						Ttn
3045	X	X		X		X											X		
3302	X	X	X	X		X							X						
		X	X										X					MG	
3302A	X	X		X		X				X			X						
	X		X	X		X												MG	
		X													X			MG	
3333A	X	X	X	X		X			X	X			X						
3354	X	X		X		X							X						
3364-2	X		X	X						X			X						
3600	X	X		X		X							X					MG	
3604	X	X		X		X				X			X					MG	
3634	X	X		X		X				X			X					MG	

Table 3-I: List of Assemblages - continued

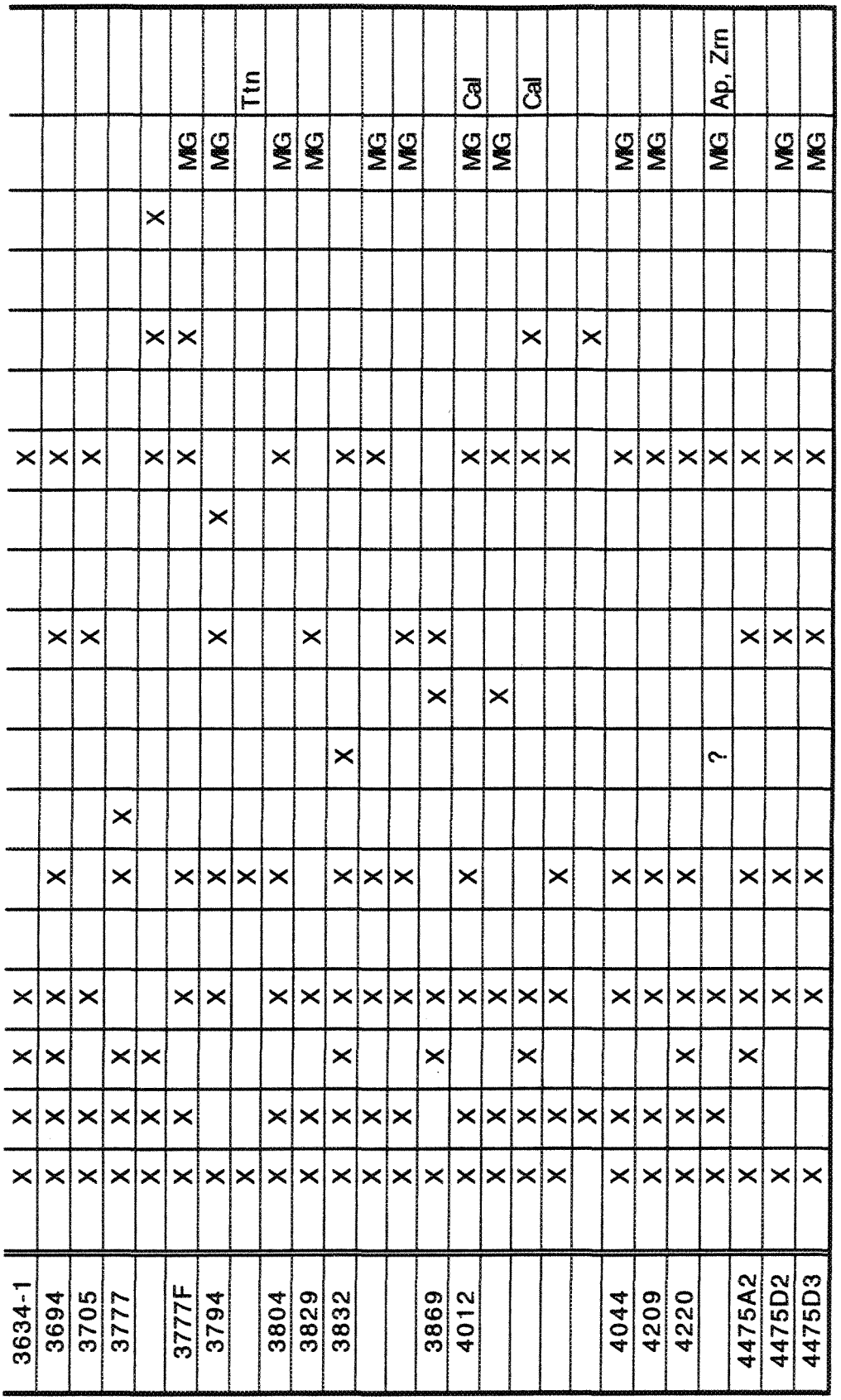

3.2 Melt-derived Assemblages

3.2a Importance of Fluid-Absent Reactions

Migmatites are formed from multiple processes involving one of, or a combination of, metasomatism, melt injection, metamorphic differentiation and partial melting (Olsen 1983). Evidence for melt-producing reactions places assemblages at pressures and temperatures above the solidus. For most rocks of approximately metapelitic composition the progression through the fluid-absent melting reactions occurs within a fairly narrow temperature interval (Figures 3-III, 3-IV). Due to the slow diffusion rates of H_2O in H_2O-undersaturated melts and the endothermic nature of these reactions, the initial stages of melting is preserved in many migmatites (LeBreton and Thompson 1988). Even the early melting reactions can be directly inferred in some migmatites where the melt fraction has not migrated far (Ashworth 1985).

Melting in the middle and deep crust involves the breakdown of mica, notably biotite, and the series of fluid-absent melting reactions have been studied experimentally in great detail (e.g. Bohlen et al. 1983; LeBreton and Thompson 1988; Vielzeuf and Holloway 1988; Jones and Brown 1990; Puziewicz and Johannes 1990; Ebadi and Johannes 1991; Patiño Douce and Johnston 1991; Clemens 1995; Vielzeuf and Montel 1994). Thus, the determination of which reactions occurred in this field area can place quite precise limits on the pressures and temperatures of melting and so provide an excellent means of verification for the results obtained from conventional geothermobarometers.

3.2b. Evidence for Melt-Producing Reactions

Annex B contains the petrographic evidence for the characteristics of the melt-producing reactions. The characteristic features and textures of the migmatitization range from layers of leucosomes with granitic composition flanked by garnet-rich layers, and biotite-rich melanosomes (samples 1475, 2401G2, 3634-1,3832) through thin (<1 mm)

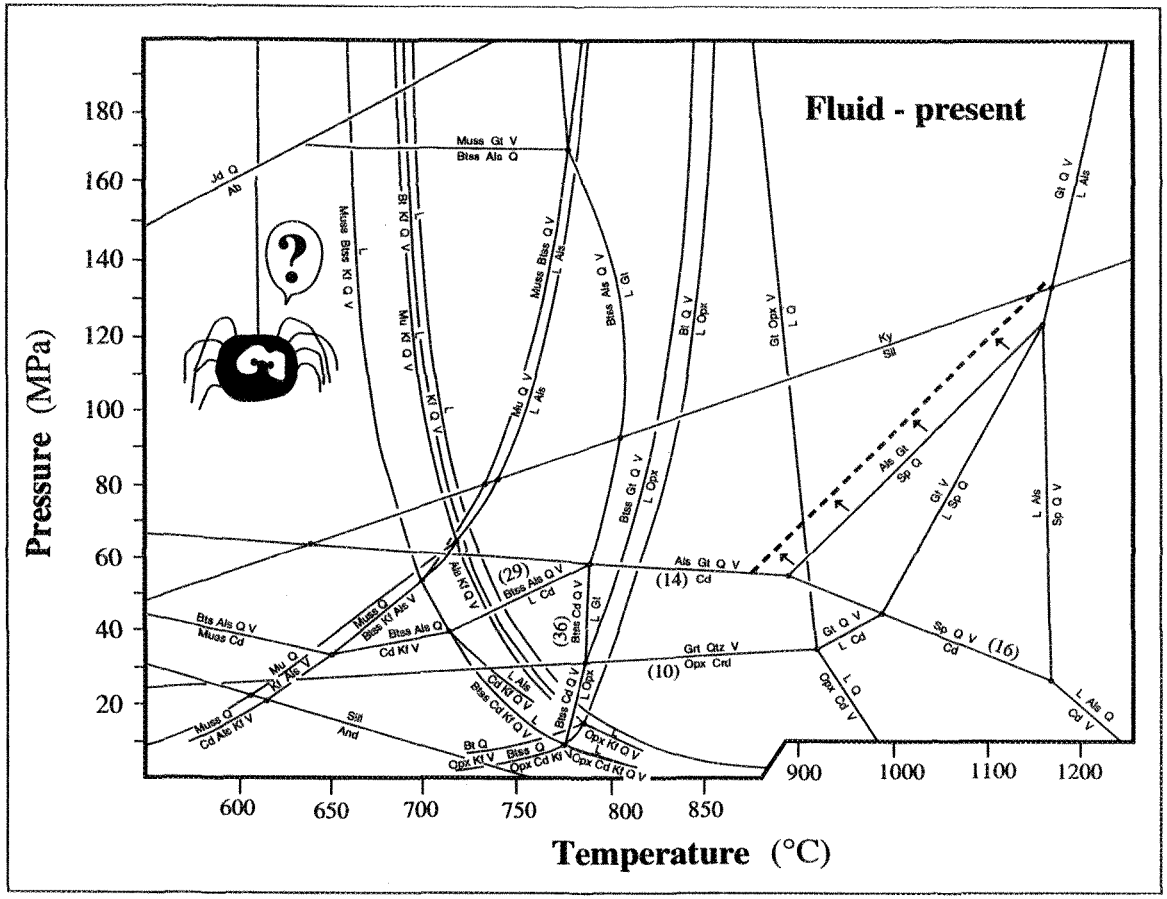

Figure 3-III: Petrogenetic grid for fluid-present (H_2O) and quartz saturated partial melting of metagraywackes and metapelites (X_{Mg} near 0.5). The mineral abbreviations are after Kretz (1983). The 'ss' after muscovite or biotite signifies solid state. Note that the temperature scale changes after 900°C (Vielzeuf and Holloway, 1988). The dashed line is the recalculated value for this study of the reaction Als + Grt = Spl + Qtz, the zinc content in these spinels caused this reaction curve to move 70°C lower (see Chapter 5 for calculations; after Vielzeuf and Holloway 1988).

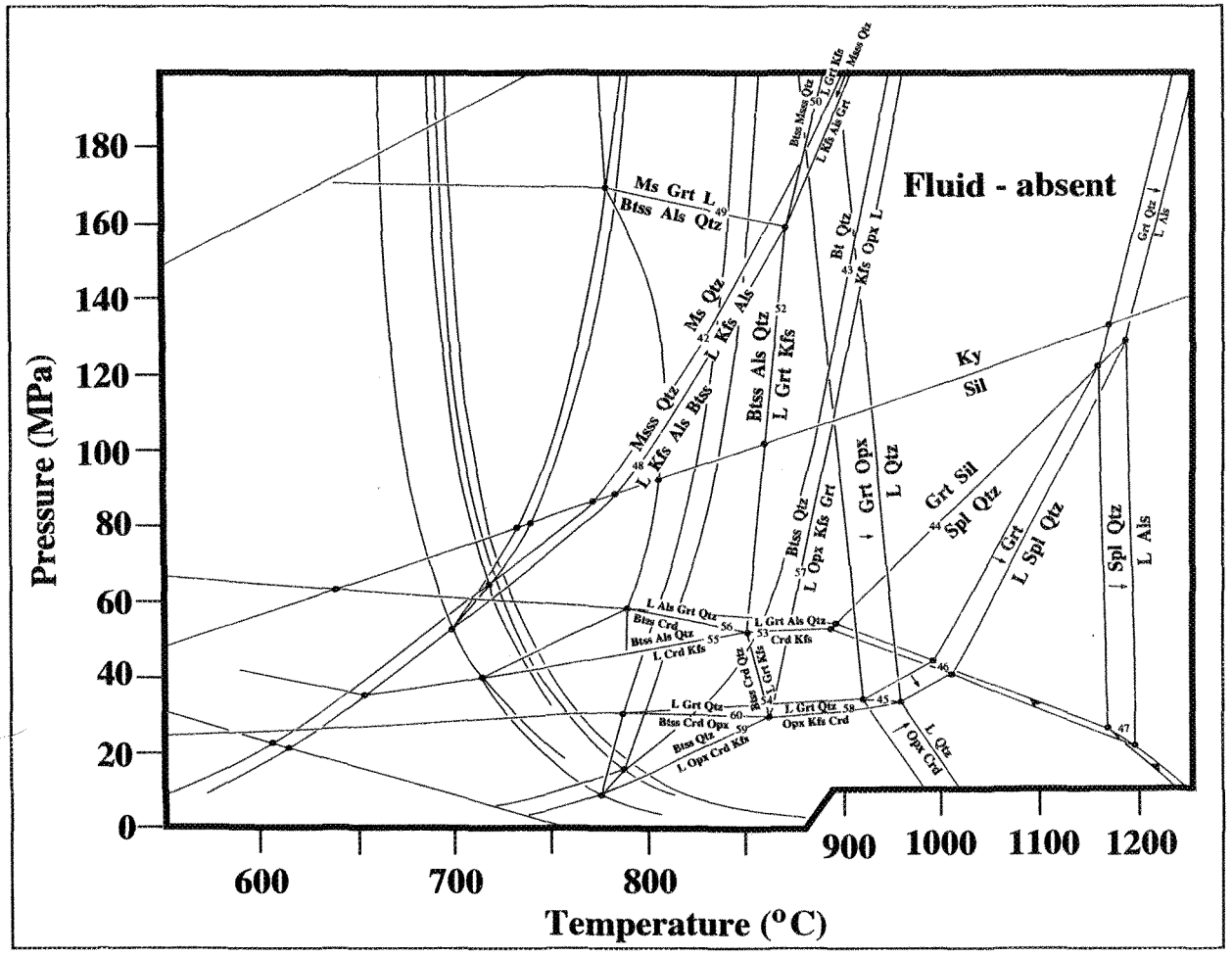

FIGURE 3-IV: Fluid-absent and quartz-saturated P-T diagram for metagraywackes and metapelites (X_{Mg} close to 0.5). The arrows indicate the displacement of the reactions involving only melt as a potential hydrous phase due to the reduction of the activity of water. The following reactions correspond to the above numbers (45) Opx + Crd = Grt + L; (46) Crd + Grt = Spl + L; (47) Crd = L + Als + Spl (after Vielzeuf & Holloway 1988). The mineral abbreviation are after Kretz (1987).

Plate I: Outcrop 4475 (BGC). Migmatized gneiss. A discrete dextral shear zone crosscuts top third of photo. Note the compositional zoning, with the dark biotite-rich melanosome bands and the light coloured granitic leucosome bands. There is a leucosome patch in the centre of this plate, located in the fold hinge.

Plate II: Outcrop 1659 (BGC). This demonstrates the flecky-gneiss texture typical of many migmatized outcrops within the study area. Here, the ortho-pyroxene porphyroblasts (black) with garnet (red) inclusions are rimmed with cordierite-rich granitic (white) leucosomes.

Plate I

Plate II

Plate III: Outcrop 1659 (BGC). Close-up of orthopyroxene porphyroblasts (black) with garnet (red), and quartz (white) inclusions surrounded by cordierite-containing granitic leucosome (white), in a biotite (black)-rich melanosome.

Plate IV: Outcrop 4475 (BGC). S-folds in migmatized gneiss. Here, there is compositional fractionation similar to Plate I, however, here the bands are thicker (1-3 cm).

Plate III

Plate IV

wispy-discontinuous (<1 cm) leucosomes (Plate I; agmatitic migmatites; samples 1280-2, 3364-2, 3869) and felsic moats surrounding garnets (Plate II, III; 'flecky' gneiss; samples 2401F2, 3694, 4012) to continuous leucosomes greater than 1 cm thick (Plates I, IV, V; stromatitic migmatites; samples 3028A, 3302A, 3777). Thus, these samples provide examples of the stages of development of a migmatite from the formation of metamorphic layering, through to the production of *in-situ* melt (discontinuous leucosomes and leucosome moats) to the channelling of the melt out of the system (i.e., continuous leucosomes; Johannes and Gupta 1982).

Many thin sections contain embayed K-feldspar grains with inclusions of biotite that formed from a melt-producing reaction (Plates VI, VII; samples 1280-2, 2401D2, 3333A, 3364-2, 3694, 4012, 4220). Other thin sections contain embayed plagioclase grains with inclusions of biotite that also formed from similar melt-producing reactions (samples 3634-1, 3694, 3777, 3832, 4012).

Appendix B also contains the evidence observed in several thin sections of at least two stages of sillimanite growth, one of which likely formed from a reaction involving melt. Thin sections 2373, 3028, 3302, 3604, 3634, 4475A, 4475B, 4475D2, 4475D3 (Plate VIII) all have well-formed equant sillimanite crystals surrounded by fibrolite. Thin sections 2401E and 3333A (Plate VI) have acicular sillimanite inclusions in garnets that are oriented in a different manner from the equant sillimanite crystals in the matrix, which implies that the matrix sillimanite formed after the growth of the garnet. It is unlikely that this difference in sillimanite orientation in sample 3333A is due to the rotation of the garnets because the sillimanite inclusions in garnets are oriented in a splayed pattern, not defining a foliation as do the matrix sillimanite (Plate VI). Thin sections 1654K, 1659H1, 1659H2, 3794, 3832 contain fibrolite, which formed either at grain boundaries, or in the cracks and embayments at the rims of garnet, orthopyroxene, cordierite and K-feldspar. This fibrolite may have also

Plate V: Outcrop 1659 (BGC). This plate, from the same outcrop as plate II, is a good example of the stromatolitic textures typical of this field area. Granitic-leucosomes (white-yellow) are rimmed with biotite-garnet rinds (black-red) which alternate with biotite-rich melanosomes (black).

Plate VI: Thin section 3333A (NCDZ). Garnet porphyroblast with wing-shaped tails (medium-relief grey) with embayments filled with sillimanite (low relief grey) - biotite (brown) - quartz (white). This texture is suggestive of a reaction producing sillimanite plus biotite from garnet (reverse reaction 3-6). Note the K-feldspar porphyrobast (white) with inclusions of biotite and quartz (pale grey specks). This porphyroblast demonstrates evidence for having grown during a melt-producing reaction (similar to the porphyroblast in Plate VII).

Plate V

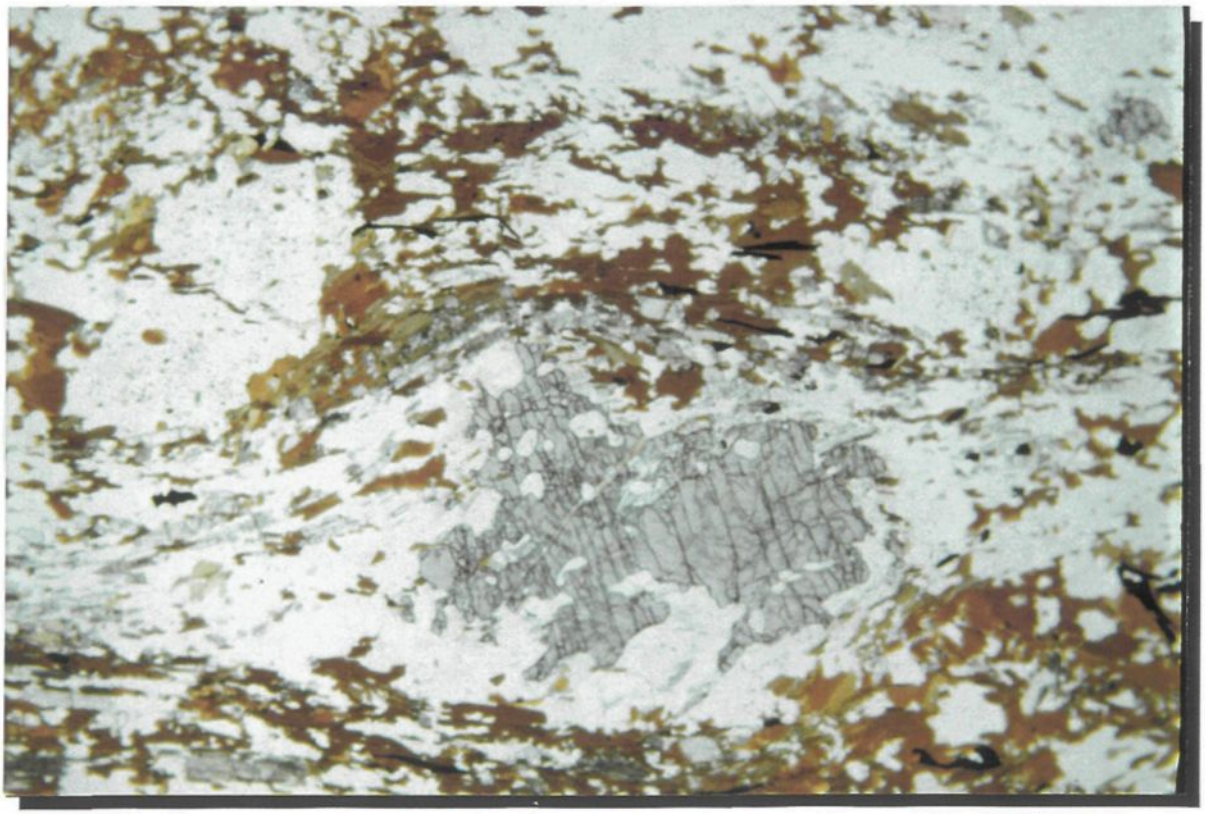

Plate VI:

2.0 mm

Plate VII: Thin section 3333A (NCDZ). K-feldspar porphyroblast. Note the embayed borders filled with quartz (grey) and biotite (brown) and inclusions of biotite (brown) and quartz (white-grey) which are evidence for K-feldspar growth due to a melt-producing reaction.

Plate VIII: Thin section 4475D3 (BGC). Garnet porphyroblast (grey) with ilmenite (black) inclusions in a mat of biotite (brown) - sillimanite (grey needles) - ilmenite. Because this is the largest garnet analyzed from the Bondy Gneiss Complex, it was expected to produce the highest temperatures from the biotite-garnet Fe-Mg exchange thermometer. However, it only produced intermediate temperatures. The presence of the ilmenite inclusions, and the associated cracks, distributed throughout this porphyroblast, are suggested to have decreased the size of the diffusion domains, allowing the effects of the retrograde diffusion to have reached the core of this garnet.

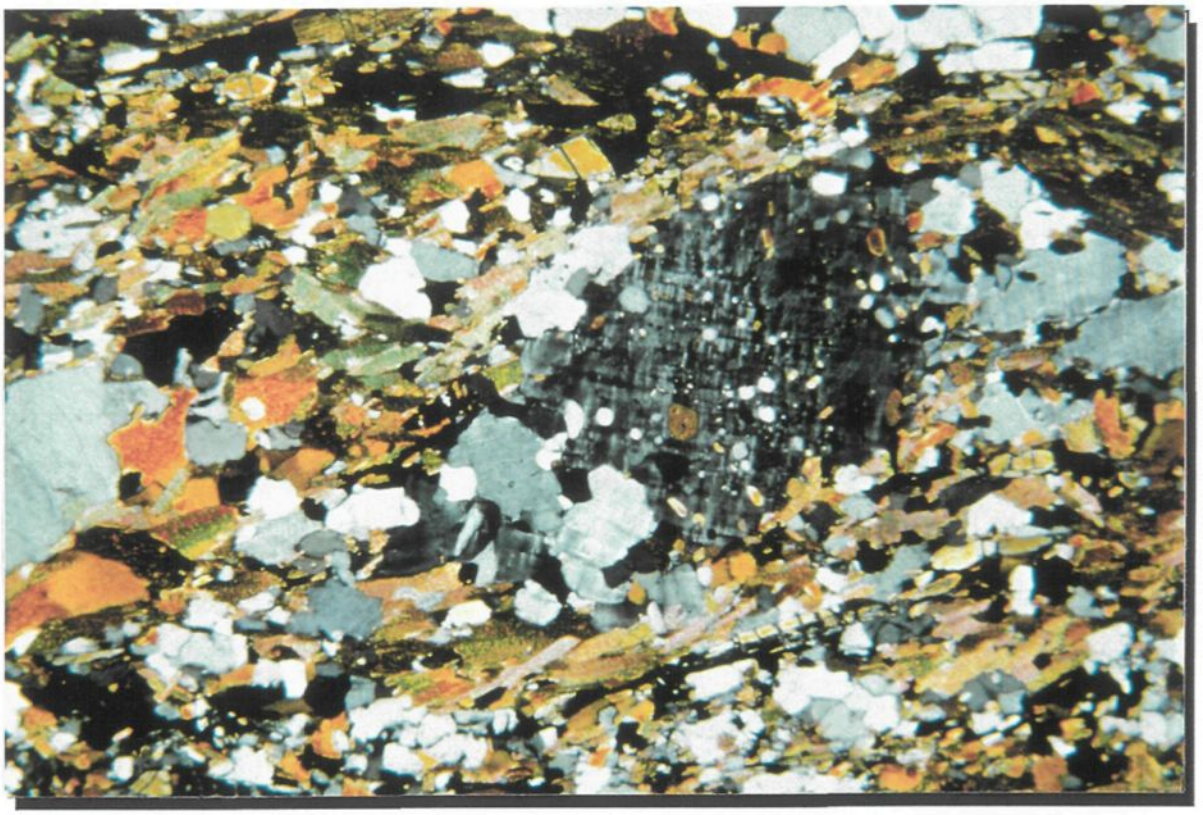

Plate VII

2.0 mm

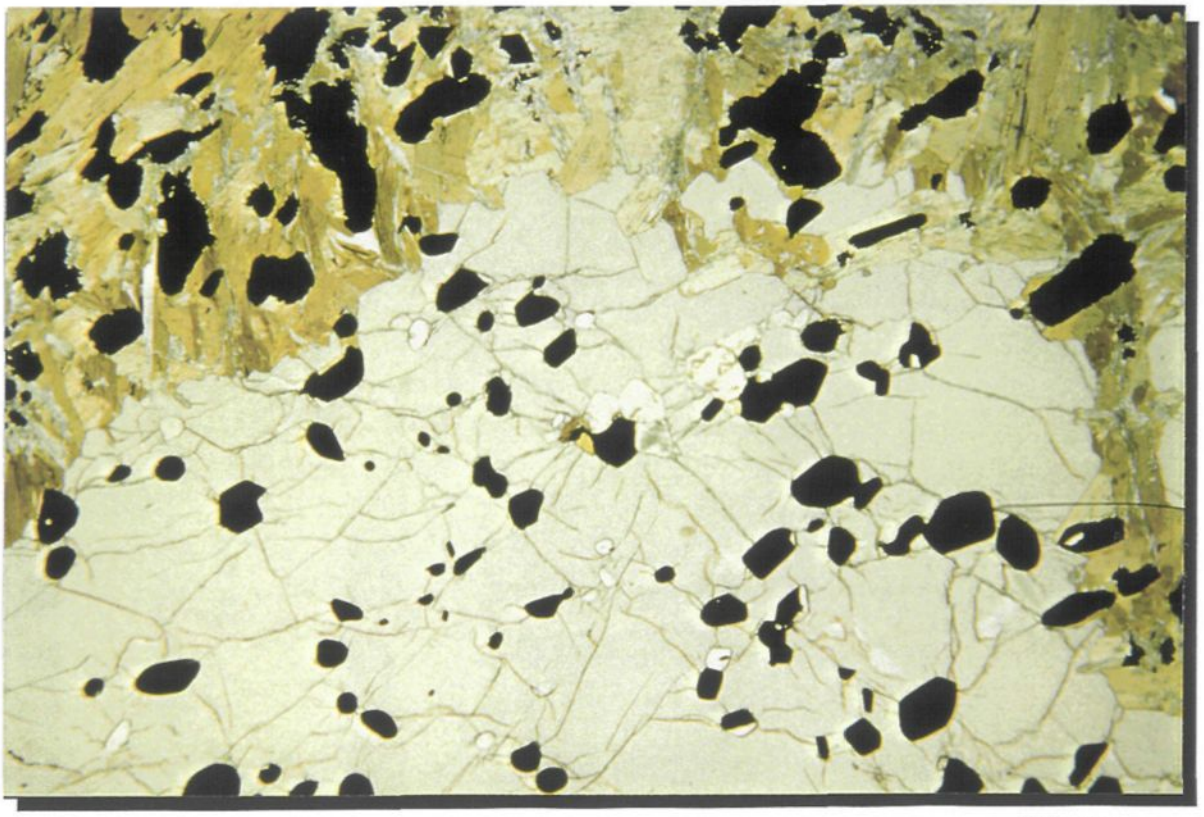

Plate VIII

2.0 mm

formed from a melt-producing reaction, hence it would be prograde fibrolite. Sillimanite in thin section 3869 crosscuts the foliation defined by biotite. In thin section 2770, sillimanite forms clots over porphyroblasts (possibly of K-feldspar?). Randomly oriented ilmenite from both thin sections 3869 and 2770 formed after the foliation, possibly from melt-producing reactions.

3.2c. Melting Reactions

According to Jones and Brown (1990), initial melting would have likely occurred at the H_2O-saturated solidus appropriate to the bulk rock composition. Thus, many metapelites that eventually became granulitic would have commenced their melting history by:

(3-1) $Ms + Bt + Qtz + V\ (+Pl) = Als + MELT$ or by

(3-2) $Or + Ab + Qtz + V\ (+An) = MELT$

which would have produced H_2O-saturated melts. These melts would have been small in volume with biotite selvages and formed stromatitic metatexites (Jones and Brown 1990).

3.2ci Peraluminous Granitoid Magmas

The anatexis of aluminous metasedimentary rocks characteristically produces peraluminous granitoid magmas (Patiño Douce and Johnston 1991). Patiño Douce and Johnston (1991) suggested the following progression through three vapour-absent reactions consistent with their experimental results at 100 MPa:

(3-3) $Ms + Bt_1 + Pl + Qtz = Bt_2 + Als + MELT$

(3-4) $Bt + Als + Qtz \pm Ilm = Grt \pm Rt + MELT$

(3-5) $Grt + Als = Spl + Qtz + MELT$

The muscovite dehydration-melting reaction (3-3) was demonstrated experimentally by Patiño Douce and Johnston (1991) to be completed between 800 and 820°C at 100 MPa. Note here that BT_2 is less hydrous than BT_1. At 100 MPa, biotite reacts out via the biotite dehydration-melting reaction (3-4) over a temperature interval of 150°C (i.e., between 825-

975°C). Generally, melting before the biotite-out reaction (3-4) will not contribute significantly to the volume of melt. Reaction (3-5) appears to increase the mafic components in the melt (Patiño Douce and Johnston 1991).

The only muscovite present in thin sections from the study area (2039A, 2995, 3705, Appendices A and B) is retrograde and, comes from the Lac Nominingue-Chénéville Deformation Zone. This suggests that retrogression possibly included the reverse of reaction (3-3), below 800°C which would have consumed biotite and aluminosilicate. Evidence for reaction (3-4) is discussed in greater detail in the following sections.

Thin sections from outcrop 2401 contain garnets with inclusions of spinel and quartz (thin sections 2401D2, 2401F2, 2401G3, 2401U). Thin section 2401D2 contains a garnet with an inclusion-free core, however, the rim (Plate IX) contains inclusions of spinel, quartz, K-feldspar and biotite. This is suggestive of crossing reaction (3-4) first to produce the garnet, followed by crossing of reaction (3-5) to produce the spinel + quartz. Crossing reaction (3-5) suggests temperatures above 1000°C at 100 MPa (Patiño Douce and Johnston 1991), or above 870°C at 55 MPa (Figure 3-III).

The spinels in this study contain zinc (see Chapter 4). The addition of zinc into the system reduces the temperature at which reaction (3-5) would occur (Nichols et al. 1992), which causes the univariant line to move to lower temperatures in P-T space. The magnitude of the effect of the presence of zinc in the spinels is calculated in Chapter 5.

Thin sections 2401D2 and 2401E do not contain spinel in contact with quartz (Plate IX). Instead spinel is included in sillimanite or garnet, which suggests that during retrogression the reaction (3-5) was reversed. The spinel is likely preserved in this thin section because it became armoured by sillimanite.

Plate IX: Thin section 2401D2 (BGC). Spinel (green-black) surrounded by garnet (medium relief, grey) or sillimanite (lower relief, grey) in biotite (brown) and quartz (white). Note that the spinel is protected from the quartz by garnet, sillimanite or biotite. These armoured the spinel and prevented it from reacting out completely to garnet + aluminosilicate (reaction (3-5)).

Plate X: Thin section 2401F2 (BGC) Garnet (grey) - orthopyroxene (green) - quartz (white) - plagioclase (white) assemblage. Note the closely intergrown garnet - orthopyroxene, with inclusions of garnet in orthopyroxene (and vice versa). Note also the plagioclase moat forming around garnet, and plagioclase eating away at embayments of orthopyroxene.

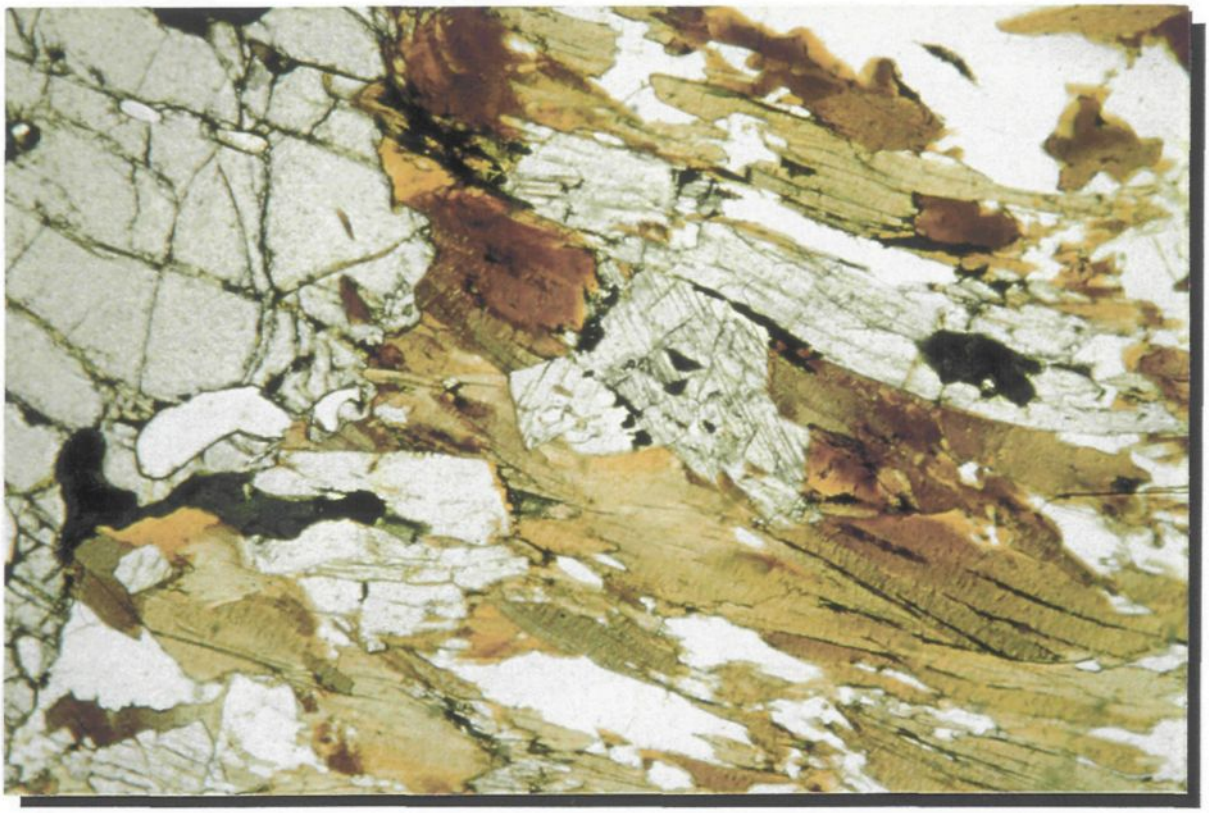

Plate IX

1.0 mm

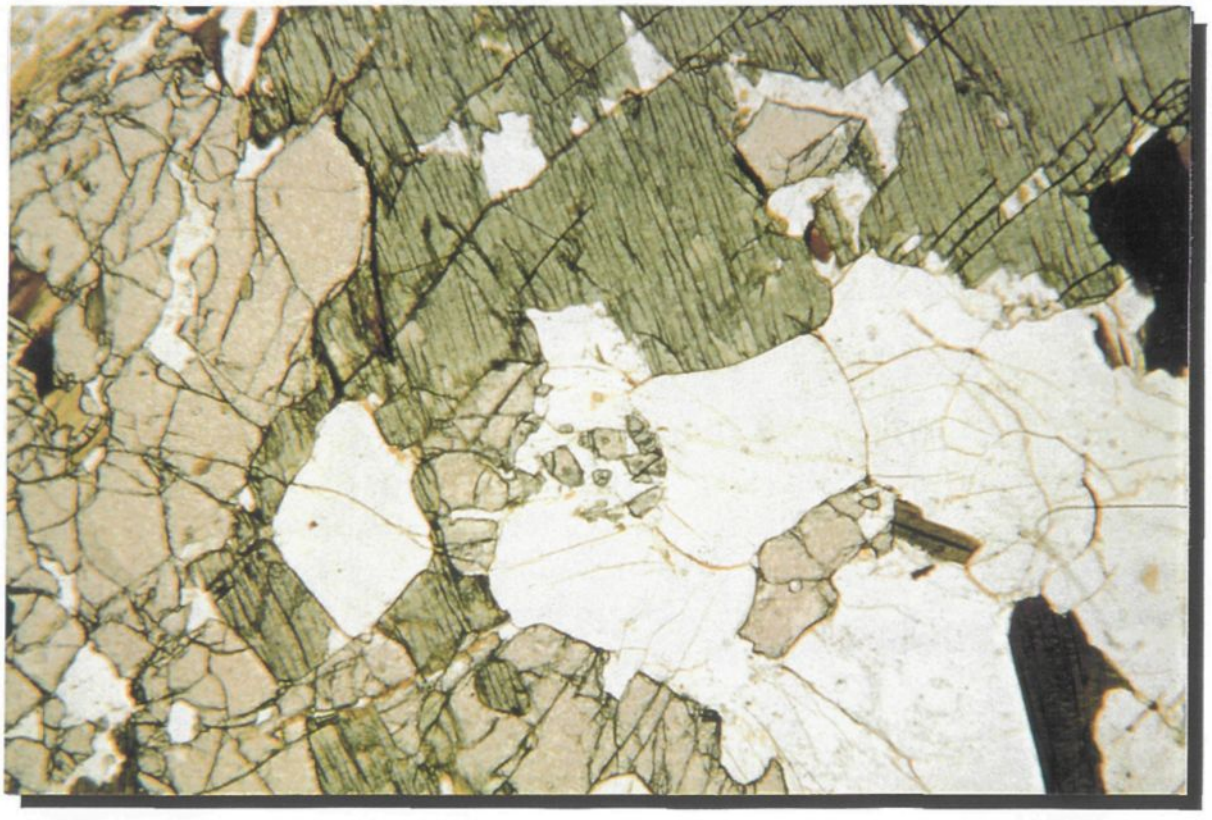

Plate X

1.0 mm

3.2cii. KFMASH System

The petrogenetic grid for the KFMASH system (Figure 3-III) contains divariant reactions that are represented by single lines for clarity (Vielzeuf and Holloway 1988). For simplicity, Fe_2O_3 and TiO_2 were excluded to omit the consideration of the Fe-Ti oxides. Furthermore neither Na_2O and CaO were considered, so as to eliminate the consideration of plagioclase. Vielzeuf and Holloway (1988) predicted that the addition of sodium would shift the melting curves to lower temperatures by approximately 100°C; however the addition of calcium would reduce this effect (Thompson and Tracy 1979).

With increasing temperature, the biotite breakdown reactions would be crossed in the following order (Figure 3-III) possibly starting with vapour present, but continuing with vapour absent dehydration melting reactions once the aqueous vapour phase was consumed:

(3-6) Bt + Als + Qtz + V = Grt + MELT

(3-7) Bt + Grt + Qtz + V = Opx + MELT

(3-8) Bt + Qtz + V = Opx + MELT

(3-9) Bt + Als + Qtz (+Pl) = Grt ± Kfs + MELT

(3-10) Bt + Qtz = Opx + Kfs + Grt + MELT

Metatexites with garnet-bearing segregations or diatexites in layers of appropriate bulk compositions would be produced by reaction (3-9) depending on the amount of melt produced. This reaction is easily distinguished by the appearance of K-feldspar (Plates VI, VII) in the residual assemblage of the melanosomes. Vielzeuf and Holloway (1988) suggested that this is the major-melt producing reaction in rocks of pelite-like composition. The experimental results of Le Breton and Thompson (1988) suggest that in natural systems this reaction occurs between 760 and 800°C at 100 MPa for biotite of intermediate X_{Mg}.

Many thin sections contain garnets with inclusions of biotite + quartz ± sillimanite and K-feldspar (1280-2, 1475A3, 2401D2, 3302A, 3333A (Plate VI), 3694, 4012, 4475A,

4475B; Appendices A and B). This is suggestive of either reaction (3-6) or (3-9) which would produce garnet in the presence of a melt. If there was any vapour present in the system, garnet would have likely been produced initially by reaction (3-6). However as reaction (3-6) progressed, the vapour in the system would have been consumed unless continually added from an external source, and the system would have progressed on to the vapour-absent reaction (3-9; Figure 3-IV) which contains K-feldspar as a solid product phase. Thin sections 1659H1 and 1659H2 (Plates II, V) contain orthopyroxene porphyroblasts that have inclusions of garnet + quartz + biotite, consistent with crossing the vapour-present reaction (3-7); in this case, garnet would have been consumed.

Figure 3-V contains numerical values (from Jones and Brown 1990 from the data of Le Breton and Thompson 1988) for the pressures and temperatures for reaction (3-9). For this reaction to have occurred, temperatures need to be above 770°C. Since sillimanite and not kyanite was observed in these thin sections, pressures at 800°C would need to be below 90 MPa; unless all kyanite has subsequently inverted to sillimanite.

Thin section 2401F2 contains garnet and orthopyroxene crystals (Plate X) which are closely associated with inclusions of idioblastic garnet in orthopyroxene and inclusions of orthopyroxene in garnet, suggesting that the orthopyroxene and garnet grew together. The matrix of the thin sections from this outcrop, contains K-feldspar grains with irregular-embayed boundaries and inclusions of biotite, suggesting that K-feldspar may have grown at the expense of biotite in a melt-forming reaction since this outcrop is migmatitic. These textural characteristics suggest that this sample crossed reaction (3-10), which is discussed further below.

3.2ciii. KFMNCASH System

Vielzeuf and Montel (1994) experimentally investigated four vapour-absent reactions involving biotite + plagioclase + quartz to simulate the partial melting of metagreywackes:

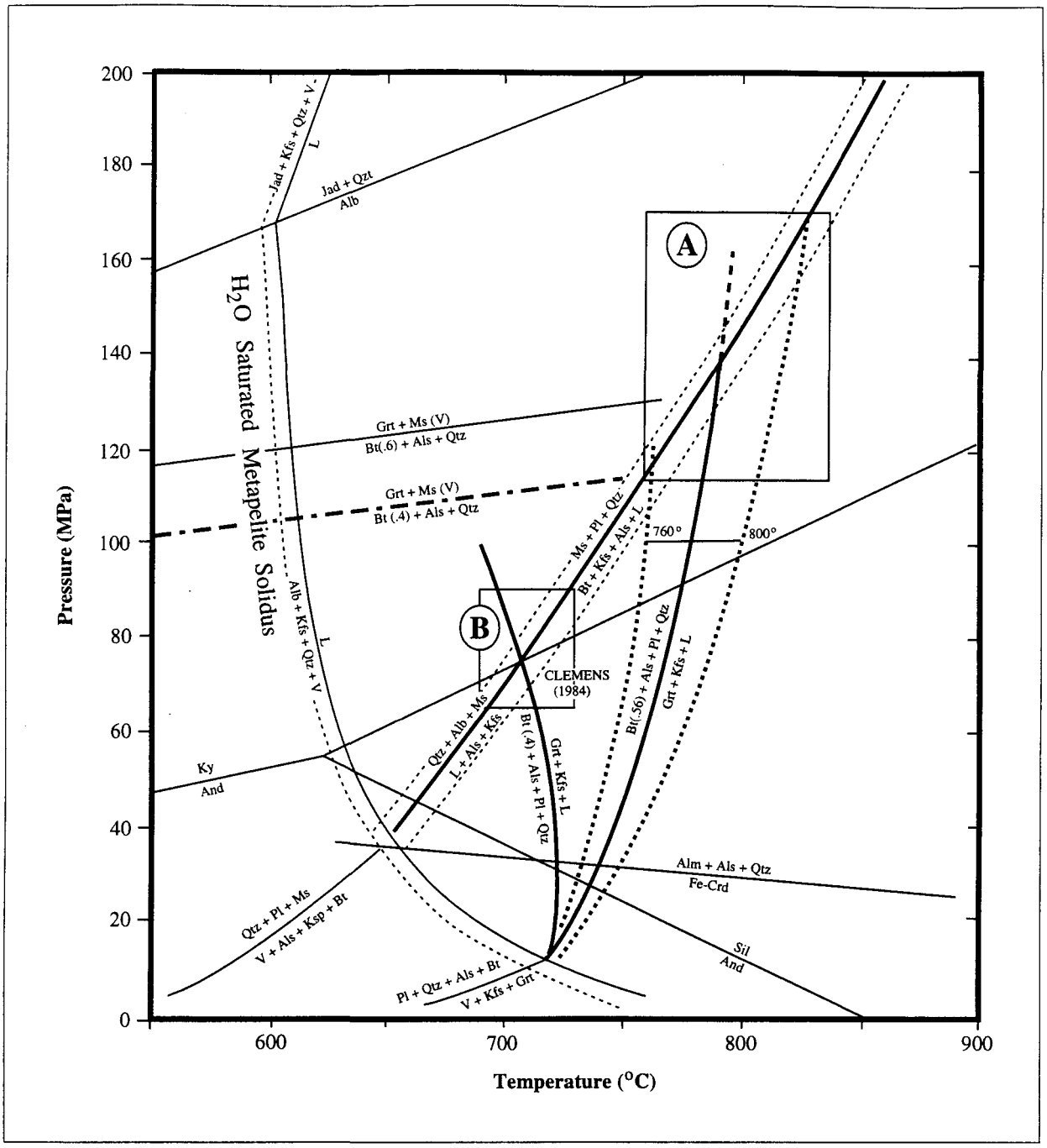

Figure 3-V: P-T diagram depicting the results of dehydration melting of biotite and muscovite in metapelites, the H_2O-saturated metapelite solidus and the biotite sides (X_{Mg}= 0.4, 0.6) of the continuous reaction Grt + Ms (V) = Bt + Als + Qtz (Thompson 1982). In box A, the results of biotite melting at100 MPa between 760 and 800°C intersect with the muscovite melting curve (Le Breton and Thompson 1988). In box B, muscovite melting intersects with the calculated backbending of biotite melting (Clemens 1984; after Le Breton and Thompson 1988).

(3-11) Bt + Pl + Qtz = Opx + Crd (+Kfs) + MELT

(3-12) Bt + Pl + Qtz = Opx + Grt (+Kfs) + MELT

(3-13) Bt + Pl + Qtz = Opx + Spl (+Kfs) + MELT

(3-14) Bt + Pl + Qtz = Grt (+Kfs) + MELT

According to their experiments, reaction (3-11) occurs below 500 MPa, reaction (3-12) above 500 MPa, reaction (3-13) at temperatures above 850°C between 300 - 500 MPa and reaction (3-14) at the low temperature side (between 780 and 850°C) of reactions (3-11), (3-12) and (3-13). Note that apart from a K-feldspar component in the melt phase, these reactions may also produce K-feldspar as a solid residual phase.

Thin section 2401F2 (Plate X) contains garnet and orthopyroxene crystals which are closely associated with inclusions of garnet in orthopyroxene and inclusions of orthopyroxene in garnet, suggesting that the orthopyroxene and garnet grew together. The garnet contains inclusions of biotite. These observations are suggestive of reaction (3-12), suggesting pressures above 500 MPa. From Figures 3-VI and 3-VII, the presence of this reaction suggests temperatures between 860 and 980°C, aH_2O <0.1 and Wt% H_2O <2.0 (Vielzeuf and Montel 1994).

Biotite is present throughout the field area (Plates, I through XXII), which suggests that the conditions for the reaction depicted in Figures 3-VI and 3-VII were not exceeded. This limits the maximum metamorphic temperature to between 860 and 980°C. If the temperature surpassed 980°C, biotite would have been completely consumed by the resultant reactions (Vielzeuf and Montel 1994).

The garnet and orthopyroxene crystals from thin section 2401F2 (Plate X) are now surrounded by a plagioclase moat. The orthopyroxene has biotite crystals forming along its cleavage traces, and the garnet has biotite forming around its rim, along cracks and embayments within it. These characteristics suggest that during the crystallization of the

Plate XI: Outcrop 3832 (SW corner of map area). Garnet-rich granitic leucosomes surrounded by biotite-rich (black) melansomes. Thin sections from this outcrop contain kornerupine which was not observed on the outcrop scale.

Plate XII: Outcrop 4475 (BGC). Garnet-rich granitic leucosome (bottom 2/3 of photo) surrounded by fine-grained biotite-rich melanosome (under pencil). Note small quartz-rich vein that crosscuts leucosome and melanosome.

Plate XI

Plate XII

Plate XIII: Outcrop 4475 (BGC). Large garnet (red) surrounded by biotite rind (black) below lens cap. Garnets in mat of biotite under lens cap. Both complexes are surroundeed by a granitic leucosome (white).

Plate XIV: Outcrop 4485 (BGC). Stretched and folded garnets (red) in biotite - quartz - feldspar groundmass.

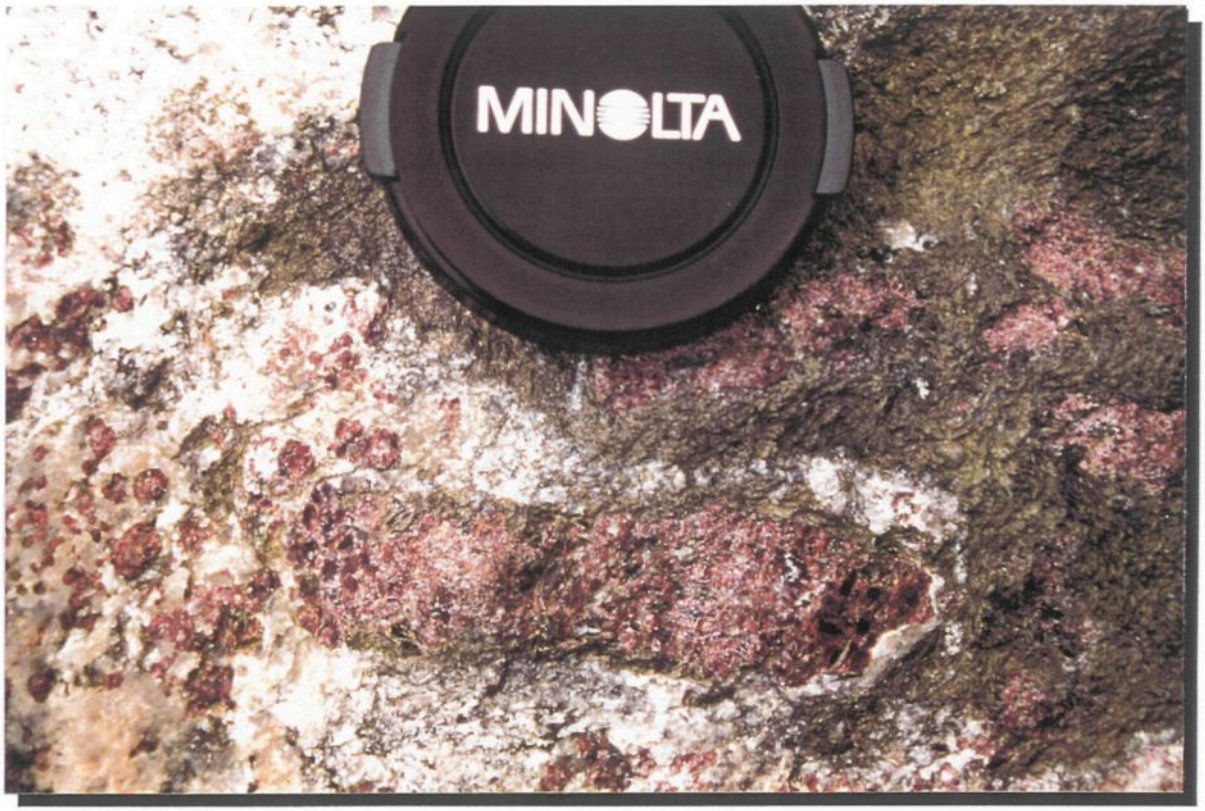

Plate XIII

Plate XIV

Plate XV: Outcrop 4044 (BGC). Symplectite located at the border of garnet (grey) with biotite (brown) and quartz (white). Note the late cracks, filled with biotite and quartz, in the garnet.

Plate XVI: Thin section 4209 (NCDZ). Garnet porphyroblast (grey) with inclusions of quartz (white) - biotite (brown) - ilmenite (black) in biotite - quartz melanosome.

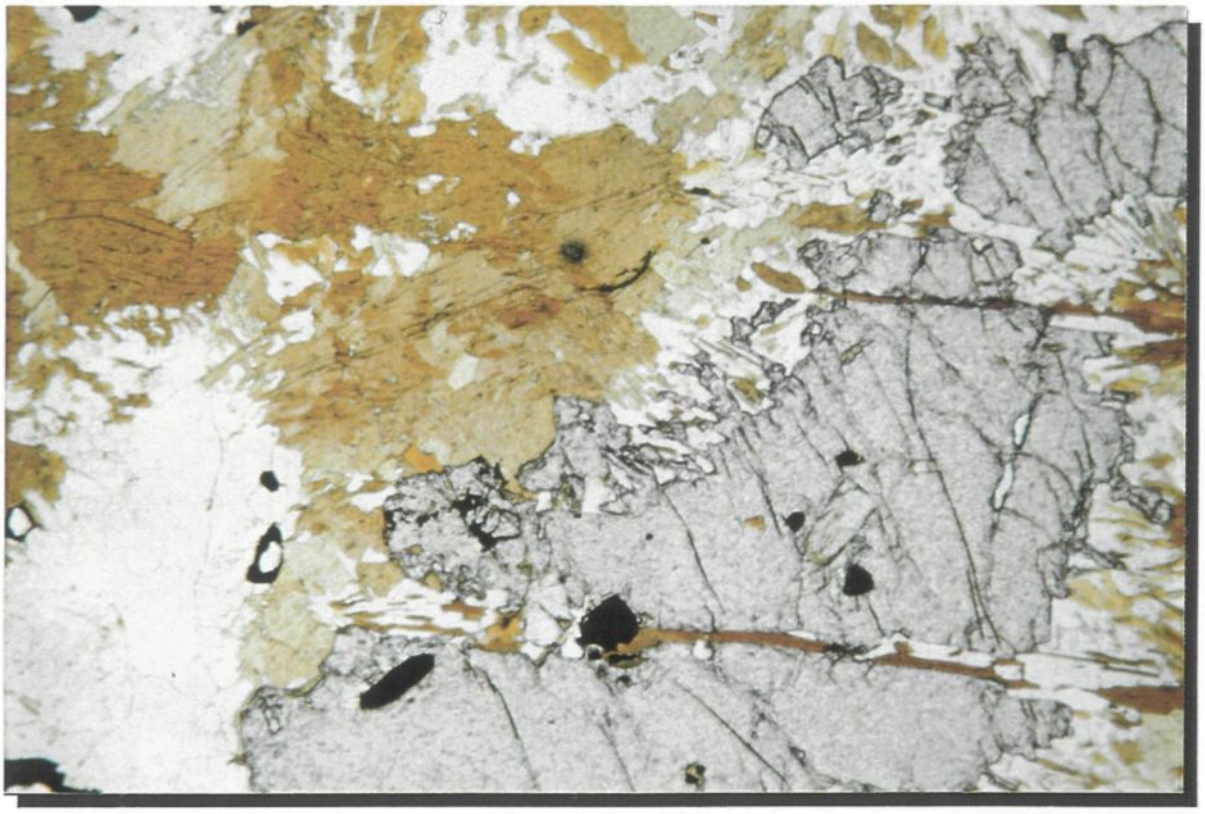

Plate XV

0.5 mm

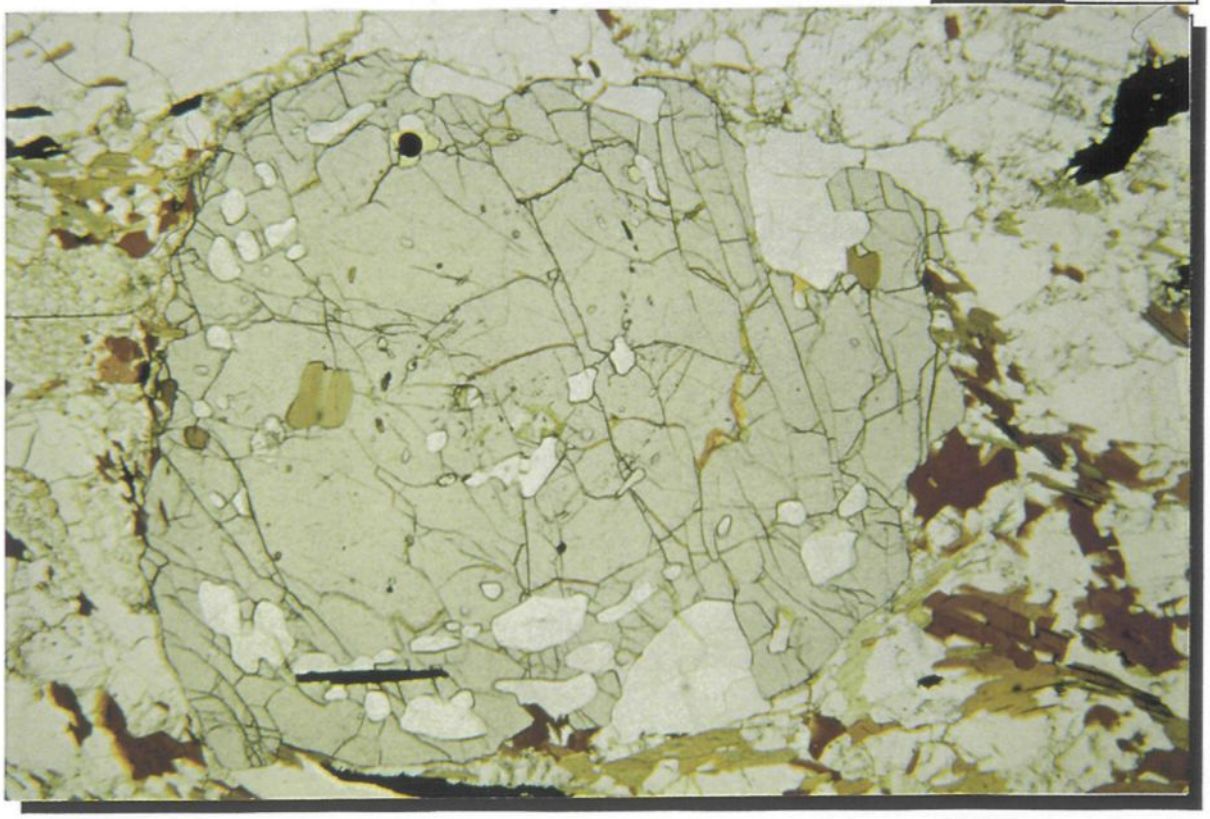

Plate XVI

2.0 mm

Plate XVII: Garnet (medium-grey, high relief) with quartz (white) and biotite (brown) in pressure shadows, from outcrop 3333 (NCDZ). Note the irregular-shaped quartz (white), biotite (brown), and needle-like sillimanite (white) inclusions in the garnet. The sillimanite inclusions in the garnet are oriented at an angle to the sillimanite (light to medium grey) in the groundmass, possibly because the garnet rotated, with respect to the groundmass, as it grew. Sillimanite in the groundmass occurs in two morphologies and/or generations. The first generation occurs as well-formed columnar crystals, the second generation is fibrolitic, which, in places, formed on the first generation columnar crystals.

Plate XVIII: Thin section 1659 (BGC). Sector twinned (white - grey - black) cordierite with garnet (black, left half of photo), quartz (untwinned white - grey - black) and biotite (yellow - blue - pink). Crossed polars.

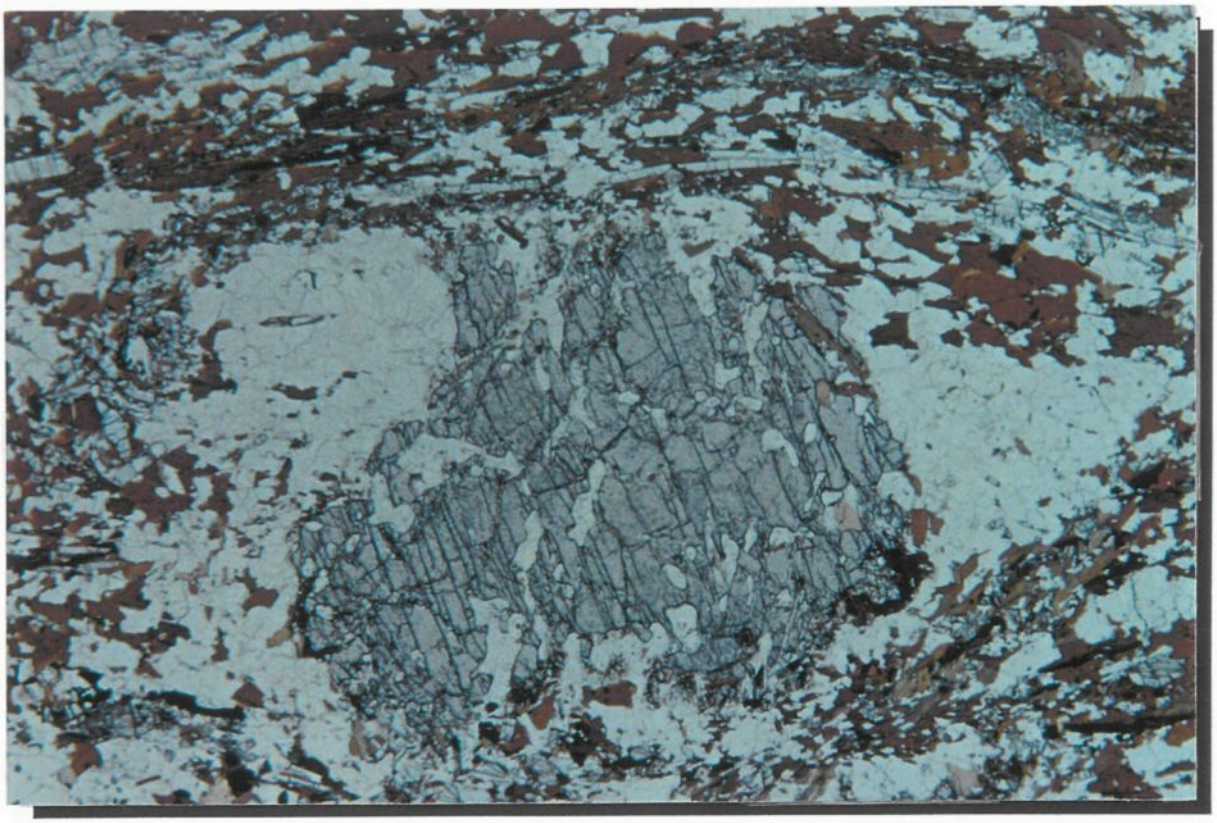

Plate XVII

2.0 mm

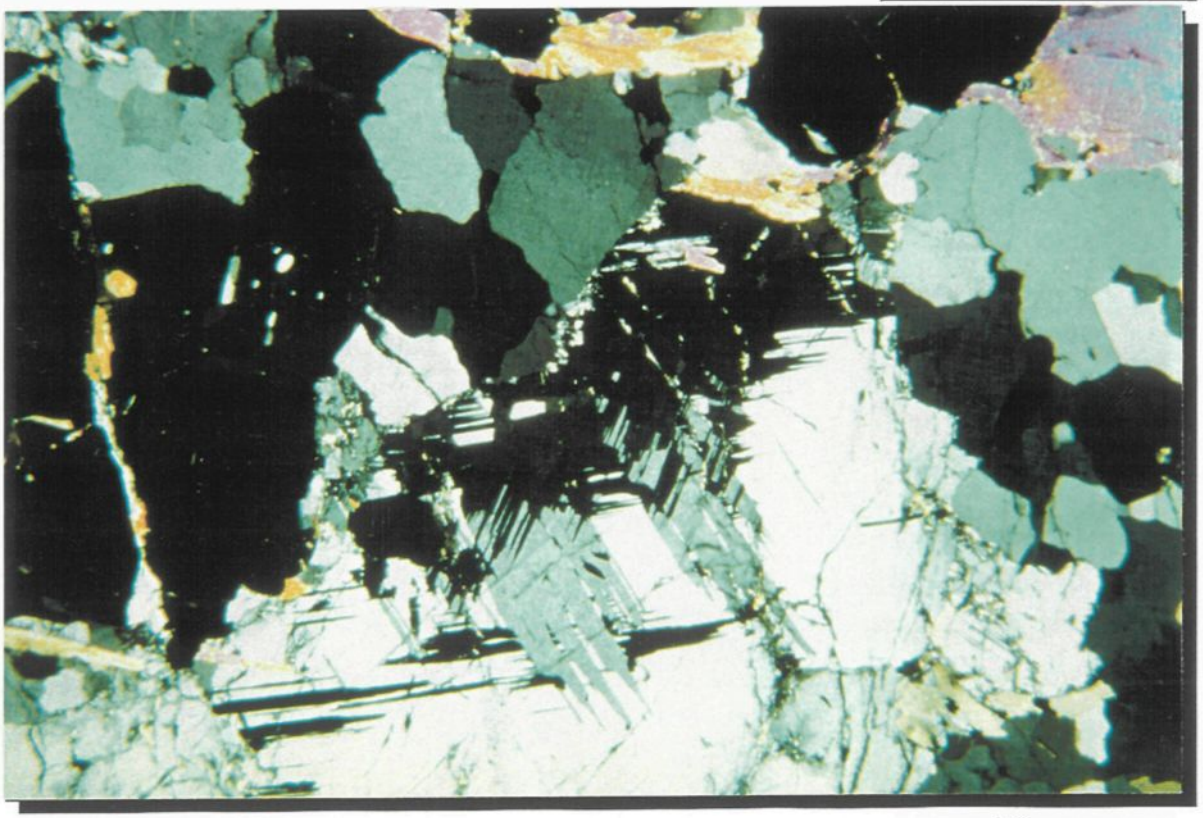

Plate XVIII

1.0 mm

Plate XIX: Outcrop 1654 (BGC). Kornerupine (green - grey) - bearing pods in quartzo-feldspathic gneiss of granitic composition. Note that this kornerupine contains inclusions of tourmaline and bronzite in thin section, which are not distinguishable in this plate.

Plate XX: Outcrop 1654 (BGC). Bronzite (brown - red) - tourmaline (black) bearing pods in quartzo-feldspathic gneiss. Cordierite is also present in these pods, but is not visible in this plate.

Plate XIX

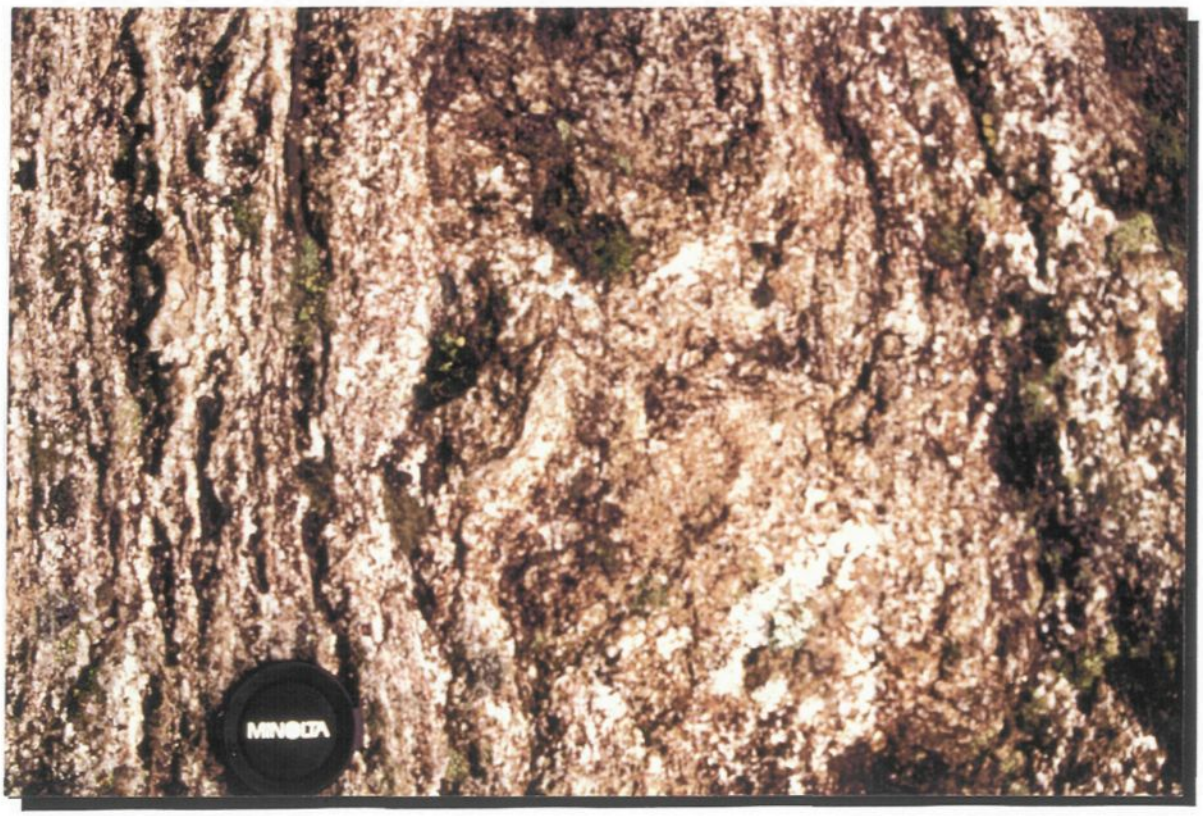

Plate XX

Plate XXI: Thin section 1654F (BGC). Kornerupine (medium grey) with inclusions of tourmaline (yellow-green), orthopyroxene (dark brown) and quartz (white), surrounded by cordierite and plagioclase (both white). This texture suggests the kornerupine-forming reaction Tur + Opx + Crd = Krn + Pl.

Plate XXII: Thin section 3832 (SW Corner). Kornerupine (blue) in garnet (brown-grey) with biotite (yellow, brown) and quartz (white). The kornerupine habit in this outcrop is very different from that of outcrop 1654. Here the kornerupine was disseminated, not concentrated in pods. This kornerupine was blue at hand specimen scale (when crushed, not seen in hand specimen, nor outcrop), and pleochroic blue-pink in thin section (closely resembling sapphirine, not apatite as in 1654).

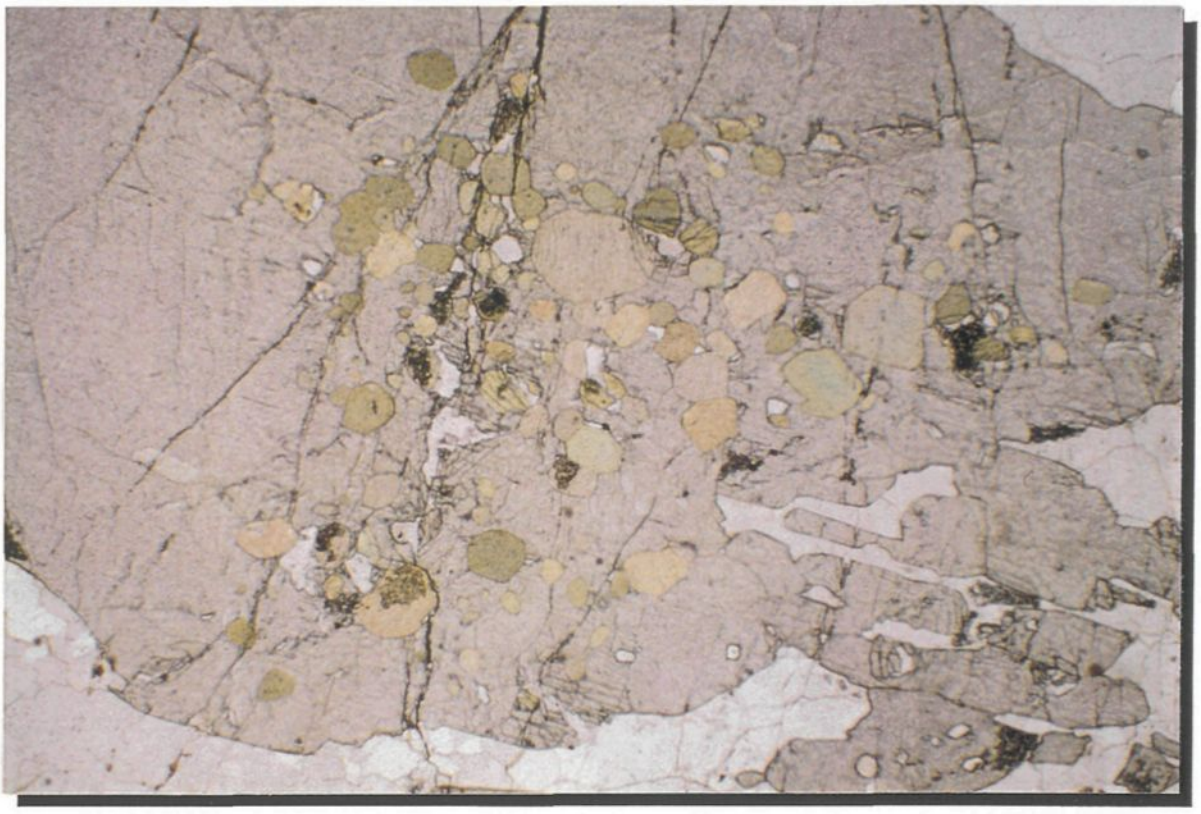

Plate XXI

1.0 mm

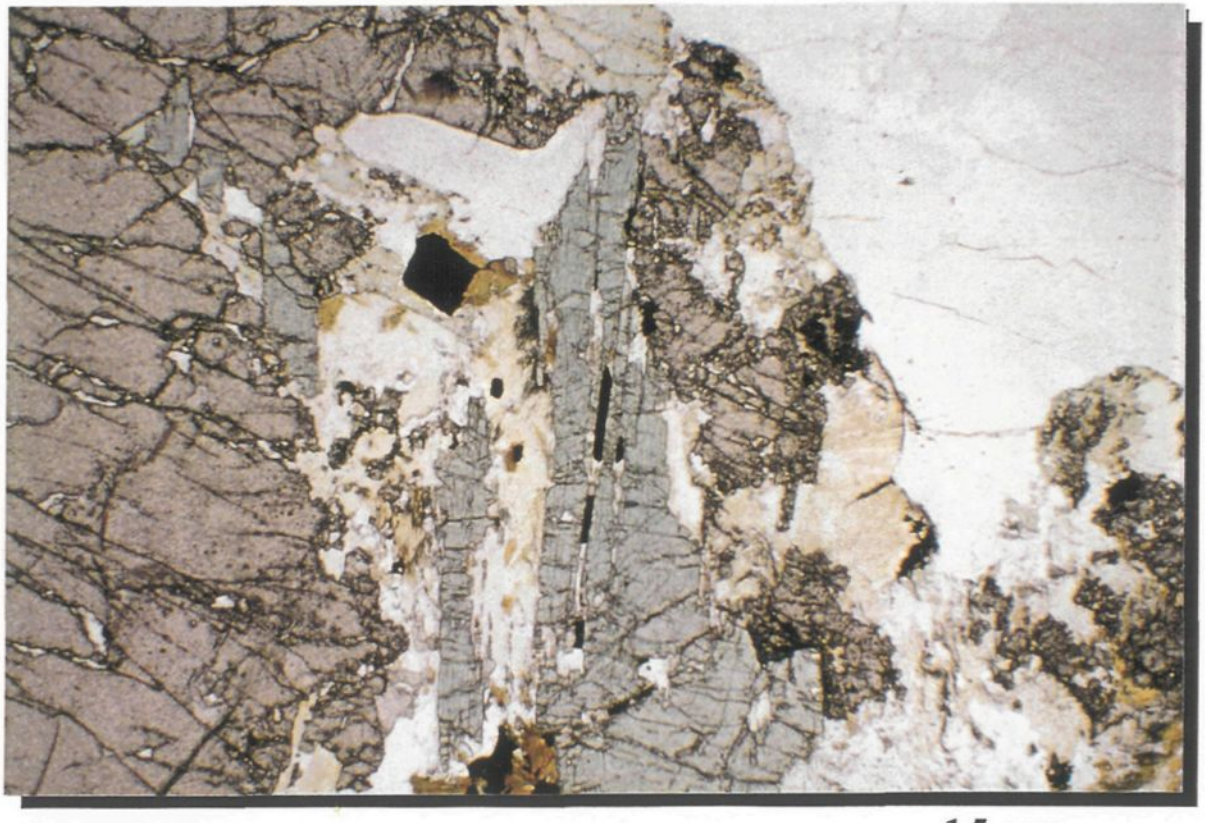

Plate XXII

1.5 mm

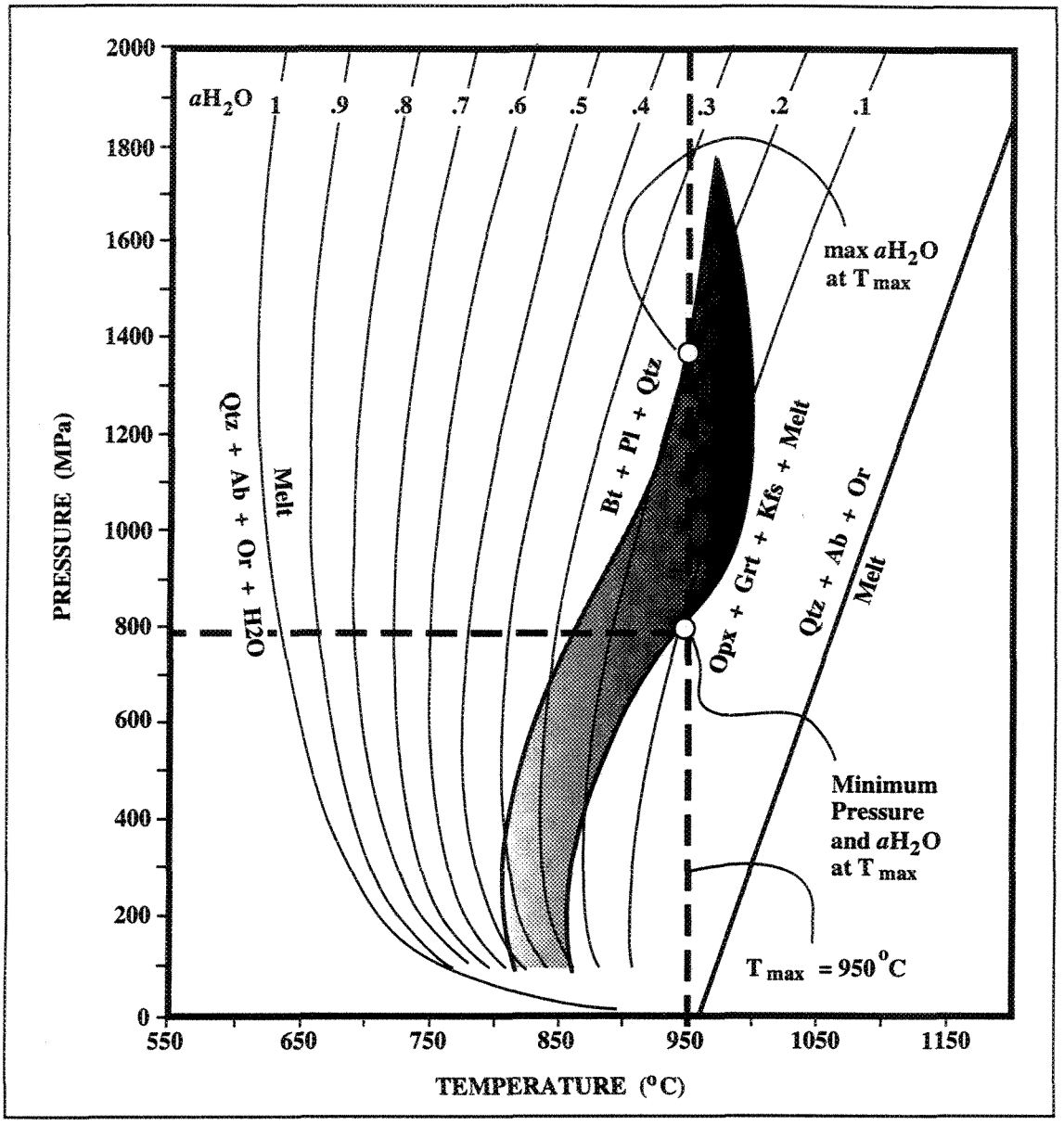

FIGURE 3-VI: A pressure-temperature diagram in the system CNKFMASH for the reaction Bt + Pl + Qtz = Opx + Grt + Kfs + Melt (after Vielzeuf and Montel 1994). The stippled area in this figures represents the stability field for this reaction. Biotite is present throughout the field area, therefore, P-T conditions are limited to the biotite-present field. Note that at the suggested Tmax of 950°C, the pressure would be above 790 MPa, and the aH_2O would be below 0.2.

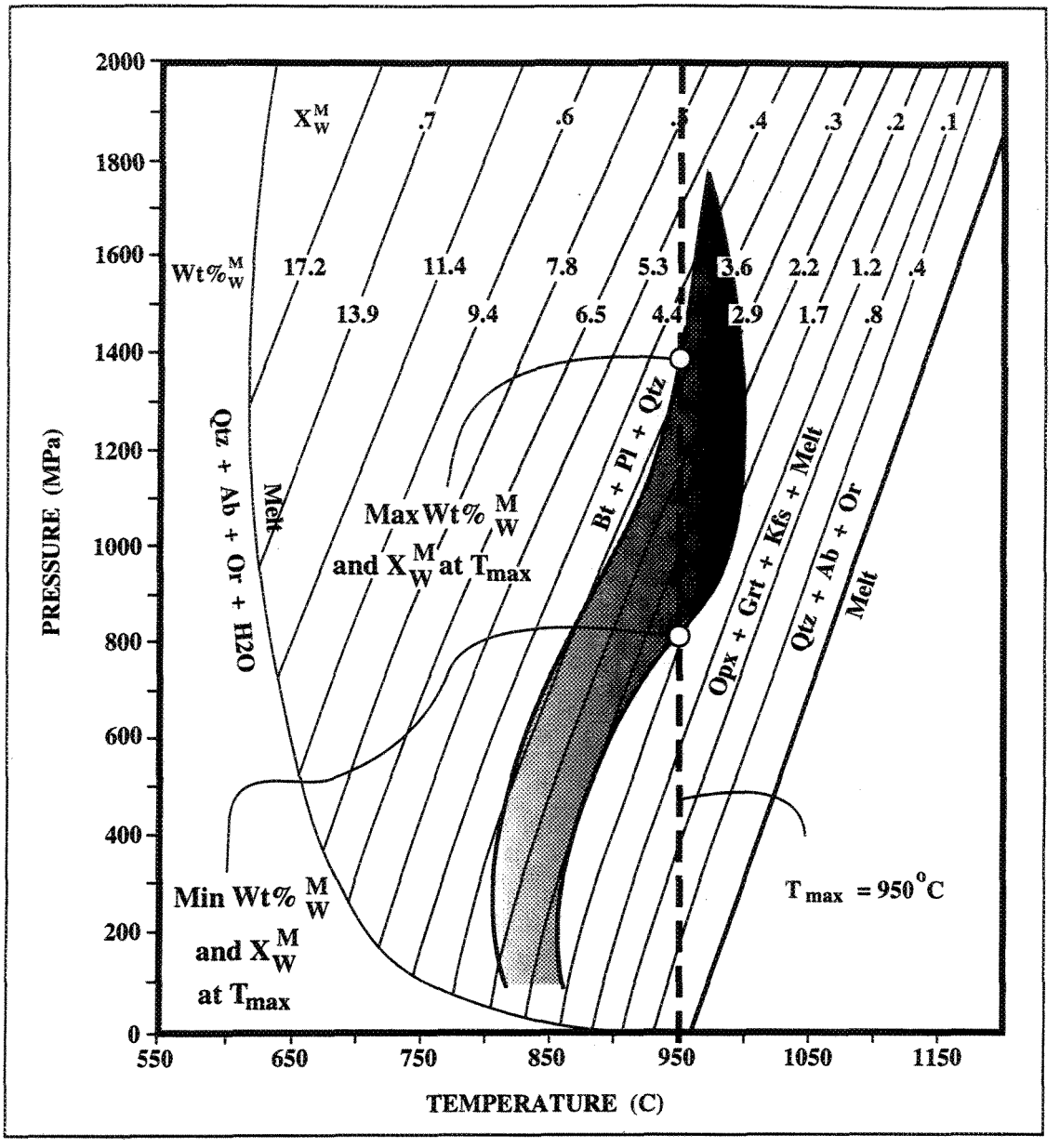

FIGURE 3-VII: The reaction Bt + Pl + Qtz = Opx + Grt + Kfs + Melt in pressure - temperature space for the system CNKFMASH (after Vielzeuf and Montel 1994). The stability field for this reaction is represented by the stippled region. Here the suggested T_{max} of 950 °C corresponds to a Wt% H_2O of < 3.6 and a $X_W^M H_2O$ of < 0.4 in the melt.

melt, this sample experienced the reverse of reaction (3-12), possibly with vapour as a reactant instead of melt. From Figures 3-VI and 3-VII, this suggests that melt then occurred at temperatures below 775°C, and was accompanied by an increase in a_{H2O} to >0.2 and an increase in the Wt% H_2O to >3.6.

Most thin sections (1280-2, 1475A1, 1475A3, 1512, 2039A, 2373, 2401D2 (Plate IX), 2401G3, 2672, 3028, 3302A, 3333A (Plates VI, XVII), 3354, 3600, 3604, 3694, 3794, 3804, 4012, 4044, 4209, 4475A, 4485B (Plate XIV)) contain garnet with inclusions of biotite, plagioclase and quartz and evidence of melt-producing reaction (3-14) (Appendices A and B). Many samples from the field area do not contain orthopyroxene. Vielzeuf and Montel (1994) noted that reaction (3-13) produced less orthopyroxene as pressure increased. Thus, the absence of orthopyroxene, and the enrichment in plagioclase, is compatible with reaction (14) at higher pressures.

Orthopyroxene, where it does occur, (outcrops 1475, 1512, 1654, 1659 (Plates II, III), 2401 (Plate X)), is idioblastic. Its boundaries are embayed and irregular, and biotite crystals have grown along its cleavage traces; a fibrolite + plagioclase + biotite + quartz subassemblage has developed along the cracks and in embayments. The orthopyroxenes are also commonly surrounded by partial or complete moats of plagioclase (Plate III, X). Regardless of whether orthopyroxene was present or not, the peak metamorphic temperatures would still have to be above 780°C (Figures 3-VI and 3-VII).

3.2civ. Retrograde Cordierite-Reactions

Outcrops 1654 and 1659 (Plates II, III, XVIII) contain unaltered cordierite in thin sections where both garnet and orthopyroxene are reacting out to form biotite + quartz + fibrolite (Appendix A). Cordierite does not occur in the presence of spinel; suggesting that reaction (16) shown on Figure 3-III did not occur. Thin sections 1659H1 and 1659H2 have garnets with embayments and cracks filled with cordierite suggestive of the reverse of

reaction (14) in Figure 3-III during retrogression. These garnets also have biotite + cordierite infilling embayments and cracks, suggestive of the reverse of reaction (36) shown on Figure 3-III. Sample 1659 also has clots of biotite + fibrolite forming in the cordierite suggestive of the reverse of Vielzeuf and Holloway's (1988) reaction (29) shown on Figure 3-III.

3.2d. Characteristics of the Melt

When fluid-absent, or H_2O-saturated anatectic pelites have molar percent ratios of iron in the following order: garnet > liquid > biotite, intermediate compositions containing biotite, garnet, aluminosilicate, plagioclase, K-feldspar and quartz would melt eutectically before Fe-richer or Mg-richer metapelites. However, near 900°C, there is a change in the relative X_{Fe} of garnet and melt (Ellis 1986), which would cause the biotite to form from a peritectic reaction with the melt during cooling (Le Breton and Thompson 1988). The formation of biotite selvages was suggested by Le Breton and Thompson (1988) to be a possible textural change during such progressive metapelite melting. The presence of biotite selvages between mafic and felsic layers (1659 (Plate II); 4475D2, 4475D3), or surrounding garnets (3694, 3832 (Plate XI), 4475 (Plates VIII, XIII), 4485 (Plate XIV)) indicates that the melt is produced by a peritectic reaction, not a eutectic reaction (Le Breton and Thompson 1988). These biotite selvages also support maximum temperatures above 900°C (Ellis 1986).

In most cases (see Appendices A and B), the composition of the partial-melt from biotite breakdown is typically (Patiño Douce and Johnston 1991) silicic (68-73 wt % SiO_2), strongly peraluminous (2-5 wt% normative corundum) and very felsic (<3 wt% FeO + MgO + TiO_2). Three notable exceptions to this are thin sections 3794, 4220, 4475D2, and 4475D3 which have between 10 and 25% biotite + garnet. The biotite and garnet from these leucosomes are likely schollen (blocks of paleosome or melanosome in the leucosome), as anatectic melts are usually silicic and felsic (Patiño Douce and Johnston 1991).

As noted above (Appendices A and B), many thin sections (1280-2, 1654E3, 2401D2, 3302, 3333A, 3364-2, 3694, 3777, 3832, 3869, 4012, 4209, 4475A2) contain K-feldspar that formed as a result of melt-forming reactions where biotite was consumed. Many thin sections also contain plagioclase that crystallized during similar melt-forming reactions. Plagioclase occurs as porphyroblasts, or aggregates of small grains forming moats around garnet and orthopyroxene porphyroblasts (2401F2, 2770, 3302A, 3333A, 3634-1, 3694, 3777, 3832, 4012, Appendices A and B). Thus, it is possible that these anatectic melts may have contained some potassium, calcium and sodium (possibly in the schollen).

As discussed above, Appendix B presents the evidence from several thin sections (2373, 2401E, 3028, 3302, 333A, 3604, 3634, 4475A, 4475B, 4475D2, 4475D3) for at least two stages of sillimanite growth, one of which may have formed from a reaction involving melt. These melts must have contained some excess alumina. However, there are also several thin sections (1654K, 1659H1, 1659H2, 2770, 3794, 3832, 3869) that contain evidence for a later, post-foliation generation of sillimanite. As noted by Patiño Douce and Johnston (1991), many melts are strongly peraluminous (2-5 wt% normative corundum).

It is interesting to note that two samples (3869 and 4220) contained apatite in the leucosomes, some of which was included within K-feldspar. Samples 3869, 333A and 4012 contained tourmaline associated with the leucosomes. Sample 3832 contained kornerupine inclusions within the plagioclase-quartz of the leucosomes. Thus, it is possible that the melt for these samples may have contained minor amounts of phosphorus and boron. A possible source for these elements may be the previously formed apatite or tourmaline.

3.2e Summary

The petrogenetic grid shown on Figure 3-VIII contains a proposed P-T trajectory based on the observed assemblages and textures plotted on a petrogenetic grid for the Bondy Gneiss Complex (BGC). The peak temperature is limited to a maximum of ~970°C due to

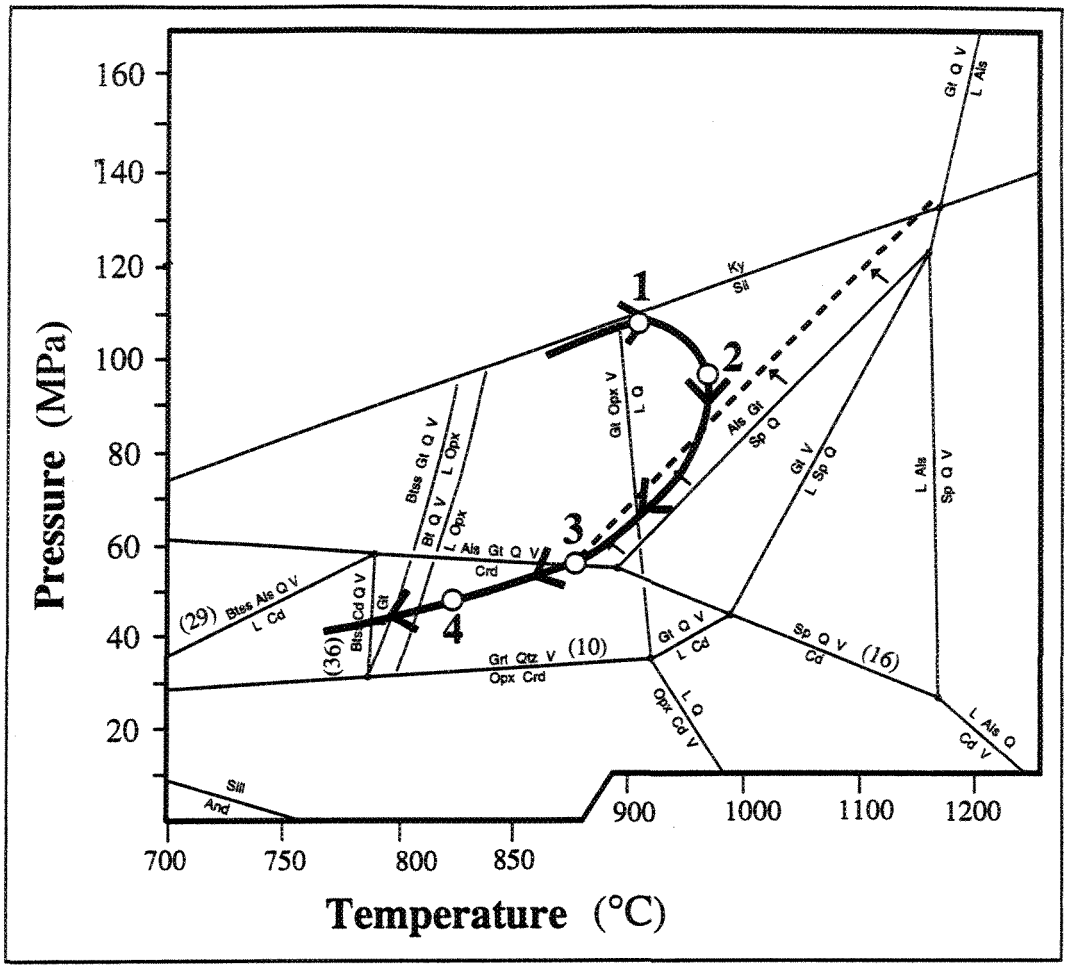

Figure 3-VIII: P-T trajectory for BGC, inferred from the mineral assemblages and textures. The maximum pressure (1) is restricted below the kyanite-in curve due to the lack of observed Ky. The T_{max} (2) is to the right of the Spl-in curve due to the presence of Spl (+ Qtz). The T_{max} is restricted to being below 980°C due to the omnipresence of biotite (Figures 3-VI, 3-VII). The absence of the preserved assemblage Spl + Qtz implies that the P-T path (3) passed through the Spl-producing reaction. The final portions of the retrograde path (4) are implied because of the presence of retrograde Crd (from Grt) with no retrograde Opx.

the omnipresence of the biotite + plagioclase + quartz subassemblage which implies that the biotite consuming reaction of Vielzeuf and Montel (1994) has not gone to completion. The absence of kyanite limits the maximum pressure, according to the assemblages, to 90 MPa at 850°C or 110 MPa at 970°C; unless kyanite has inverted to sillimanite. The same limits for peak metamorphic conditions would apply to the Nominingue-Chénéville Deformation Zone (Figure 3-IX).

During retrogression from peak metamorphic temperature of 970°C, the trajectory is inferred to follow reaction (15) (in Figure 3-VIII) closely because of the production of spinel, followed closely by the consumption of spinel. The absence of the assemblage spinel + cordierite implies that reaction (16) (in Figure 3-VIII) did not occur, limiting the temperatures to below 900°C for the retrograde cordierite-producing reactions. Porphyroblasts of garnet from sample 1659 commonly have partial coronas of cordierite suggesting reaction (3-19). The cordierite coronas surrounding garnet in sample 1659 contain retrograde biotite, suggestive of reaction (36) (Figure 3-III). Biotite + cordierite aggregates also have fibrolite associated with them, implying the crossing of reaction (29) (Figure 3-VIII). These retrograde cordierite-producing reactions limit the retrograde conditions to having passed between 35 to 60 MPa and 900 to 720°C.

3.3 Possible Prograde Discontinuous Reactions

At the outcrop scale (1659 (Plates II, III)), large (up to 3 cm across) porphyroblasts of cordierite, garnet and orthopyroxene are observed, they are separated by moats (1 to 2 cm thick) of leucosome (cordierite + quartz + K-feldspar + plagioclase?). These porphyroblasts are too large for all three, together with the leucosome moats, to be contained within a thin section (e.g., Plate XVIII). Thus it is not possible to say unequivocally that these three phases were in equilibrium. However if garnet, cordierite and orthopyroxene were stable together, then this suggests the possible progression through a series of discontinuous

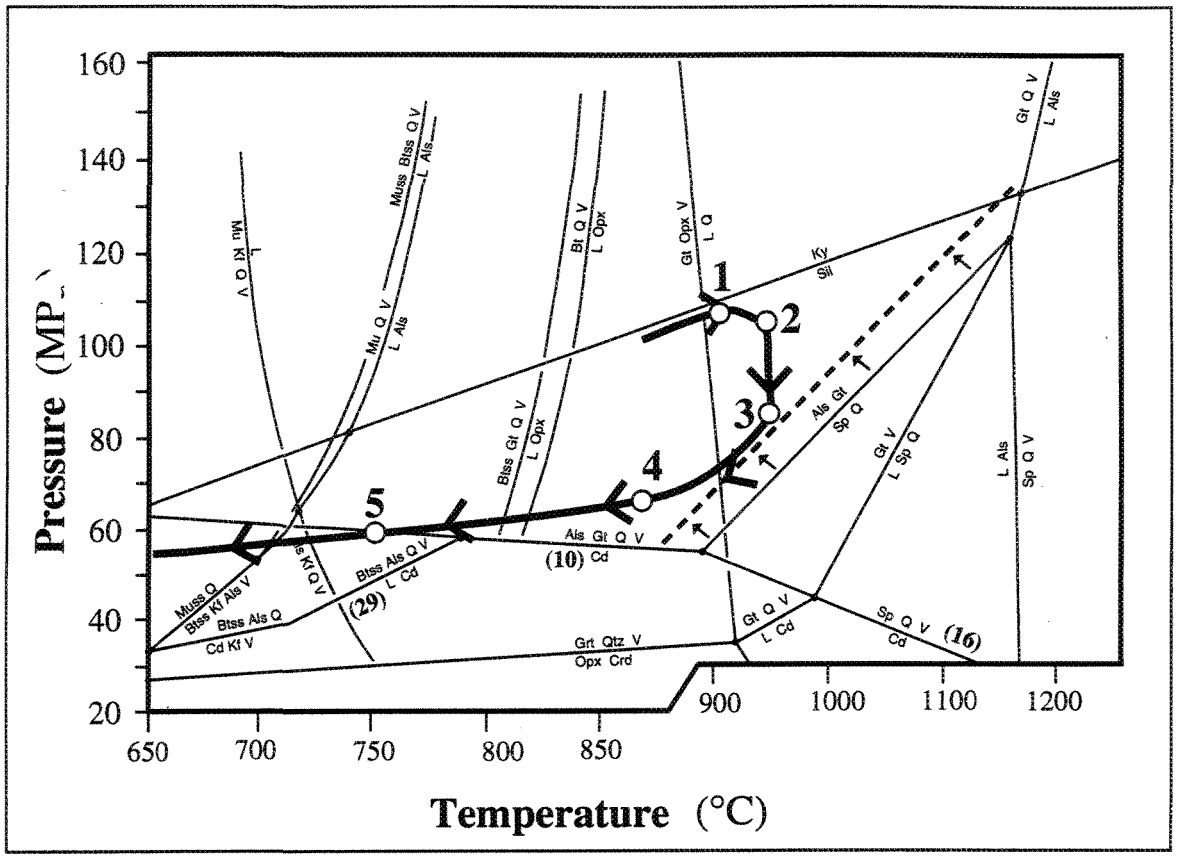

FIGURE 3-IX: P-T path for NCDZ, inferred from assemblages and textures. The prograde conditions were approximately the same for the whole study area, therefore positions (1) and (2) are the same for both the BGC and the NCDZ (compare with Figure 3-VIII). There is structural evidence within the NCDZ for extension, implying position (3). Neither Spl nor Crd was observed in the NCDZ, which restricts the retrograde path to the left of the Spl-in curve, and above the various Crd-in curves (4). Ms is present in the NCDZ, however, never in assemblage with Kfs, which defines position (5). This petrogenetic grid was simplified from Figure 3-III.

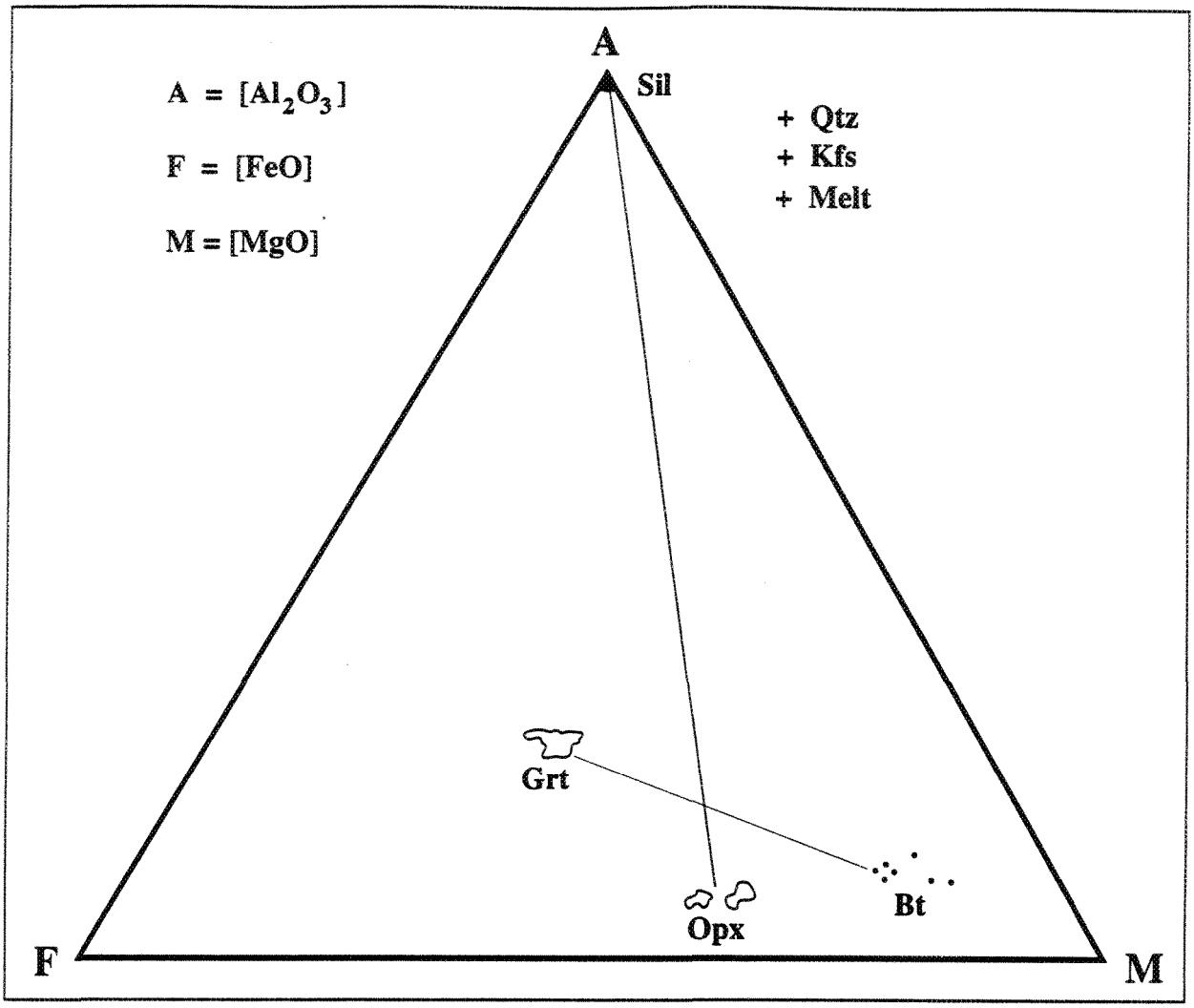

FIGURE 3-X: AFM projection from Kfs for sample 1659 suggesting the reaction Grt + Bt + Qtz = Sil + Opx + MELT.

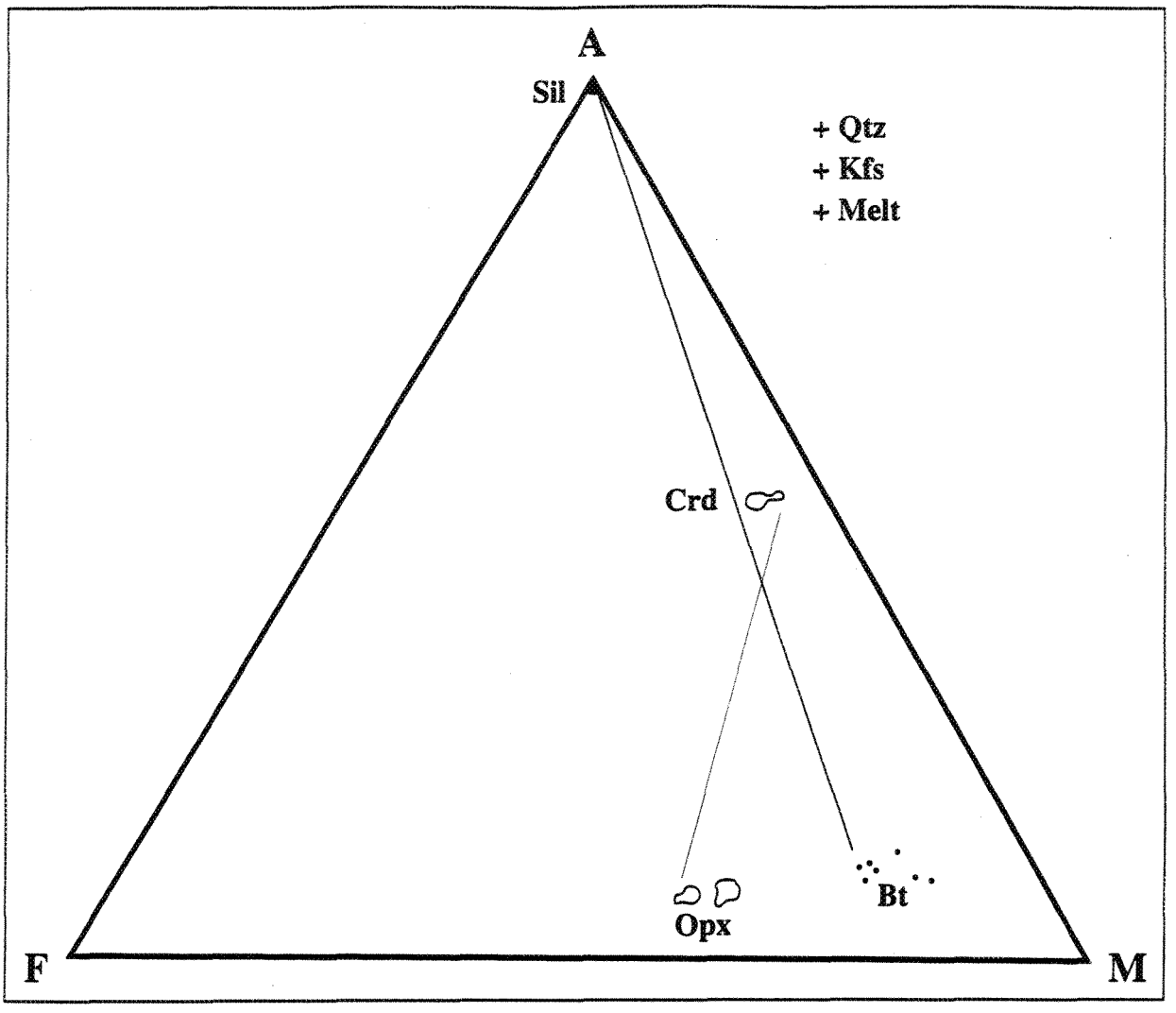

FIGURE 3-XI: AFM projection from Kfs for sample 1659 suggesting reaction Bt + Sil + Kfs + Qtz = Crd + Opx + MELT.

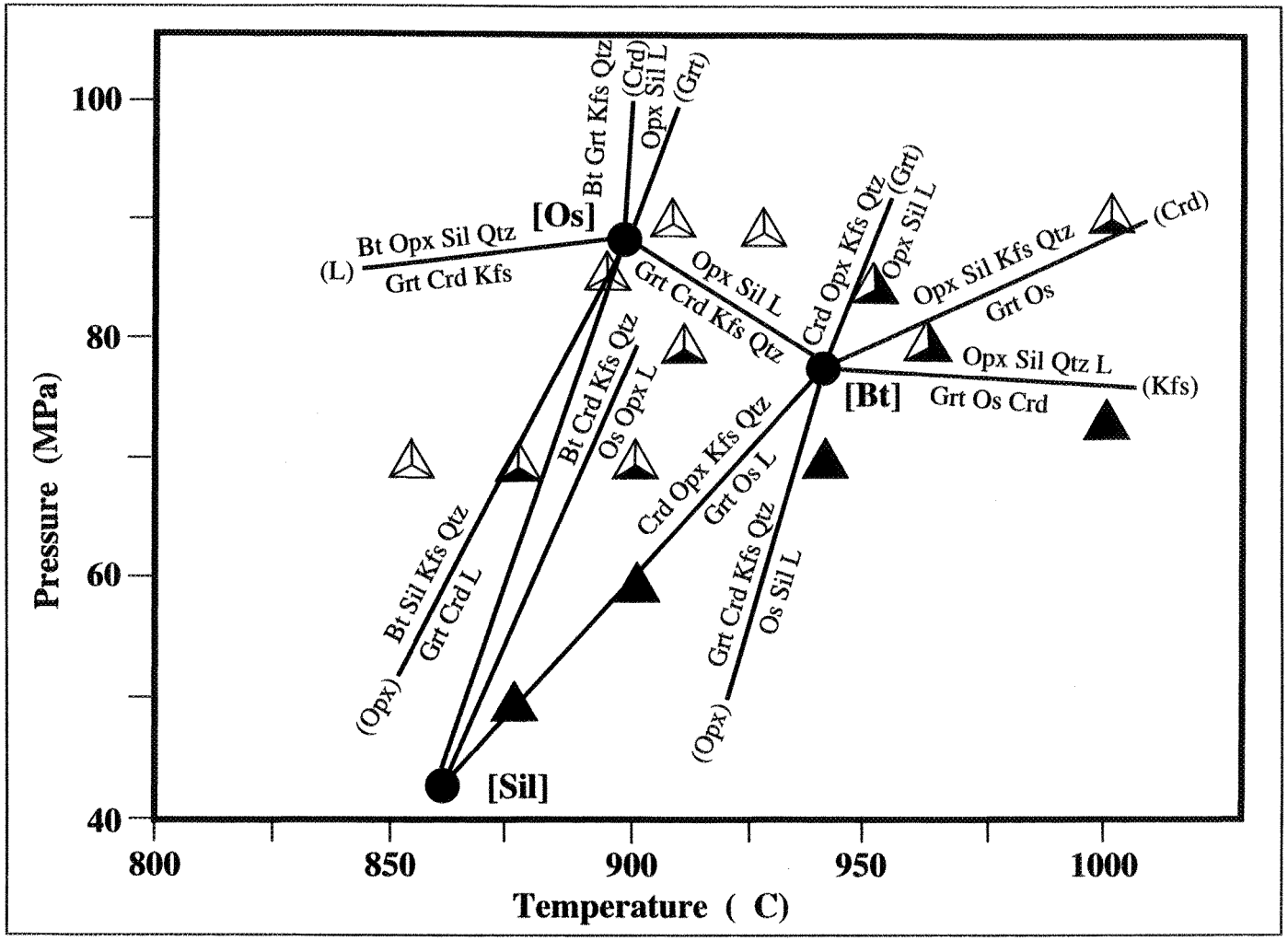

FIGURE 3-XII: Discontinuous osumilite-bearing reactions in P-T diagram (after experimental work of Carrington and Harley 1995). Unlabelled reactions are (Os, Grt) Bt + Sil + Kfs + Qtz = Crd + Opx + L; (Os, Sil); Bt + Grt + Kfs + Qtz = Crd + Opx + L. The reactions inferred by the textures and assemblages in this study are discussed in the text with the aid of the AFM projections (Figures 3-X, 3-XI, 4-XXX, 4-XXXI).

reactions whose positions in P-T space overlap those suggested by the melt-producing biotite-dehydration reactions previously discussed.

As suggested by crossing tie-lines in AFM diagrams (sample 1659) in Figures 3-X and 3-XI, the following two discontinuous prograde reactions could be proposed:

(3-15) Grt + Bt + Kfs + Qtz = Sil + Opx + MELT

(3-16) Sil + Bt + Kfs + Qtz = Crd + Opx + MELT

At outcrop 1659, orthopyroxene is observed to contain idioblastic garnet inclusions both in the hand specimen and thin section (Plates II, III). This is consistent with the prograde discontinuous reaction (3-15). The second discontinuous reaction (3-16) is not suggested by any textural relationship; however, to reach the peak metamorphic temperature of 970°C suggested by the melt-producing reactions, the conditions for this reaction were likely surpassed. These reactions correspond to the two reactions located at pressures above the [osumilite] invariant point in Figure 3-XII from Carrington and Harley (1995) who place this invariant point at 900°C and 90 MPa, which is consistent with the limit deduced from the biotite + quartz + plagioclase breakdown reaction of Vielzeuf and Montel (1994).

Whether these possible discontinuous reactions, which all involve biotite in the granulite facies, are truly discontinuous in reality is questionable, due to the complicated solid solution involved in biotite. Patiño Douce et al. (1993) demonstrated that natural biotite departs from the ideal phlogopite-annite join; in their experiments, Al^{6+} and excess Al^{4+} ($=Al^{4+-1}$) varied as a function of temperature at 70 and 100 MPa. During their experiments, temperature also caused the antithetical variation of Fe^{2+} and Ti in biotite (Patiño Douce et al. 1993). These experiments demonstrated that the solid solutions occurring within biotite during granulite-grade metamorphism result in the gradual disappearance of biotite over a wide temperature interval, similar to what is expected from a continuous reaction. However, regardless of the effect of the solid solution in biotite, if garnet, orthopyroxene and cordierite

were in stable equilibrium and one could argue in favour of two discontinuous reactions, then it is possible to infer a lower limit to the peak metamorphic conditions (900°C and 90 MPa).

3.4 Geothermobarometric Assemblages

The assemblages:

-biotite + garnet,

-cordierite + garnet and

-garnet + orthopyroxene

were used as geothermometers. The following assemblages:

-aluminous orthopyroxene + garnet,

-garnet + sillimanite + spinel + quartz,

-biotite + garnet + plagioclase + sillimanite + quartz (GASP), and

-cordierite + garnet + sillimanite + quartz

were used as geobarometers. The thin sections which contain these assemblages are listed in Table 3-II. The following portion of this section describes the textures of the assemblages suitable for geothermobarometry.

3.4a Garnet+Sillimanite+Spinel+Quartz Assemblage

This assemblage was not observed in the field area. However, it is inferred from outcrop 2401 (Plate IX) where hercynite occurs as inclusions within both garnet and sillimanite. Quartz is not observed in contact with spinel, however small grains (<1 mm) of quartz do occur throughout the matrix and as inclusions within garnet. This reaction cannot be seen on AFM projections (Figure 3-XIII) because the presence of quartz is assumed in the projection. However, on an ASF projection (Figure 3-XIV), crossing tielines display this reaction graphically. A possible balanced reaction for this equation is:

(3-17) $3FeAl_2O_4 + 5SiO_2 = Fe_3Al_2(SiO_4)_3 + 2Al_2SiO_5$

Hercynite Quartz Almandine Sillimanite

Table 3-II: Assemblages Used For Geothermobarometry

Sample	Bt-Grt	Grt-Opx	Spl-Grt	GASP	Sil	Al in Opx	Crd-Grt
1280-2	x						
1475-A1	x						
1475-A3	x	X				x	
1475-B1	x						
1475-B2	x						
1512	x			X	x		
1654A1						X	
1654C1						X	
1654C2						X	
1654D					X	X	
1654-E3					?		
1654F2						X	
1654H						X	
1654L						X	
1659H1	X	X			X	X	x
1659H2	X	X			X	X	x
2039-A	x						
2039-B	x						
2373	x			X	x		
2401	x	X	X	X	X	x	
2401D1	x	X	X	X		x	
2401D2	x	X	x	X	x	X	
2401E	x		x		x		
2401F2	x	X	X			X	
2401F2	x	X	X			x	
2401G1	x	X				x	
2401G2	x						
2401G3	x					x	
2672	x			X	x		
2672	x			X	x		
2770	x			X	x		
3028B				X	X		
3045	x						
3045A1	x						
3045A2	x						
3045A2	x						
3302	x			X	X		
3302A	x			X	X		
3333A	x			X	x		
3333B	x			X			

Table 3-II: Assemblages Used For Geothermobarometry - continued

3354		X						
3364-2					X	X		
3600		X						
3604		X			X	X		
3634		X			X	X		
3634-1								
3694		X			X	X		
3705						X		
3777		X						X
3777F		X						
3794		X			X	X		
3804		X						
3829						X		
3832		X			X	X		
3869						X		
4012		X						
4044		X						
4209		X						
4220		X						
4475A2		X				X		
4475D2		X				X		
4475D3		X				X		

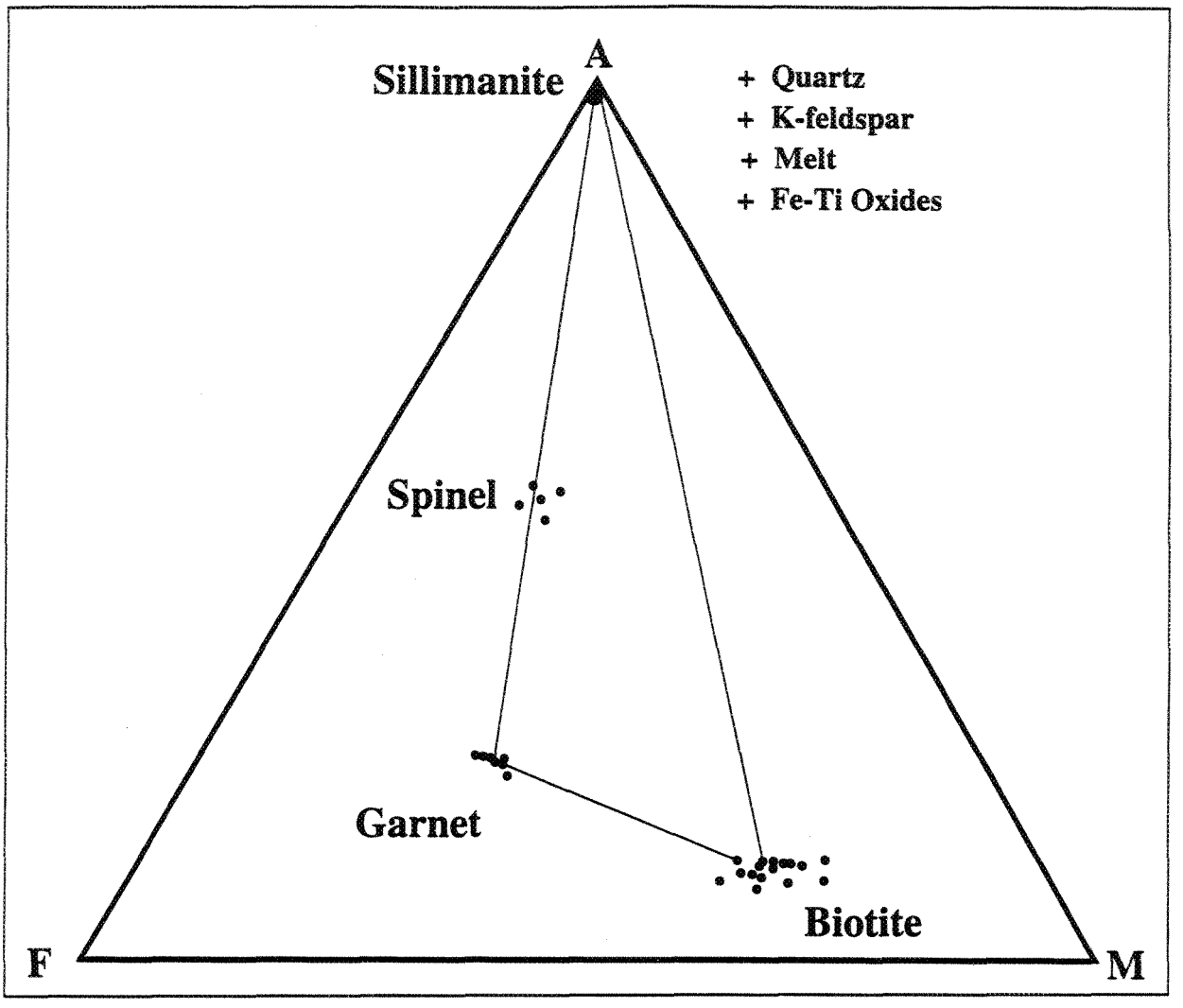

FIGURE 3-XIII: An AFM projection from K-feldspar for sample 2401D2 (BGC). Spinel lies near the tieline between garnet and sillimanite suggesting a possible reaction (which is demonstrated by the textures (Plate IX) and the ASF projection from this sample (Figure 3-XIV)). Biotite is probably not involved in the reaction since another K_2O bearing phase would be required on the opposite side of the reaction. Quartz, sillimanite, spinel and garnet relations are examined in the AFS plot (Figure 3-XIV).

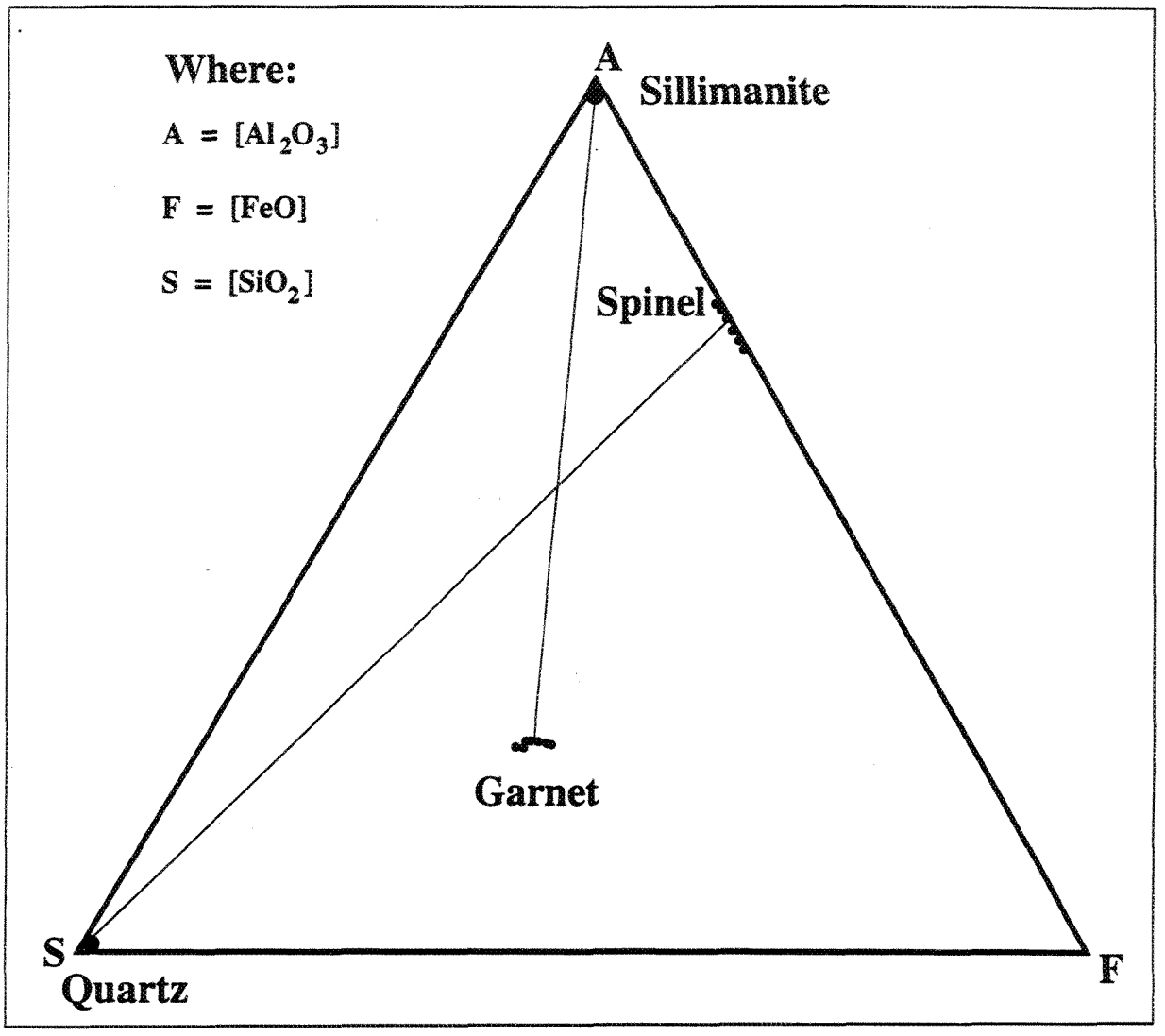

FIGURE 3-XIV: An ASF plot for sample 2401D2 (BGC). This projection was necessary to include quartz in the projection in order to represent the reaction Qtz + Spl = Grt + Sil, which is shown here by the crossing tielines.

This reaction was suggested by Sengupta et al. (1991) in their study of spinel granulites from Araku, Eastern Ghats, India. The Indian granulites contained spinel rimmed by an intergrowth of sillimanite and garnet, a texture which was not observed in this study.

3.4b Biotite+Garnet+Plagioclase+Sillimanite+Quartz Assemblage

This assemblage was observed in several outcrops (Table 3-II). Thin section 3333A (Plate VI) contained a classic reaction texture typical of this assemblage. Garnet porphyroblasts with wing-shaped projections, were broken and extremely fractured with embayed boundaries. Both the fractures and the embayments are filled with biotite and sillimanite. This replacement texture suggests the rehydration reaction:

(3-18) $4Fe_3Al_2(SiO_4)_3 + 7SiO_2 + 6H_2O + 6K_2O + O_2 = Al_2SiO_5 + 6K_2Fe_2(OH)_2(AlSi_3O_{10})$

Almandine Quartz (Melt) Sillimanite Biotite

Samples 1512, 2373, 2672, 2770, 3302, 3333A and 3604 all demonstrate evidence for two periods of sillimanite growth. The first episode is clearly shown by coarse-grained blades that are visible to the naked eye in the hand specimen. Sillimanite formed during the second period of growth is visible only at the microscopic scale, as fibrolitic growths on the sillimanite blades and rims on the garnets. The sillimanite in thin section 2373 occurs in concentrations up to 15%.

Throughout the field area, reaction (3-18) appears to have proceeded to varying extents in different outcrops. For example thin section 3354 demonstrates only an incipient reaction, as sillimanite occurs only as local narrow fibrolitic rims on garnets. Many garnets occur as islands in a sea of biotite. Sample 3302 represents the opposite extreme in which small fragments of garnet that are completely isolated in moats of fibrolitic sillimanite and biotite.

Other than in samples 3302 and 3604, the garnet porphyroblasts are poikiloblastic, extremely so in thin section 2672, the garnets are crowded with inclusions of quartz and opaque minerals. Sample 3333A (Plate VI) contains garnet porphyroblasts which are full of quartz and sillimanite inclusions.

The garnets in samples 1512 and 2373 are zoned with respect to their inclusions. The garnet cores in thin section 1512 are relatively inclusion-free, an intermediate ring contains quartz and biotite inclusions, whereas the rims contain abundant sillimanite, biotite and quartz inclusions. In sample 2373, garnets are full of quartz inclusions throughout, however, they appear to contain sillimanite inclusions only in their rims.

The biotite in all of these samples is located predominantly within the groundmass around the garnet porphyroblasts. It ranges in morphology from lepidoblastic in thin sections 1512, 2373 and 3333A to irregular patches associated with garnet and sillimanite in 2672, 3302 and 3604. In sample 2770 biotite defines the foliation in the groundmass. Biotite in sample 2770 also occurs as pressure shadows around the garnet porphyroblasts. Sample 3604 contains symplectic biotite-quartz around the rims of some garnets.

3.4c Cordierite-garnet-sillimanite-quartz Assemblage

Mukhopday and Holdaway (1994), Holdaway and Lee (1977), Hensen (1977), Hensen and Green (1971, 1973) and Currie (1971) have all conducted experiments on this reaction:

(3-19) $3(Mg,Fe)_2Al_3(AlSi_5)O_{18} = 2(Mg,Fe)_3Al_2Si_3O_{12} + 4Al_2SiO_5 + 5SiO_2$
Cordierite Garnet Sillimanite Quartz

as a potential geothermobarometer. The petrography of thin sections in this study indicate the possibility that this reaction occurred in outcrop 1659. In thin sections 1659H1 and 1659H2 the garnets are surrounded by quartz and cordierite (Plates II, III, XVIII). In places, the cordierite is separated from the garnet by a thin rind of quartz. Quartz inclusions are typically located within the garnets. Isolated islands of fibrolitic sillimanite, and tiny garnets (<<1

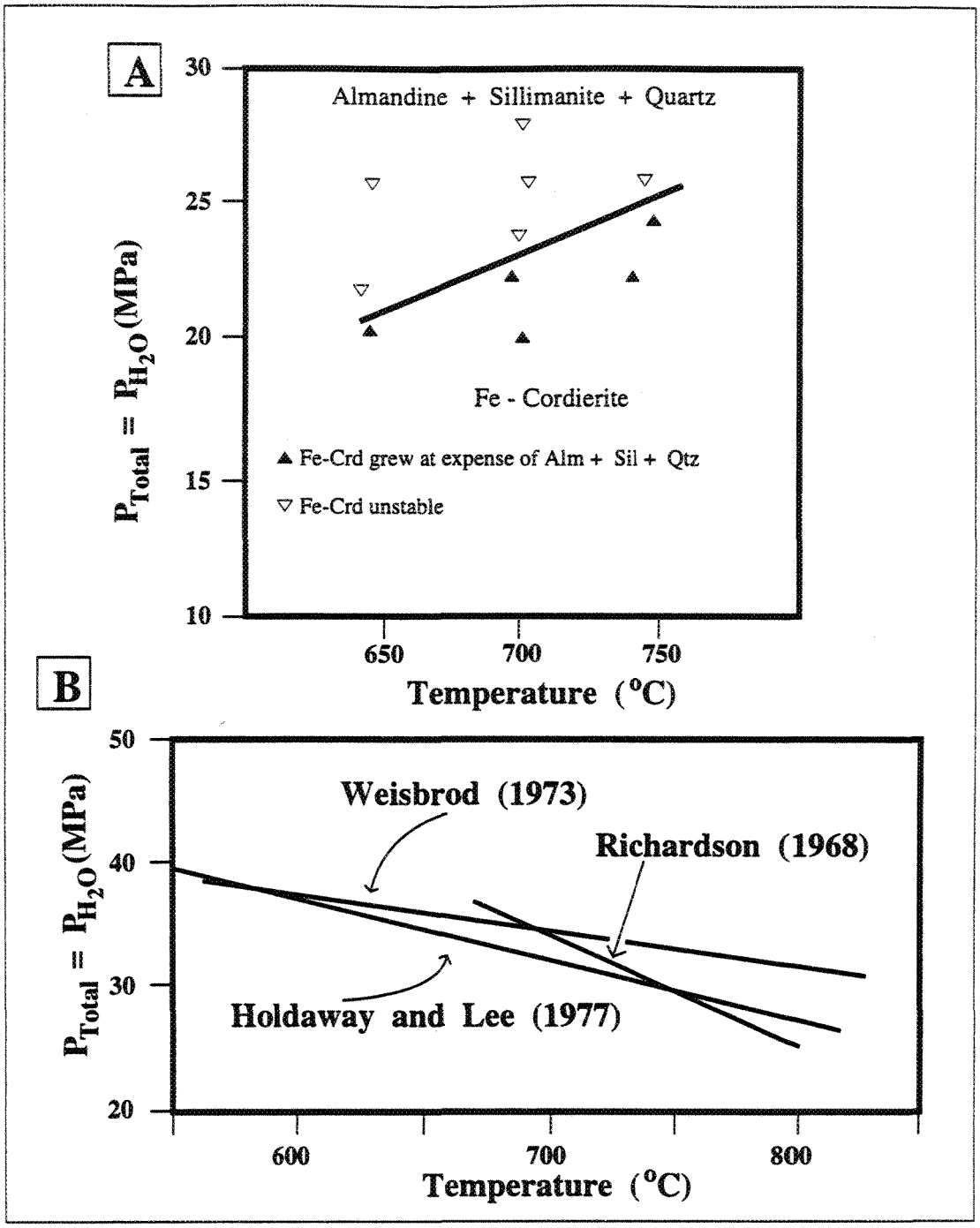

Figure 3-XV: Experimental calibration of the pure end member reaction Fe-Crd = Alm + Sil + Qtz + V under conditions of $P_{H_2O} = P_{Total}$. "A" represents work by Mukhopadhay and Holdaway (1994). The orientation of the reaction curve in "A" is preferred by the authors, as this orientation does not require an increase in pressure during the retrograde portion of the P-T trajectory. "B" represents the previous experimental calibrations

3.4d Garnet-quartz-cordierite-orthopyroxene Assemblage

Thin sections 1659H1 and 1659H2 (Plates II, III) both contain large orthopyroxene porphyroblasts (>20 mm x >30 mm) to which the following equilibrium reaction can be applied:

(3-20) $2(Mg,Fe)_3Al_2Si_3O_{12} + 5SiO_2 = 3(Mg,Fe)_2Al_3(AlSi_5)O_{18} + 4(Mg,Fe)SiO_3$
Garnet Quartz Cordierite Orthopyroxene

suggested by Hensen and Green (1971, 1972, 1973) and Hensen (1977). This reaction is demonstrated more explicitly in thin section 1659H2 where the orthopyroxene contains inclusions of both the reactants garnet and quartz and is surrounded by cordierite. The orthopyroxene in sample 1659H1 only contains inclusions of quartz suggesting that the garnet may have reacted-out completely in this location. This assemblage was not suitable for geothermobarometry because the orthopyroxene was prograde and was therefore not involved in the retrograde reactions, i.e., the cordierite and orthopyroxene are believed to have grown at different times.

3.5 Pyroxene - Bearing Assemblages

Two outcrops of migmatitic gneisses (1475, 2401 (Plate X)) contain the assemblage plagioclase + garnet + pyroxene (orthopyroxene) + quartz. This assemblage occurs within the leucosomes. The orthopyroxene porphyroblasts are up to 7 mm x 15 mm in thin sections 1475A3, 2401D1 and 2401F2.

In the melanosomes of thin sections 2401G1 and 2401G3 orthopyroxene occurs mostly as tiny grains (<1 mm) in a biotite-rich groundmass not in contact with garnets. Thin sections 2401D2, 2401G2, 1475A1 and 1475A2 contained no orthopyroxene. This diversity of orthopyroxene texture and occurrence from two outcrops demonstrates the diverse nature of these migmatites. The porphyroblasts of orthopyroxene and garnet are so large that it is very difficult to examine this full assemblage in one thin section.

Thin section 2401G3 contains two porphyroblasts of orthopyroxene which illustrate the reaction that eliminates this mineral. One porphyroblast is almost pristine with only minor inclusions of biotite along cleavages, and a thin rim of biotite; the second porphyroblast contains almost 35% biotite occurring along the cleavages. The orthopyroxene in 1475A3 also contains inclusions of plagioclase and oxides along the cleavages which implies that orthopyroxene is also altering to plagioclase and oxides. In both outcrops, orthopyroxene is usually separated from garnet by moats of plagioclase or biotite which possibly indicate that garnet could be involved in the breakdown of orthopyroxene to plagioclase and biotite (and possibly oxides). A possible balanced equation for this reaction is:

(3-21) $Fe_3Al_2(SiO_4)_3 + (Mg,Fe)SiO_3 + 2SiO_2 + H_2O + 3H^+ + (Ca,Na) + K^+ =$
Almandine Hypersthene Quartz (Melt)

$2K_2(Mg,Fe)_2(OH)_2(AlSi_3O_{10}) + (Ca,Na)AlSi_3O_8$
Biotite Plagioclase

This reaction was suggested by Harley (1988) for the Rauer Group, East Antarctica. The Antarctica granulites also have plagioclase moats that separated the garnets from the orthopyroxenes. A symplectic intergrowth of orthopyroxene and plagioclase observed in the East Antarctic rocks was not observed in this study.

Garnet occurs in all thin sections from outcrops 1475 and 2401 (Plate IX) ranging in size from <1 mm to 8 mm x 8 mm. Garnets are poikiloblastic and fractured (with inclusions of quartz, plagioclase, biotite, K-feldspar, and even hercynite (outcrop 2401)). Commonly the borders are embayed with biotite + quartz + oxides, and have partial retrograde coronas of biotite.

Biotite occurs both as rims and inclusions on orthopyroxene and garnet porphyroblasts. It is also the dominant mineral within the melanosomes of outcrop 2401 where the resultant texture is lepidoblastic.

Plagioclase is the principal groundmass mineral of the leucosomes in outcrop 1475, whereas, in outcrop 2401 it occurs primarily as moats between garnet and orthopyroxene. In both outcrops, the plagioclase has minor alteration to biotite along twin planes.

Outcrop 1659 also contained the plagioclase-garnet-orthopyroxene-quartz assemblage. However, sillimanite and cordierite are present in this outcrop, therefore, it is described in the cordierite assemblage section.

3.6 Kornerupine-bearing Assemblages

Kornerupine occurs in outcrops 1654 (Plates XIX, XX, XXI) and 3832 (Plate XXII). In thin sections from 1654 (Plate XXI), it is closely associated with orthopyroxene, tourmaline, phlogopite, cordierite, quartz and plagioclase; and it closely resembles apatite (both in hand specimen and thin section). In places, the kornerupine contains tourmaline, orthopyroxene and quartz inclusions. In outcrop, it typically appears as sea green prisms up to 2 mm x 15 mm in size. In thin section this kornerupine is colourless and uniaxial positive with low birefringence. Pods up to 15 cm x 4 cm in size contain this assemblage and have their long axis in the foliation plane of this white quartzo-feldspathic gneiss. This implies that these pods formed, or were aligned, during the deformation that formed the foliation.

One possible kornerupine-producing reaction involves the breakdown of tourmaline (source of boron for kornerupine-formation):

(3-22) $NaMg_3B_3Al_3(OH)_4(Al_3Si_6O_{27}) + 3MgSiO_3 + Mg_2Al_3(AlSi_5)O_{18}$
Tourmaline Orthopyroxene Cordierite

$+ O_2 = Mg_8Al_9B_3Si_7O_{40} + NaAlSi_3O_8 + 4H_2O + 4SiO_2$
Kornerupine Plagioclase

This reaction is possible because kornerupine has been observed to contain inclusions of both orthopyroxene and tourmaline, and cordierite is also frequently closely associated with kornerupine.

Reaction (22) is very similar to that suggested by Waters and Moore (1985) in their study of kornerupine-bearing gneisses in Namaqualand, South Africa. There the kornerupine occurs as coarse intergrowths with orthopyroxene and as idioblastic prisms in phlogopite. The South African kornerupine also contained tourmaline inclusions. One reaction suggested by Waters and Moore (1985) was:

(3-23) Tourmaline + cordierite + spinel + orthopyroxene = kornerupine + plagioclase

Spinel was not observed in either outcrop 1654 or 3832, however, it was not necessary to balance the reaction suggested by the textures in the thin sections from outcrop 1654. The isopleths for kornerupine-bearing reactions have not been well established in P-T space, however, the presence of this kornerupine-bearing assemblages does suggest temperatures greater than 740°C and pressures above 46 MPa (Waters and Moore 1985).

An X-ray diffraction analysis of a blue mineral separate from outcrop 3832 determined that kornerupine is also present at this outcrop (Plate XXII), however it was not observed visually (Plate XI). In thin section, this kornerupine is pleochroic blue-salmon pink with low birefringence. Here, it closely resembles sapphirine, except that the kornerupine is uniaxial positive. This assemblage is very different from that at outcrop 1654. In these thin sections, there is no evidence of tourmaline or orthopyroxene. Here the kornerupine is closely associated with biotite and garnet. The typical assemblage is: garnet + biotite + kornerupine + quartz + plagioclase + K-feldspar + oxides.

Outcrop 3832 is migmatitic with compositional layering (Plate XI). Kornerupine occurs with biotite in plagioclase and quartz in the leucosomes. This suggests that the plagioclase + quartz likely formed around the kornerupine from a melt produced by a biotite-consuming reaction. It is likely that the kornerupine formed from a tourmaline-consuming reaction, possibly at the same time as the biotite-consuming reaction formed the melt to

produce the plagioclase + quartz leucosomes, however, there is no evidence preserved in this sample for such a reaction.

3.7 Kyanite

Kyanite was not observed in any thin section, however because first generation sillimanite typically occurs as large blades and is concentrated in macroscopic domains, it is suggested that such sillimanite may represent pseudomorphs after kyanite. Thus, it is possible that the prograde P-T-t path may lie in part in the kyanite stability field. Thus, the peak metamorphic pressure could actually have been above 90 MPa at 850°C (and not below as suggested by the presence of only sillimanite).

3.8 Summary

3.8a Bondy Gneiss Complex

The P-T-t trajectory suggested by the assemblages from the Bondy Gneiss Complex (BGC) is contained in Figure 3-VIII. Peak metamorphic pressures above 90 MPa are suggested by the possible presence of the two discontinuous reactions (3-15) and (3-16) of Carrington and Harley (1995). The presence of spinel produced from reaction (3-5) and the omnipresence of biotite which suggests that the biotite-dehydration reactions did not continue to completion (Vielzeuf and Montel 1994) limits the maximum temperatures to between 920 and 980°C.

Cordierite is not observed in contact with spinel, suggesting that reaction (16) from Figure 3-VIII was not involved in the retrograde path. Cordierite is only in contact with primary orthopyroxene suggesting that reaction (10) from Figure 3-VIII was not crossed during the retrograde path. This limits the pressure to above 30 MPa at 920 to 700°C. Tiny garnet fragments are located in cordierite (thin section 1659F2) suggesting that reaction (3-19) from Figure 3-VIII was crossed, implying pressure below 60 MPa somewhere between 900 and 780°C during retrogression.

3.8b Nominingue-Chénéville Deformation Zone

It is likely that the Bondy Gneiss Complex and the Nominingue-Chénéville Deformation Zone (NCDZ) experienced similar prograde P-T-t conditions. Thus, even though no spinel, cordierite or orthopyroxene was observed in thin sections from the NCDZ, a prograde trajectory similar in form to that of the Bandy Gneiss Complex is assumed (Figure 3-VIII).

The BGC has not been deformed after the emplacement of the 1165 Ma magmas along the NCDZ, whereas the NCDZ was, implying that the NCDZ experienced retrograde conditions different from those of the BGC. Muscovite is observed in several thin sections from the NCDZ (Chapter 3). It is not observed in thin sections from the BGC. This suggests that fluids (not present in the BGC) may have been channelled through the deformation zone that allowed the reactions to produce muscovite during cooling.

The absence of observed cordierite in the NCDZ suggests that the retrograde conditions were nearly isobaric above reaction (14) on Figure 3-IX at least to 58 MPa at 780°C. Muscovite is not observed in contact with K-feldspar suggesting that reaction (3) (Figure 3-IX) likely was not crossed, limiting the retrograde conditions to below 50 MPa at 725°C Thus, due to the observed assemblages, it is proposed that the retrograde pressures in the NCDZ may have been 10 to 20 MPa higher than in the BGC (Figures 3-3-VIII, 3-IX).

CHAPTER 4

ANALYTICAL RESULTS

4.1 Purpose and Outline

This chapter contains the results from the microprobe analyses. The primary purpose of this data is to use it in the various geothermobarometers in order to obtain pressures and temperatures with which to construct the P-T-t trajectories (Chapter 5 and 6). The analyses of transects across minerals are necessary to determine the existence, magnitude, and affects of post-peak metamorphic diffusion.

Figure 4-I is a map, showing the location of individual samples for which microprobe data were obtained. Tables 4-I through 4-XII contain the analyses of the minerals. The effects of retrograde cation exchange on the garnets are shown in Figures 4-VIII through 4-XXII. Figures 4-XXIII through 4-XXX contain the AFM projections for several samples. The tables of mineral analyses and the AFM projections both demonstrate a Mg-enrichment in the Bondy Gneiss Complex when compared to the Nominingue-Chénéville Deformation Zone. Several reactions suggested by the assemblages (Chapter 3) are also reinforced by the AFM (ASF) projections.

4.2 Sample Selection

Seventeen samples from across the field area were chosen for microprobe analyses (Figure 4-I). These samples represent each of the main mineral assemblages and were chosen in order to construct a thermobarometric transect across the field area (Chapter 5). Three samples (1280, 3302 and 3832) were chosen because they contain monazite, zircon and rutile suitable for the geochronological part of the study (Chapter 6).

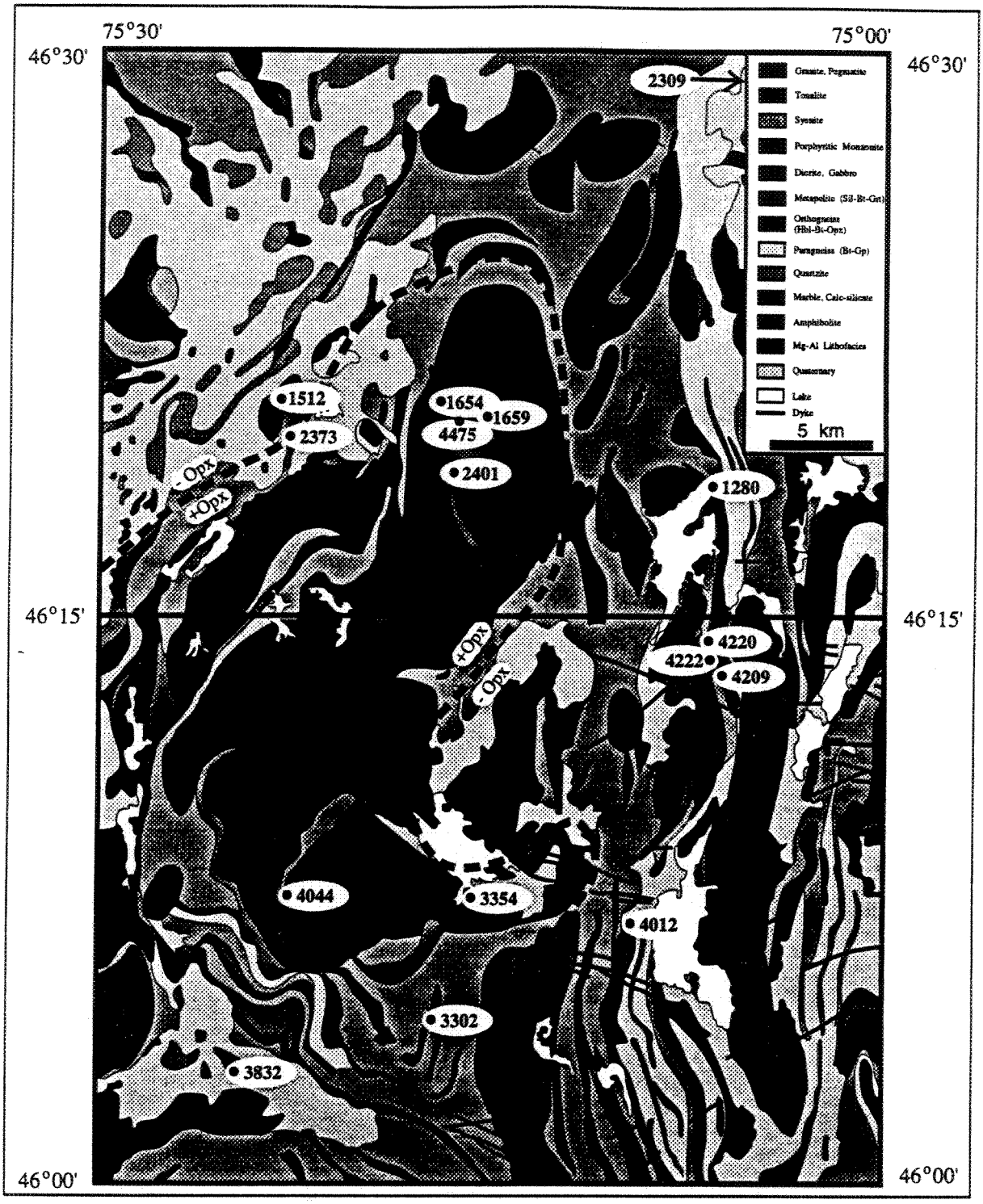

Figure 4-I: Geological map of field area with outcrops from which samples were analyzed by microprobe (simplified after Figure 2-I; after Corriveau et al, 1994).

4.3 Analytical Conditions

The ARL-SEMQ II electron microprobe at the Université du Québec à Chicoutimi was used to obtain mineral compositions. This machine is equipped with a NORAN energy detector with a berillium window giving a resolution of 143 eV. The microprobe is controlled by the quantitative microanalysis system TN-5500: Series II from NORAN. The analytical results of silicates were corrected using the Bence-Albee matrix corrections.

The diameter of the beam is approximately 5 microns which restrains the analyzed surface to a grain size of about 8 microns. An accelerating voltage of 15 kV was used, with a electron beam current of 10 nA. Counts for each element (oxide) were made for 100 seconds. The program MICROQ was used to reduce the analyses to weight percent oxides.

4.4 Consistency of Microprobe Data, Sources of Error

There are two principal types of errors in microprobe analysis:

1. a variation from day to day caused by small variation in the standardizing procedure and
2. a drift during use, due principally to variations in current supply

To assess these errors, one spot on a garnet of sample 2401D2 was chosen as a test site. The same spot was analysed each day, and ten times one day. The means, standard deviation and coefficient of variation were calculated for each oxide. For the 5 main oxides in this garnet (SiO_2, Al_2O_3, FeO, MgO, CaO), the coefficients of variation were less than 3.6% of the oxide concentration for both the day to day consistency, and the consistency during a day. For iron, the coefficient of variation was 0.7% over one day, and 1.8% over the ten days of analysis. The coefficients of variation for magnesium were slightly higher at 1.8% for one day's analysis, and 3.3% for the ten days of microprobe analysis. The 17.7% for manganese is disproportionately high due to the low abundance of manganese present in the test site. For an oxide concentration under 2%, any small variation would result in high

standard deviation and coefficient of variation values which are not representative of the overall accuracy obtained for the oxide analyses.

4.5 Corrections of Systematic Errors in Microprobe Data

Two methods have been used to correct for the two sources of error discussed in section 4.2, recalculation of stoichiometric values by the use of; a) plagioclase analyses and, b) repetitive standard analyses. When present, plagioclase was analysed to provide a control for the calibration of silicon and aluminium during microprobe standardisation. Because of the coupled substitution between silicon and aluminium, and calcium and sodium, it is possible to predict the silicon and aluminium content from the mole fraction of anorthite. These correction values were applied to the weight percent oxides analysed by the microprobe before the stoichiometric values were calculated.

4.5a Plagioclase Correction

Figure 4-II shows the analysis of plagioclase from point 15 of sample 1280. The plot indicates that the calcium and sodium contents both gave the same mole fraction An_{48}, this suggests that the calibration values for Ca and Na are correct and hence their correction factors are 1.00. However, the silica value needed to be lowered by a factor of 0.996 to obtain an An value of 0.48 from the measured value; and the alumina value needed to be raised by a factor of 1.006. These correction factors were then applied to the other minerals measured during the same time interval.

4.5b Standard Correction

For the analysis of sample 1659, repetitive analysis of known garnet standards were used to correct the measured results without readjusting the microprobe standardisation file. The known standard values were divided by the measured values to obtain a correction factor for each oxide measurement. These correction factors were then applied to the mineral

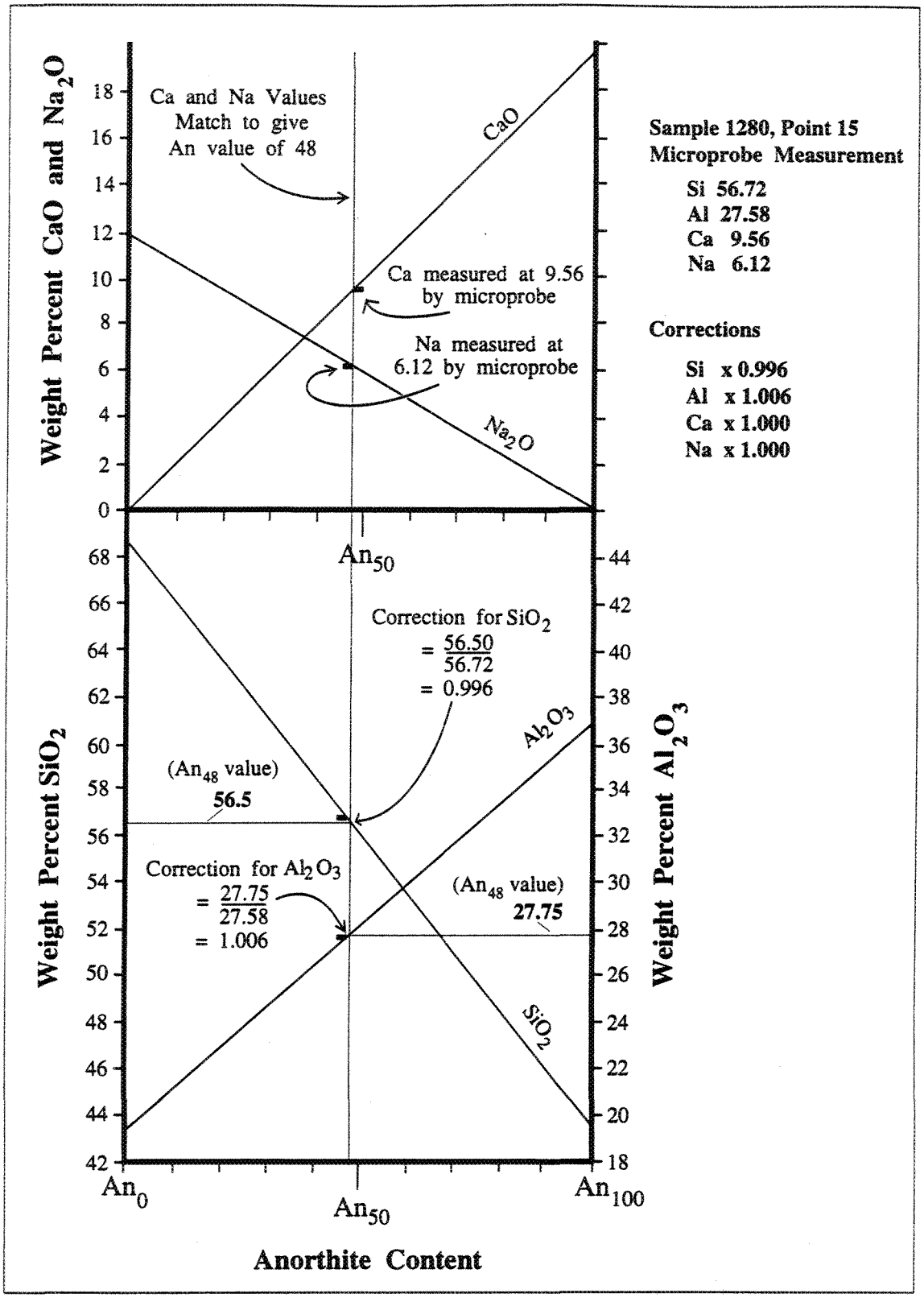

Figure 4-II: Demonstration of the plagioclase correction for microprobe data.

analyses that were made closest in time to that particular standard. Other phases were also corrected using these correction factors.

4.6 Criteria for Accepting Microprobe Analysis

Geothermobarometers are sensitive to small changes in the oxide analysis and would thus be susceptible to inconsistencies if the analysis were unreliable. Thus the choice of reliable mineral analysis is important in the determination of pressure and temperature from geothermobarometers.

To start with, the totals were examined. For anhydrous minerals, if the totals were not between 99.0% and 101.0%, the analysis was rejected. For biotites and cordierites, if the totals were not between 95.0% and 97.0%, the analyses were rejected.

For anhydrous minerals, the site occupancy was calculated to determine the analysis reliability further. For example, the accepted values for the three site occupancies in garnets are 3.0 for silica, 2.0 for aluminium and 3.0 for the M1 site (Fe + Mg + Mn + Ca). The acceptable relative error values would be equivalent to the coefficient of variance: $\pm$ 2.0% for silicon; $\pm$ 2.0% for aluminium, $\pm$ 2.1% for iron, $\pm$ 3.6% for magnesium and $\pm$ 3.3% for calcium.

4.7 Mineral Chemistry

4.7a.i. Plagioclase

The plagioclase analyses from 8 different samples throughout the study area (Table 4-I) range in mole fraction anorthite content from 0.25 to 0.88 (mostly within the labradorite range with one value in the oligoclase range and one value in the bytownite range), with a median value of 0.58 (labradorite). The plagioclase analysis from sample 4012 had an anomalously high value of anorthite at An_{88}, more than 20 mol percent An higher than other plagioclase analyses within the study area. Conversely, the plagioclase analysis from sample 3302 had an anomalously low value of An_{25}, more than 30 mol percent An lower that other

Table 4-I: Plagioclase Analyses

Sample	SiO2	Al2O3	CaO	Na2O	Total	XAn	NCDZ XAn	BGC XAn
1280-7	56.97	27.41	9.526	6.398	100.3	0.622	0.622	
8	57.71	27.01	8.66	6.65	100	0.59	0.59	
34	58.92	25.53	7.897	7.198	99.55	0.548	0.548	
44	57.45	27.11	8.999	6.479	100	0.606	0.606	
45	57.49	27.11	8.998	6.602	100.2	0.601	0.601	
46	57.3	27.22	9.06	6.438	100	0.609	0.609	
15	56.55	27.77	9.56	6.12	100	0.633	0.633	
2039-41	57.29	27.3	8.696	6.502	99.78	0.596	0.596	
42	56.43	27.89	9.69	5.98	99.98	0.642	0.642	
53	56.38	27.9	9.61	5.93	99.81	0.642	0.642	
2401-53	56.41	27.8	9.65	5.96	99.82	0.642		0.642
54	56.47	27.8	9.6	6.01	99.89	0.638		0.638
3045-23	55.59	28.39	10.43	5.69	100.1	0.503	0.503	
28	53.15	29.91	12.23	4.61	99.9	0.594	0.594	
25	55.09	28.76	10.71	5.44	100	0.521	0.521	
26	55.58	28.41	10.4	5.601	100	0.506	0.506	
27	53.92	29.41	11.6	5.001	99.94	0.562	0.562	
59	53.66	29.69	11.8	4.9	100.1	0.571	0.571	
61	53.42	29.79	11.87	4.9	99.98	0.572	0.572	
3302-64	61.76	24.01	5.277	8.688	99.73	0.251		0.251
4012-74	46.11	34.93	18.04	1.313	100.4	0.884		0.884
4209-25	58.88	26.2	7.88	7.19	100.1	0.548	0.548	
26	58.59	26.12	7.87	7.24	99.82	0.546	0.546	
27	58.89	26.21	7.802	7.2	100.1	0.545	0.545	
29	58.67	26.41	8.001	7.102	100.2	0.555	0.555	
30	58.92	26.2	8.02	7.24	100.4	0.55	0.55	
31	59.12	25.99	7.68	7.29	100.1	0.538	0.538	

Note that in these tables, elements not represented are below detection level (bdl)

plagioclase analyses. The physical appearance of these plagioclases and the minerals that they are associated with, does not show any obvious explanation for their anomalous compositions. However, outcrops 3302 and 4012 are located along the edges of the Bondy Gneiss Complex which Corriveau et al. (1995) proposed to be hydrothermally altered. It is possible these unusual compositions could be a result of that hydrothermal alteration (i.e. sodium depletion). The mole fraction anorthite from the Nominingue-Chénéville Deformation Zone samples range from 0.51 to 0.64 (labradorite) with an average of 0.58.

There were no consistent zoning patterns observed in the plagioclase. In most cases, such as samples 1280 and 2401D2 (Plate IX), the plagioclase grains were too small to analyse multiple times in order to test for zoning. Many of these plagioclase grain analyses such as points 44, 45, 46 of sample 1280 were inclusions (0.05 mm x 0.05 to 0.11 mm x 0.27 mm) within garnet. However, samples 3045 and 4209 (Plate XVI) both contained plagioclase grains large enough for multiple analyses. The 5 analyses from a transect across the plagioclase grain in sample 3045 varied non-systematically in mole fraction anorthite from 0.50 to 0.59; whereas the 6-point transect across the plagioclase porphyroblast in sample 4209 only ranged from 0.53 to 0.55. Thus, where present, the zoning of plagioclase, appears to be patchy or irregular.

4.7a.ii. Alkali-feldspar

The alkali-feldspar analyses are contained within Table 4-II. The orthoclase/sanidine mole fraction values for these 24 analyses from 4 samples range from $Or_{70}Ab_{17}An_{13}$ to $Or_{89}Ab_{11}An_{0}$ with an average value of $Or_{85}Ab_{12}An_{3}$. The two analyses (2401D-52; 3302-65) which represent the extremes of the alkali-feldspar compositions are both from within the Bondy Gneiss Complex. The 5 analyses from 2 samples within the Nominingue-Chénéville Deformation Zone have orthoclase/sanidine mole fractions that range from $Or_{86}Ab_{11}An_{3}$ to $Or_{89}Ab_{8}An_{3}$.

Table 4-II: K-feldspar Analyses

Sample	SiO2	Al2O3	CaO	Na2O	K2O	Total	XOr	XAb	XAn	BGC K2O	NCDZ K2O
1280-40	64.1	19	0.26	1.23	14.7	99.31	0.86	0.11	0.03		14.7
53	64.1	18.6	0.11	1.32	14.6	98.7	0.87	0.12	0.01		14.6
54	64.3	18.7	0.25	1.27	14.8	99.36	0.86	0.11	0.02		14.8
55	64.3	18.8	0.21	1.1	14.9	99.4	0.88	0.1	0.02		14.9
2401D38	64.9	18.8	0.19	1.65	14.9	100.4	0.84	0.14	0.02	14.9	
39	65	18.5	0.36	1.76	14.5	100.1	0.82	0.15	0.03	14.5	
41	64.7	18.9	0.14	1.66	14.7	100.1	0.84	0.14	0.01	14.7	
42	64.7	19.1	0.24	1.06	15.4	100.5	0.88	0.09	0.02	15.4	
43	64.6	18.7	0.19	1.37	15	99.81	0.86	0.12	0.02	15	
44	64.1	19	0.23	1.39	15	99.67	0.86	0.12	0.02	15	
44	64	20.1	0.22	1.39	15	100.8	0.86	0.12	0.02	15	
45	65.2	18.8	0.25	1.72	14.6	100.6	0.83	0.15	0.02	14.6	
46	64.7	18.9	0.39	1.98	13.9	99.95	0.79	0.17	0.04	13.9	
47	64.6	18.8	0.25	1.43	15.1	100.1	0.85	0.12	0.02	15.1	
48	64.3	18.9	0.15	1.52	14.9	99.7	0.85	0.13	0.01	14.9	
49	65.1	18.7	0.08	1.36	15.3	100.5	0.87	0.12	0.01	15.3	
50	64.5	19	0	1.58	15.2	100.3	0.86	0.14	0	15.2	
51	65	18.9	0.34	1.43	14.9	100.6	0.84	0.12	0.03	14.9	
52	63.7	20	1.48	2.07	13	100.1	0.7	0.17	0.13	13	
55	64.4	19.1	0.1	1.3	15.1	100.1	0.88	0.11	0.01	15.1	
3302-65	63.9	19.5	0	1.14	14.7	99.17	0.89	0.11	0	14.7	
66	63.7	19.3	0.41	1.16	14.7	99.26	0.86	0.1	0.04	14.7	
68	63.8	19.4	0.32	1.25	14.4	99.26	0.86	0.11	0.03	14.4	
4220-5	64.7	18.2	0.3	0.94	15.2	99.37	0.89	0.08	0.03		15.2

Elements not shown are below detection level

The mole fraction albite in the K-feldspar ranges from Ab_8 (point 5 sample 4220) to Ab17 (point 46 sample 2401D2), the anorthite content up to An_{13} (point 52, sample 2401D2). These ternary alkali feldspars were sanidines before exsolution.

Perthitic exsolution textures in alkali-feldspar were observed in several thin sections (Appendix A); e.g., 1280 from within the Nominingue-Chénéville Deformation Zone. The four analyses from this sample do not provide evidence for exsolution as the orthoclase values only vary from Or_{86} Ab_{11} An_3 to Or_{88} Ab_{10} An_2. However, the grains from this sample were all too small (0.05 mm x 0.05 mm) to analyse a transect. In contrast, the seven analyses from matrix K-feldspar of sample 2401D2, from the Bondy Gneiss Complex, do demonstrate exsolution. These analyses show a range from Or_{70} Ab_{17} An_{13} to Or_{88} Ab_{11} An_1, a difference of 18% Or which is likely due to exsolution of a sodic plagioclase from the initial, homogeneous ternary feldspar. Samples 2401D2 and 2401E both contained alkali-feldspar grains as inclusions within garnet porphyroblasts.

4.7b Calcite

Calcite was only observed and analysed in two metapelitic samples, sample 1280 and 2039 (see Table 4-III), both of which were located within the Nominingue-Chénéville Deformation Zone. The mole percent calcite varied from 0.90 to 1.00, rhodochrosite up to 0.03, ankerite up to 0.03, and dolomite up to 0.06. The CO_2 content (calculated by subtracting the totals of the weight percent oxides from 100%) ranged from 36.6% to 45.4%.

4.7c Quartz

The quartz analyses are contained within Table 4-IV. The 16 analyses from 3 samples consist of mostly pure silica containing < 1% weight oxide impurities. Typically, TiO_2 is < 0.14%, Al_2O_3 is < 0.08%, FeO is < 0.5%, MgO is < 0.12%, MnO is < 0.22% and CaO is < 0.08%. These can be attributed to analytical "noise".

Table 4-III: Analyses of Carbonate Minerals

Sample	CaO	MnO	FeO	MgO	Total	CO2	XCc	XRds	XAnk	XDol
1280-24	55.8	0	0.25	0	56.1	43.9	1	0	0	0
28	55.9	0	0	0.07	55.9	44.1	1	0	0	0
2039-54	57	0.19	0	0	57.2	42.8	1	0	0	0
55	56.6	1.95	2.19	2.64	63.4	36.6	0.89	0.03	0.03	0.04
56	49.2	1.78	1.62	1.96	54.6	45.4	0.9	0.03	0.03	0.04

Elements not represented here were below detection level

Table 4-IV: Quartz Analyses

Sample	SiO2	TiO2	Al2O3	FeO	MgO	MnO	CaO	Total
1280-32	100.6			0.22	0.08		0.08	101
36	99.05			0.39	0.12			99.56
50	101.1				0.07			101.1
28	100.1					0.08		100.2
10	100.3							100.3
18	100.8			0.21				101.1
19	100.1			0.38				100.5
20	100.2	0.08		0.27		0.22		100.8
2401-8	99.06	0.14	0.08			0.12		99.4
2	100.1			0.2				100.3
4220-6	99.95							99.95
75	99.96			0.47				100.4
78	99.76							99.76
79	99.8							99.8
80	99.57							99.57
81	99.41	0.14						99.55

Elements not represented are bdl

4.7d Cordierite

The 27 analyses of cordierite from sample 1659 (Plate XVIII) in the Bondy Gneiss Complex are given in Table 4-V. The SiO_2 values range from 48.1% to 49.7% (average 49.0%), Al_2O_3 from 32.8% to 33.8% (average 33.3%), and the Fe/(Fe+Mg) ratio from 0.12 to 0.17 (average 0.15). The transects across these two cordierite grains produced erratic or patchy zoning profiles. However, as the contact with garnet was approached, the X_{Mg} of cordierite changed from 0.408 to 0.414 while the X_{Fe} changed from 0.066 to 0.077 gradually over a distance of 0.75 mm (see Figure 4-III).

4.7e Orthopyroxene

The 16 analyses of orthopyroxene from sample 1659 (Plates II, III) in the Bondy Gneiss Complex are given in Table 4-VI. The SiO_2 values range from 46.7% to 49.3% (average 48.7%), Al_2O_3 from 5.5% to 7.7% (average 6.5%), $TiO_2 < 0.7\%$, FeO from 20.4% to 25.9% (average 22.5%) and MgO from 20.6% to 23.3% (average 21.7%). The Fe/(Fe+Mg) ratios range from 0.33 to 0.41 (hypersthene) with an average of 0.37. The points number 22 through 27 (Table 4-VI) describe a partial transect from the core towards the rim of the large orthopyroxene crystal. As can be seen from Figure 4-IV, the resultant zoning profile is flat. However, as can be seen from Table 4-VI, the Fe/(Fe+Mg) values do vary 0.08 from 0.33 for point 27 (adjacent to a garnet inclusion) to 0.41 for point 17 (core of the orthopyroxene). This variation suggests patchy irregular zoning within the orthopyroxene, possibly due to adjacent ferromagnesian minerals.

4.7f Spinel

The 6 analyses of spinel from sample 2401D2 (Plate IX) from the Bondy Gneiss Complex are given within Table 4-VII. The weight percent Al_2O_3 ranges from 59.2% to 62.9% (average 61.6%), FeO from 22.6% to 26.0% (average 24.5%), MgO from 7.3% to 9.8% (average 8.7%), ZnO from 3.0% to 7.9% (average 5.2%), MnO <0.2%, CoO <0.2%,

Table 4-V: Cordierite Analyses

Sample	SiO2	Al2O3	FeO	MgO	Total	XFe	XMg
1659-30	48.1	33.32	3.181	10.59	95.18	0.144	0.856
31	48.32	33	3.355	10.42	95.1	0.153	0.847
33	48.85	33	3.437	10.37	95.65	0.157	0.843
34	48.39	33.43	3.375	10.61	95.8	0.151	0.849
36	48.42	33.21	3.776	10.57	95.98	0.167	0.833
38	48.84	32.93	3.396	10.19	95.35	0.158	0.842
39	48.37	32.8	3.725	10.49	95.39	0.166	0.834
40	48.55	33.05	3.313	10.56	95.48	0.15	0.85
41	48.22	33.08	3.488	10.55	95.35	0.156	0.844
72	49.1	33.71	3.338	10.65	96.8	0.15	0.85
73	49.1	33.33	3.453	10.65	96.53	0.154	0.846
74	49.3	33.59	3.39	10.31	96.59	0.156	0.844
77	49.4	33.54	3.297	10.48	96.71	0.15	0.85
31	49.62	33.43	2.932	10.56	96.55	0.135	0.865
7	49.31	33.33	2.286	10.73	95.66	0.107	0.893
13	49.67	33.5	2.829	10.49	96.5	0.131	0.869
15	49.34	33.77	2.665	10.62	96.4	0.123	0.877
10	49.22	33.49	3.024	10.18	95.92	0.143	0.857
22	49.27	33.42	2.942	10.17	95.8	0.14	0.86
23	49.13	33.33	3.116	10.31	95.89	0.145	0.855
24	49.67	33.41	3.516	10.2	96.79	0.162	0.838
25	49.17	33.59	3.383	10.45	96.59	0.154	0.846
27	49.07	33.25	3.27	10.23	95.83	0.152	0.848
28	49.28	33.6	2.952	10.14	95.98	0.14	0.86
29	48.91	33.25	3.075	10.24	95.48	0.144	0.856
30	48.97	33.26	3.454	10.16	95.85	0.16	0.84
66	48.66	33.46	2.707	11.07	95.89	0.121	0.879

Other elements bdl

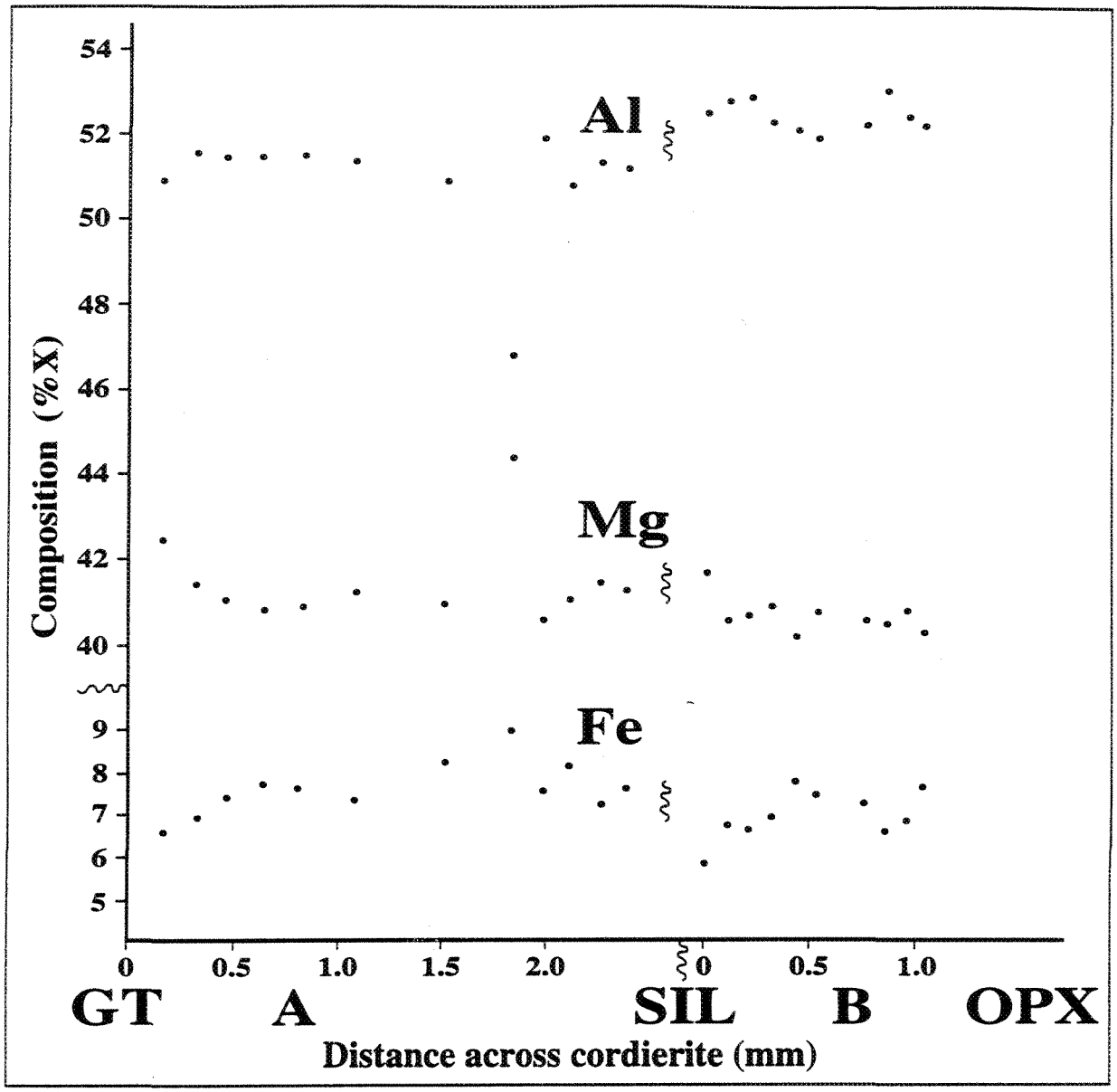

Figure 4-III: Profile across cordierite (A) from garnet to sillimanite and (B) from sillimanite to coridierite. There is no regular trend from the core to rim for cordierite, however, when the transects approached garnet, the iron content decreased 1.3% from 7.8 to 6.5 over 0.7 mm from the rim of the garnet. The magnesium content increased over this same interval 1.7% from 40.8 to 42.5. There were no obvious trends when the transects approached the sillimanite or the orthopyroxene. Other than near garnet, zoning within cordierite appears to be patchy with no regular trends.

Table 4-VI: Orthopyroxene Analyses

S	SiO2	Al2O3	TiO2	FeO	MgO	Total	XFe	XMg
1659-9	48.33	6.546	0.11	23.63	20.56	99.17	0.392	0.608
12	47.46	6.285	0.13	24.37	20.59	98.83	0.399	0.601
22	49.1	7.328	0	20.83	22.54	99.8	0.341	0.659
23	48.81	7.661	0	20.44	22.25	99.15	0.34	0.66
24	49.15	7.5	0.11	21.37	22.18	100.3	0.351	0.649
25	48.81	7.59	0	21.02	22.33	99.75	0.346	0.654
26	49.03	6.784	0.12	20.72	22.32	98.98	0.343	0.657
27	49.87	6.149	0	20.58	23.29	99.88	0.332	0.668
17	47.58	6.209	0	24.06	21.17	99.01	0.389	0.611
8	47.93	6.623	0	23.49	20.83	98.88	0.388	0.612
17	46.67	5.594	0.65	25.9	20.8	99.62	0.411	0.589
34	49.11	5.709	0	22.56	21.77	99.14	0.368	0.632
37	49.32	5.658	0	21.64	22.27	98.89	0.353	0.647
38	49.35	5.504	0.08	21.84	21.98	98.75	0.358	0.642
76	48.61	6.386	0	23.54	20.68	99.21	0.39	0.61
78	49.21	6.376	0	23.31	21.03	99.92	0.383	0.617

Other elements bdl

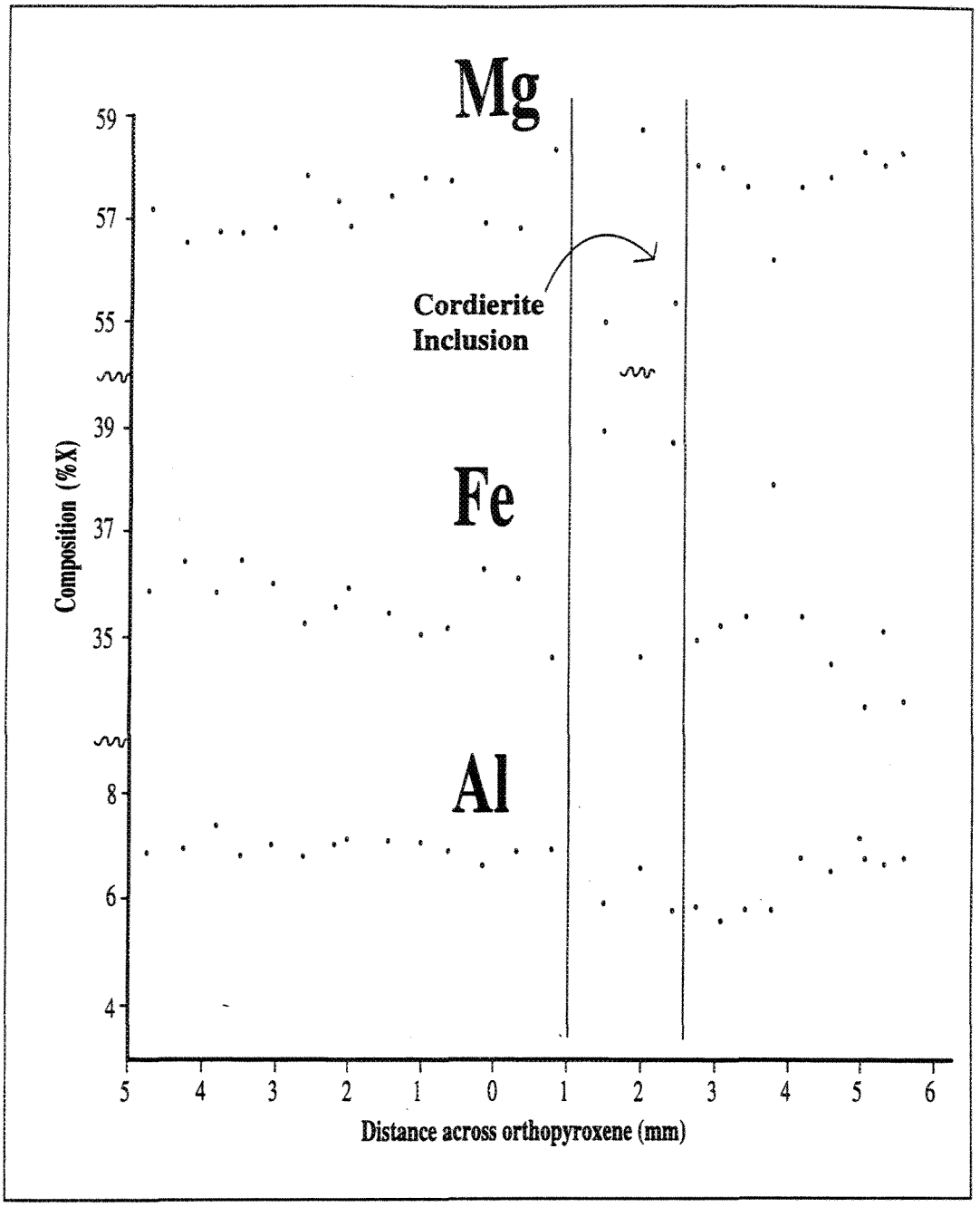

Figure 4-IV: Profile across orthopyroxene crystal from cordierite to cordierite. There is no regular trend from the core out towards the rim. The Al content remains homogenous (within <1%) throughout the profile. The profile passed near an inclusion of cordierite, where the iron content increased 4%, and the magnesium content decreased 4%.

Table 4-VII: Spinel Analyses

Sample	SiO2	Al2O3	FeO	MgO	CoO	ZnO	Total		XFe	XMg	XZN
2401D2											
59	0	62.3	22.6	9.66	0	5.04	99.6		0.51	0.39	0.1
65	0	62	24.6	8.59	0	4.44	99.7		0.56	0.35	0.09
67	0.68	61.3	22.6	7.68	0.17	6.63	99		0.54	0.33	0.14
71	0	62.1	25.9	9.84	0	2.96	101		0.56	0.38	0.06
50	0	62.9	25.1	8.84	0	4.31	101		0.56	0.35	0.09
32	0.14	59.2	26	7.38	0	7.91	101		0.56	0.29	0.15

elements not represented are bdl

TABLE 4-VIIa: Compilation of Spinel Analyses From the Literature

Sample	Fe	Mg	Zn	Total	XFe	XMg	XZn
Dietvorst							
SP1a	14	1.38	27.1	42.4	0.33	0.03	0.64
SP1b	20	1.73	19.8	41.5	0.48	0.04	0.48
SP2a	12.9	1.8	27.1	41.8	0.31	0.04	0.65
SP2b	13.4	2.14	26	41.5	0.32	0.05	0.63
SP3a	9.16	1	32.8	42.9	0.21	0.02	0.76
SP3b	15.9	1.71	24.6	42.3	0.38	0.04	0.58
SP4c	10.1	2.87	29.1	42	0.24	0.07	0.69
SP4d	6.08	1.86	33.9	41.8	0.15	0.04	0.81
SP5a	11.4	1.81	28.6	41.8	0.27	0.04	0.68
SP5b	8.74	1.76	31.7	42.2	0.21	0.04	0.75
A&G							
188	9.99	15.1	8.51	33.6	0.3	0.45	0.25
315a	18.1	15.3	2.68	36	0.5	0.42	0.07
333b	23.4	11.8	1.95	37.1	0.63	0.32	0.05
354a	15	7.26	16.5	38.8	0.39	0.19	0.43
Florence							
92-2C2	1.01	0.1	0.03	1.14	0.89	0.09	0.02
92-2C4	0.89	0.16	0.06	1.11	0.8	0.14	0.05
92-C6	0.92	0.19	0.04	1.14	0.8	0.16	0.03
92-3A	0.68	0.18	0.13	0.99	0.69	0.18	0.13
92-8A	0.88	0.11	0.06	1.04	0.85	0.1	0.05
BD-03b	0.73	0.1	0.18	1.01	0.72	0.1	0.18
Stoddard							
1	20.6	5.9	14.6	41.1	0.5	0.14	0.36
2	24.2	7.44	9.66	41.3	0.59	0.18	0.23
3	18.7	4.44	19.8	42.9	0.44	0.1	0.46
4	33.9	1.59	3.45	38.9	0.87	0.04	0.09

Table 4-VIIa: Compilation of Spinel Analyses From the Literature - continued

5	16.6	2.36	24	43	0.39	0.05	0.56
6	26.4	9.9	1.25	37.5	0.7	0.26	0.03
7	36.1	2.67	7.02	45.7	0.79	0.06	0.15
8	15.7	4.59	21.7	42	0.37	0.11	0.52
S&S							
S&SI-1	9.61	0	32.9	42.6	0.23	0	0.77
2	7.46	0.16	37	44.6	0.17	0	0.83
3	6.41	0.83	35.3	42.5	0.15	0.02	0.83
4	10.9	0	40.5	51.4	0.21	0	0.79
5	5.29	1.14	40.9	47.3	0.11	0.02	0.86
6	5.39	1.54	37.7	44.6	0.12	0.03	0.84
7	5.77	1.16	36.9	43.8	0.13	0.03	0.84
8	5.2	1.66	35.8	42.6	0.12	0.04	0.84
9	7.29	1.76	33.4	42.5	0.17	0.04	0.79
10	7.6	1.93	33	42.5	0.18	0.05	0.78
11	4.39	1.09	40.5	45.9	0.1	0.02	0.88
12	5.19	1.72	35.4	42.3	0.12	0.04	0.84
13	6.06	1.9	36.8	44.8	0.14	0.04	0.82
14	5.89	0.59	35.4	41.8	0.14	0.01	0.85
15	5.45	1.92	35.6	43	0.13	0.04	0.83
16	5.42	1.71	35.6	42.7	0.13	0.04	0.83
S&SII-1	8.37	0.35	33.1	41.8	0.2	0.01	0.79
2	6.81	2.26	32.1	41.2	0.17	0.05	0.78
3	6.65	1.3	35	42.9	0.15	0.03	0.81
4	11.8	3.07	27.1	41.9	0.28	0.07	0.65
5	9.15	8.48	22.7	40.3	0.23	0.21	0.56
6	5.43	23.1	6.98	35.5	0.15	0.65	0.2

and $SiO_2 < 0.7\%$. The mole fractions of these ternary spinels vary from $spinel_{29}$ $hercynite_{56}$ $gahnite_5$ to $spinel_{39}$ $hercynite_{51}$ $gahnite_{10}$ with an average $spinel_{35}$ $hercynite_{55}$ $gahnite_{10}$.

In granulite grade rocks, zinc is partitioned into gahnite (Hand et al. 1994). The addition of zinc causes the KFMASHT invariant reactions to become KFMASHT + Zn divariant fields. An increase of zinc content causes the stability field of spinel to increase (Nichols et al. 1992). With zinc present, the reaction Bt + Als = Spl + Crd will proceed; without zinc only cordierite would be produced (Hand et al. 1994). Therefore, the presence of gahnite is important. The effect of the zinc content on the spinel stability is calculated in Chapter 5.

Figure 4-V contains an FMZ plot of the spinels from the Mont Laurier Region, and various other studies. Florence et al. (1995) have analysed spinels from the western Adirondack Highlands of New York and found mole percentage of gahnite to vary between 0.03 and 0.36 (the lower range is similar to the Mont Laurier Region spinels; Figure 4-V). They observed that the highest Zn contents occurred in the rocks with the highest Mn contents in their garnets. This link could not be investigated in this study, as all of the analysed spinels came from one outcrop. All garnets analysed in this study contain ≤ 0.02 X_{sps}, which is far smaller than the spessartine content in the spinels from the Adirondacks.

Arima and Gower (1990), in their study of osumilite-bearing granulites from the Eastern Grenville Province, Eastern Labrador, found spinels with between 5 and 43 Wt% ZnO. The spinels from this study are similar to those in the lower range of the those from Labrador (Figure 4-V).

Dalziel (1991), Hoffman (1991), Moores (1991), and Young (1992) proposed that a reconstruction of the Grenville Orogeny linked the Grenville Province in North America with Madagascar, western/northern Antarctica (including Dronning Maud Land), eastern India (including Eastern Ghats), and central Australia (including the Albany-Fraser Belt and the

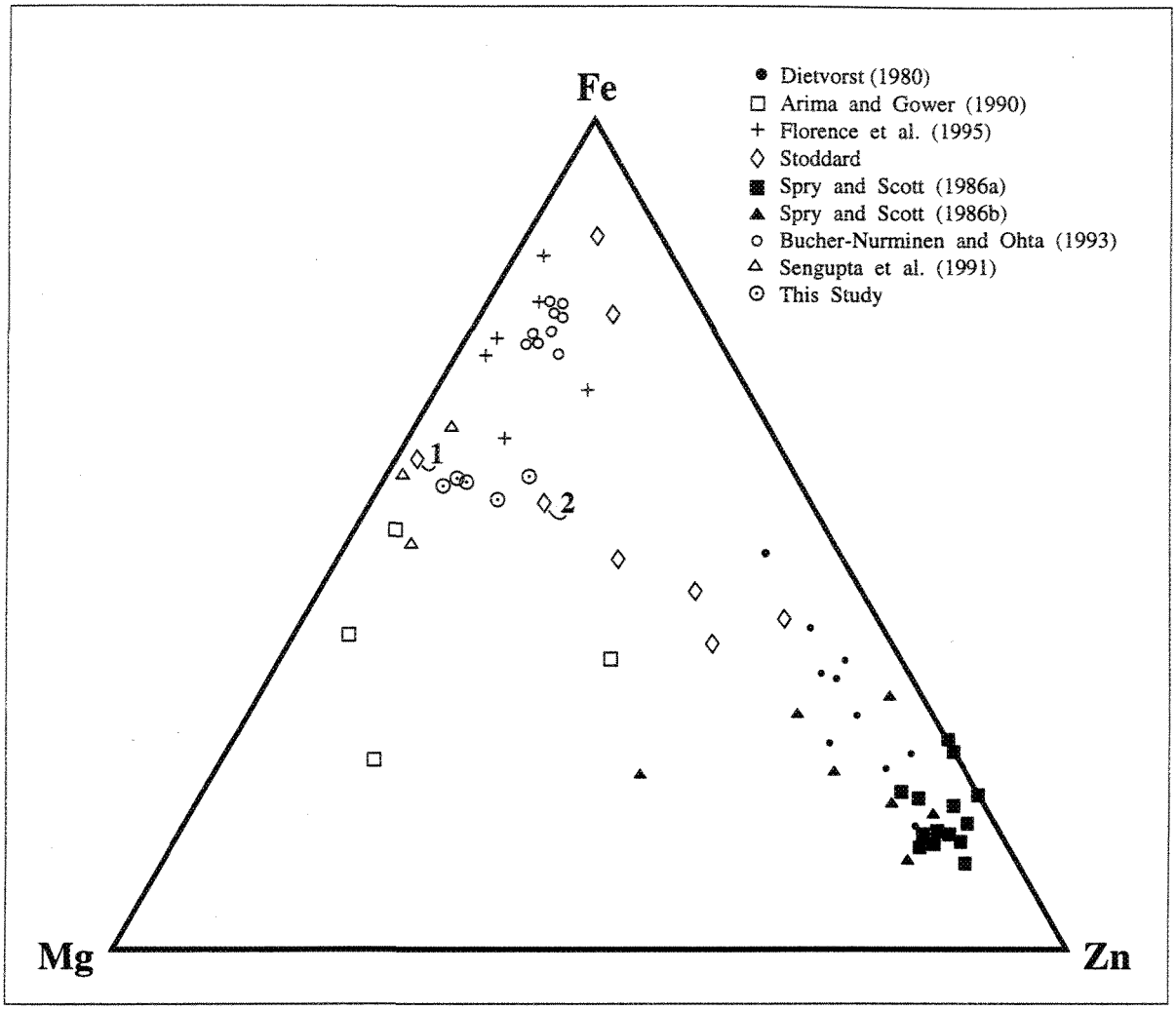

Figure 4-V: FMZ plot of spinel analyses from this study and other literature values from Finland (Dietvorst 1980), Eastern Labrador (Arima and Gower 1990), Adirondack Highlands (Florence et al. 1995; 1 and 2 of Stoddard, 1979), Appalachians and Caledonides (Spry and Scott 1986a), Dronning Maud Land, Antarctica (Bucher-Nurminen and Ohta 1993) and the Eastern Ghats, India (Sengupta et al. 1991). The remaining analyses of Stoddard are from other non Grenville age locations in the U.S., and the analyses of Spry and Scott (1986b) are from non Greville age locations throughout the world. The spinel analyses with similar zinc content as the analyses from the Mont Laurier Region are the ones from the various regions that were linked together with the Grenville Province at 0.8 Ga (Figure 2-VI).

Musgrave Block; Figure 2-VI). Sengupta et al. (1991) analysed spinels from the Eastern Ghats Belt in India, their spinels contain between 0.01 and 0.07 X_{gahn}, which plots near to the spinels from this study (Figure 4-V). A plot of Bucher-Nurminen and Ohta's (1993) spinel data from Dronning Maud Land, Antarctica resulted in a concentration richer in hercynite than the spinels in this study, but with gahnite contents of between five and ten mole% which is similar to the spinels in this study (Figure 4-V). Thus, the spinels from the Mont Laurier region of the Grenville Province are not anomalously rich in zinc in comparison with those from the reconstructed Grenville Province (Figure 4-V).

Spry and Scott (1986a 1986b) and Dietvorst (1980) analysed spinels associated with massive sulphide deposits. Their spinels contain between 43 and 85 mole% gahnite. These spinels are much richer in zinc than the ones from this study (Figure 4-V).

4.7g Sillimanite

Table 4-VIII contains the 19 analyses of sillimanite from four samples. The measured ranges of weight oxides ranged from 36.2% to 37.6% SiO_2 (average 37.0%), from 61.1% to 63.1% Al_2O_3 (average 62.3%), < 0.2% TiO_2, < 1.1% Fe_2O_3, < 0.5% MgO and < 0.1% MnO.

4.7h Ti-Rich Phases

The three analyses from two samples with greater than 50% TiO2 are contained within Table 4-IX. The two ilmenite analyses from sample 4220 contains 53% TiO_2, 45% FeO, < 0.7% SiO_2, < 0.14% Al_2O_3 and < 0.17% CrO. The rutile analysis from sample 4475D2 contains 89% TiO_2, 10% FeO, 0.9% SiO_2, 0.5% Al_2O_3.

4.7i Fe-Oxides and Sulphides

Table 4-X contains the 19 analyses of opaque phases from six samples. The one opaque analysed in sample 2039 was too small for an accurate measurement and was thus contaminated by the surrounding quartz. A second analysis from sample 1280 was poor.

Table 4-VIII: Sillimanite Analyses

Sample	SiO2	Al2O3	TiO2	Fe2O3	MgO	MnO	Total	XFe
2401D2-1	35.99	63.86	0	0.789	0.33	0.09	101	0.012
18	36.02	63.5	0	1.123	0.25	0	100.8	0.017
2	35.99	63.63	0.23	1.056	0.38	0	101.2	0.016
20	35.77	63.57	0	0.878	0.21	0	100.3	0.014
24	35.39	63.28	0	1.034	0.3	0	99.9	0.016
28	35.61	62.32	0.08	0.667	0.31	0	98.92	0.011
12	35.37	62.56	0	0.978	0.23	0	99.03	0.015
33	35.52	62.86	0.08	1.167	0.34	0	99.86	0.018
2770-12	36.42	64.2	0	0.233	0.26	0	101.1	0.004
11	35.95	63.64	0	0.133	0.32	0.14	100.2	0.002
3333-76	37.2	63.01	0	0.449	0	0	100.6	0.007
67	37.3	63.73	0	0	0	0	101	0
61	37.31	63.02	0	0	0	0	100.3	0
62	36.83	63.55	0.12	0	0	0	100.5	0
3832-27	36.76	62.87	0	1.081	0.45	0	101.1	0.017

Other elements bdl

Table 4-IX: Analyses of Ti-rich Minerals

SAmple	SiO2	Al2O3	TiO2	FeO	MgO	CrO	ZnO	Total	ID?
4220-88	0.69	0.14	53.32	45.36	bdl	bdl	bdl	99.51	ILM
85	0.58	bdl	53.35	44.6	bdl	0.17	bdl	98.7	ILM
4475D2-113	0.88	0.53	89.23	9.99	bdl	bdl	bdl	100.6	RUT

Other elements bdl

Table 4-X: Analyses of Fe Oxides and Sulphides

Sample	SiO2	Al2O3	TiO2	FeO	MgO	MnO	CaO	CrO	Total	XFe
2401D-30	10.96	12.15	2.79	64.15	1.6	0	0.1	0.5	92.16	0.704
14	0.57	3.52	0	88.58	0.1	0	0	0.4	93.21	0.963
9	1.09	5.43	0.13	83.62	0.1	0.3	0	0.1	90.72	0.939
17	0.42	0.21	0	74.99	0	0	0	0	75.62	0.991
30	0.45	0.64	0.23	89.63	0.2	0.2	0	0.2	91.62	0.982
31	0.41	0	0	56.96	0.2	0.1	0	0	57.66	0.986
3333-2	2.38	3.68	0	72.32	0.5	0.3	0	0	79.16	0.921
3	0.29	0.17	0	89.4	0	0	0	0	89.86	0.995
4012-25	0.61	0	0	83.31	0	0	0	0	83.92	0.991
4220-10	3.61	3.69	0.21	31.83	0	0	0	0	39.34	0.817
11	14.44	7.68	0.2	39.02	1	0	0.9	0	63.26	0.613
12	4.07	6.25	0	58.42	0	0	0	0	68.74	0.863
17	2.98	4.91	0.18	35.27	0	0	0	0	43.34	0.831

Other elements bdl

The remaining analyses were dominated by iron, measured weight percent FeO was between 31.8 and 89.6. Those analyses with mole percent iron above 70% are likely to be magnetite, less than 70% likely pyrite or pyrrhotite (Table 4-X).

4.7j Biotite

The five representative analyses with total measured weight percent oxides between 95.0% and 97.0% from each of the 17 analysed samples are shown in Table 4-XI. The weight percent measured SiO_2 ranges from 35.6 to 40.8 (average of 38.5), Al_2O_3 from 16.1 to 20.9 (average of 17.8), TiO_2 from 1.0 to 5.1 (average 3.3), FeO from 5.8 to 18.6 (average of 12.4), MgO from 10.2 to 21.6 (average of 16.2) and K_2O from 8.4 to 10.6 (average of 9.8). MnO values are < 0.3%, CaO from 0% < 0.4% and NaO is < 0.5%

The ratio of Mg:Fe, Mg# = Mg/(Mg + Fe) x 100, and %Al = (Al + Ti)/(Al + Ti + Si) x 100 were calculated to identify the species of biotite. The resultant values were plotted in Figure 4-VI which shows that the samples plot within the biotite and phlogopite fields. An interesting point to note is that the analyses from the Nominingue-Chénéville Deformation Zone plot as a well-defined group within the biotite field, except for sample 4012 which plots in the top portion of the phlogopite field. All of the analyses from rocks metamorphosed in the shear zone plot above Fe#68. In contrast, the analyses from the Bondy Gneiss Complex and the southwestern corner of the study area all plot in the phlogopite field. Thus, the biotite from the Bondy Gneiss Complex are notably more Mg-rich than the biotites from the NCDZ or the SW corner.

One exception to this trend is the analysis for point 25 of sample 1280 which plots in the phlogopite field. This sample is located in the northeast corner of the study area in the Nominingue-Chénéville Deformation Zone. The other four points from the same sample plot within the biotite field with all the other data from within the Nominingue-Chénéville Deformation Zone. Point 25 is from a biotite inclusion within a leucosome garnet whereas

Table 4-XI: Representative Biotite Analyses

Sample	SiO2	Al2O3	TiO2	FeO	MgO	MnO	CaO	Na2O	K2O	Total
1280-25	37.8	17.1	1.93	10.6	17.8	0	0.08	0.28	9.83	95.5
36	36.1	16.5	4.14	18	11.3	0	0.07	0.16	9.61	96
48	36.3	16.6	4.2	17.5	11.3	0	0.06	0.29	9.73	95.9
56	36.5	16.6	4.12	17.4	11.5	0.14	0.16	0.27	9.37	96
59	36.5	16.3	4.02	17.4	11.1	0.11	0.12	0.24	9.73	95.5
1659-50	40.8	17.5	0.65	7.03	21.4	0	0.27	0	8.5	96.2
43	39.9	16.1	1.78	8.97	20.4	0	0.27	0	8.75	96.1
41	39.7	16.7	1.73	9.15	20.5	0	0.23	0	8.4	96.4
39	39.8	16.3	1.58	9.05	20.8	0	0.28	0	8.82	96.6
2039-10	36.1	17.1	2.95	16.8	12.9	0.16	0.13	0.45	9.22	95.7
14	35.7	16.9	2.96	17.1	12.8	0.25	0.25	0.5	9.33	95.8
15	36.4	16.9	2.81	16.8	12.8	0.17	0.19	0.47	9.14	95.6
12	35.9	17.2	2.96	16.8	12.8	0.25	0.09	0.45	9.61	96.1
16	36	17.2	2.49	16.9	13	0.29	0.12	0.35	9.12	95.4
2401D2-18	37	18.6	4.16	12.4	14	0.17	0	0.26	10.1	96.7
2401-101	36.3	16.9	4.96	11.4	16.8	0	0	0	9.62	96
134	36.6	18.6	3.99	10.1	17.2	0	0	0	10.2	96.6
135	36.5	17.9	4.42	10.1	17.1	0	0	0	10.1	96.1
2770-7	35.8	19.8	3.59	17.3	9.95	0	0.11	0.38	9.7	96.7
17	35.8	20	3.59	17.4	9.93	0	0.1	0.29	9.5	96.5
20	34.9	19.3	3.11	18.6	9.57	0	0.07	0.34	9.14	95.1
22	35.6	20.8	2.78	18	9.93	0	0.26	0.27	9.22	96.9
3302-44	38.8	17	3.63	7.19	19.4	0	0.29	0	9.24	95.6
32	38.6	17.6	4.16	7.89	18.6	0	0	0	9.61	96.5
32	38.2	17.4	4.09	7.92	18.3	0	0	0	9.94	95.8
32	37.6	17.7	3.82	7.82	18.6	0	0	0	9.74	95.3
3354-19	46.7	33.3	0	3.22	4.06	0	0	0	8.57	95.9
26	37.9	16	5.06	8.85	17.4	0	0	0	9.99	95.3
3832-12	39.3	16	2.24	8.27	19.7	0	0.36	0	9.86	95.8
23	39.6	16.7	2.17	5.82	21.1	0	0.22	0	9.79	95.4
4012-78	37.9	17.4	3.11	13.6	15.1	0	0	0	9.62	96.7
4209-5	36.5	18	4.4	16.9	11	0	0	0	9.93	96.7
6	36.6	18.1	4.56	16.2	10.9	0	0	0	9.49	95.8
10	37	17.9	4.42	16.3	11.6	0	0	0	9.82	97
7	36.3	18	4.54	16.2	11.1	0	0	0	9.51	95.7
8	36.7	18.2	4.41	16.1	11.1	0	0	0	9.49	96
4220-17	37.5	17.1	4.87	16.9	10.9	0	0	0	9.66	97
13	38	16.9	4.87	16.2	11.4	0	0	0	9.54	97
4475A-39	38.4	18.2	0.96	12.5	16.6	0	0.27	0	10	96.8
38	38.2	18.2	1.11	12.5	16.3	0	0.25	0	9.81	96.4
40	38.3	18.1	0.95	10.8	18.2	0	0	0	9.86	96.3
40	38.5	18.8	1.38	7.48	20.5	0	0	0	9.61	96.2
4475D2-117	40.5	16.6	1.97	7.41	21.1	0	0	0	8.82	96.4
115	40.2	16.8	1.9	6.82	21.3	0	0	0	9.36	96.4
116	40.2	16.7	2.16	6.21	21.4	0	0	0	9.14	95.8
118	40	17.8	1.95	6.66	20.7	0	0	0	9.21	96.4
119	40.1	16.9	2.54	8.23	19.8	0	0	0	9.14	96.8
4475D3-2	39.1	16.1	2.53	9.53	19.1	0	0.25	0	9.62	96.2
3	39.1	16.9	2.32	8.56	20.2	0	0	0	9.6	96.7

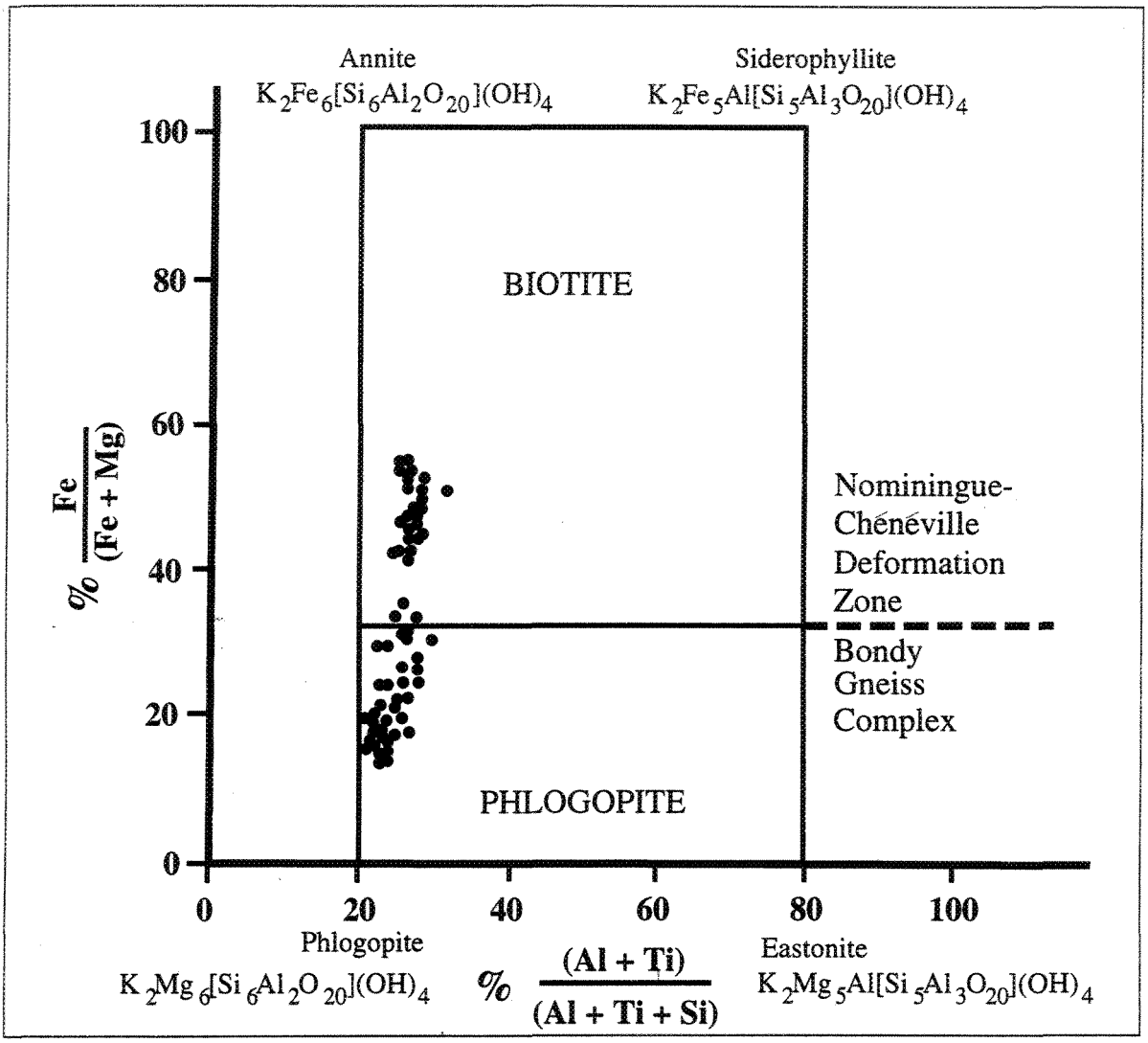

Figure 4-VI: Classification of biotite analyses. Note that the NCDZ biotites consistently plot in the more iron rich biotite field, whereas the BGC biotites plot in the phlogopite field. The Mg-enrichment of the BGC biotite may be due to the proposed hydrothermal alteration of rocks in this region (Corriveau et al. 1995). The classification scheme was chosen from Deer et al. (1966) who arbitrarily chose the division at Mg:Fe = 2:1

the other biotite points from the same sample are all matrix biotites, hence there may be two generations of biotite in this sample. Thus it appears that micas within the leucosomes of the Nominingue-Chénéville Deformation Zone also plot within the phlogopite field. Two points (59 and 44) from the Bondy Gneiss Complex sample 3302 also are inclusions within leucosome garnets, thus in general, it appears that biotite inclusions within leucosome garnets plot in the phlogopite field of Figure 4-VI.

4.7k Garnet

The weight percent oxides and the totals for five representative analyses from each sample analysed are in Table 4-XII. The Wt% SiO_2 ranges from 37.0 to 40.0%, Al_2O_3 from 21.3 to 23.0%, FeO from 25.2 to 35.4%, MgO from 7.0 to 11.8%, CaO from 0.34 to 3.6%, with TiO_2 <0.15% and MnO <5.8%. The mole fraction of pyrope, almandine, spessartine and grossular for the cores and rims of the garnets within each sample are given in Table 4-XIII. These garnets were dominantly almandine (X_{Fe} 0.50 to 0.78), with large fractions of pyrope (X_{Mg} 0.14 to 0.48), comparatively small fractions of grossular (X_{Ca} 0.01 to 0.16) and minute quantities of spessartine (X_{Mn} <0.03). Therefore, these are well approximated as ternary garnets.

4.7k.i. Garnet zoning profiles

In order to examine the effects of post-peak metamorphic diffusion in the garnets, transects were completed across most of the garnets. The growth development and subsequent modification of garnet by diffusion during cooling of a sample garnet are depicted schematically in Figure VII. During growth under low- to mid-amphibolite facies conditions (STAGE I), Mg-zoning profiles through a hypothetical garnet would be bell-shaped (and Fe-zoning profiles U-shaped) with the composition at the rim corresponding to the P-T conditions during garnet growth. If during peak metamorphic (STAGE II) temperatures were >625°C, then diffusion within the garnet leads to a homogenisation and a flat

Table 4-XII: Representative Garnet Analyses

Sample	SiO2	Al2O3	TiO2	FeO	MgO	MnO	CaO	Total
1280-1	37.11	21.45	0.08	32.07	0.71	5.35	3.29	100.1
2	37.42	21.37	0	31.43	0.98	5.67	3.34	100.2
3	37.3	21.36	0.07	31.16	0.94	5.58	3.49	99.9
4	37.17	21.76	0	31.3	0.97	5.78	3.61	100.6
5	37.52	21.44	0	31.14	0.87	5.4	3.62	99.99
1659-29	38.64	21.64	0	27.17	11.9	0	0.407	99.75
30	38.59	21.76	0	26.76	11.8	0	0.477	99.39
31	38.89	21.91	0	26.74	11.6	0.448	0.338	99.93
28	38.73	21.88	0	26.23	11.61	0.306	0.447	99.2
43	39.97	21.87	0	26.19	11.77	0.368	0.482	100.6
2401D2-1	38.07	23.03	0	26.34	9.33	0.97	3.07	100.8
3	38.33	22.96	0	25.15	9.26	1.17	3.7	100.6
5	38.04	22.79	0	27.48	9.11	1.16	2.27	100.8
10	37.91	22.54	0	28.65	9.04	0.92	1.86	100.9
11	37.91	22.83	0	28	9.12	1.06	1.67	100.6
2770-4	36.51	21.76	0	35.41	3.79	1.15	1.477	100.1
1	36.36	21.66	0	34.92	4.48	0.92	1.487	99.83
2	37.03	21.91	0	33.83	5.07	0.86	1.667	100.4
3	37.03	21.82	0	34.05	5.1	0.97	1.527	100.5
20	36.47	21.88	0	35.64	3.9	1.14	1.467	100.5
3302-1	38.57	22.44	0.14	25.91	10.54	0.43	1.661	99.7
2	38.48	22.33	0	26.34	10.7	0	1.814	99.67
3	38.03	22.25	0	26.25	10.29	0	2.118	98.93
4	38.42	21.95	0	26.7	10.35	0.41	2.328	100.2
5	37.79	22.55	0	26.5	10.1	0.49	2.41	99.84
3333-53	37.73	21.77	0	32.36	4.75	1.696	1.717	100
46	37.79	21.54	0	32.22	4.99	1.586	1.834	99.96
47	37.81	21.9	0	32.85	5.36	1.457	1.756	101.1
48	37.69	22.04	0.11	32.53	5.01	1.614	1.707	100.7
49	37.4	21.85	0	32.36	4.88	1.733	1.746	99.97
3354-7	38.45	22.44	0	27.69	10.61	0.46	1.252	100.9
9	37.98	22.33	0	26.66	10.49	0.52	1.088	99.06
10	38.06	22.52	0	26.28	10.96	0	1.112	98.92
11	37.78	22.46	0	26.97	10.66	0.53	1.182	99.58
12	38.05	22.29	0	26.21	11.17	0.54	1.229	99.48
3832-17	39.41	21.99	0	27.44	11.41	0	0.385	100.6
19	39.2	21.7	0	27.24	10.98	0	0.395	99.5
45	39.39	22.02	0	27.41	11.3	0	0.414	100.5
46	39.18	21.82	0	27.24	11.43	0	0.479	100.2

Table 4-XII: Representative Garnet Analyses - continued

47	39.49	21.81	0	26.06	11.95	0	0.537	99.84
4012-42	38.57	21.98	0	25.81	9.45	0.751	3.515	100.1
43	38.34	22.16	0	25.41	9.566	0.827	3.62	99.91
44	38.35	21.92	0	26.03	9.291	0.835	3.487	99.91
45	38.52	22.26	0	25.63	9.111	0.927	3.515	99.96
46	38.45	22.28	0	25.97	8.974	0.958	3.496	100.1
4209-2	38.03	21.65	0.15	29.92	5.964	1.26	3.247	100.2
3	38.13	22.03	0	30.41	5.565	1.16	3.138	100.4
4	37.98	21.86	0	30.38	5.841	1.14	2.969	100.2
5	38.02	22.01	0	30.86	5.504	1.11	2.949	100.5
6	37.88	21.88	0	31.07	5.667	1.36	2.502	100.4
4475D3-3	39.06	22.54	0	27.34	11.3	0	0.302	100.5
4	39.27	21.9	0	27	11.51	0	0.36	100
5	39.47	22.48	0	26.69	11	0	0.36	99.99
6	38.98	22.46	0	27.08	11.2	0	0.468	100.2
7	39.42	22.76	0	27.04	11.52	0	0.399	101.1

Table 4-XIII: Molar Percent Alm, Pyp, Grs, Sps

Sample	CORE %Fe	%Mg	%Mn	%Ca	Rim %Fe	%Mg	%Mn	%Ca
1659-1	0.502	0.477	0.017	0	0.582	0.4	0.013	0
2	0.511	0.478	0.014	0	0.574	0.426	0	0
3	0.534	0.443	0.015	0	0.512	0.466	0.007	0
2401D2-1	0.556	0.363	0.011	0.078	0.645	0.263	0.01	0.047
2	0.513	0.369	0.007	0.101	0.666	0.232	0.007	0.043
2401-E	0.628	0.319	0.011	0.04	0.556	0.356	0.019	0.07
2770-1	0.743	0.186	0.024	0.047	0.771	0.151	0.027	0.051
2770-2	0.739	0.199	0.022	0.042	0.783	0.139	0.026	0.042
3045	0.604	0.246	0.03	0.126	0.551	0.314	0.028	0.107
3302-AB	0.566	0.347	0.014	0.074	0.617	0.349	0.019	0.052
CD	0.584	0.329	0.013	0.082	0.641	0.296	0.031	0.054
E	0.619	0.321	0.01	0.044	0.621	0.324	0.017	0.045
LEUC	0.55	0.37	0.01	0.07	0.56	0.39	0.01	0.05
3333-AB(36)	0.674	0.254	0.051	0.021	0.721	0.191	0.039	0.045
AB(35)	0.679	0.243	0.026	0.046	0.722	0.183	0.044	0.053
3354	0.541	0.406	0.012	0.034	0.643	0.324	0	0.025
3832-23	0.539	0.444	0	0.015	0.644	0.336	0.013	0.008
17	0.553	0.043	0	0.011	0.574	0.411	0.008	0.016
16	0.558	0.429	0	0.011	0.603	0.349	0.007	0.011
4209-13/14	0.644	0.245	0.029	0.098	0.721	0.173	0.039	0.041
16	0.709	0.198	0.029	0.062	0.755	0.145	0.041	0.058
17	0.682	0.221	0.024	0.044	0.73	0.163	0.039	0.062
4220-19	0.651	0.198	0.022	0.125	0.698	0.149	0.013	0.162
20	0.685	0.194	0.026	0.101	0.668	0.149	0.014	0.162
21	-0.649	0.208	0.015	0.129	0.698	0.152	0.017	0.152
4475D3	0.559	0.428	0	0.007	0.693	0.276	0.02	0.016
Total	15.77	7.958	0.431	1.408	16.95	7.107	0.507	1.371
Average	0.607	0.306	0.017	0.054	0.652	0.273	0.019	0.053

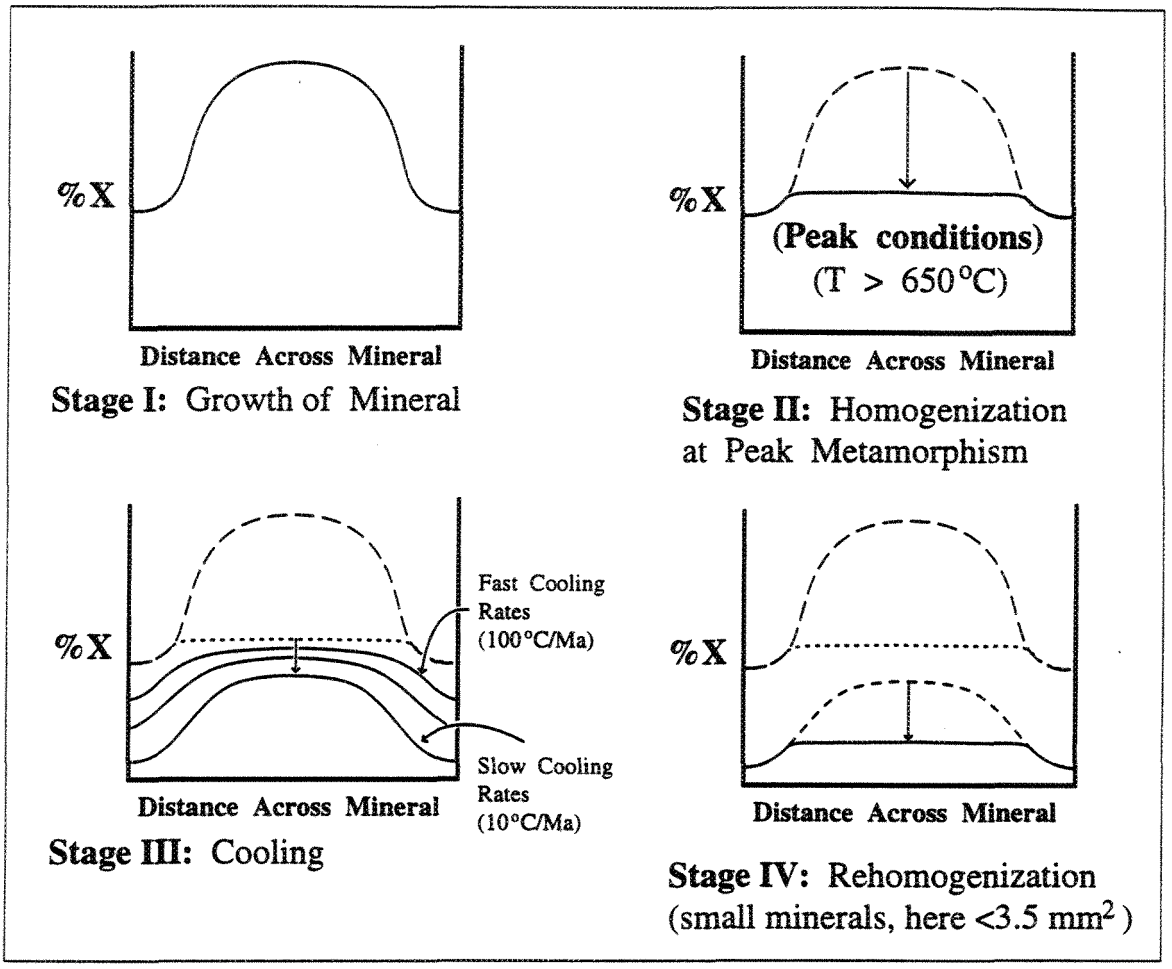

Figure 4-VII: The development of mineral profiles during geological history (after Spear, 1991). For the Mont Laurier Region, there would have initially been homogenization (Stage II) because the peak temperatures were 950° C, there were slow cooling rates below 650° C, and the small garnets were rehomogenized. These bell-shaped profiles are representative of the almandine profiles in the Mont Laurier garnets.

compositional profile results. Diffusion in from the matrix serves to change the garnet interior composition until it is the same as the rim and records the peak metamorphic temperature. At this time, the core conditions may have been altered so that they no longer preserve evidence of pre-peak metamorphic conditions. As diffusion continues during post-peak metamorphic conditions (STAGE III), the garnet may develop a second bell-shaped zoning profile with compositions at the rim responding first to decreasing temperature. If cooling is slow enough, core compositions will also be changed and the bell-shaped secondary profile will flatten. Spear (1991) suggested that if the cooling rate was fast (>100°C/Ma) then the profile would closer resemble STAGE II, with the bell-shaped profile in STAGE III being more extreme the slower the cooling rate (down to <10°C/Ma). If the garnets are small (here the data suggests <3.5 mm^2) then the zoning profile may even be completely homogenised a second time (STAGE IV). Because the maximum metamorphic temperature suggested by the assemblages is 950°C (i.e., over 625°C), a bell-shaped profile indicates the effects of post-peak metamorphic diffusion (Spear 1991).

The compositional variation (X_{Fe}, X_{Mg}, X_{Ca}, X_{Mn}) across garnets are plotted against distance from the centre of the garnet (or from the rim if the transect was only partial or did not cross the garnet's centre). The physical centre of the garnets was considered to be the intersection of the two lines representing the middle points of the longest and the shortest axes of the garnet. These profiles were plotted primarily in order to assess the extent of the post-peak metamorphic diffusional effects on the garnets. They were also plotted in order to study the effects of surrounding minerals, inclusions (size, chemistry and concentration), embayments and garnet size on the composition of the garnets. Post-peak metamorphic diffusional effects and any resultant chemical changes on the garnets could effect the results of the geothermobarometry (Chapter 5).

4.7k.ii. Iron and Magnesium Trends

Magnesium gradually increases and iron gradually decreases inwards from the garnet rims towards the cores, in the garnets that were not entirely homogenised by post-peak metamorphic diffusion. Two good examples of these trends are the samples 4209 (Plate XVI) and 4475D3 (Plates VIII, XII; Figures 4-VIII, 4-IX). The zoning profiles for both these garnets are smooth bell-curves, suggestive of STAGE III (Spear 1991). This suggests that these bell-shaped profiles are not due to growth, but re-equilibration. The mole fraction almandine (X_{Alm}) in sample 4209 decreases from 0.71 at the rim to 0.64 in the core, while the mole fraction pyrope (X_{Py}) increases from 0.17 to 0.25. In sample 4475D3, the X_{Alm} decreases inwards from 0.69 to 0.56 where X_{Py} increases from 0.28 to 0.43. Both these garnets are rounded with irregular boundaries. They are both large; 4209 (Figure 4-X) has an area of 15.6 mm^2, 4475D3 (Figure 4-XI) has an area of 76.4 mm^2. Both garnets contain abundant inclusions which tend to be concentrated in the outer portions of the garnets.

Overall the average mole fraction almandine decreases from 0.55 to 0.78 at the rim to 0.50 to 0.74 in the core where the average mole fraction pyrope increases from 0.14 to 0.47 at the rim to 0.19 to 0.48 in the core. One exception to this trend is the garnet traverse of sample 3045 where at first glance the trends appear to show the reverse with almandine increasing inwards from 0.55 to 0.60 and pyrope decreasing inwards from 0.31 to 0.25 (Figure 4-XII). This garnet is deeply embayed with many inclusions (Figure 4-XIII). The influence of these characteristics on the zoning profiles will be discussed in sections 4.7k.iv and 4.7k.v.

The general trends of these mole fraction almandine and pyrope profiles are similar to those studied by Indares and Martignole (1990a) in their transect across the Central Metasedimentary Belt of Quebec. These trends are also similar to those of Martignole and Pouget (1993) in their study of the Cabonga reservoir Terrane and to those of Tucillo et al.

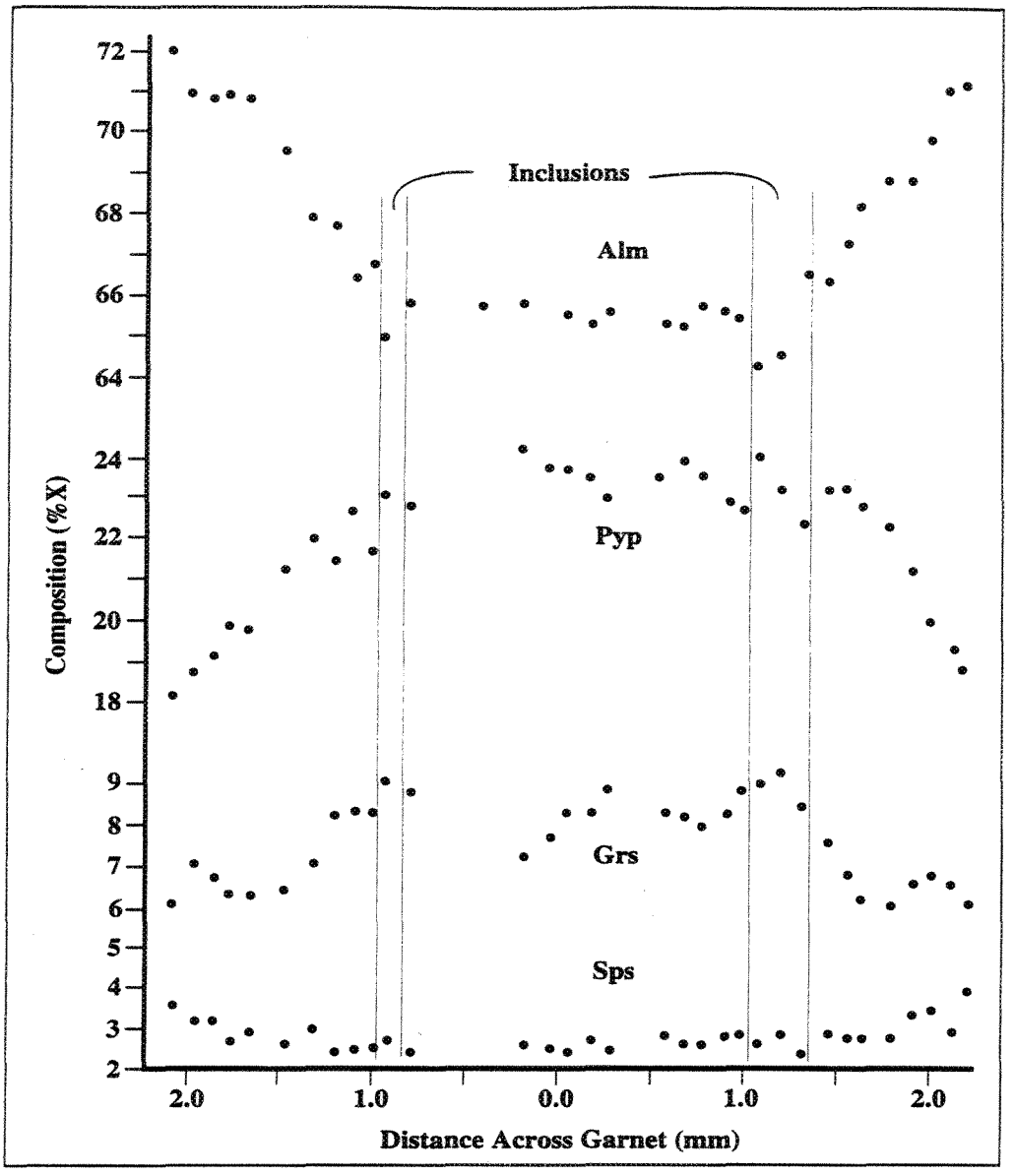

FIGURE 4-VIII: Compositional profile of garnet transect "A" from photo 5-13/14, sample 4209 (NCDZ). Note that the almandine content decreases (8%) towards the core (0.0) as the pyrope content increases (6%). These two curves describe bell- and U-shaped profiles. Generally, grossular increases (3%) towards the core where spessartine increases by 1% about 0.75mm from the rims. The increase in grossular content towards the core of the garnet, while the almandine and pyrope profiles remain flat, was observed by Indares and Martignole (1990a). They interpreted it to indicate isothermic decompression. A similar pattern was observed in the inclusion-free cores of sample 2401D2 (Figure 4-XV).

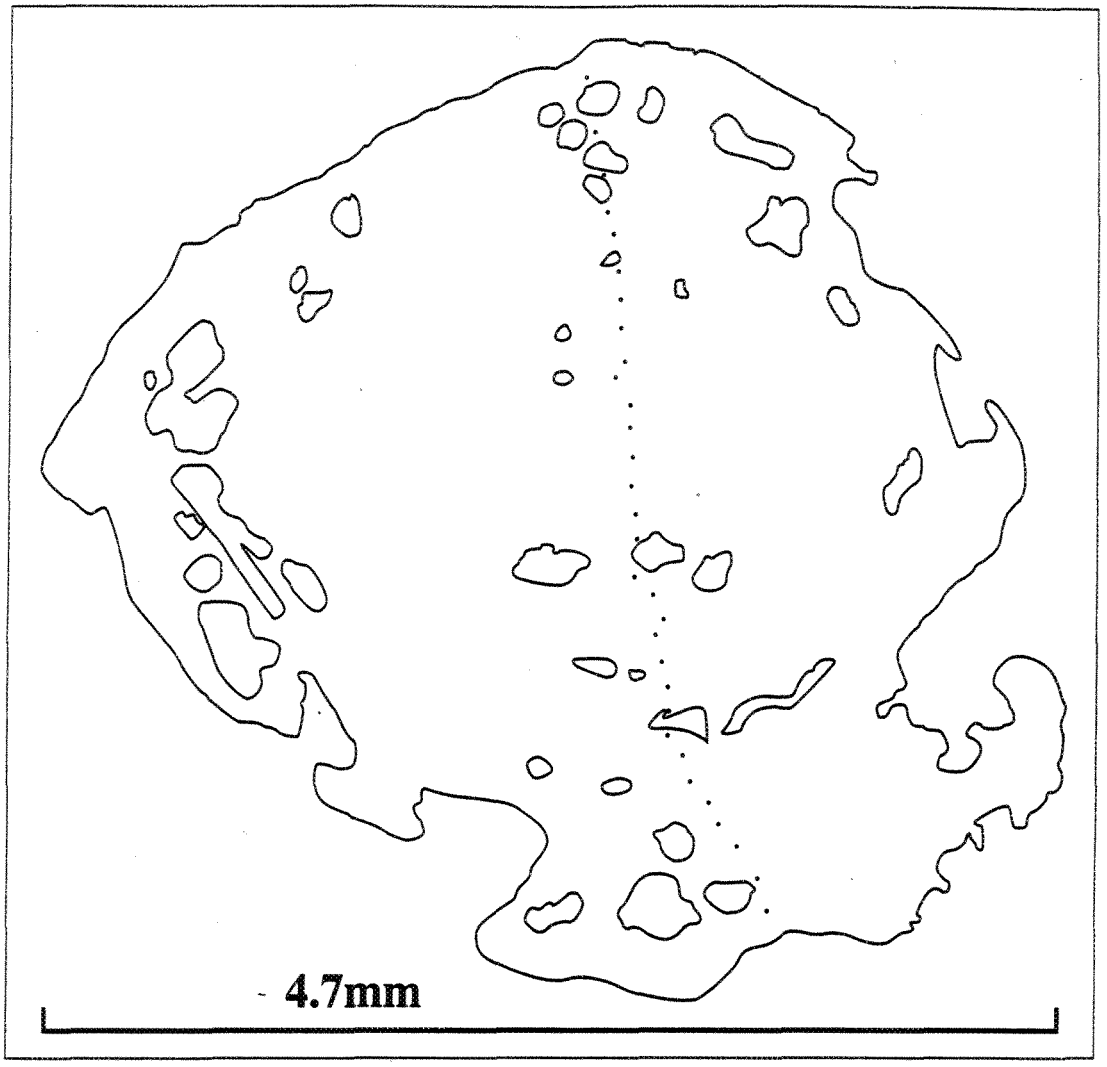

Figure 4-X: Garnet from sample 4209 (Plate XVI). This garnet is quite small, and was thus not expected to preserve evidence of the peak metamorphic conditions. However, it is compositionally zoned (profile Figure 4-VIII), and, therefore,not completely rehomogenized.

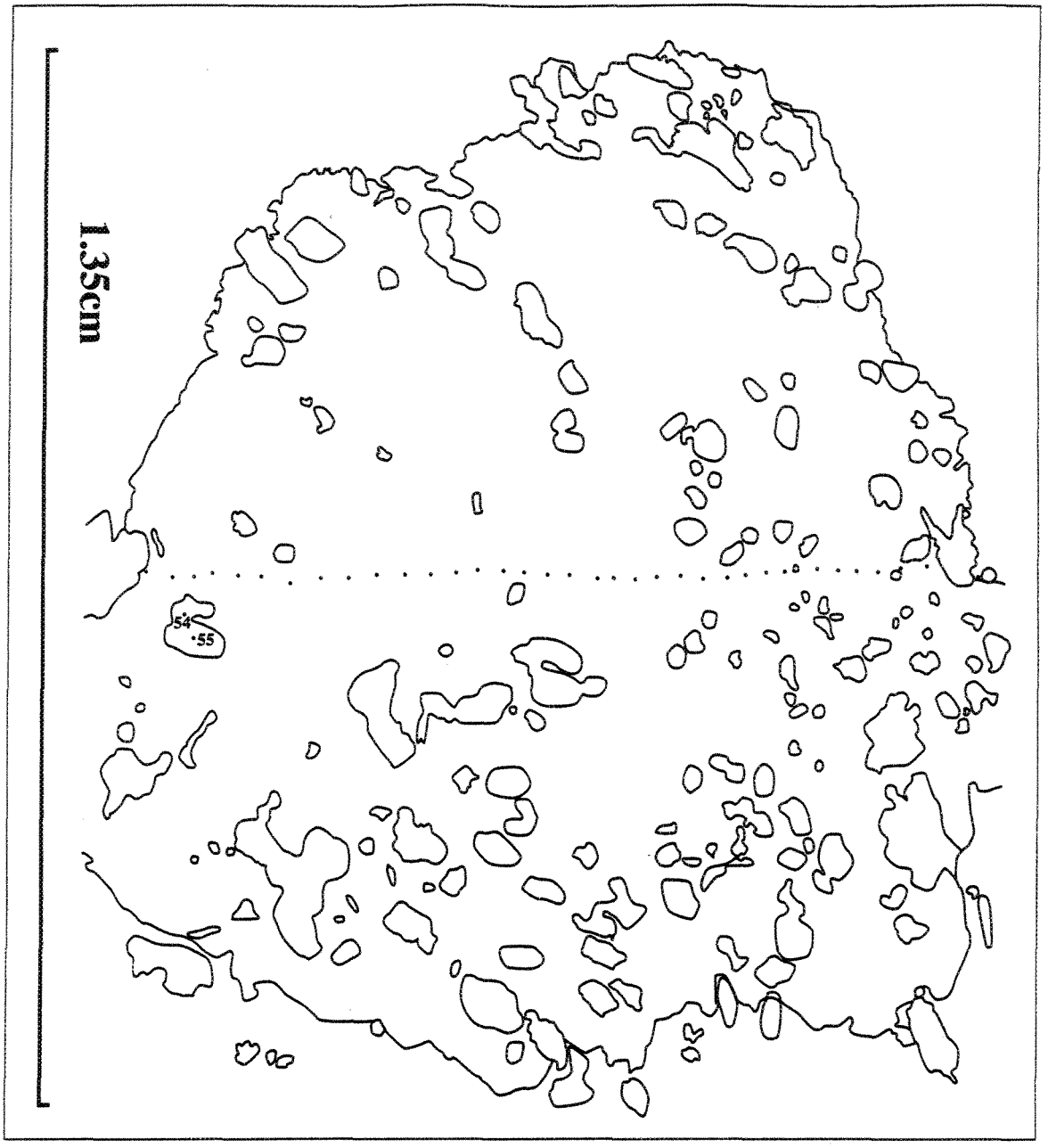

FIGURE 4-XI: Garnet in sample 4475D3 (Plate VIII). The transect on this figure corresponds to the transect in Figure 4-IX. This is one of the largest garnets from the study area, and was thus expected to preserve evidence of peak metamorphic conditions. However, it is full of ilmenite inclusions, which opened the interior of the garnet to the effects of retrograde cation exchange, by decreasing the size of the diffusion domaines.

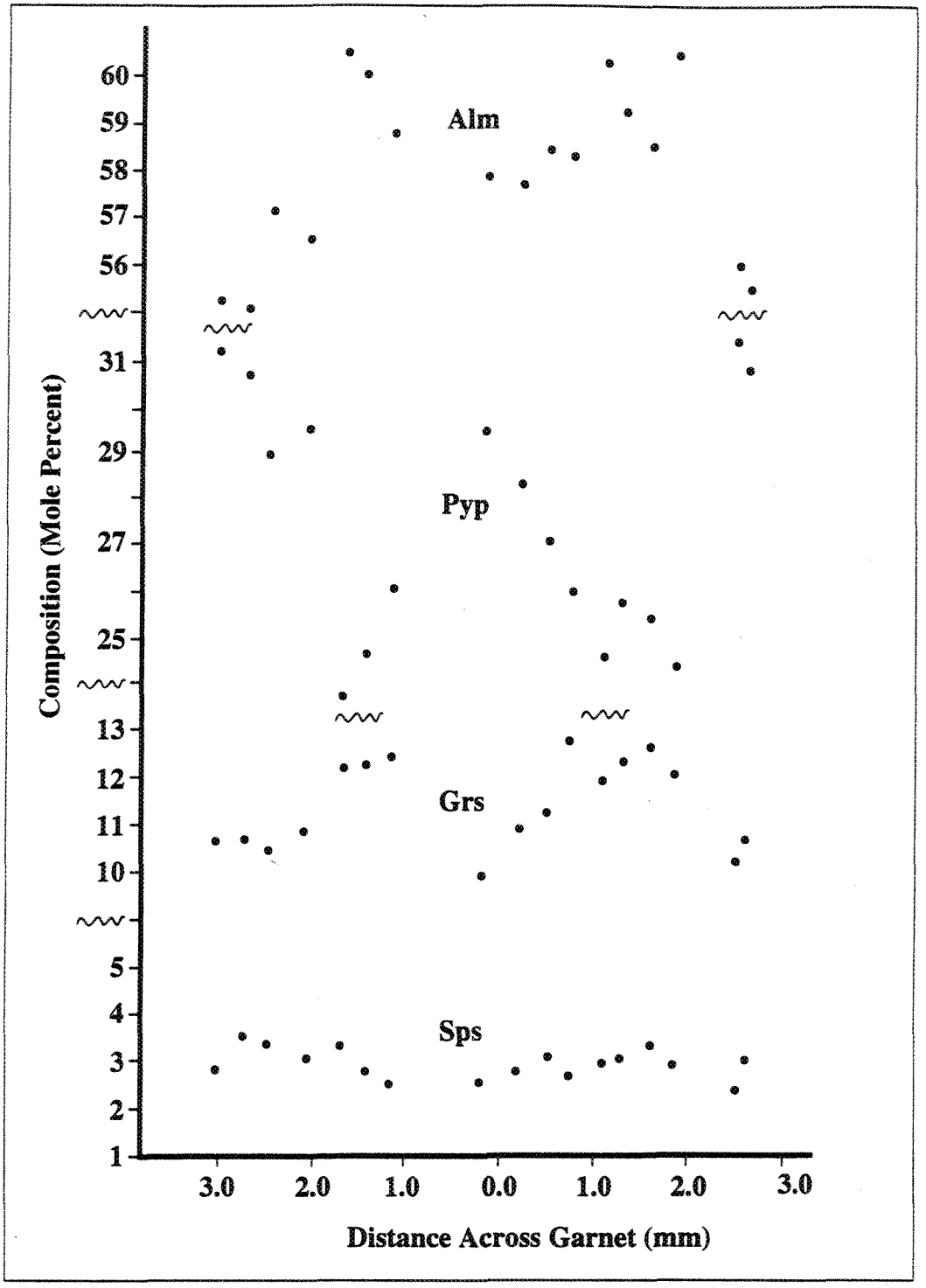

FIGURE 4-XII: Composition profile across garnet from sample 3045. Note how distorted this profile is due to the inclusions and embayments in the garnet (Figure 4-XIII).

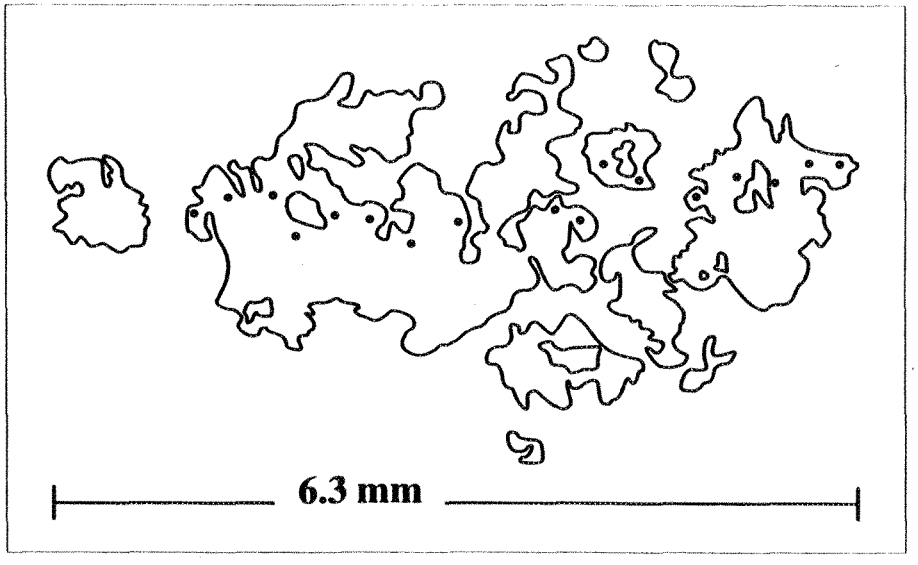

Figure 4-XIII: Garnet from sample 3045. This garnet is full of inclusions and crosscut by embayments, therefore the profile across this garnet (Figure 4-XII) is very irregular.

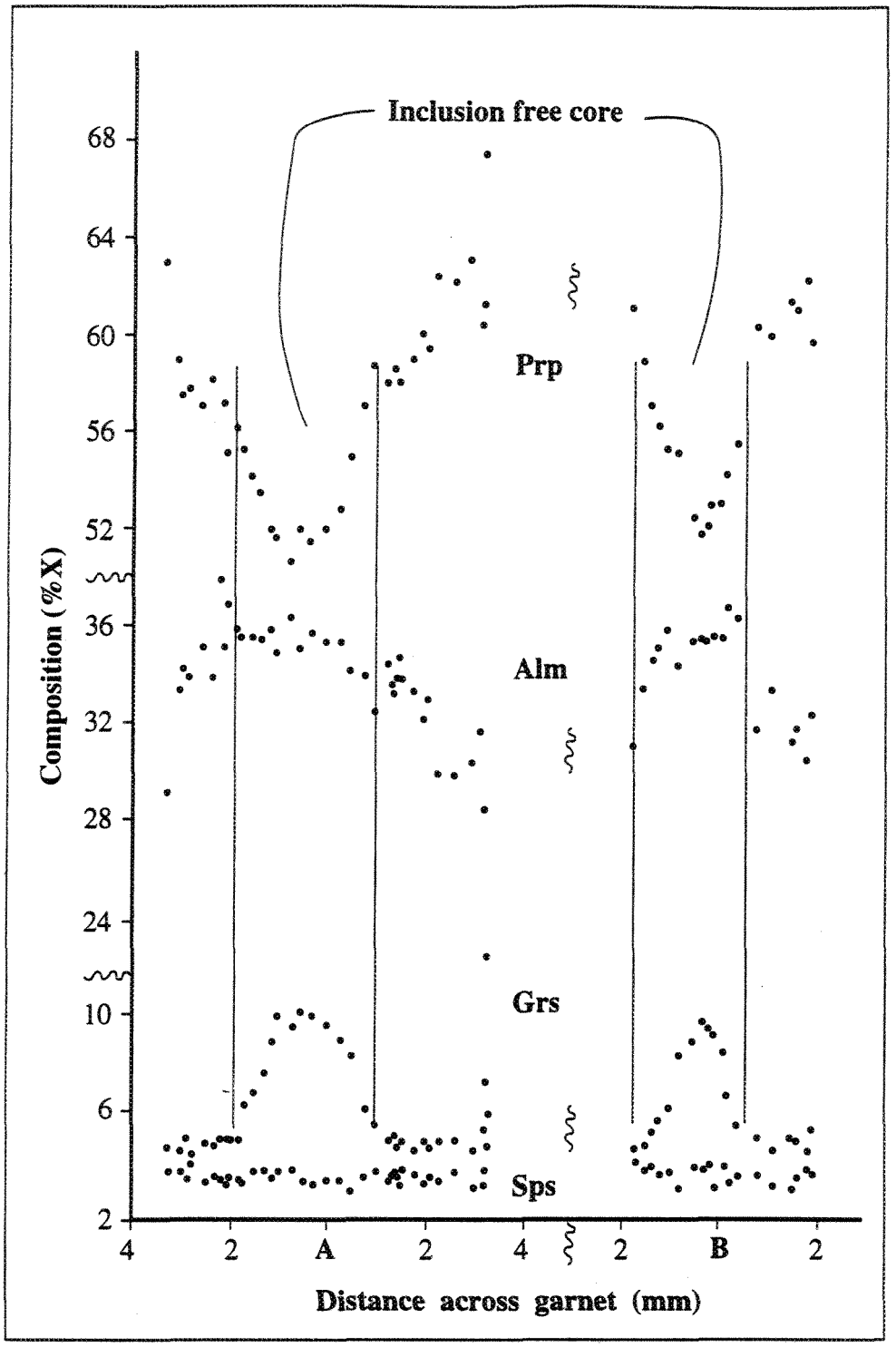

Figure 4-XIV: Profile of garnet from sample 2401D2 (BGC). This corresponds to the sketch in Figure 4-XVI. Note the abrupt changes in the Grs, Alm and Pyp profiles once the inclusion-free core is traversed. Indares and Martignole (1990a) proposed that the increase in Grs content, when the Alm content remained flat, indicated isothermal decompression. This corresponds with the structural evidence in the NCDZ for extension.

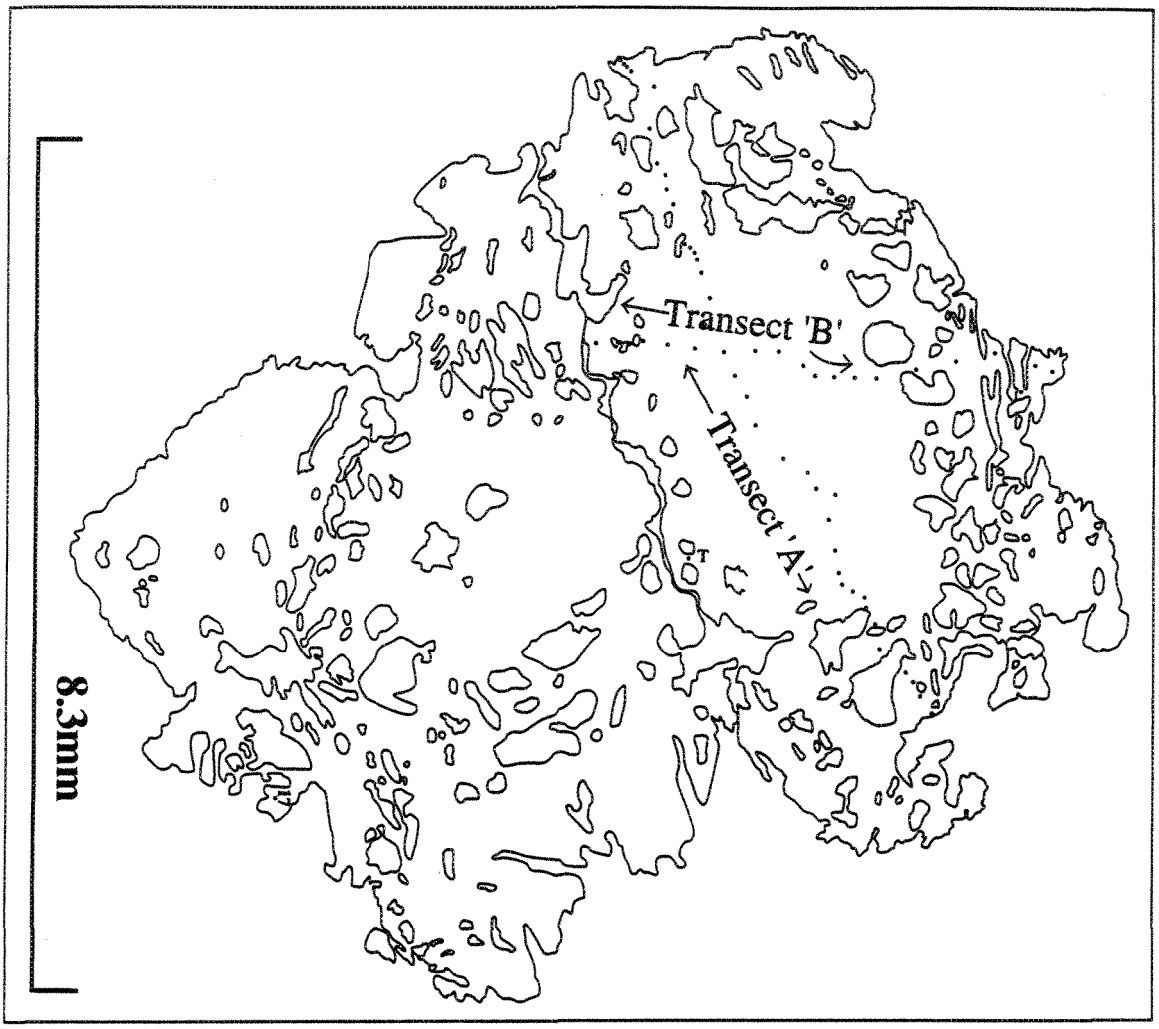

Figure 4-XV: Garnet from sample 2401D2. This is a larger intermediate-sized garnet from the field area that preserves an inclusion-free core. The garnet analyses from this core resulted in the peak metamorphic temperatures. This garnet also contains spinel inclusions, but only in the rim (Plate IX). This, and the profile, suggest that the core of the garnet grew during or at pre-peak conditions; and that the spinel inclusion-containing rim grew during the isothermic decompression conditions suggested by the profile (Figure 4-XIV).

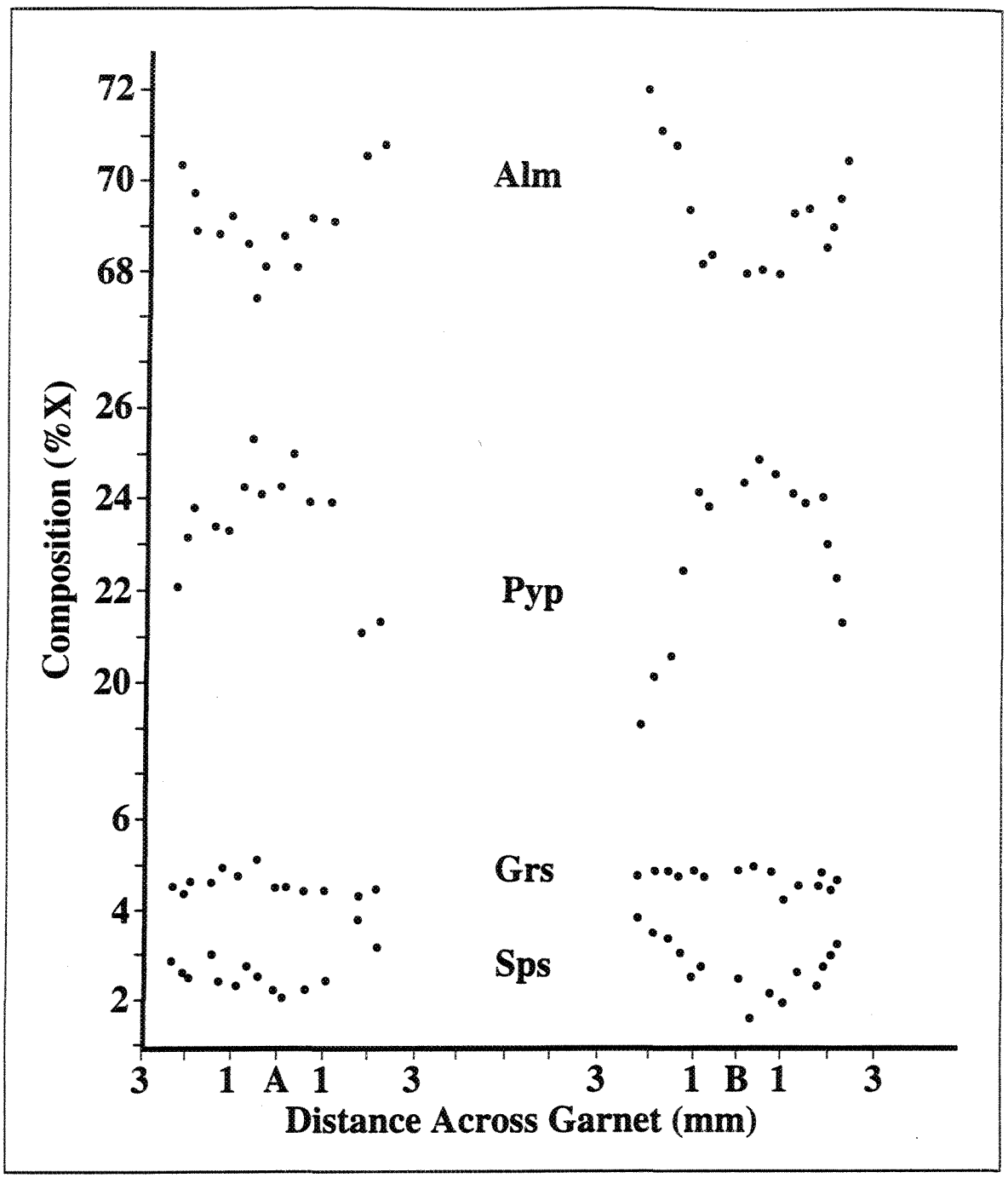

FIGURE 4-XVI: Compositional profile for a garnet from sample 3333A. Note the typical decrease of almandine towards the core, and the corresponding increase of pyrope. Transect B is one of the few transects from this study that demonstrates a trend with the spessartine content profile; the manganese trend in this profile decreases 2.5% from the rims inwards.

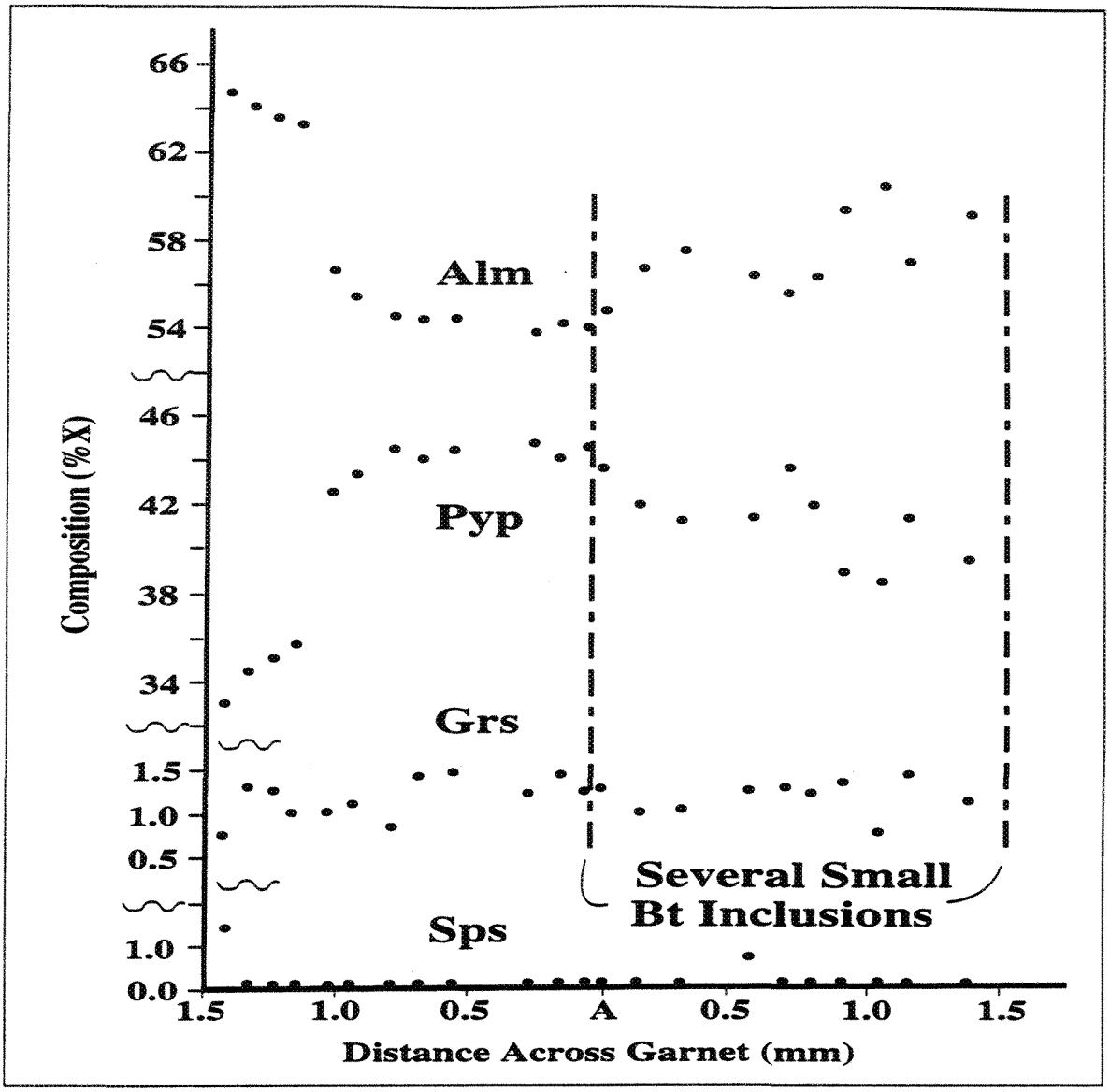

FIGURE 4-XVII: Compositional profile across a garnet from sample 3832 (photo 6-23). This profile follows the overall general trend of increasing almandine content towards the rims accompanied with decreasing pyrope content. This garnet is poikiloblastic, full of plagioclase, biotite and quartz inclusions. The left portion of this profile crossed near several small plagioclase inclusions, which did not disturb the almandine or pyrope profiles, but may have distorted the grossular profile (difficult to determine from this profile). The several small biotite inclusions that the right portion of the profile crossed distorted both the almandine and pyrope profiles.

flat, Indares and Martignole (1990a) proposed that there was a metamorphic history involving isothermal decompression. The garnet cores from sample 2401D2 demonstrate this trend.

In three garnets (4475D3, 4209 and 3333), manganese contents tend to decrease gradually from the rims inwards towards the central portions of the garnets. In some cases such as sample 4475D3 (Figure 4-IX), the X_{Sps} decreases to below detection level, 0.5 to 1.5 mm from the rims. However, in the other two samples (4209 and 3333A; Figures 4-VIII, 4-XVI), the X_{Sps} contents drop from 0.03-0.04 down to 0.01-0.02, 0.5 to 1.0 mm inwards from the rims. The X_{Sps} trend in sample 4220 garnet is anomalous; in this garnet, the X_{Sps} content increases gradually from 0.012 to 0.025 in a bell-shaped pattern 0.5 mm inwards from the rim. In samples 3832 (Figure 4-XVII) and 3354 (Figure 4-XVIII), as is the case for most of the garnet profiles, X_{Sps} tends to vary erratically from the detection limit to 0.015.

4.7k.iv. The Effect of Embayments

In most cases, the size and positioning of embayments within the garnets strongly affect the compositional profiles. For example, the garnet in sample 3354 (Figure 4-XIX) is almost cut in two by embayments filled with biotite and quartz. Even though this is one garnet, the profiles behave as if it were two (Figure 4-XVIII). FeO decreases inwards from both edges, but then increases towards the middle where the garnet is cut by the embayments. MgO also indicates the same effect with the values decreasing on both sides of the embayment. The CaO and MnO contents show no consistent trend. Even minute embayments such as that of the biotite-filled crack between the two portions of the large garnet in sample 2401D2 (Figure 4-XV) have an effect on the compositional profiles.

Embayments that only partly invade the garnet, such as that of sample 2401E, (Figures 4-XX, 4-XXI) produce a similar effect on the composition profiles, making it

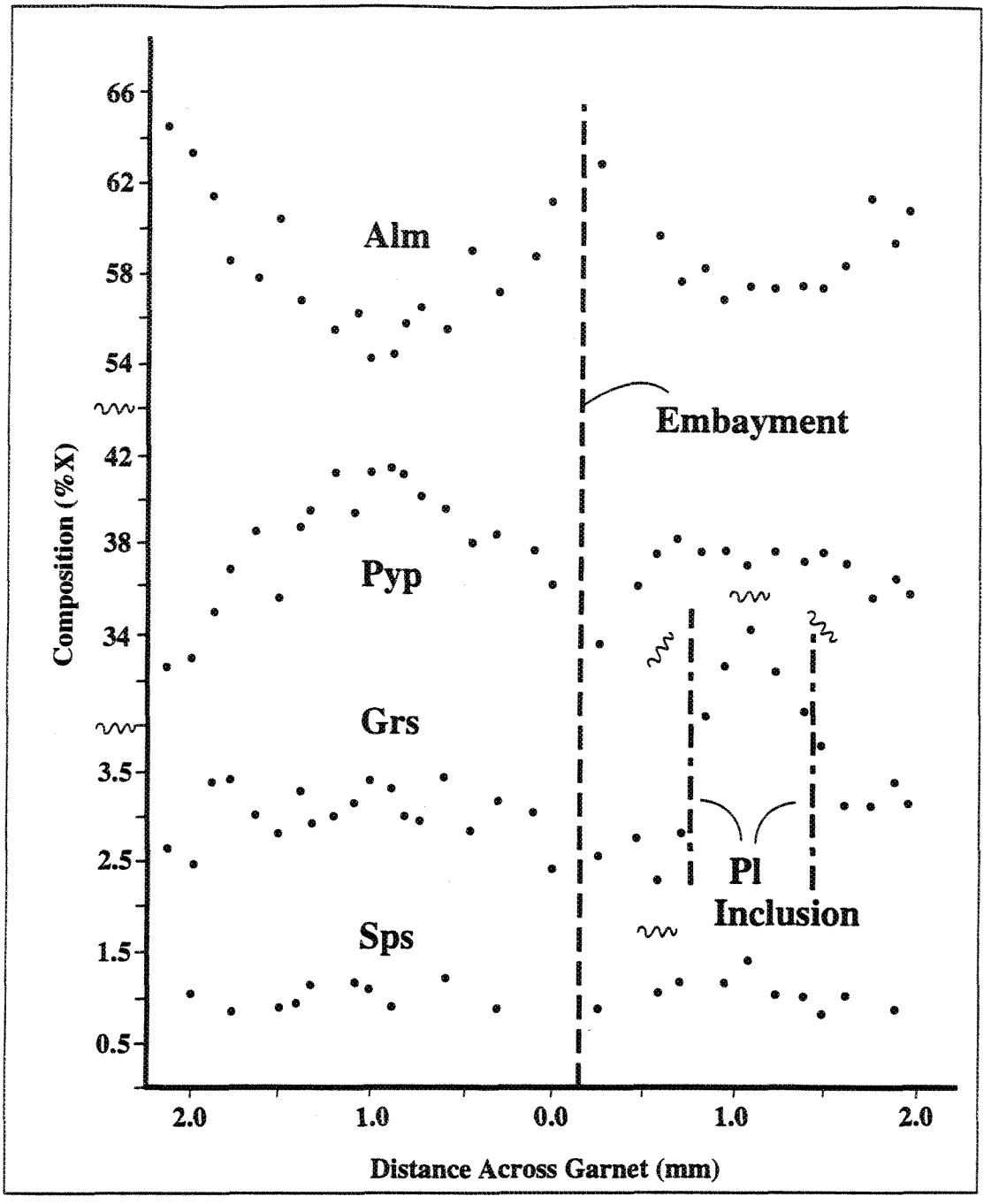

FIGURE 4-XVIII: Compositional profile across a garnet from sample 3354. This garnet is almost bisected by an embayment filled with biotite and plagioclase (Figure XX). This profile appears as if the embayment caused the garnet composition to behave as if it were two garnets. The almandine content increases both towards the rims and the boundaries of the embayment, and the pyrope content increases towards the core of both portions of the garnet. There is also a large plagioclase inclusion in the core of one portion of this garnet. The grossular content increases almost 3% as the profile approaches the inclusion.

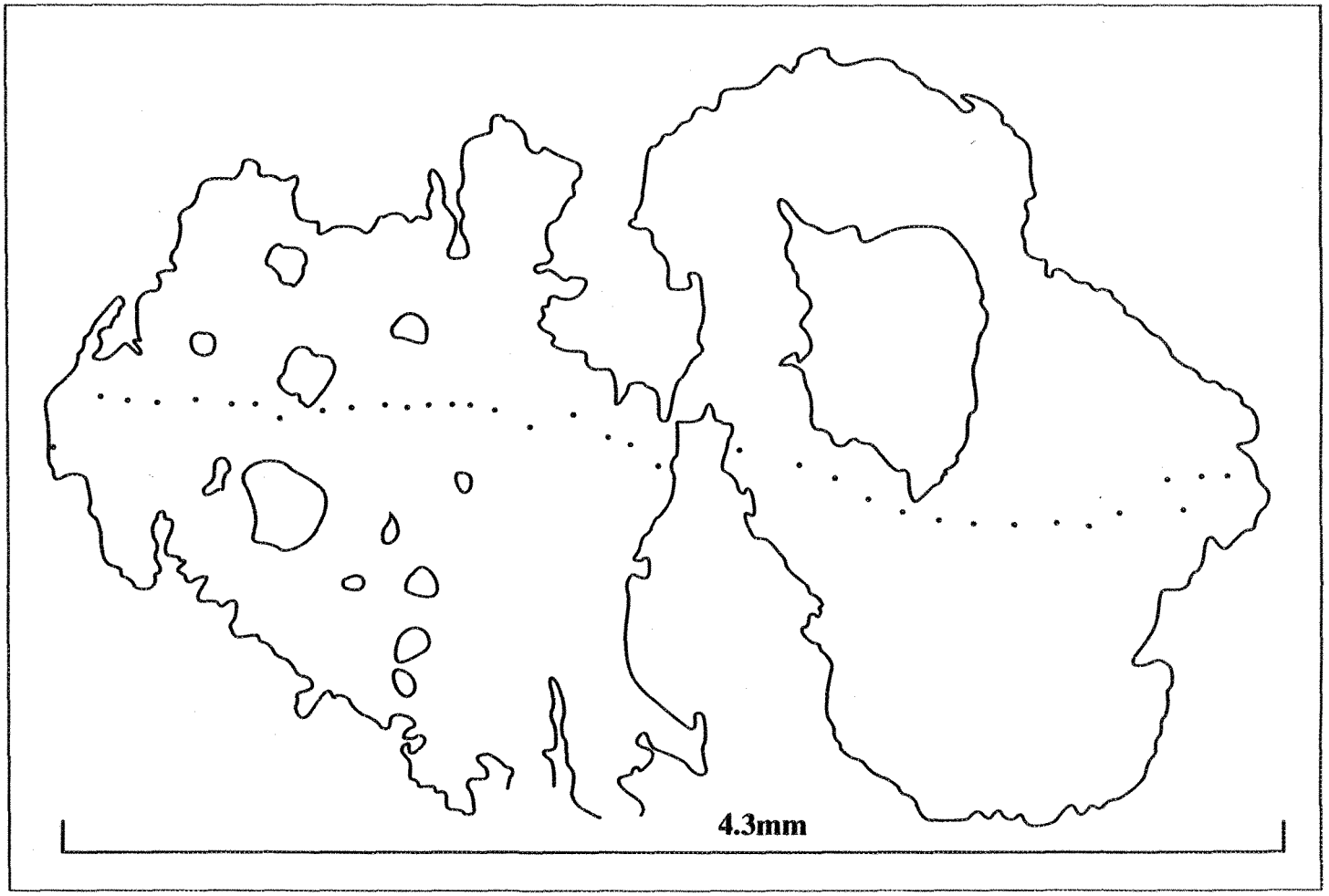

Figure 4-XIX: Garnet from sample 3354. This corresponds to the profile in Figure 4-XVIII. Note the deep embayment that almost bisects this garnet, and the large plagioclase inclusion in the right half of the garnet.

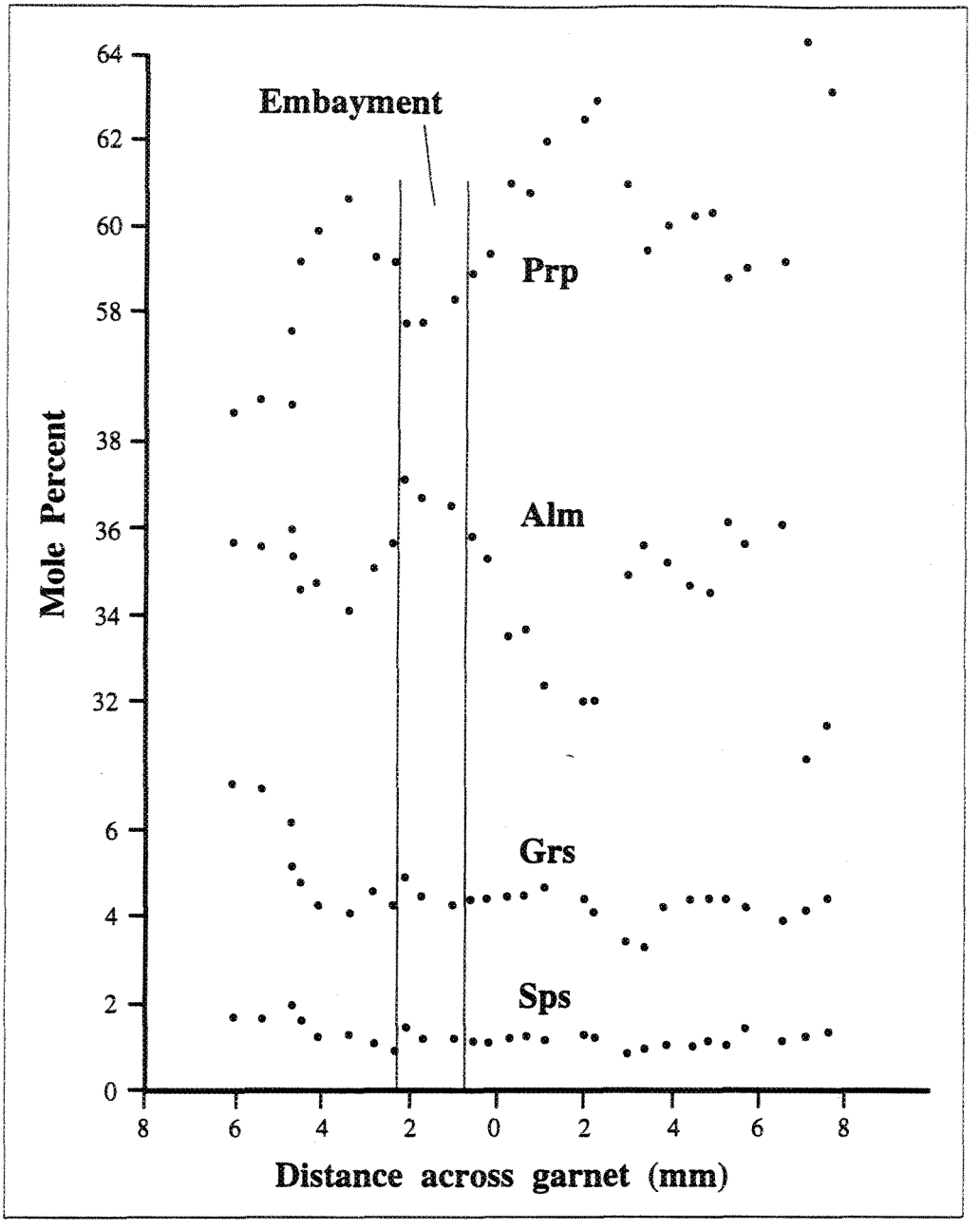

Figure 4-XX: Profile across garnet from sample 2401E. This garnet is from the same outcrop as 2401D2 (Figures 4-XIV, 4-XV), but does not have the inclusion-free core. It is crosscut by embayments, and is full of spinel and biotite inclusions. This is one of the larger garnets from the study, and was thus expected to produce one of the highest temperatures from the biotite-garnet thermometer. However, as with the garnet from sample 4475D3 (Figures 4-IX, 4-XI), it only produced intermediate temperatures, likely because of the inclusions.

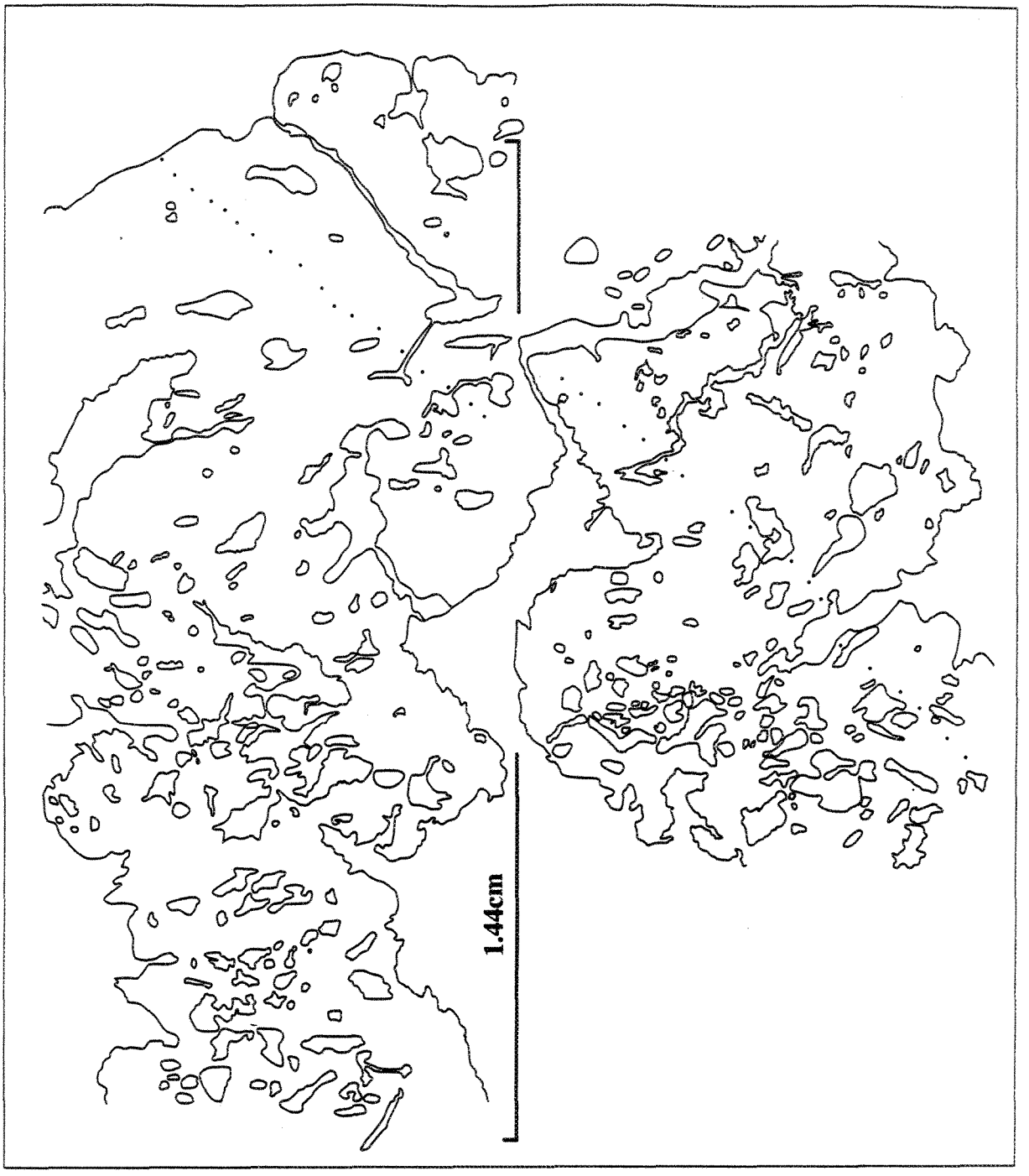

FIGURE 4-XXI: Garnet from sample 2401E. This is one of the largest garnets in the field area. Unlike the garnet from sample 2401D2, it does not have an inclusion-free core, and thus does not preserve evidence for the peak metamorphic temperatures. Note the large embayments, and the high concentration of inclusions throughout this garnet.

appear as if the profile cut through two unattached garnets. The embayments in sample 3045 (Figure 4-XIII) completely distort the zoning profiles of this garnet (Figure 4-XII). Smaller rounded, unembayed garnets from this same thin section produced profiles with no disturbances.

In their study of garnet rims and cracks from central Vermont, and western Conneticut, Hames and Menard (1993) suggested that these features opened the crystal structure to metasomatic fluids, thus shortening the path for diffusion. Embayments would therefore act as a highway for fluids, and would open the crystallographic structure to the effects of retrograde cation exchange. Thus, for the thermobarometers, analyses near rims, cracks or embayments should be avoided.

4.7k.v. The Effect of Inclusions

The presence of inclusions, depending on mineral type, size, number, and location, can also influence or distort the composition profiles of the garnets. For example, the transect of the garnet from sample 4209 (Plate XVI) crosses a cluster of three small (0.16 mm x 0.21-0.35 mm) irregular plagioclase inclusions (Figures 4-VIII, X). The zoning profile demonstrates the presence of these inclusions by an abrupt increase in FeO and MgO and an abrupt decrease in CaO. Other than this distortion, the bell-curves of this zoning profile is smooth. The garnet in sample 3354 also contains one large (0.72 mm x 1.09 mm) irregular plagioclase inclusion (Figure 4-XIX). The transect across this garnet passes slightly to one side of this inclusion. The FeO and MgO contents do not alter their shape, however the CaO content increases abruptly from 2.5% to 5.1% in the vicinity of this inclusion (Figure 4-XVIII).

Other mineral inclusions also alter the appearance of the zoning profiles. For example the larger, irregularly shaped garnet in sample 3832 contains an U-shaped biotite inclusion near its middle (Figure 4-XXII). Where the transect passes close to this inclusion,

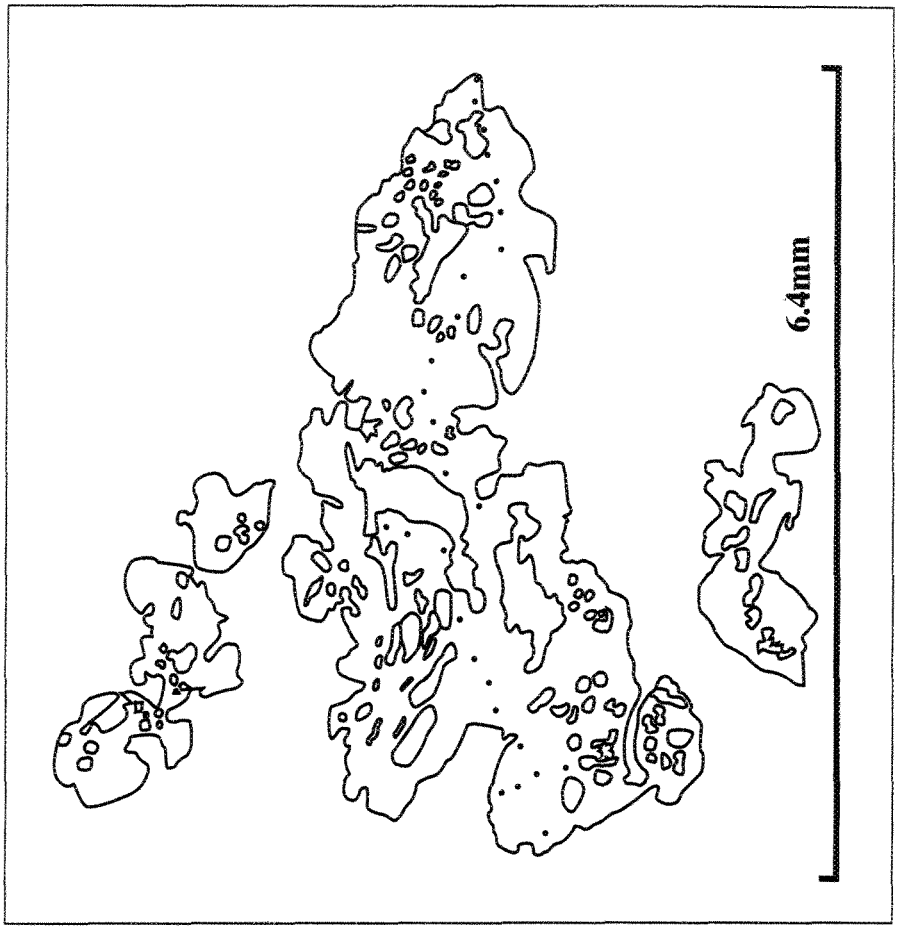

Figure 4-XXII: Garnet from sample 3832. This corresponds to the profile in Figure 4-XVII. The inclusions in the top half of this garnet are all plagioclase and quartz, and therefore, do not distort the chemical profiles. In the bottom half, the larger inclusions are biotite, the corresponding portions of the garnet profiles are distorted.

the FeO content increases, MgO decreases and CaO appears to decrease slightly (Figure 4-XVII). The presence of oxides and hercynite in the inclusion-rich outer rim of the garnet in sample 2401D2 (Plate IX; Figure 4-XV) also distort the zoning profile through the rim (Figure 4-XIV). However, in this case, the influence of individual mineral inclusions is difficult to determine due to the density and variety of the inclusions.

Hames and Menard (1993) also observed that mineral inclusions within garnets promoted the movement of fluids along the inclusion boundaries. The presence of mineral inclusions within the garnets also aids in making the cores of garnets susceptible to the affects of retrograde cation exchange. Thus, the analyses near inclusions should be avoided for the thermobarometric calculations.

The absence of inclusions, such as in the inclusion-free core of sample 2401D2 (Figure 4-XV), results in relatively smooth zoning profiles. This suggests that this core would have been relatively impervious to fluid circulation. Therefore, this core may provide geologically significant information about peak metamorphic conditions (Chapter 5).

4.7k.vi Post-peak Metamorphic Diffusion?

Because the garnets in this study area all formed at temperatures above 650°C (Chapters 3, 5), these garnets would be expected to have had smooth (i.e. flat) compositional profiles at the peak metamorphic temperatures (STAGE II from Figure 4-VII). However, the zoning profiles from garnets 4475D3 (Figure 4-IX), 3354 (Figure 4- XVIII), and 2401D2 (Figure 4-XIV) are bell-shaped with a similar form to the hypothetical low cooling-rate model outline in STAGE III on Figure 4-VIII, implying that these garnets have experienced post-peak metamorphic diffusion with a low cooling rate (Chapter 6).

The influence of embayments and inclusions on the zoning profiles also provides further evidence of the effects of post-peak metamorphic diffusion. The same argument holds for bell-shaped modifications of profiles where they were influenced by inclusions or

embayments. Good examples of these bell-shaped alterations of profiles due to embayments and inclusions are samples 2401D2 (Figure 4-XIV), 3045 (Figure 4-XII), 3832 (Figure 4-XVII) and 4209 (Figure 4-VIII).

4.8 AFM Projections

For each thin section, the mineral analyses were plotted on an AFM diagram projected from K-feldspar and quartz (Thompson 1957). The co-ordinates used to plot the microprobe analysis on the AFM plots were as follows:

$$A = Al - [Ca + Na + K]$$

$$F = [Fe]$$

$$M = [Mg]$$

$$A + F + M = 100$$

The resultant position of individual mineral analysis on the AFM diagrams were examined with respect to other analyses of the same mineral species in the rock to determine whether:

a. systematic compositional variations related to position in the mineral e.g. core, rim etc., and

b. cross-cutting tie line relationships were indicative of a reaction relationship between phases.

In most cases such as sample 1280, assemblages defined at the thin section scale are two phase fields and hence preserve no evidence of reaction relationships (Figure 4-XXIII).

4.8a Garnet Zoning Patterns From AFM Diagrams

A transect across each mineral within the thin sections was analysed to test for zoning. Garnet is the only mineral that demonstrated any schematic zoning patterns. This zoning can be observed in the AFM projections for samples 1280, 3354, 2770, 4209, 4475D3 (Figures XXIII through XXVII), 16 of the 17 thin sections demonstrated a general trend where the core was enriched in Mg and depleted in Fe gradually becoming depleted in Mg and enriched in Fe towards the rims. Sample 2401E did not follow this trend, possibly

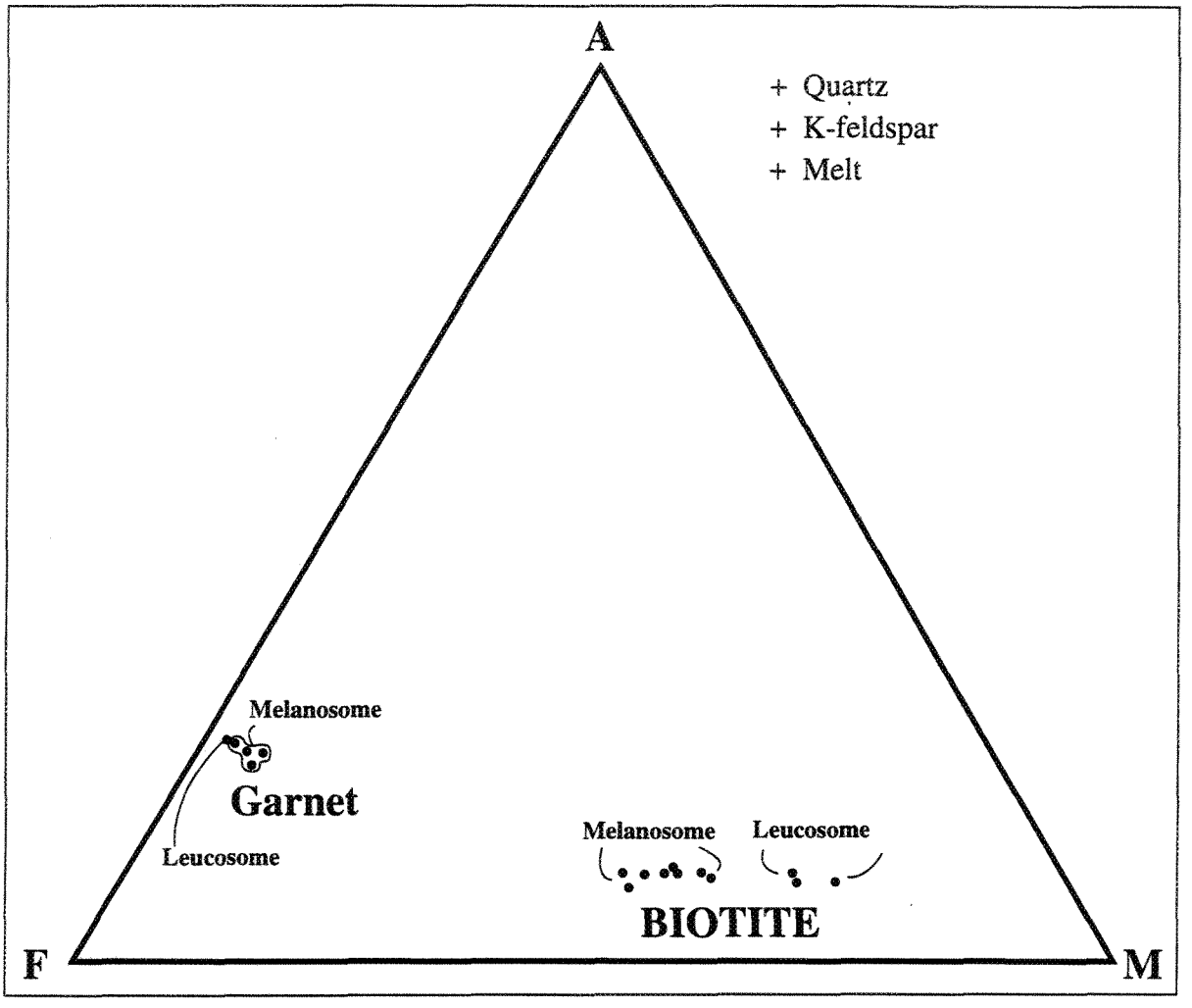

FIGURE 4-XXIII: An AFM projection from K-feldspar for sample 1280 (NCDZ). This thin section contains both leucosome and melanosome. Leucosome biotites have up to 20% more magnesium than the melanosome biotites. The leucosome garnets contained between 1 and 5 Wt% more aluminum, 1 to 5 Wt% more iron, and 1-5 Wt% less magnesium.

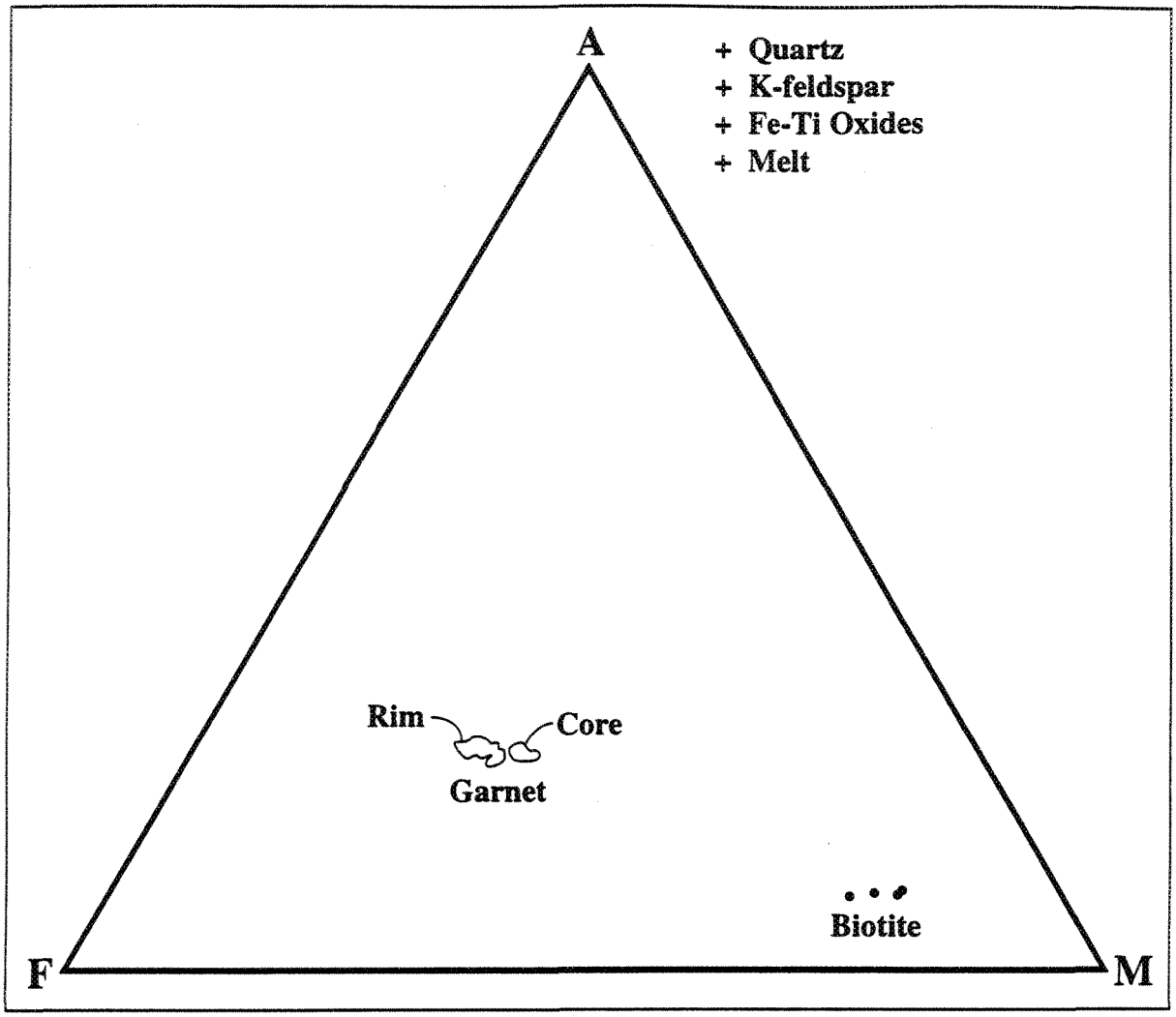

FIGURE 4-XXIV: An AFM projection from K-feldspar for sample 3354 (BGC). Here there are only two phases to plot, biotite and garnet, thus there are no reactions implied by crossing tielines. However, the garnet plot does demonstrate one of the typical trends for garnets, that the core analyses are more magnesian (by 5-10%) than the rim analyses.

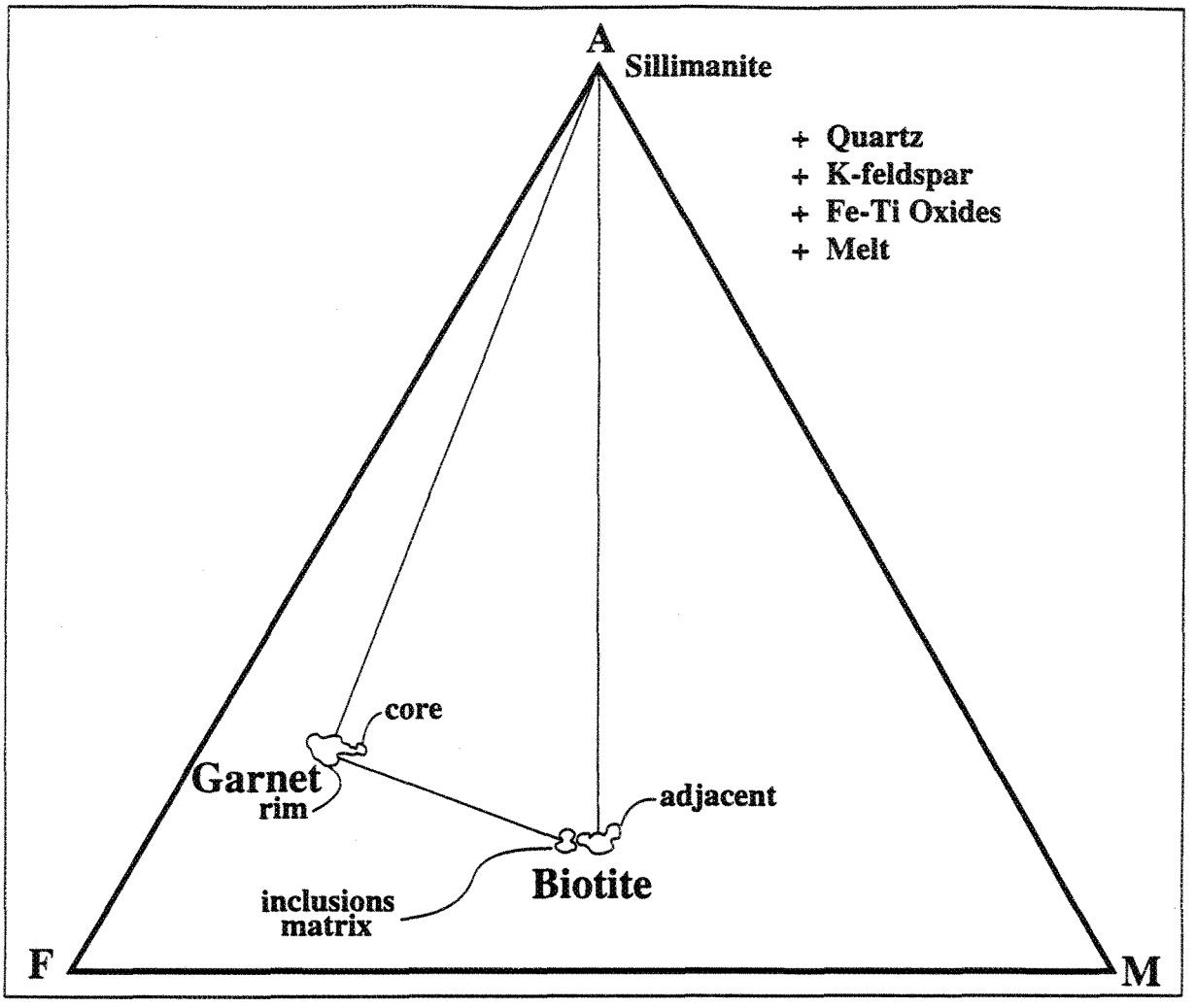

FIGURE 4-XXV: An AFM projection from K-feldspar for sample 2770 (NCDZ). The garnets from this outcrop demonstrate the same chemical patterns as those of the previous Figure XXV, with the core being enriched in magnesium and the rim being enriched in iron. Here, the biotites also demonstrate a trend with the adjacent matrix biotites being magesium rich, and the inclusion/distant matrix biotites being iron-rich. This sample is from the NCDZ. A direct comparison between this AFM projection and Figure XXV (BGC) shows that the BGC garnets and biotites, and therefore whole rock compositions, are much more magnesium-rich than the NCDZ garnets and biotites. These biotites are up to 30% more iron-rich, and the garnets are up to 20% more iron-rich than the same minerals from the BGC.

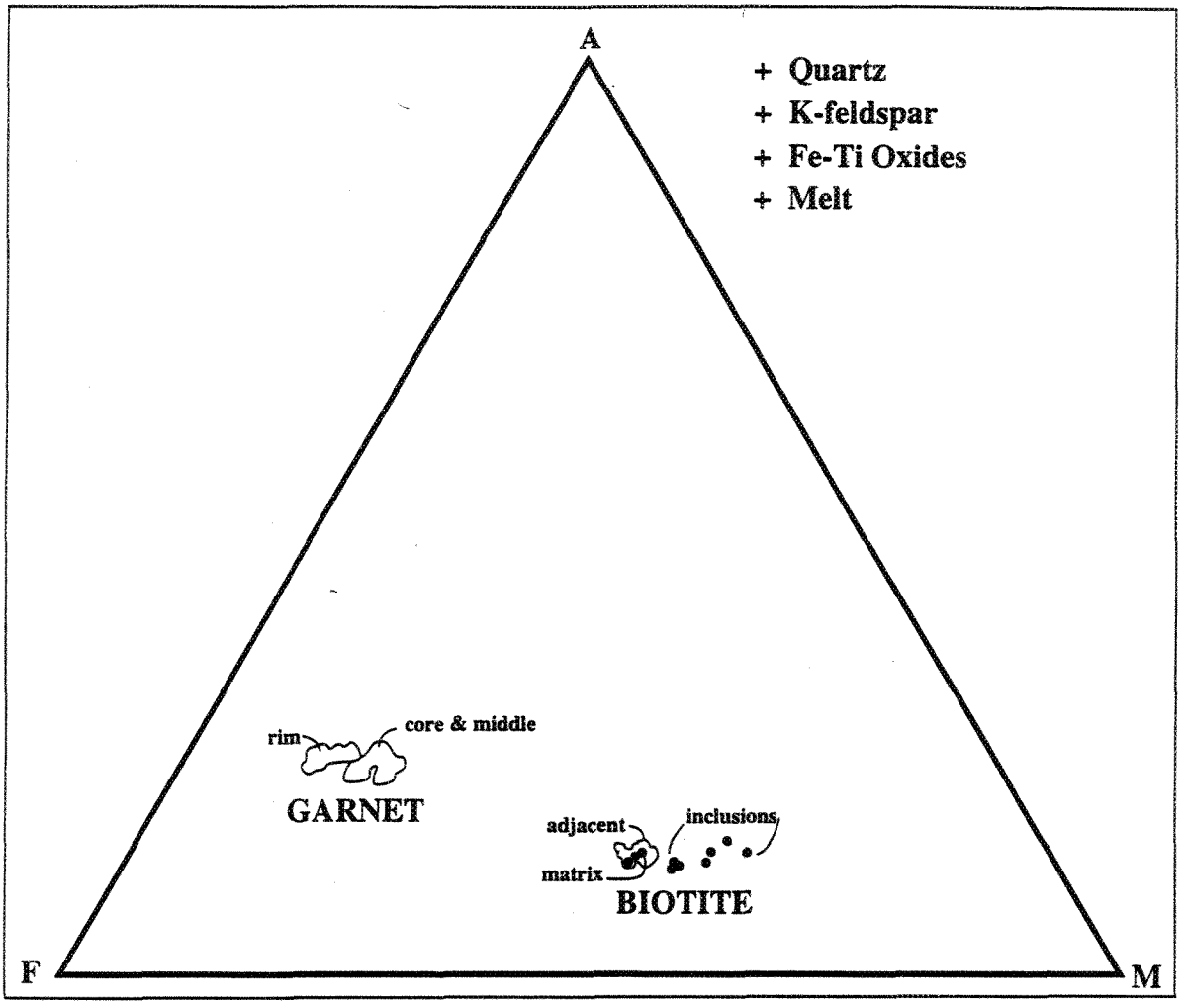

FIGURE 4-XVI: AFM projection from K-feldspar for sample 4209. Note here that both the core-middle garnets and the biotite inclusions inside the garnets are 5-10% richer in Mg, than the rim garnets and the adjacent-matrix biotites. This sample is from the NCDZ, and is thus poorer in Mg than the analyses from the BGC. A direct comparison with samples 4475D3 (from the BGC) demonstrates that these NCDZ garnets are up to 20% poorer in Mg and the biotites are up to 30% poorer in Mg.

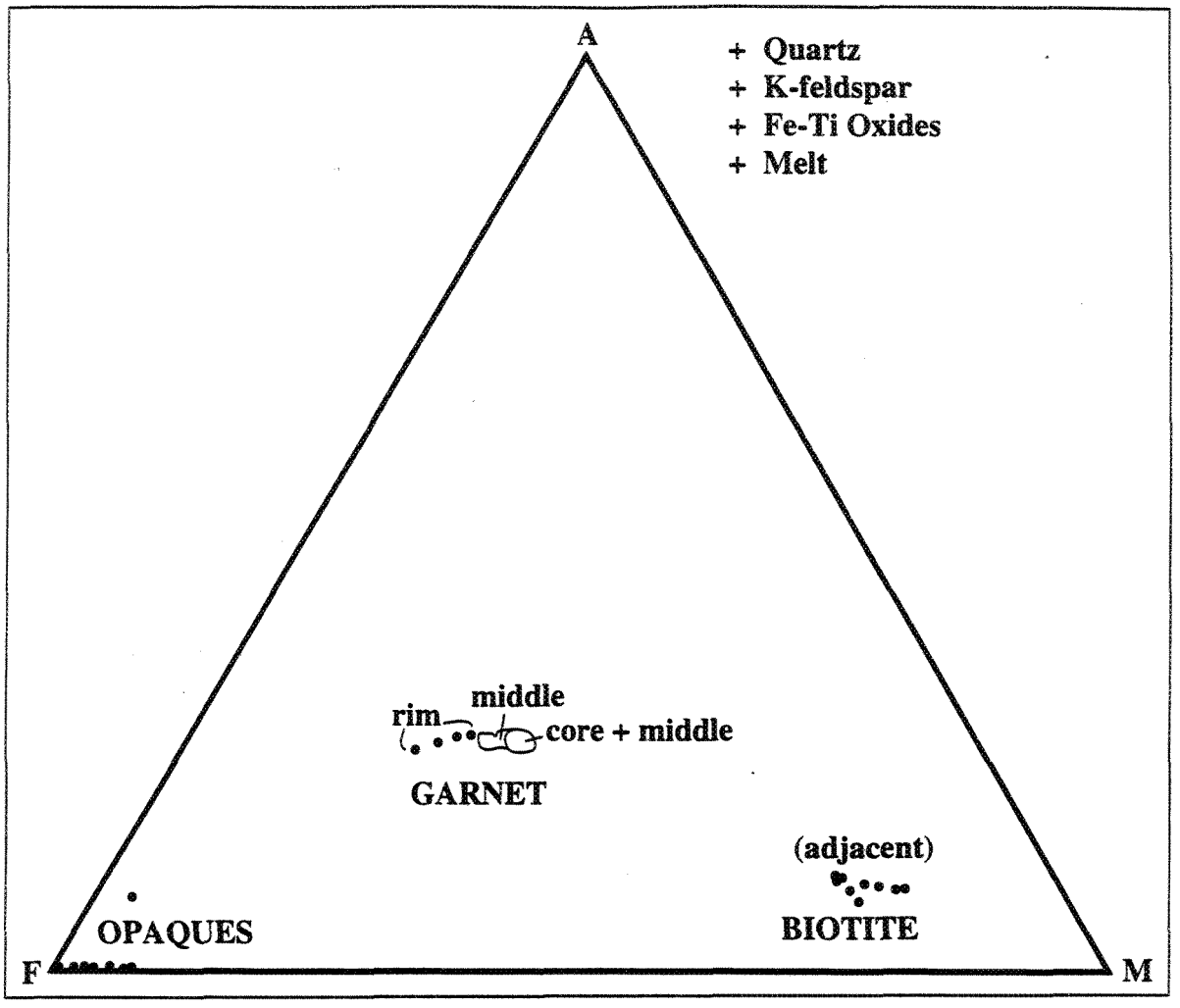

FIGURE 4-XXVII: AFM projection from K-feldspar for sample 4475D3 (BGC). This projection demonstrates the typical trend of the garnet analyses from this field area, with the core being up to 10% richer in Mg than the rim analyses. This sample, being from the BGC, is more magnesian than the samples from the NCDZ. Here, the garnets are up to 20% richer in Mg, and the biotites are up to 30% richer in Mg, than the analyses from the NCDZ samples. Here the biotites are also up to 5% poorer in Al than the biotites from the NCDZ.

because not enough analyses were completed on the garnets in this thin section, sample 2401D2 from the same outcrop does exhibit the normal zoning pattern. Three samples (3045, 4012 and 4220; Figure 4-XXVIII) had garnets that were progressively enriched in Ca outwards from the cores to the rims.

4.8b Trends From AFM Diagrams

Mineral analyses from grains included within garnets and/or orthopyroxenes were compared with those from the matrix to test for a chemical difference between the two groups of grains. As can be seen from the AFM diagrams, there are differences between the chemical analysis of biotite included within garnets and the biotites occurring in the matrix. In ten of the seventeen thin sections examined, the biotites included within garnets had consistently more magnesium and less iron than those biotites located in the matrix (both those located adjacent to the garnets and remote from the garnets; e.g. sample 4209; Figure 4-XXVI). Of the remaining seven thin sections, five did not include enough acceptable biotite analyses to provide support to these observations. The remaining two thin sections demonstrated opposing trends, in sample 2770 (Figure 4-XXV), the biotites adjacent to garnets were enriched in magnesium and depleted in iron, whereas the biotites included within garnets and those matrix biotites remote from garnets were similarly depleted in magnesium and enriched in iron. In sample 4220, the biotites adjacent to garnet are enriched in magnesium and depleted in iron, whereas, the included biotites are depleted in magnesium and enriched in iron with the remote matrix biotites showing intermediate compositional trends. These two separate groups of grains were also analysed to observe the effects of their chemical differences on the geothermometers (Chapter 5).

A second interesting trend is evident in the AFM projection of sample 1280 (Figure 4-XXIII). The analyses of biotite and garnet from leucosomes and restites were plotted separately. The restite biotites were richer in magnesium than the leucosome biotites;

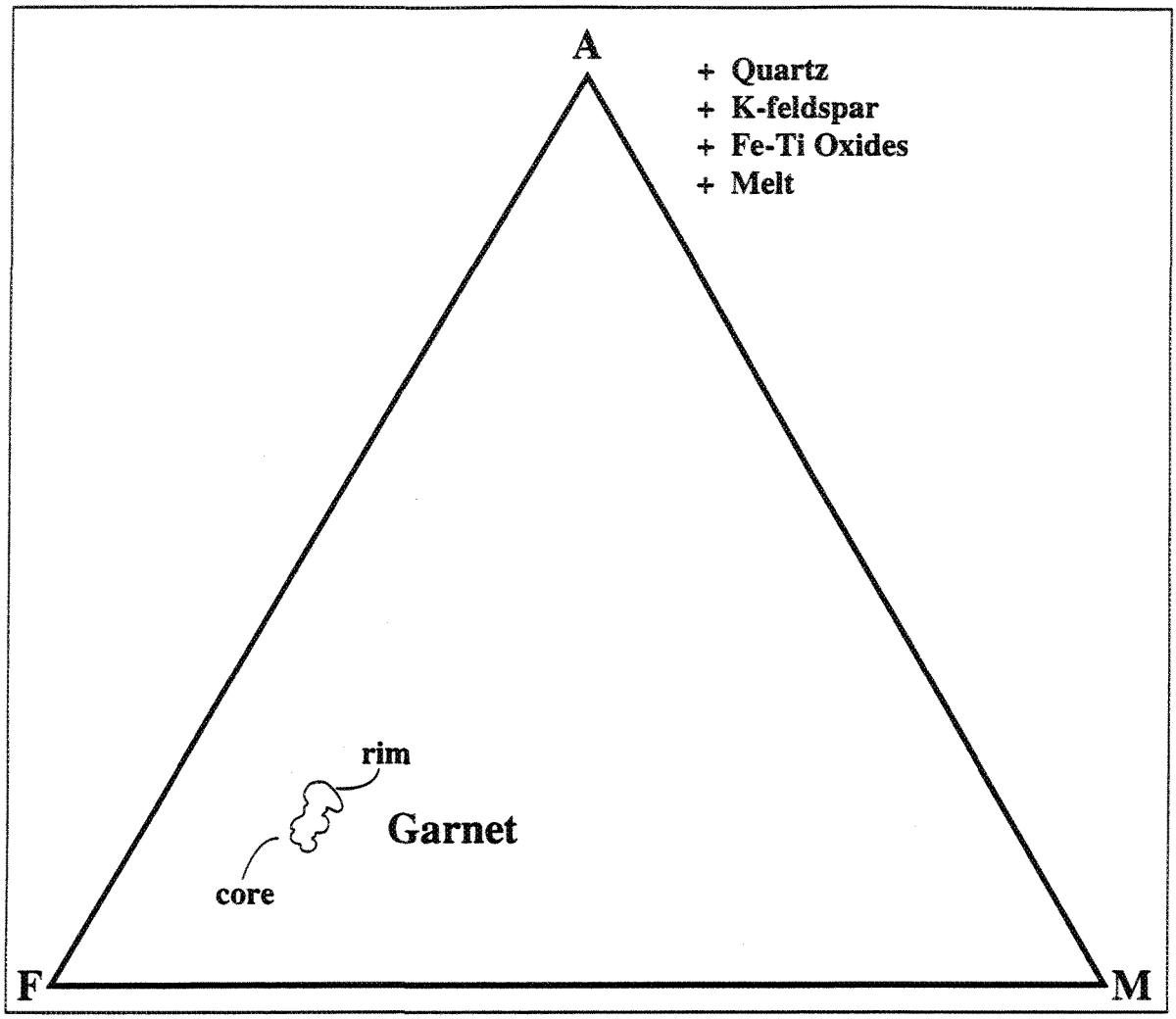

FIGURE 4-XXVIII: An AFM prjection from K-feldspar for sample 4220 (NCDZ). A direct comparison between the location of these garnets and those from the BGC sample in Figure XXV show that these garnets from the NCDZ are up to 20% richer in iron.

whereas the restite garnets were richer in iron than the leucosome garnets (Figure 4-XXIII). This chemical relationship between garnets and biotites in the restite and leucosome imply that the temperatures were reduced during the formation of the leucosomes (Chapter 5; section 5.3).

4.8c Reactions Inferred From AFM Diagrams

4.8c.i Spinel+Quartz

The addition of spinel and sillimanite into the system in samples 2401D2 made the AFM projections more informative (Figure 3-XIII). In order to represent adequately the reaction suggested by the microtextures, an ASF plot must be used since the reaction of interest is quartz consuming and the product assemblage is quartz-free (Figure 3-XIV). The ASF projection was from plagioclase with the following equations:

$$A = Al - [Ca + Na]$$

$$S = Si$$

$$F = Fe$$

The crossing tie lines in Figure 3-XIV and the microtextures (Plate IX) suggest the balanced reaction:

(3.1ci-3) $3FeAl_2O_4 + 11SiO_2 = 4AlSi_2O_5 + Fe_3Al_2Si_3O_{12} + O_2$
3Spinel + 11Quartz = 4Sillimanite + Garnet

4.8c.ii Cordierite + Orthopyroxene

The most informative AFM projections are those for sample 1659 (Figures 3-X, 3-XI, 4-XXIX, 4-XXX). The crossing tie lines in Figures 3-X, 3-XI and the observed textures (Chapter 3) suggest the following discontinuous prograde reactions (Figure 3-XII):

(30) garnet + biotite + K-feldspar + quartz = sillimanite + orthopyroxene + melt

(31) sillimanite + biotite + K-feldspar + quartz = cordierite + orthopyroxene + melt

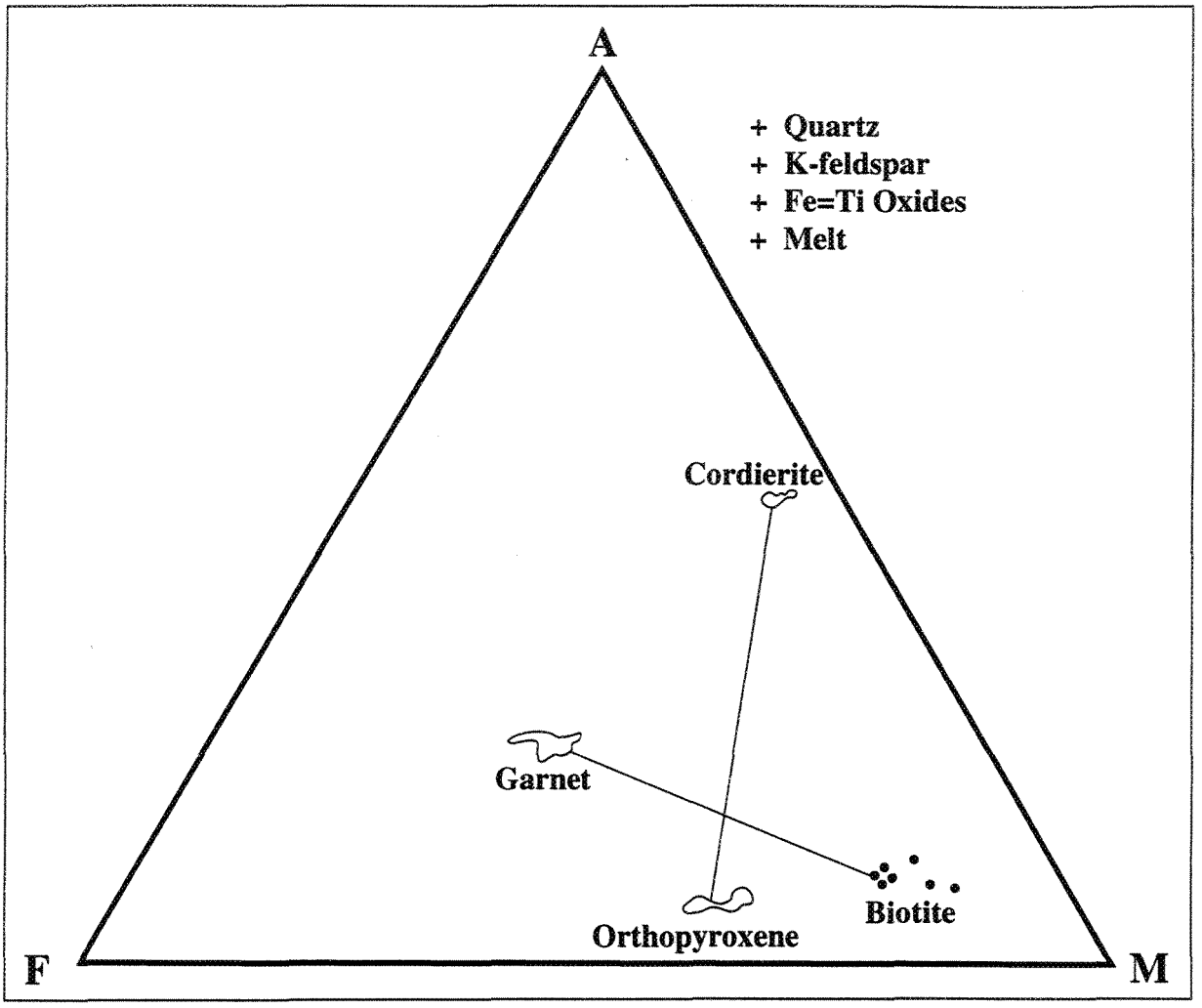

FIGURE 4-XXIX: An AFM projection from K-feldspar for sample CQA1659D3 (BGC). Here, the addition of retrograde biotite results in the configuration of crossing tie-lines that suggests the reaction Opx + Crd = Grt + Bt + Qtz. This reaction corresponds to reaction 10 from Vielzeuf and Holloway's (1988) petrogenetic grid (Figure 3-III).

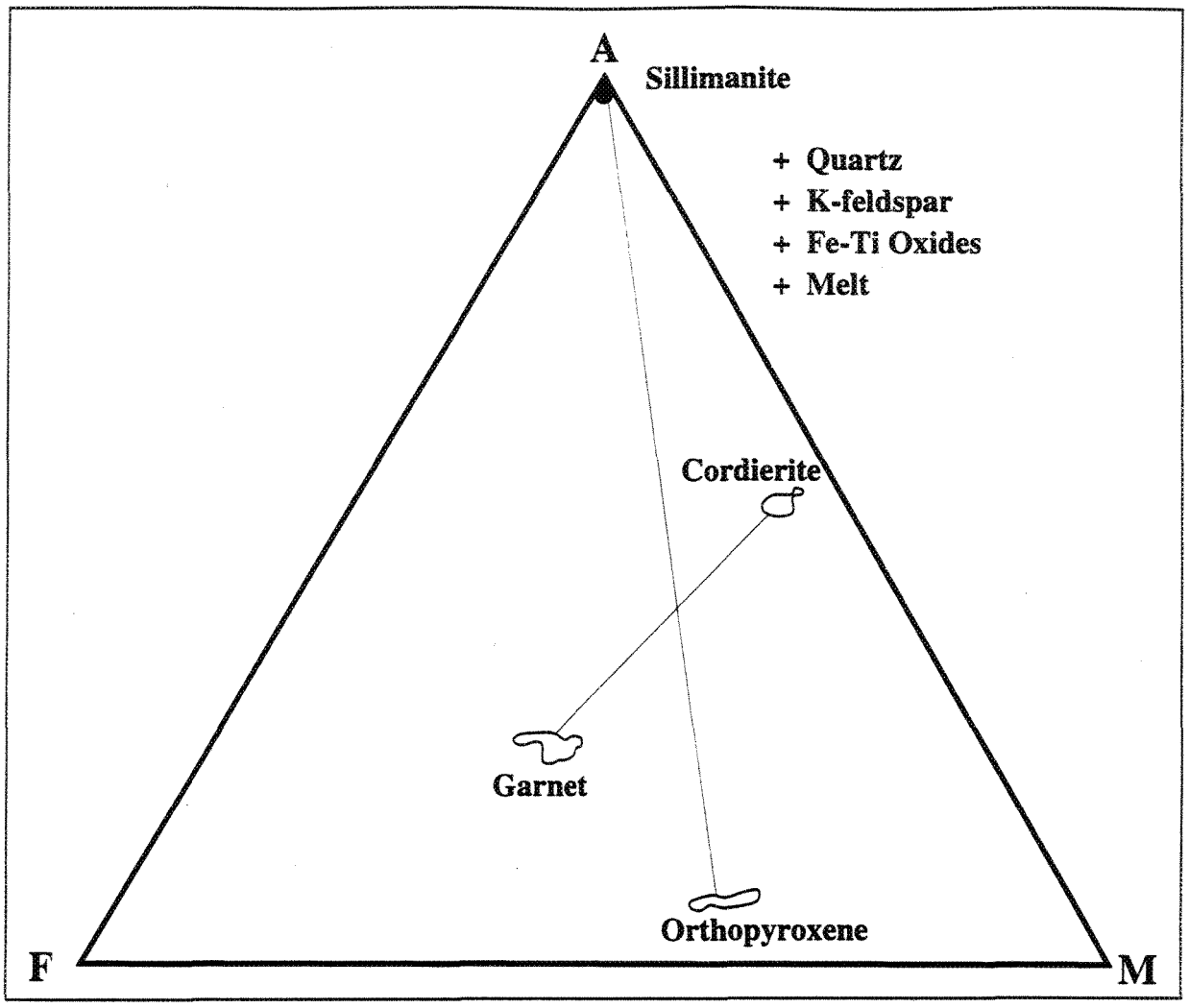

FIGURE 4-XXX: An AFM projection from K-feldspar for sample 1659D3 (BGC). The addition of the phases cordierite and orthopyroxene to this sample from the above confirguation of crossing tielines that depict the discontinuous prograde reaction (32) Opx + Sil (+ Melt) = Grt + Crd (+Kfs + Qtz). This reaction corresponds to the (bt) reaction between [Os] and [Bt] on Figure 3-XII.

The crossing tie lines in Figures 4-XXIX, 4-XXX and the observed textures (Chapter 3) suggest the following retrograde reactions:

(32) orthopyroxene + sillimanite + melt = garnet + cordierite + K-feldspar + quartz

(33) garnet + quartz + vapour = cordierite + orthopyroxene

(34) melt + garnet + cordierite = sillimanite + biotite

(35) melt + orthopyroxene + cordierite = sillimanite + biotite

The discontinuous reaction (32) is defined in P-T space by Carrington and Harley (1995; Figure 3-XII), reaction (33) is defined in P-T space by Vielzeuf and Holloway (1988; Figure 3-III). These reactions were used in Chapter 3 to define portions of both the prograde and retrograde P-T trajectories for both the Bondy Gneiss Complex and the Nominingue-Chénéville Deformation Zone.

4.9 Summary

4.9a Bondy Gneiss Complex

The plagioclase analyses from the Bondy Gneiss Complex vary from oligoclase through labradorite to bytownite This is possibly due to the hydrothermal alteration proposed by Corriveau et al. (1995). The alkali feldspars from this complex also demonstrate a large variation in composition from $Or_{70}Ab_{17}An_{13}$ to $Or_{89}Ab_{11}An_{0}$. All of the biotite within the BGC plot within the phlogopite field.

A comparison of the AFM plots demonstrates an interesting trend between the BGC and the NCDZ. The minerals in the BGC consistently plot in a more magnesian-enriched field than the minerals from the NCDZ. For example, the biotites plot between 58 and 70% MgO, and the garnets plot between 20 and 30% MgO (Samples 3354, 4475D3, 1659D3, 2401D2; Figures 4-XXIV, 4-XXVII, 4-XXIX, 3-XIII). This suggests a possible enrichment of MgO in these rocks by the hydrothermal alteration proposed by Corriveau et al. (1995). Figure 4-I contain a summary of these characteristics.

4.9b Nominingue-Chénéville Deformation Zone

The mole fraction anorthite from the Nominingue-Chénéville Deformation Zone samples range from 0.51 to 0.64 (labradorite). This is a much smaller range than the BGC. The K-feldspar analyses are also more consistent than the BGC, ranging from $Or_{86}Ab_{11}An_3$ to $Or_{89}Ab_8An_3$. The biotite from the NCDZ (other than inclusions within leucosome garnets from sample 1280) plot within the biotite field.

As mentioned above, the minerals from the NCDZ plot in a more iron-enriched field on AFM plots than the minerals from the BGC. For example, the biotites plot between 35 and 58% MgO, whereas the garnets plot between 3 and 18% MgO (Samples 1280, 2770, 4209, 4220; Figures 4-XXIII, 4-XXV, 4-XVI, 4-XXVIII). These differences are summarised in Figure 4-I.

CHAPTER 5

GEOTHERMOBAROMETRY

5.1 Purpose and Outline

The use of assemblages and textures to predict the morphology of a P-T trajectory provides only approximate positions for the peak pressures and temperatures, for either the prograde or the retrograde paths. The results from geothermobarometric calculations can be used to provide more accurate points in P-T space. With good microprobe analyses, an accurate position for the peak metamorphic pressures and temperatures, and points along the prograde or retrograde paths, may be plotted. Thus, the geothermobarometer results may be used to "fine tune" the P-T trajectories suggested by the assemblages and textures in Chapter 3.

The calculated temperatures from the garnet-biotite Fe-Mg exchange thermometer were plotted against garnet size to determine the effects of retrograde cation exchange on the preserved garnets. Histograms of calculated temperatures for the orthopyroxene garnet thermometer were plotted to determine which was the actual peak temperature. The peak pressure was calculated from the GASP and Al in orthopyroxene barometers. Structural evidence, and garnet zoning profiles suggest an initial episode of isothermal decompression following peak temperature, therefore, the pressure that corresponds to the peak temperature was calculated from the spinel-garnet barometer. Retrograde pressures were then calculated from the cordierite-garnet barometer. The resultant P-T trajectories for the Bondy Gneiss Complex and the Nominingue-Chénéville Deformation Zone were then plotted considering both the geothermobarometer results and the assemblage/textures.

5.2 Method

The significant effects of post-peak diffusion have altered the chemical profiles of the garnets (Chapter 4). Thus all geothermobarometers would record lower diffusion-based post-peak metamorphic temperatures, especially those sensitive to retrograde cation exchange such as the biotite-garnet Fe-Mg exchange geothermometer. It is therefore important to choose geothermobarometers that are insensitive to Fe-Mg re-equilibration, such as those involving alumina net-transfer reactions.

Also, it is likely that the Fe-Mg exchange thermometers have closure temperatures for cation exchange below those of granulite metamorphism (O'Hara 1977; O'Hara and Yarwood 1978; Lasaga 1983). Straightforward insertion of the stoichiometric data into the databases would fail to allow for a close examination of the effects of the low closure temperatures for cation exchange. This would have dire consequences on the reliability of the resultant calculated P-T values as stated by Frost and Chacko (1989), Harley (1989), Selverstone and Chamberlain (1990), Spear (1991, 1992) and Spear and Florence (1992).

5.3 Biotite-Garnet Fe-Mg Exchange Thermometer

5.3a Literature

As temperature increases, garnet becomes enriched in Mg and biotite in Fe with the following exchange reaction:

(5-1) Fe-garnet + Mg-biotite = Mg-garnet + Fe-biotite.

The Gibb's energy for this reaction is effected by both temperature and pressure:

(5-2) $\Delta G = \Delta H - T\Delta S + (P-1)\Delta V$

Where G = Gibb's Free Energy, H = Heat Capacity, T = Temperature, P = Pressure, V = volume. However, the volume change of this reaction is small (0.057 cal/bar; Ferry and Spear 1978) indicating that pressure only has a minor influence on the Gibb's energy, therefore this reaction is an ideal geothermometer (Chipera and Perkins 1988).

The equilibrium constant (K) for reaction (5-1) has both an "ideal" (distribution coefficient Kd) and "non-ideal" component described by the ratio of activity coefficients K¥ :

$$K = \frac{(X_{Mg}/X_{Fe})_{gt}}{(X_{Mg}/X_{Fe})_{bt}} * \frac{(¥_{Mg}/¥_{Fe})_{gt}}{(¥_{Mg}/¥_{Fe})_{bt}} \quad (5\text{-}3)$$

$$K = Kd * K¥ \quad (5\text{-}4)$$

In studies where ideal mixing is assumed, activity coefficients and K¥ are equal to 1, making the equilibrium constant (K) equal to the distribution equilibrium coefficient (Kd). This may be justified (and may not produce significant errors) if:

a) the deviations from ideality of biotite and garnet are small, or

b) the deviations from ideality of biotite and garnet cancel each other.

Thompson 1976b, calibrated his thermometer by correlating Kd values of natural biotite-garnet assemblages with estimated temperatures from experimental phase equilibria. Goldman and Albee (1977) compared the biotite-garnet compositions to temperatures obtained by quartz-magnetite oxygen isotope thermometry. The Ferry and Spear (1978) thermometer was experimentally calibrated in systems with Fe/Fe + Mg held at ~0.9. The Perchuk and Lavrent'eva (1983) thermometer was also calibrated experimentally in systems at ~ 0.6 Fe/Fe+Mg. Ganguly and Saxena (1985) developed a thermodynamic model based on the experimental model of Ferry and Spear (1978) and implementing ideal mixing in biotite, but non-ideal mixing in garnet.

The partitioning of cations between coexisting phases may also be dependent on bulk composition (Bohlen and Essene 1980). A statistical investigation (Goldman and Albee 1977) of the compositional effects on $\ln_{Kd}$ due to Ti and Al_{VI} in biotite and Ca and Mn in garnet demonstrated that increasing Ti in biotite increases the temperatures and that an increase in Ca and Mn in garnet and Al_{VI} in biotite decreases the temperatures obtained from this calibration. Ferry (1980) found that Goldman and Albee's (1977) approach may occasionally over-compensate for these compositional effects. Indares and Martignole

(1985) combined natural data with the experimental data of Ferry and Spear to derive an empirical thermometer that corrects for garnet and biotite dilutents (Patiño Douce et al. 1993).

Chipera and Perkins (1988) applied several calibrations (Thompson 1976a; 1976b; Goldman and Albee 1977; Ferry and Spear 1978; Perchuk and Lavrent'eva 1983; Ganguly and Saxena 1984; and Indares and Martignole 1985) of the garnet-biotite geothermometer to the English River subprovince of western Ontario, in order to examine their respective accuracy and precision. Accuracy was assessed by comparing experimental phase equilibria with the derived temperatures. Precision was evaluated by a least-squares regression (trend surface analysis) to determine the fit of the temperatures on the regional temperature surface across the study area. An F-test was used to analyse the variance for each degree of regression in a trend:

(5-5) $$\text{F ratio} = \frac{(SSR_n - SSR_{n-1})/(DFR_n - DRF_{n-1})}{(SSD_n/DFD_n)}$$

(SSR = Sum of Squares Regression; SSD = Sum of Squares Deviation; DFR = Degrees Freedom Regression; DFD - Degrees Freedom Deviation; n= Order of Equation)

Chipera and Perkins (1988) determined that the Goldman and Albee thermometer produced temperatures lower than those indicated by the prograde reactions, whereas Ferry and Spear's (1978) thermometer resulted in temperatures above those indicated by the reactions. The remaining calibrations were observed to produce reasonable results with that of Perchuk and Lavrent'eva being the most reasonable and consistent. As mentioned in Chapter 1 and above (section 5.1), it has recently been determined that many exchange thermometers may underestimate peak temperatures due to the offset from the peak temperature and peak pressure of the P-T paths by retrograde cation exchange. Thus, it is quite possible that the Ferry and Spear (1978) thermometer actually recorded, by chance, temperatures that were closer to the real peak temperatures than previously considered. For

this study only the Ferry and Spear thermometer was used because it may be more accurate as recently suggested (Spear 1991).

5.3b Retrograde Cation Exchange

As can be observed from the garnet zoning profiles discussed in chapter 4, the garnets in this study have been subjected to retrograde cation exchange. Thus the garnet rims do not record peak metamorphic conditions. It is also possible that few or none, of the garnet cores, especially the smaller garnets, preserve peak metamorphic characteristics. In order to examine the effect of this post metamorphic peak diffusion on the temperatures derived from Ferry and Spear's (1978) biotite-garnet thermometer, graphs of garnet size versus derived temperatures were plotted. The temperatures obtained for each garnet core was plotted in several categories; i) the overall range when paired with all the biotites, ii) those paired with included biotites in the core of garnets, iii) those paired with included biotites in the rims of garnets, iv) those paired with biotites adjacent to the garnets and v) those paired with matrix biotites remote from the garnets. The temperature ranges were plotted for several groups of garnets: individual garnets, tectonostratigraphic units, and overall field area. For the purpose of discussion, only the maximum temperatures were considered, as these are the temperatures that are likely to have been least affected by retrograde cation exchange.

Florence and Spear (1991) suggested that if peak temperatures are thought to be greater than 620°C, with a metamorphic history over 20 to 30 Ma and a heating/cooling rate of 2-5°C/Ma, that grains with radii >2 mm should be chosen to reconstruct P-T path models and accurate P-T histories. In this study, the peak temperatures are near 950°C, the metamorphic history over 40 Ma, and the cooling rates below 5°C/Ma for temperatures < 600°C (Chapters 5, and 6). In order to test this hypothesis, all the garnets were analysed,

and the results from the garnet-biotite Fe-Mg exchange thermometer were compared against the garnet's size.

5.3b.i. Individual Thin Sections

As can be observed in Figure 5-I (Sample 4220), the general overall trend is that the smaller garnet cores record maximum temperatures (T_{max}) that are lower than those for larger garnet cores. For this sample, the smallest garnet has an area of 0.47 mm^2 with a derived T_{max} of 778°C whereas the largest garnet has an area of 11.02 mm^2 with a derived T_{max} of 846°C. An interesting aside is the trend of temperature ranges with respect to the location of the biotite analysis. For example, the biotites included within the core of the garnets yielded a range of temperatures that represents the lower half of the overall temperature range; whereas the biotites included within the rims of the garnets represent a range of temperatures that include the lower two thirds of the overall range. Biotites adjacent to the garnets represent the upper half of the overall temperature range, whereas the matrix biotites that do not contact garnets represent a small range of temperatures in the middle of the overall range.

The same overall general trend for garnet size versus Tmax is also seen in Figure 5-II (sample 4012) where garnets of smaller size have lower maximum temperatures than garnets of larger size. For example four of the six garnets with areas less than 6 mm^2 have a T_{max} of between 750 and 796°C, whereas a larger (19.5 mm^2) garnet has a T_{max} of 986°C. Here, it is also interesting to note the distribution of the temperature ranges. The biotites included in the cores of the garnets resulted in temperatures in the lower half of the overall temperature ranges while the biotites included in the garnet rims gave temperatures that correspond to the overall range. The biotites located adjacent to garnets gave temperatures in the middle third of the overall range.

The five garnets from sample 3832 do not show the general trend observed in the other samples (Figure 5-III). These garnets, which range in size from 0.9 to 3.3 mm^2, give

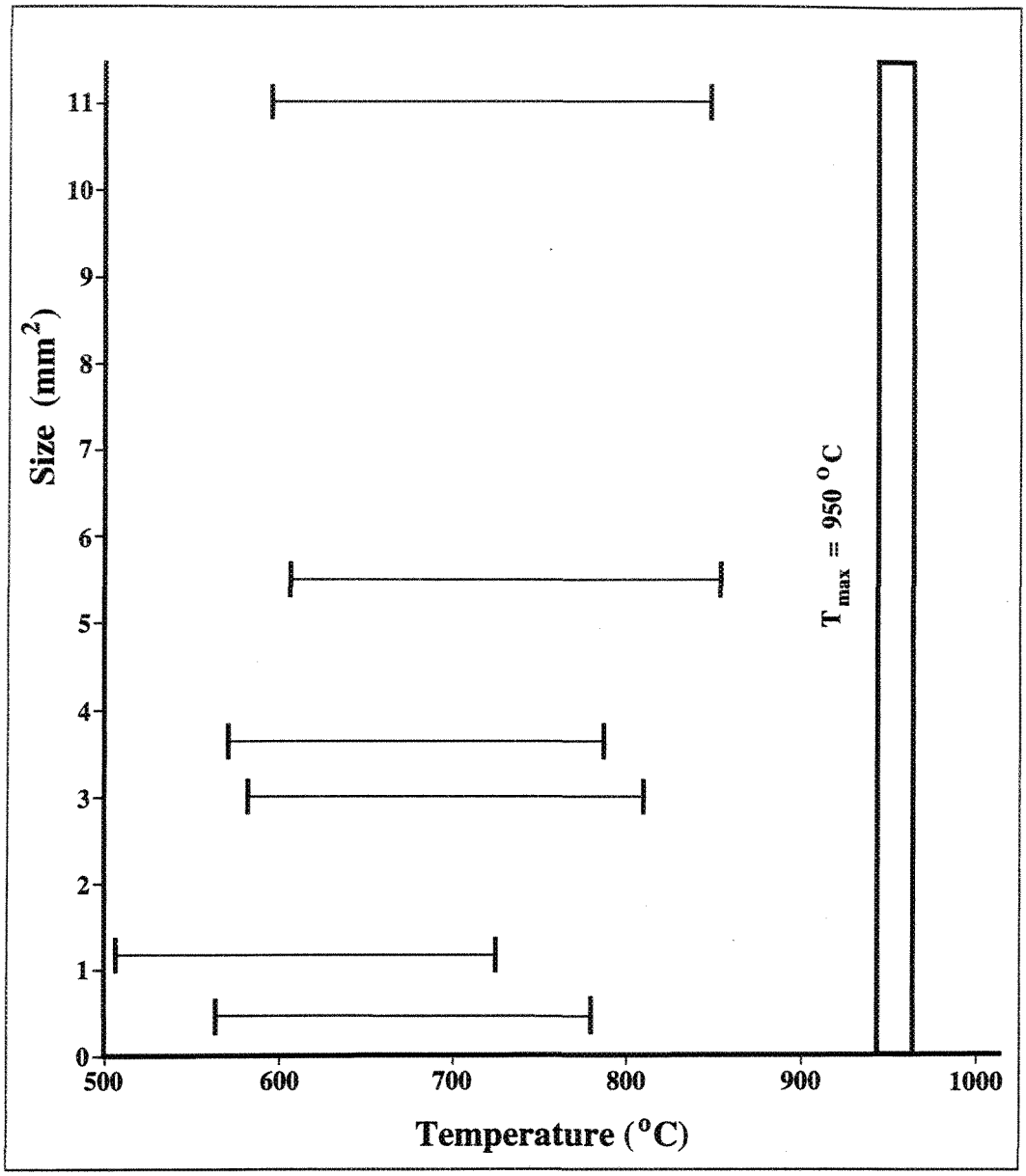

FIGURE 5-I: Plot of temperature from Ferry and Spear's (1978) biotite-garnet Fe-Mg exchange thermometer versus size of garnet for sample 4220. The complete range of data was plotted, however, for discussion purposes, only the maximum temperatures were used. This is the value most likely to record the actual peak conditions due to the effects of retrograde cation exchange. These seven garnets demonstrate the overall general trend, that the smaller garnets record temperatures lower than the larger garnets. Here the temperature difference is 70 °C, between the 850°C of the largest garnet and the 780 °C of the smallest garnet. In this sample, even the larger samples were affected by retrograde cation exchange, they record temperature 100 °C below the proposed peak temperature for the field area.

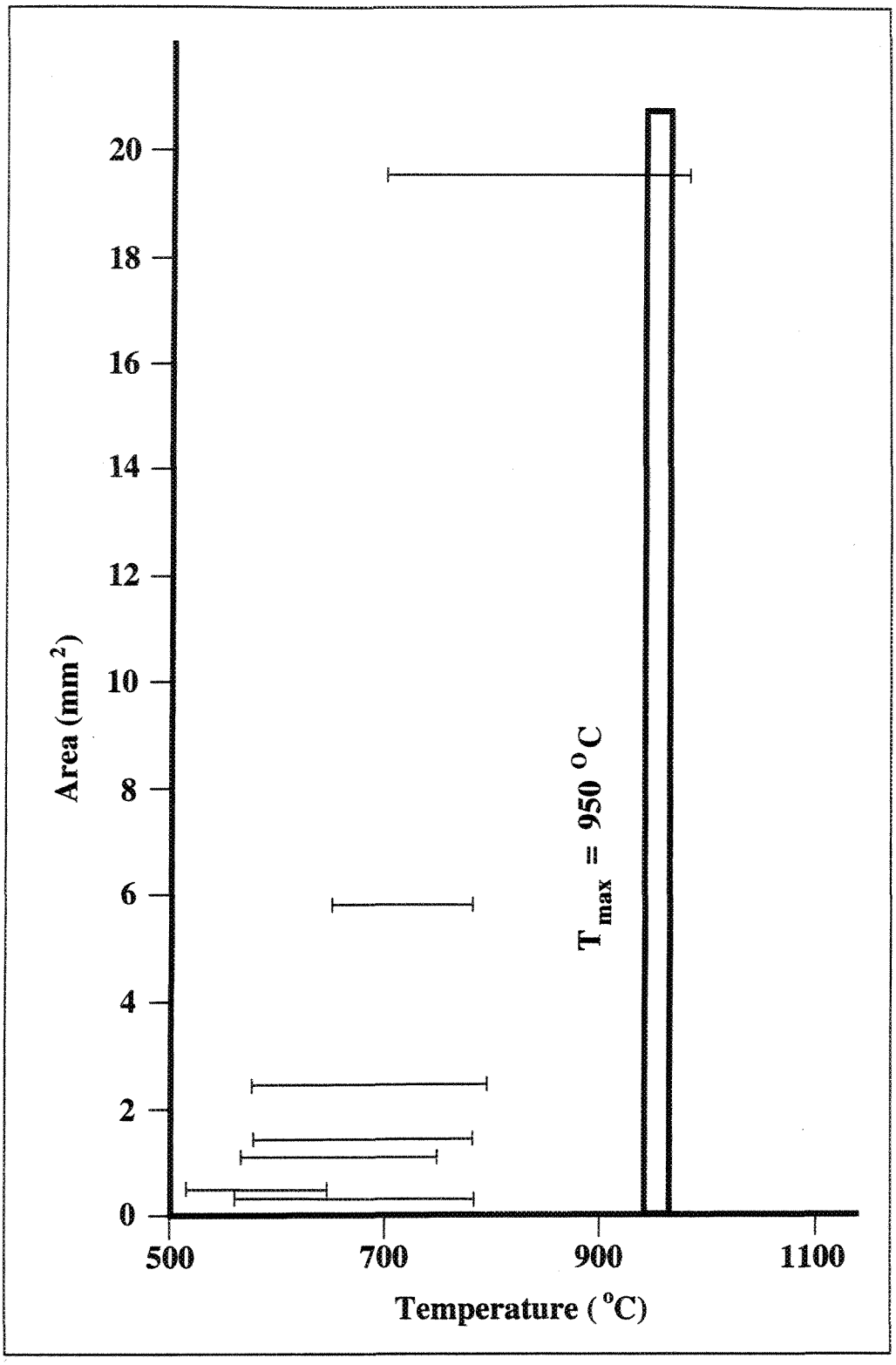

FIGURE 5-II: Garnet size versus temperature results from Ferry & Spear (1978) biotite-garnet Fe-Mg exchange geothermometer for sample 4012. These garnets follow the general trend for the study area with the larger garnets recording higher maximum temperatures than the smaller garnets. Here the 19.5 mm^2 garnet recorded a maximum temperature 100°C above those maximum temperatures recorded by the garnets below 6mm^2 in area.

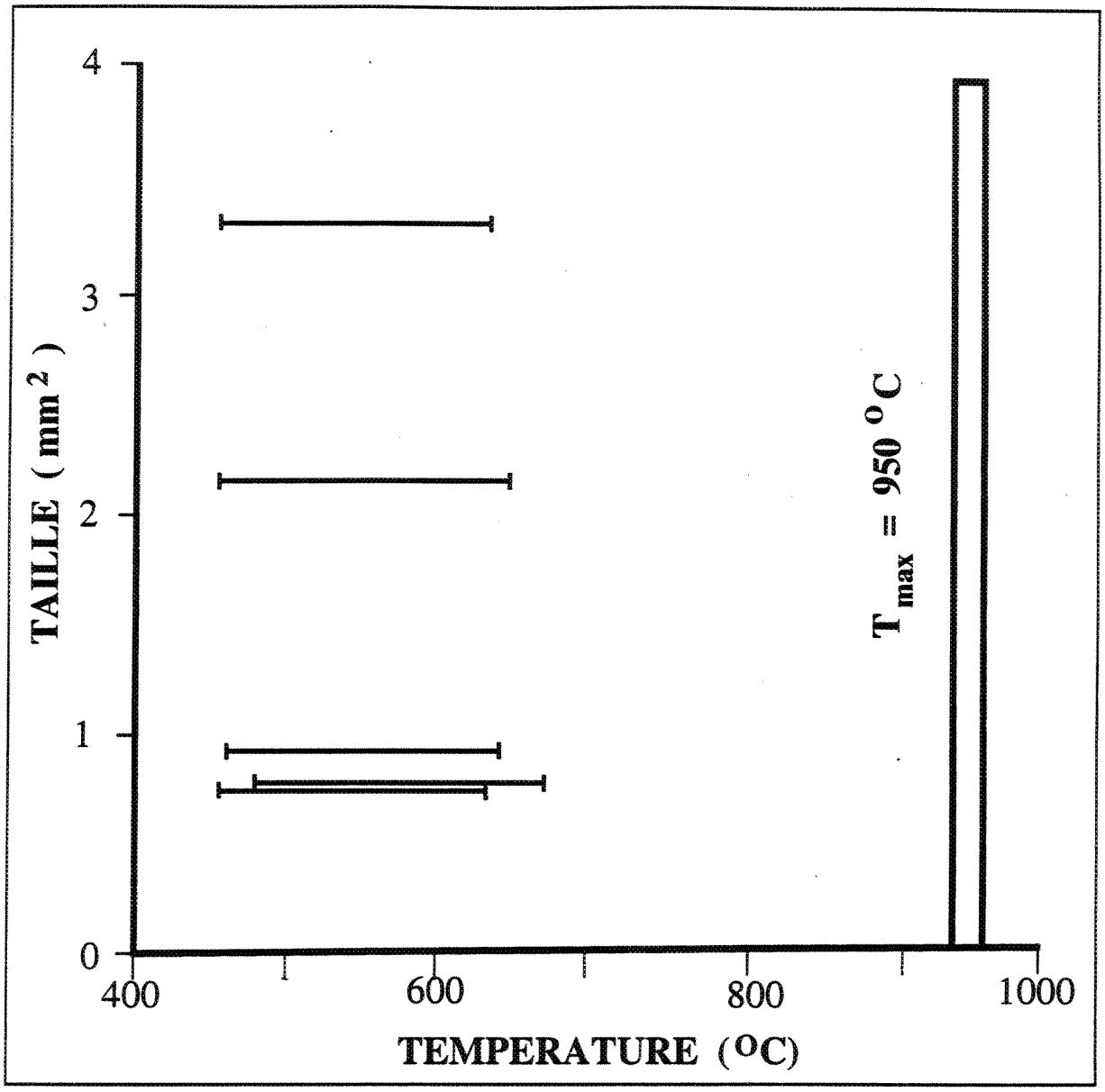

Figure 5-III: Garnet size versus temperature results from Ferry and Spear (1978) biotite-garnet Fe-Mg exchange geothermometer for sample 3832. These five garnets demonstrate the homogenization of small garnets (here < 3.5 mm^2). These garnets preserved temperatures of 680°C, 270°C below the maximum temperature for the study area.

maximum temperatures ranging from 614-652°C irrespective of garnet size. This suggests that these garnets have all been affected by retrograde cation exchange to such an extent that the cores have been partially homogenised. Thus, in the southwest corner of the 31J3 map sheet, garnets smaller than 3.3 mm^2 have substantially re-equilibrated during cooling. Larger garnets may show a lesser degree of resetting.

5.3b.ii. Regional Trends

To examine regional trends, the range of temperature for the garnets from all thin sections were plotted against the garnet size for both the Bandy Gneiss Complex and the Nominingue-Chénéville Deformation Zone. As can be observed from Figures 5-IV, 5-V, the same general trend is preserved, where smaller garnets have lower maximum temperatures than larger garnets. However, it is the intermediate-sized (samples 4012 from the NCDZ at 980°C, and sample 2401D2 from the BGC at 980°C; between 19 and 55 mm^2) garnets that have the highest maximum temperatures. Significantly, these two garnets have inclusion-free cores which give these higher maximum temperatures (Figure 4-XV).

The zoning profile in Figure 4-XIV demonstrates an abrupt change as it crosses the boundary between this inclusion-free core and the inclusion-rich rim. It is possible that this inclusion-rich rim shielded the core from the influence of the retrograde cation exchange, preserving conditions closer to the actual peak in this garnet core.

The largest garnets from samples 4209 (63 mm^2), 2401E (138 mm^2) and 4475D3 (60 mm^2) were entirely poikiloblastic and lack inclusion-free cores. Sample 4209 (Plate XVI, Figure 4-X) contained inclusions of ilmenite, quartz, and plagioclase, 2401E inclusions of spinel, quartz, plagioclase, K-feldspar, ilmenite, and rutile, and 4475D3 (Plate VIII, Figure 4-XI) inclusions of ilmenite and rutile. The presence of these inclusions likely enhanced diffusion in the cores of these garnets during cooling, and permitted retrograde cation

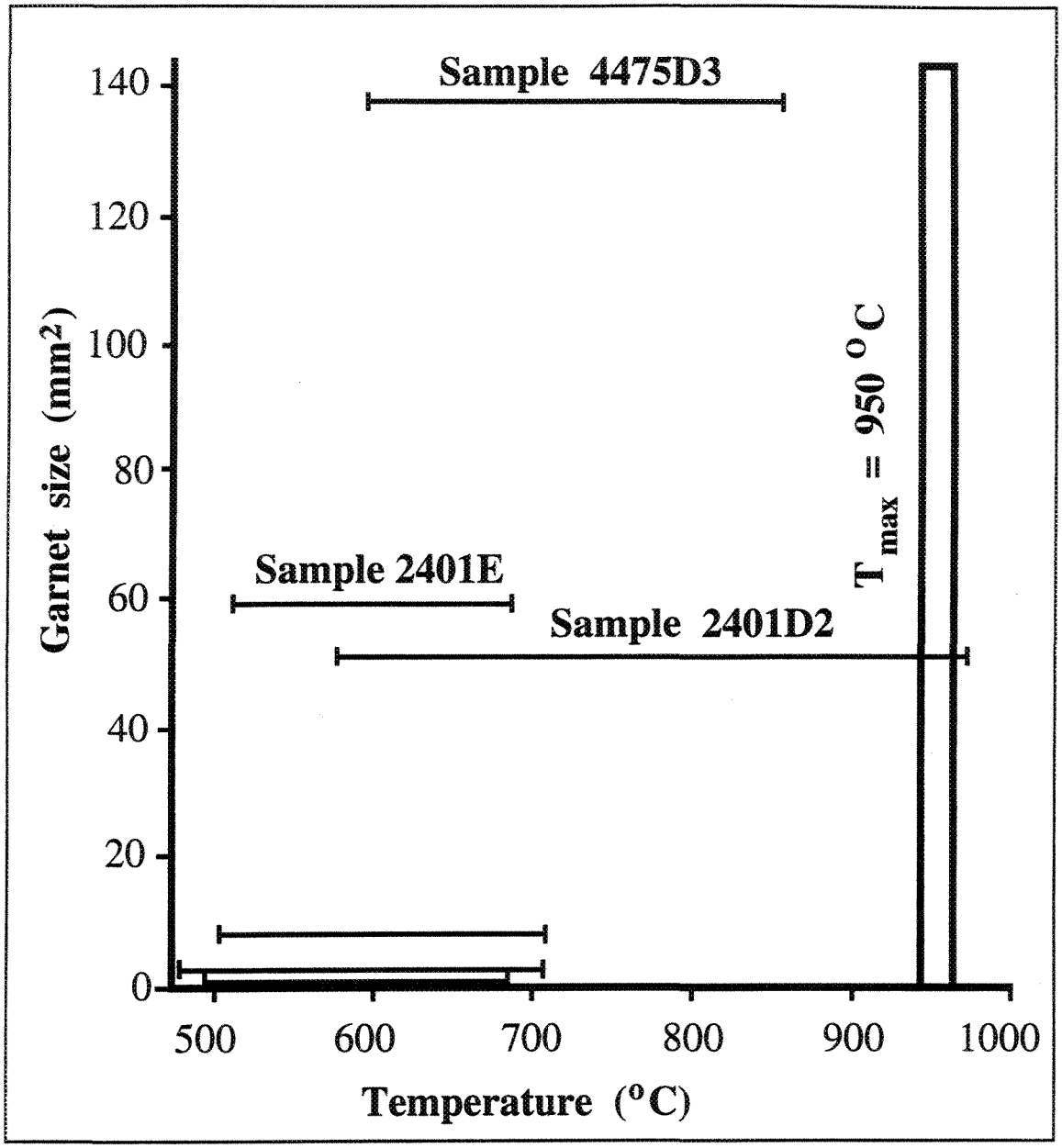

Figure 5-IV: Garnet size versus calculated temperature from the biotite garnet Fe-Mg exchange thermometer (Ferry and Spear 1978) for the Bondy Gneiss Complex. Here the intermediate sized garnet with an inclusion free core (2401D2; see Figure 4-XV) recorded the highest temperatures. The larger garnets (2401E and 4475D3) were expected to record the highest temperatures, however, they are full of inclusions (Figures 4-XI, 4-XXI; Plate VIII) which decreased the diffusion domain size, opening the core of these garnets to the effects of retrograde cation diffusion. These effects were not observed in the garnet profiles (Figures 4-IX, 4-XX).

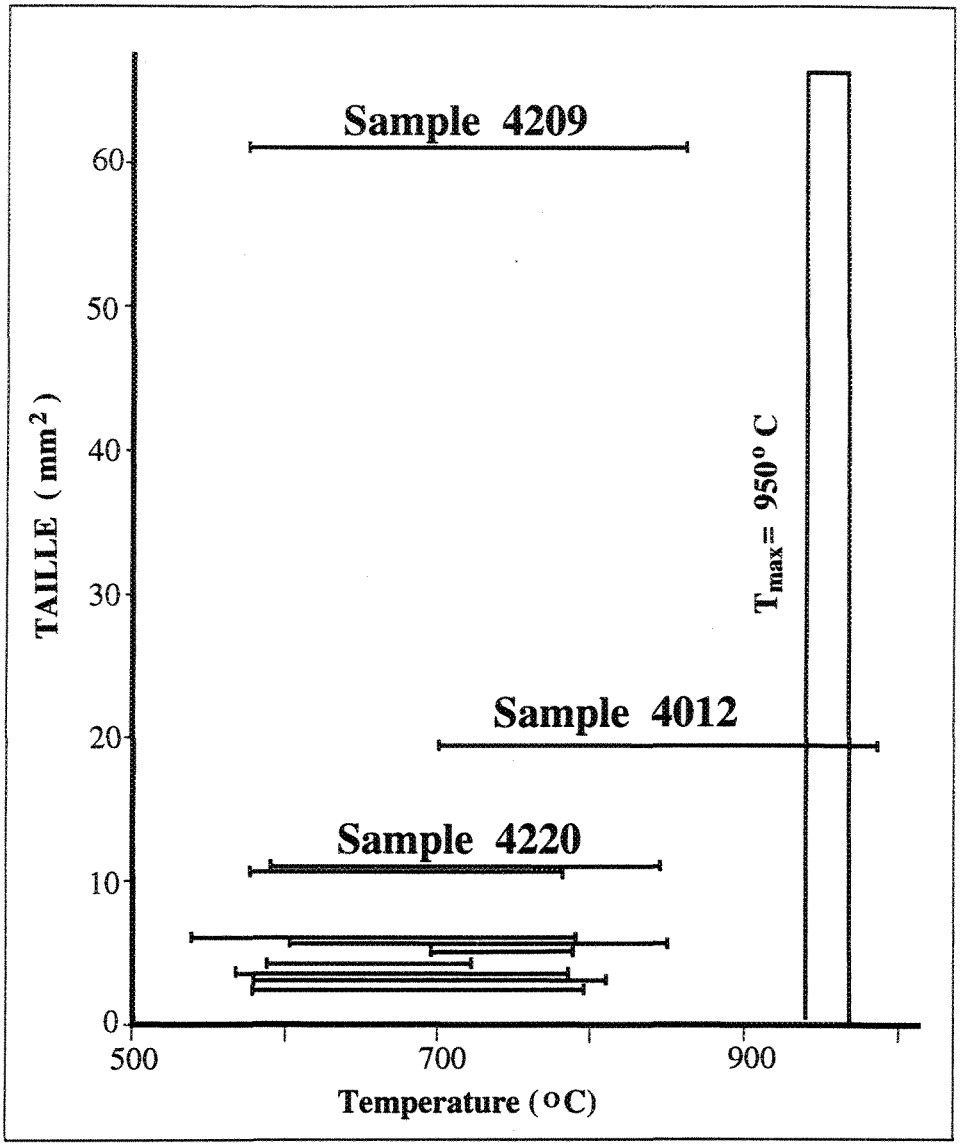

Figure 5-V: Garnet size versus temperature results from Ferry and Spear (1978) biotite-garnet Fe-Mg exchange geothermometer for the garnets within the Nominingue-Chénéville Deformation Zone (>2 mm^2). The garnets from this tectonostratigraphic unit also follow the general trend for the study area with the larger garnets recording higher maximum temperatures than the smaller garnets. Here, the medium sized garnet with the inclusion-free core records the highest temperature (the peak metamorphic temperature). Here, the garnets under 5 mm ^{2}, resulted in temperatures up to 230 °C below that of the peak metamorphic temperature.

exchange, which caused the lowering of the temperatures recorded by the Fe-Mg exchange biotite-garnet geothermometer.

5.4 Garnet-Orthopyroxene Thermometer

5.4a. Literature

The garnet-biotite thermometer calibrated by Ferry and Spear (1978) will, according to Sen and Bhattacharya (1984) produce unreasonable results if the $(Al^{VI} + Ti)/(Al^{VI} = Ti + Mg + Fe^{2+})$ biotite ratios are greater than 0.15; a condition common in granulite facies biotites. Also, in many granulite facies rocks, biotite may have grown during a second equilibration event, which could correspond to temperatures other than the peak metamorphic conditions (Sen and Bhattacharya 1984). As noted in Chapter 4, the garnets in this field area have undergone retrograde cation exchange, which would severely affect the temperature-sensitive Fe-Mg exchange biotite-garnet thermometer (as shown in the above section). Therefore it is desirable to use a thermometer which is less sensitive to processes undergone during retrogression from granulite-facies conditions. Sen and Bhattacharya (1984) suggest that the Fe-Mg exchange garnet-orthopyroxene thermometer is just such a tool.

Using diffusion profiles in coexisting garnet-clinopyroxene pairs, Anovitz (1991) estimated that the Ca-Mg-Fe diffusion in pyroxenes would be slower than in garnets by approximately one order of magnitude over the temperature range 600 to 800°C. This agrees with experimental data (Miyamoto and Takeda 1977; Brady and McCallister 1983; Freer et al. 1982; Reitmeijer 1983) and with estimated kinetics (Ganguly and Chakraborty 1990). Thus, by using orthopyroxene instead of biotite (which has a faster diffusion rate than garnet), the thermometer will be less susceptible to the influence of retrograde cation exchange.

The following reaction:

(5-6) $3MgSiO_3 + Fe_3Al_2Si_3O_{12} = 3FeSiO_3 + Mg_3Al_2Si_3O_{12}$
enstatite almandine ferrosilite pyrope

represents the partitioning of Mg and Fe^{2+} between garnet and orthopyroxene. This reaction has been experimentally calibrated as a thermometer by both Harley (1984a) and Lee and Ganguly (1988). The thermometric equations are similar, however Harley's (1984a) equation yields temperatures between 50 and 90°C lower than Lee and Ganguly's calibration. Carswell and Harley (1990) derived a best fit equation to both data sets. The calibration of Sen and Bhattacharya (1984) was derived by calculation from existing thermodynamic data. Bhattacharya et al. (1991) have proposed a new calibration of this reaction; however their experimental data does not include the data necessary for crustal metamorphic calculations. They claim that this version of the garnet-orthopyroxene thermometer produces temperatures between those obtained with the Harley (1984a) and the Lee and Ganguly (1988) calibrations. Lal (1993) refined the calibration of this geothermometer using a dataset of natural analyses from the FeO-MgO-Al_2O_3-SiO_2 (FMAS) and CaO-FeO-MgO-Al_2O_3-SiO_2-H_2O (CFMASH) systems in the P-T range 50-500 MPa and 700-1400°C.

5.4b Results

Three calibrations were used for this study; Lal (1993), Sen and Bhattacharya (1984), and Harley (1984a). The results from these calibrations for garnet-orthopyroxene pairs from sample 1659 are in Table 5-I. The Sen and Bhattacharya (1984) and the Harley (1984a) calibrations agree within 2°C of each other. The Lal (1993) calibration consistently gives temperatures 200°C below the other two. The results from Sen and Bhattacharya (1984) and from Harley (1984a) give maximum temperatures of 1000°C when core garnets are paired with core orthopyroxenes. These values are somewhat higher than the 970°C suggested by the assemblages, but are only 20°C higher than the maximum temperatures of 950°C suggested from the inclusion-free cores of two garnets with the Fe-Mg exchange biotite-garnet thermometer. Generally, the garnet-orthopyroxene temperatures support a T_{max} of approximately 950°C (Figure 5-VI).

Table 5-I: Results From Orthopyroxene-Garnet Thermometer

Pair	Harley T (C)	S&B T (C)	Lal T (C)
GT-OPX			
C40-34	1009	1010	795
37	941	942	751
38	963	964	768
C41-34	992	991	785
37	926	925	743
38	947	946	759
R35-34	932	930	745
37	872	870	707
38	891	890	722
R36-34	947	947	756
37	885	886	717
38	905	906	732
R39-34	979	978	774
37	915	913	733
38	936	934	749

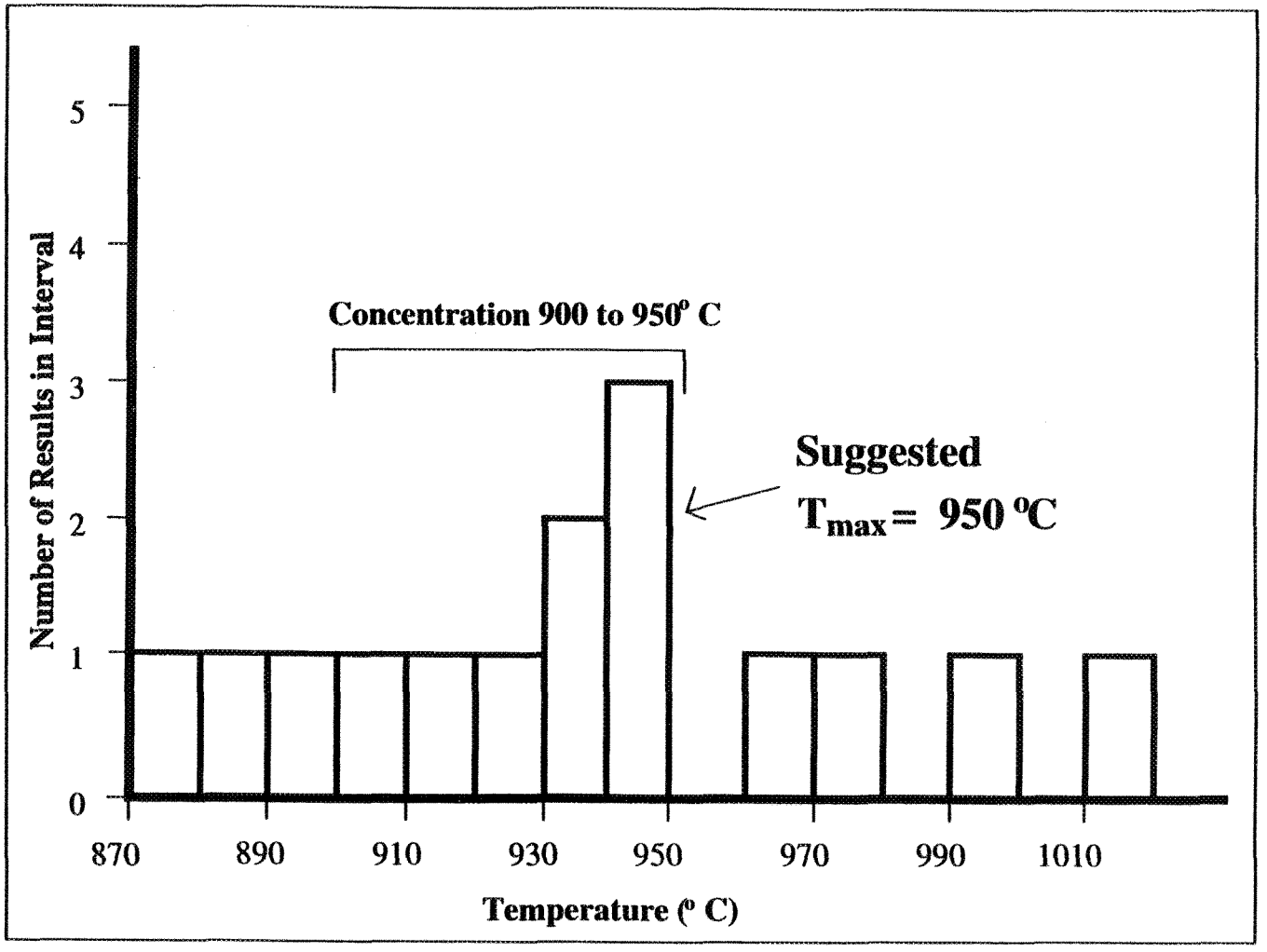

FIGURE 5-VI: Histogram of results from garnet-orthopyroxene thermometer. A maximum temperature of 950° C is proposed due to the concentration of results in the interval 940 - 950 ° C. This value agrees with the values for peak metamorphic temperature obtained from the biotite-garnet Fe-Mg exchange thermometer (Figures 5-I, 5-II, 5-III, 5-IV), and the mineral assemblages.

Vielzeuf and Montel (1994) suggested with their study of fluid-absent melting of metagreywackes, that orthopyroxene would form at lower pressures than garnet. Outcrop 1659 did not contain primary sillimanite, and would therefore behave in a manner similar, chemically, to metagreywackes. If the orthopyroxene formed before garnet, at lower pressures and temperatures than the peak conditions, the high peak temperatures would reset the conditions preserved within the orthopyroxene-garnet pairs, to that of the peak temperature. Thus, this peak temperature of 950°C, not only agrees with the results from the biotite-garnet pairs and the assemblages, but it agrees with what would be expected from chemical reactions during high temperatures.

5.5 Alumina Solubility in Orthopyroxene Barometer

5.5a. Literature

The Ca-Mg-Fe zoning profiles of granulite facies pyroxenes suggest that many pyroxenes may retain their peak condition core compositions (Anovitz 1991). If Al diffusion is slower than Ca-Mg-Fe diffusion, then it is possible that Al zoning in pyroxenes may be a relic from peak metamorphic conditions. Because diffusion processes in pyroxenes are slower than those of garnets or biotites, this alumina solubility in orthopyroxene barometer should be relatively insensitive to the retrograde cation exchange demonstrated in the garnets of the study area (Chapter 4). This should be especially true if the analyses of the core orthopyroxenes are considered (Anovitz 1991).

The solubility of alumina in orthopyroxene is controlled by the following reaction:

(5-7) $$\underset{\text{garnet}}{(Fe, Mg)_3Al_2Si_3O_{12}} = \underset{\text{orthopyroxene solid solution}}{(Fe, Mg)Al_2SiO_6 + (Fe, Mg)_2Si_2O_6}$$

Many of the calibrations of this barometer (Wood 1974) are applicable only when considering magnesian assemblages; however, the thermodynamically based model of Harley (1984b) and the semi-empirical model of Harley and Green (1982) use experimental data for a wide range of compositions. Harley's experiments were originally in the FeO-MgO-Al_2O_3-

SiO_2 (FMAS) system, but were expanded into the CaO-FeO-MgO-Al_2O_3-SiO_2 (CFMAS) system.

5.5b Results

Orthopyroxene was formed during the prograde portion of the P-T trajectory (Chapter 3). Because orthopyroxene is produced at lower pressures than garnet in metapelitic rocks (Vielzeuf and Montel 1994), it is possible that the Al in orthopyroxene barometer would either record pre-peak pressures, or provide a lower limit for the peak pressures. The maximum pressure is not necessarily recorded at the same time as the maximum temperature (Chapter 1), therefore, temperatures of 850°C and 750°C were used to calculate the pressures. Because of the structural evidence for extension following peak metamorphic conditions, in the Nominingue-Chénéville Deformation Zone, an initial episode of isothermal decompression is predicted following peak metamorphic conditions. This is supported by the bell-shaped mole percent grossular profile and the flat mole percent pyrope profile in the inclusion-free core garnets of thin section 2401D2. Indares and Martignole (1990a) proposed that this zoning pattern in garnets occurred due to isothermal decompression. The Bondy Gneiss Complex was likely uplifted during this extensional episode, and then protected from the post-peak deformation and syn-tectonic intrusions that occurred in the NCDZ as these processes were channelled into the less-competent NCDZ. The maximum temperature of 950°C was, therefore, used to calculate a pressure for the beginning of the extensional episode in both the NCDZ and the BGC. These calculated pressures would provide a lower limit for the maximum pressure.

Harley's (1984b) calibration was used because it is the most recent, it also covers the widest compositional system. The results for sample 1659 (Bondy Gneiss Complex) obtained using this calibration are given in Table 5-II. A histogram of the results from this calibration (Figure 5-VII) give a maximum pressure mode of 93 MPa at 950°C, 80 MPa at

Table 5-II: Results From Al in Orthopyroxene Barometer

(C)	750	850	950
(MPa)			
34-35	45.33	57.97	71.69
36	48.64	61.62	75.68
39	53.58	67.03	81.56
40	58.28	72.2	87.19
41	55.61	69.26	83.99
43	57.62	71.47	86.4
46	61.45	75.69	91.01
47	56.43	70.15	84.95
37-36	42.11	54.7	68.42
39	47.05	60.11	74.3
40	51.75	65.27	79.93
41	49.07	62.33	76.73
43	51.09	64.54	79.13
46	54.92	68.76	83.75
47	49.9	63.23	77.69
38-36	47.08	60	74.04
39	52.02	65.41	79.92
40	56.72	70.58	85.55
41	54.05	67.64	82.35
43	56.06	69.85	84.76
46	59.89	74.07	89.37
47	54.87	68.53	83.31
39-36	50.12	63.15	77.17
39	55.06	68.56	83.05
40	59.76	73.73	88.68
41	57.09	70.79	85.48
43	59.1	73	87.88
46	62.93	77.22	92.5
47	57.92	71.68	86.43
17-36	72.09	86.63	102.1
39	77.03	92.04	108
40	81.73	97.21	113.6
41	79.06	94.27	110.4
43	81.07	96.48	112.8
46	84.9	100.7	117.4
47	79.88	95.16	111.3

(C)	750	850	950
(MPa)			
25-1	54.06	67.84	82.73
2	47.64	90.84	75.14
3	53.4	97.12	81.94
4	57.16	71.27	86.47
5	62.22	76.7	92.29
6	57.72	71.77	86.9
7	56.32	70.3	85.37
8	68.45	83.68	100
9	62.15	76.77	92.47
10	59.74	74.1	89.56
26-1	53.48	67.34	82.37
2	47.06	60.34	74.78
3	52.83	66.62	81.59
4	56.59	70.72	86.12
5	61.64	76.2	91.93
6	57.15	71.26	86.55
7	55.74	69.79	85.02
8	67.87	83.17	99.65
9	61.58	76.26	92.12
10	59.16	73.59	89.2
27-1	60.12	74.3	89.53
2	53.7	67.29	81.94
3	69.46	73.58	88.75
4	63.22	77.72	93.28
5	68.28	83.16	99.09
6	63.78	78.22	93.71
7	62.38	76.75	92.18
8	74.51	90.13	106.8
9	68.22	83.22	99.28
10	65.8	80.55	96.36

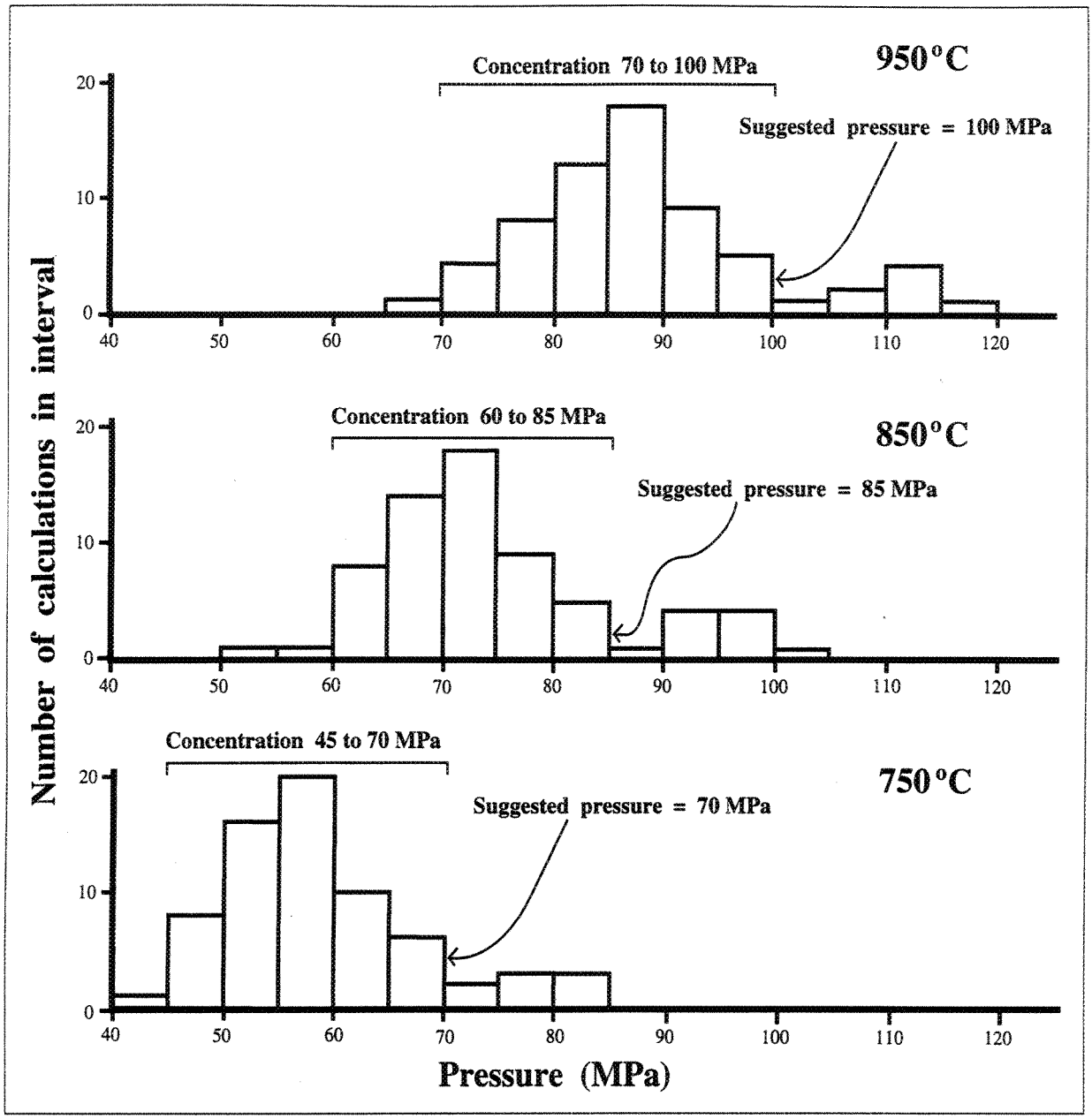

Figure 5-VII: Histogram of results from the Al in orthopyroxene barometer for 750, 850, and 950°C. The concentration of values is noted, however, the shoulder of these concentrations is the pressure that is suggested for that temperature. This is due to the effects of the retrograde cation diffusion. This process would tend to push the results to a lower pressure value, thus the higher pressure values of these concentration is likely to be more representative of the actual peak conditions than the average.

850°C and 65 MPa at 750°C. It is possible that the high peak metamorphic temperatures would have reset these calculated pressures, however, even if these calculated pressures are geologically meaningless, they do provide a lower limit for the maximum pressure.

5.6 Plagioclase-Garnet-Aluminosilicate-Quartz Barometer (GASP)

5.6a Literature

The assemblage garnet + plagioclase + aluminosilicate + quartz is common in medium to high-grade metamorphic rocks over a wide range of pressures and temperatures and thus provides a widely applied barometer with the following reaction:

(5-8) $3CaAl_2Si_2O_8 = Ca_3Al_2Si_3O_{12} + 2Al_2SiO_5 + SiO_2$
anorthite grossular aluminosilicate quartz

Boyd and England (1961) first identified the products of the anorthite breakdown. Several other experimental studies of this calibration include Hays (1967), Hariya and Kennedy (1968), Schmid et al. (1978), Goldsmith (1980) and Gasparik (1984); most of which were conducted at temperatures and pressures well above crustal metamorphic conditions and thus require large extrapolations to obtain pressures. Hodges and McKenna (1987) demonstrated that this large extrapolation along with limited experimental P-T ranges and wide bracketing uncertainties contribute to the large uncertainty in pressure estimates from this barometer.

Koziol and Newton (1988) used a nonaqueous molten flux (Li_2MoO_4) to promote equilibration of the experimental charges in order to bracket the reversals more tightly at lower temperatures. They also used two zoisite-forming reactions (precisely determined in gas-pressure apparatus at lower pressures) to bracket the equilibrium curve at 650°C, 128 to 141 MPa. This places the resultant data in the P-T limit of crustal metamorphism, hence eliminating the need for such large extrapolations.

5.6b Results

In this field area, the major proportion of garnet was formed, in the presence of plagioclase, during the prograde portion of the P-T trajectory. Indeed the highest temperature

melt-forming reaction generated garnet as a residual phase. This suggests that the GASP barometer would have recorded the maximum pressure. As with the Al in orthopyroxene barometer, the maximum pressure does not necessarily occur at the same time as the maximum temperature (Chapter 1), thus 850°C and 750°C were used to calculate the maximum pressure. Due to the possibility of isothermal decompression, during the initial period of cooling, the pressure was also calculated at 950°C.

Koziol and Newton's (1988) calibration was used because it requires the least extrapolation. The results from this calibration are in Table 5-III. A histogram of the results (Figure 5-VIII) produced a concentration with a maximum pressure of 105 MPa at 950°C, 95 MPa at 850°C and 70 MPa at 750°C. The calculated pressures from this barometer are between 5 and 15 MPa higher than those of the Al in orthopyroxene barometer.

Due to the high peak temperature, and the resultant resetting, it is difficult to determine at what temperature the peak pressure occurred. Because of the predicted episode of isothermal decompression, it is likely that the maximum pressure occurred at, or near, the maximum temperature. Therefore, the maximum pressure was considered to be 105 MPa, the value calculated for 950°C. This value is below the upper limit of 110 MPa and above the 93 MPa at 950°C value calculated from the Al in orthopyroxene barometer. Because of the retrograde cation exchange experienced by these rocks, the net transfer reactions may also have been reset (Fitzsimmons and Harley 1994) , and the results would therefore, represent a lower limit for the peak pressure.

5.7 Maximum Pressure

Maximum pressure is constrained to be less than 110 MPa due to the absence of observed kyanite (Figure 3-III), assuming a maximum temperature of 950°C. It is possible that kyanite was once present in these rocks, and that it has since been transformed completely to sillimanite. The slow cooling rate (Chapter 6) and the high peak temperature

Table 5-III: Results From GASP Barometer

(C) (MPa)	750	850	950
2401D2			
28	53.9	84.82	109.5
31	54.24	76.61	101.2
25	53.69	75.16	99.84
35	53.61	74.16	98.85
14	53.95	75.04	99.68
2401E			
18	44.94	71.95	94.37
68	45.06	77.28	94.46
77	44.78	74.31	94.26
96	44.72	80.01	94.22
3302			
L-5	106	132.5	153.3
6	103.5	130.1	153.3
7	107.3	133.8	153.5
6	106	130.9	159.8
7	109.3	134.3	159.9
M-21	111.9	138.7	152.3
22	108.5	135.1	152.8
49	78.91	105.5	153.1
50	85.47	112.1	152.9
51	82.67	109.3	153
21	98.79	125	154.8
23	102.6	128.9	154.6

(C) (MPa)	750	850	950
4012			
35	61.82	92.3	104.2
36	62.07	92.57	104.6
39	62.27	90.75	104.7
41	59.34	86.66	102.7
15	58.86	74.97	102.4
55	61.85	93.17	104.4
65	61.92	90.21	104.5
48	59.19	83.12	102.6
57	78.61	102.2	116.1
33	58.96	87.08	102.4
4209			
15	66.01	94.61	119.3
16	66.5	95.39	119.7
17	66.3	94.12	119.5
17	67.18	102.9	120.1
26	67.76	108.6	120.5
27	67.85	113.1	120.6
25	68.56	96.92	121.1
14	66.4	92.97	119.6
18	66.39	9.9	119.6
19	66.2	98.55	119.5
34	67.31	117.8	120.2
36	67.51	107.3	120.4
18	67.33	116.7	120.2

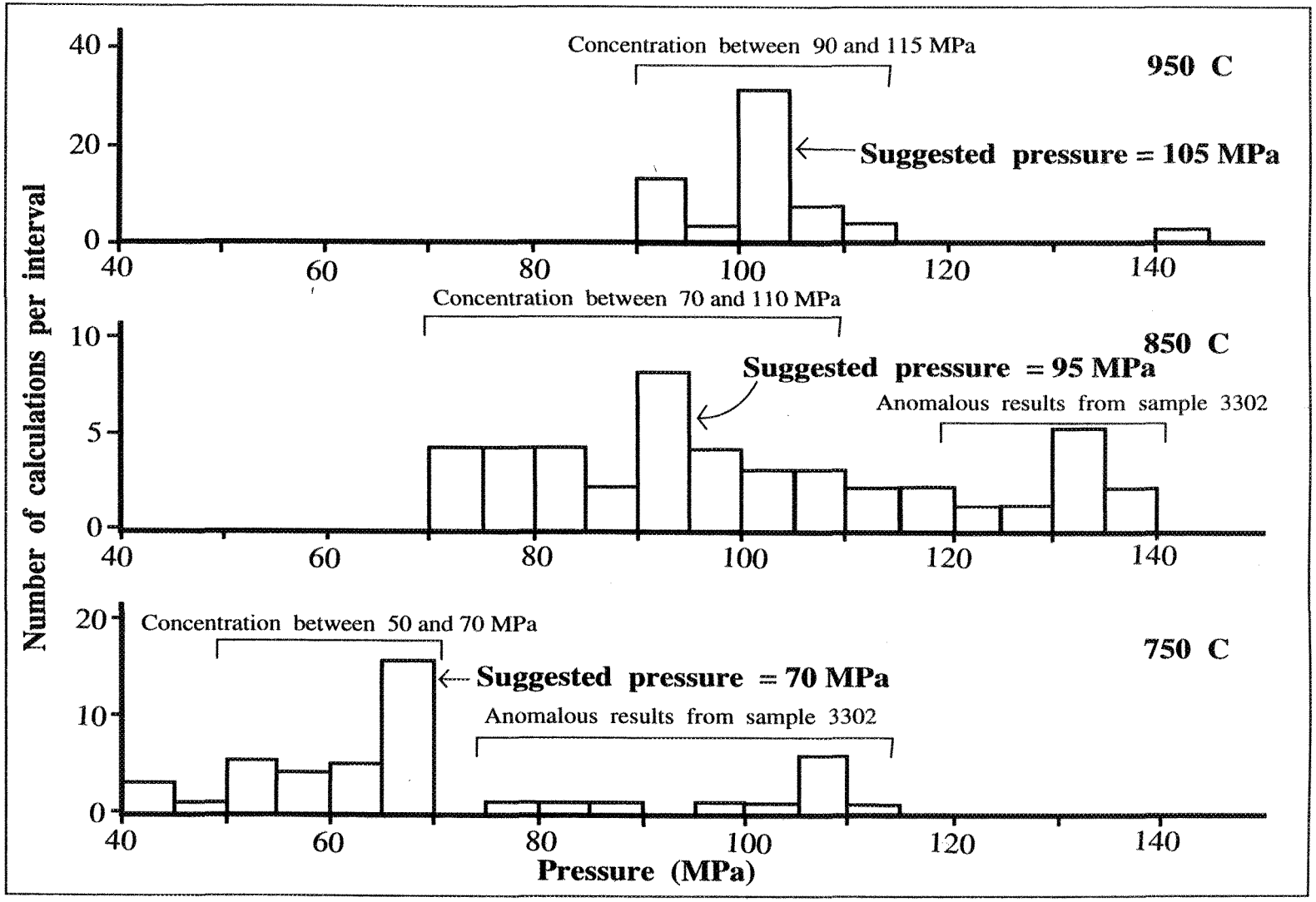

Figure 5-VIII: Histogram of results from GASP barometer. These results were more difficult to interpret than the results from the Al in Opx barometer due to the irregular distribution. At 750°C, the right shoulder corresponded with the strongest concentraion. At 850°C, there was no strong concentration. At 950°C, the strongest concentration contained by far the most calculated results. According to the experimental results of Vielzeuf and Montel (1994), garnet is formed at the expense of orthopyroxene at higher pressures. Therefore, the pressures from this barometer would likely represent the closest estimate to peak pressures, possibly a lower limit due to the effects of retrograde cation exchange.

would have assisted this phase transformation. It is possible that the peak pressure could have been above 110 MPa, though unlikely. As noted in Chapter 1, there is no reason to suppose that the maximum pressure and maximum temperature were recorded at the same time. Since the pressures were determined by equilibrium using Al and Ca using the GASP barometer, they are less likely to be reset by the high T_{max}. We believe the peak pressure to predate the peak temperature, however the temperature at the peak pressure cannot be estimated. An initial cooling curve from the T_{max} is considered to involve isothermal decompression due to garnet zoning profiles and structural evidence. Thus the calculated pressure of 105 MPa at 950°C from GASP is considered to be a point on the P-T trajectory, though this is not necessarily the P_{max}.

5.8 Spinel-Garnet Barometer

5.8a Literature

Nichols et al. (1992) experimentally quantified the equilibrium:

(4) $(Mg,Fe,Zn)_3Al_2Si_3O_{12} + 2Al_2SiO_5 = 3(Mg,Fe,Zn)Al_2O_4 + 5SiO_2$
garnet aluminosilicate spinel quartz

They derived a ternary Fe-Mg-Zn symmetric mixing model for spinels in equilibrium with garnets to account for the increase in the gahnitic end-member with increasing pressure and decreasing temperature. Berman's (1990) garnet model was used in order to minimise W_{Grt} (FeMg) in the calculation of an spinel activity model.

5.8b Results

The calculated values for the spinel-garnet pairs of thin section 2401D2 are in Table 5-IV. The resultant pressures for temperatures of 750, 850, 950 and 1050 °C (Figure 5-IX) were used to reposition the univariant curve for this reaction on the petrogenetic grid of Vielzeuf and Holloway (1988). The resultant curve moved ~90°C towards lower temperatures due to the zinc content in the spinels (as predicted by Nichols et al. 1992).

Table 5-IV: Results From Spinel-Garnet Barometer

Sample	Spl	Her	Spn	Her	Spl	Her	Spl	Her
(C)	750	750	850	850	950	950	1050	1050
(MPa)								
P72	39.79	47.28	59.08	72.757	78.32	98.2	97.58	123.7
70	40.16	45.96	59.537	71.29	78.85	96.58	98.2	121.9
69	39.07	48.32	58.216	73.914	77.31	99.47	96.43	125.1
68	40.25	45.97	59.48	71.421	78.65	96.84	97.85	122.3
66	41.19	44.07	60.483	69.402	79.72	94.7	98.98	120
64	40.8	44.81	60.15	70.136	79.44	95.42	98.76	120.7
63	39.05	48.72	58.288	74.288	77.46	99.82	96.67	125.4
60	41.18	43.72	60.583	68.939	79.93	94.12	99.31	119.3
61	41.6	42.68	61.047	67.826	80.43	92.94	99.85	118.1
R40	40.37	44.24	59.785	69.398	79.14	94.52	98.53	119.7
41	40.41	43.78	59.883	68.853	79.29	93.89	98.74	119
42	39	47.47	58.217	72.921	77.38	98.34	96.57	123.8
43	38.98	47.11	58.195	72.532	77.35	97.91	96.54	123.3
44	38.74	48.29	58.005	73.755	77.22	99.18	96.45	124.6
45	40.79	43.77	60.15	68.981	79.45	94.15	98.78	119.4
46	41.79	41.82	60.868	67.12	79.89	92.38	98.94	117.7
47	35.53	52.45	54.017	78.48	72.45	104.5	90.91	130.5
P72	41.22	40.7	60.787	65.472	80.3	90.2	99.84	115
70	41.59	39.38	61.245	64.004	80.84	88.59	100.5	113.2
69	40.5	41.74	59.923	66.628	79.29	91.48	98.69	116.4
68	41.68	39.39	61.187	64.135	80.63	88.84	100.1	113.6
66	42.62	37.49	62.19	62.116	81.7	86.7	101.2	111.3
64	42.23	38.24	61.857	62.85	81.43	87.42	101	112
63	40.48	42.14	59.996	67.002	79.45	91.83	98.93	116.7
60	42.61	37.14	62.29	61.653	81.91	86.13	101.6	110.6
61	43.03	36.1	62.754	60.54	82.42	84.94	102.1	109.4
R40	41.8	37.66	61.493	62.112	81.13	86.53	100.8	111
41	41.84	37.2	61.591	61.567	81.28	85.89	101	110.3
42	40.43	40.89	59.925	65.635	79.36	90.34	98.83	115.1
43	40.41	40.54	59.902	65.246	79.34	89.92	98.8	114.6
44	40.17	41.71	59.712	66.469	79.2	91.19	98.71	115.9
45	42.22	37.19	61.857	61.695	81.43	86.16	101	110.7
46	43.22	35.25	62.576	59.834	81.87	84.38	101.2	109
47	36.96	45.88	55.725	71.194	74.43	96.47	93.17	121.8
P72	43.15	44.99	62.899	70.1	82.59	95.17	102.3	120.3
70	43.52	43.67	63.357	68.632	83.13	93.56	102.9	118.5
69	42.43	46.03	62.035	71.256	81.58	96.44	101.2	121.7
68	43.61	43.68	63.299	68.763	82.92	93.81	102.6	118.9
66	44.55	41.78	64.302	66.744	83.99	91.67	103.7	116.6

Table 5-IV: Results From Spinel-Garnet Barometer - continued

64	44.16	42.53	63.969	67.478	83.72	92.39	103.5	117.3
63	42.41	46.43	62.107	71.63	81.74	96.79	101.4	122
60	44.54	41.43	64.402	66.281	84.21	91.1	104	115.9
61	44.96	40.39	64.866	65.168	84.71	89.91	104.6	114.7
R40	43.73	41.95	63.605	66.74	83.42	91.49	103.3	116.3
41	43.77	41.49	63.703	66.195	83.57	90.86	103.5	115.6
42	42.36	45.18	62.037	70.263	81.65	95.31	101.3	120.4
43	42.34	44.83	62.014	69.874	81.63	94.88	101.3	119.9
44	42.1	46	61.824	71.097	81.49	96.15	101.2	121.2
45	44.15	41.48	63.969	66.323	83.73	91.13	103.5	116
46	45.15	39.54	64.687	64.462	84.16	89.35	103.7	114.3
47	38.89	50.16	57.836	75.822	76.73	101.4	95.65	127.1
P72	44.9	39.74	64.242	64.476	83.53	89.18	102.8	113.9
70	45.27	38.41	64.7	63.008	84.07	87.57	103.5	112.2
69	44.18	40.77	63.378	65.632	82.52	90.45	101.7	115.3
68	45.36	38.42	64.642	63.139	83.86	87.82	103.1	112.5
66	46.3	36.52	65.645	61.12	84.93	85.68	104.3	110.3
64	45.91	37.27	65.313	61.854	84.66	86.4	104	111
63	44.16	41.17	63.451	66.007	82.68	90.8	101.9	115.6
60	46.29	36.17	65.745	60.657	85.15	85.11	104.6	109.6
61	46.71	35.13	66.209	59.545	85.65	83.92	105.1	108.3
R40	45.48	36.69	64.948	61.117	84.36	85.5	103.8	109.9
41	45.52	36.23	65.046	60.571	84.51	84.87	104	109.2
42	44.11	39.92	63.38	64.64	82.59	89.32	101.8	114
43	44.09	39.57	63.357	64.251	82.57	88.89	101.8	113.6
44	43.85	40.74	63.167	65.473	82.43	90.16	101.7	114.9
45	45.9	36.23	65.312	60.7	84.67	85.14	104	109.6
46	46.9	34.28	66.031	58.839	85.1	83.36	104.2	107.9
47	40.64	44.91	59.18	70.199	77.67	95.45	96.18	120.7

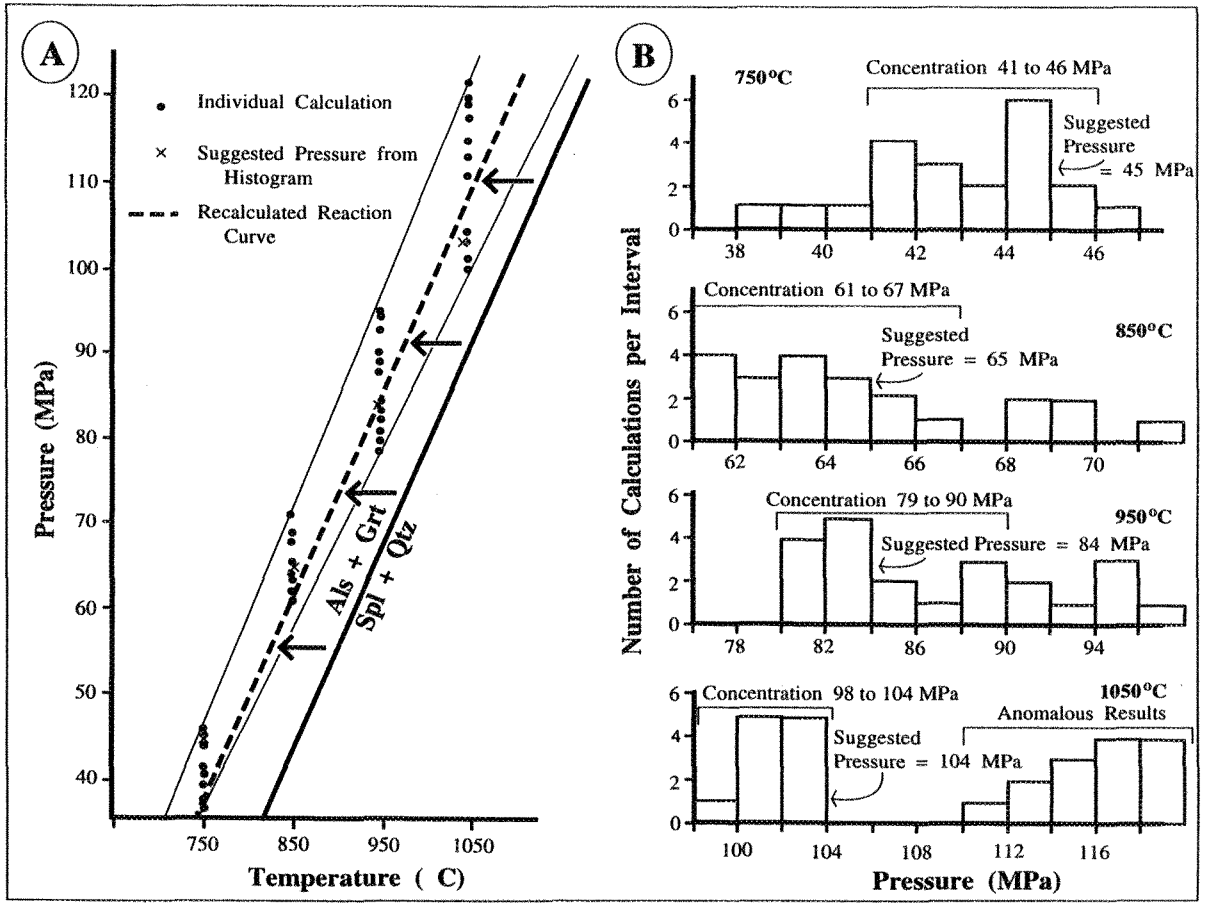

Figure 5-IX: Results from the spinel-garnet barometer (Nichols et al. 1992) for sample 2401D2 (BGC). "A" contains the P-T diagram of the recalculated Als + Grt = Spl + Qtz curve. The recalculated curve was 80°C lower than the value from Figure 3-III due to the zinc content in the spinels. "B" contains the histogram of the results from the Spl-Grt barometer at 750, 850, 950 and 1050°C, which were used to reposition the reaction curve. Isothermal decompression was proposed from peak temperatures. The position of the spinel inclusions in sample 2401D2 (Figure 4-XVI: Plate IX) implies that the spinel reacted out to garnet during this decompression, which suggests that the calculated pressure of 84 MPa at 950°C, near the end of the isothermal decompression in the BGC, is a position on the P-T trajectory for the BGC.

Due to the predicted isothermal decompression, a pressure of 84 MPa at 950°C calculated from this barometer, was plotted as a position on the P-T-t trajectory. The position of the spinel inclusions in the garnet rims, from thin section 2401D2, imply that isothermal decompression likely stopped once this univariant curve was crossed. As discussed in chapter 3, the absence of the spinel-quartz assemblage in this thin section, suggests that this reaction was crossed in the reverse direction, during the retrograde path. Thus, the trajectory would have crossed this reaction curve somewhere between 64 MPa at 850°C and 52 MPa at 800°C.

5.9 Garnet-Cordierite Barometer

5.9a Literature

One cordierite-breakdown reaction based on the Fe-end members, suitable to the peraluminous assemblages in this study, was reformulated by Bhattacharya (1986):

(6) $3Fe_2Al_4Si_5O_{18} = 2Fe_3Al_2Si_3O_{12} + 4Al_2SiO_5 + 5SiO_2$
Fe-cordierite almandine aluminosilicate quartz

Previous geobarometers based on the assemblage cordierite-garnet-sillimanite-quartz (Hutcheson et al. 1974; Thompson 1976a; 1976b; Holdaway and Lee 1977; Newton and Wood 1979; Martignole and Sisi 1981; Lonker 1981; Bhattacharya and Sen 1985) resulted in calculated pressures that disagreed (Bhattacharya 1986). Bhattacharya (1986) re-examined these geobarometers, and removed the inaccuracies that caused these disagreements.

The variability of partial pressure of H_2O and metastability of Mg-cordierite in wet and dry systems created difficulties in controlling the reversibility of cordierite equilibria (Currie 1971; Hensen and Green 1971, 1972, 1973). These same problems created obstacles when attempting to locate the cordierite-garnet-orthopyroxene-quartz reaction in P-T space (Hensen and Green 1973). However, the experimentally calibrated Fe-cordierite reaction for the cordierite-garnet-sillimanite-quartz assemblage (used by Bhattacharya 1986) has been located accurately (Weisbrod 1973a, 1973b; Richardson 1968; Holdaway and Lee

1977). Previous authors also ignored the variability of X_{H2O} in cordierite on the computed pressures (Hutcheson et al. 1974; Thompson 1976a; 1976b; Vielzeuf 1980; Harris 1981). Bhattacharya and Sen (1985) used experimental data at $P(H_2O) = P(total)$ to develop a one-site mixing model in the $Mg_2Al_4Si_5O_{18}$ - $Mg_2Al_4Si_5O_{18}\cdot H_2O$ system to improve the comprehension of the activity-composition relationship of hydrated cordierites. This was incorporated into the Bhattacharya (1986) model.

Until Bhattacharya (1986), the geobarometric models involving cordierite-bearing equilibria assumed that the Fe-Mg mixing in cordierites, and the other phases, was ideal. As mentioned by Dahl (1980); Ganguly (1979); and Ganguly and Saxena (1985), experimental and natural studies indicate non-ideality, especially in multi-component garnet solutions.

5.9b Results

Bhattacharya's (1986) formulation was used to calculate the pressures for the garnet-cordierite-sillimanite-quartz assemblages because he used the Fe-cordierite end-member, and Bhattacharya and Sen's (1985) activity-composition relationship of hydrated cordierites, and accounted for the non-ideality of mixing in garnets. The assemblage garnet-sillimanite-cordierite-quartz was only observed in one outcrop (1659) from the Bondy Gneiss Complex. As discussed in Chapter 3, the free water was probably consumed during the early prograde path, therefore, the X_{H2O} in cordierite must have been low (between 0.3 and 0.1).

The results from the cordierite-garnet pairs from thin section 1659 are in Table 5-V. The calculated pressures of 83 to 85 MPa at 800°C with a X_{H2O} of 0.3 from garnet 1659-24 are consistently 20 to 30 MPa higher than the 53 to 63 MPa at 800°C with a X_{H2O} of 0.3 from garnet 1659-4 (Figure 5-X). The garnet-cordierite pairs from garnet 1659-24 do not occur with sillimanite, it was assumed that the sillimanite had reacted out completely to produce cordierite. However, the pressures from these garnet-cordierite pairs are

Table 5-V: Results From Cordierite-Garnet Barometer

				Pressure (MPa)					
T(C)		750			800			850	
aH2O	0.1	0.3	0.5	0.1	0.3	0.5	0.1	0.3	0.5
Photo6-4									
31	44.3	52.7	63.9	43.6	52.5	64.2	43.1	52.3	64.6
	46.3	54.7	65.9	45.8	54.6	66.4	45.3	54.5	66.8
	45.9	54.3	65.5	45.4	54.2	65.9	44.8	54	66.3
	46.2	54.6	65.8	45.7	54.5	66.3	45.2	54.4	66.7
	46.4	54.8	66	45.9	54.7	66.5	45.4	54.6	66.9
7	52	60.4	71.6	51.8	60.6	72.4	51.6	60.8	73.1
	54.1	62.5	73.7	54	62.7	74.5	53.8	63	75.3
	53.6	62	73.2	53.5	62.3	74	53.3	62.5	74.8
	54	62.4	73.6	53.9	62.6	74.4	53.7	62.9	75.2
	54.2	62.5	73.7	54	62.8	74.6	53.9	63.1	75.4
13	45.3	53.7	64.9	44.7	53.5	65.3	44.2	53.4	65.7
	47.3	55.7	66.9	46.9	55.7	67.4	46.4	55.6	67.9
	46.9	55.3	66.5	46.4	55.2	67	45.9	55.1	67.4
	47.3	55.6	6.8	46.8	55.6	67.3	46.3	55.5	67.8
	47.4	55.8	67	47	55.7	67.5	46.5	55.7	68
15	47.4	55.8	67	47	55.7	67.5	46.5	55.7	68
	47.4	57.8	69	49.1	57.9	69.6	48.7	57.9	70.2
	49	57.4	68.6	48.6	57.4	69.2	48.2	57.4	69.7
	49.4	57.7	68.9	49	57.8	69.5	48.6	57.8	70.1
	49.5	57.9	69.1	49.2	57.9	69.7	48.8	58	70.3
24-Jun									
72	77.1	86.3	96.8	76.2	85	96.8	75.3	83.7	94.9
	76.8	86	96.5	75.9	84.7	96.5	75	83.4	94.6
	77	86.2	96.7	76.1	84.9	96.7	75.2	83.6	94.8
	76.8	86	96.4	75.9	84.7	96.5	75	83.3	94.6
73	76.2	85.4	95.9	75.3	84.1	95.9	74.4	82.8	94
	75.8	85	95.5	75	83.8	95.5	74.1	82.5	93.7
	76.1	85.3	95.7	75.2	84	95.7	74.3	82.7	93.9
	75.8	85	95.5	75	83.8	95.5	74.1	82.5	93.7
74	75.7	84.9	95.4	74.9	83.6	95.4	74	82.4	93.6
	75.4	84.6	95.1	74.5	83.3	95.1	73.7	82.1	93.3
	75.6	84.8	95.3	74.7	83.5	95.3	73.9	82.3	93.5
	75.4	84.6	95.1	74.5	83.3	95.1	73.7	82.1	93.3

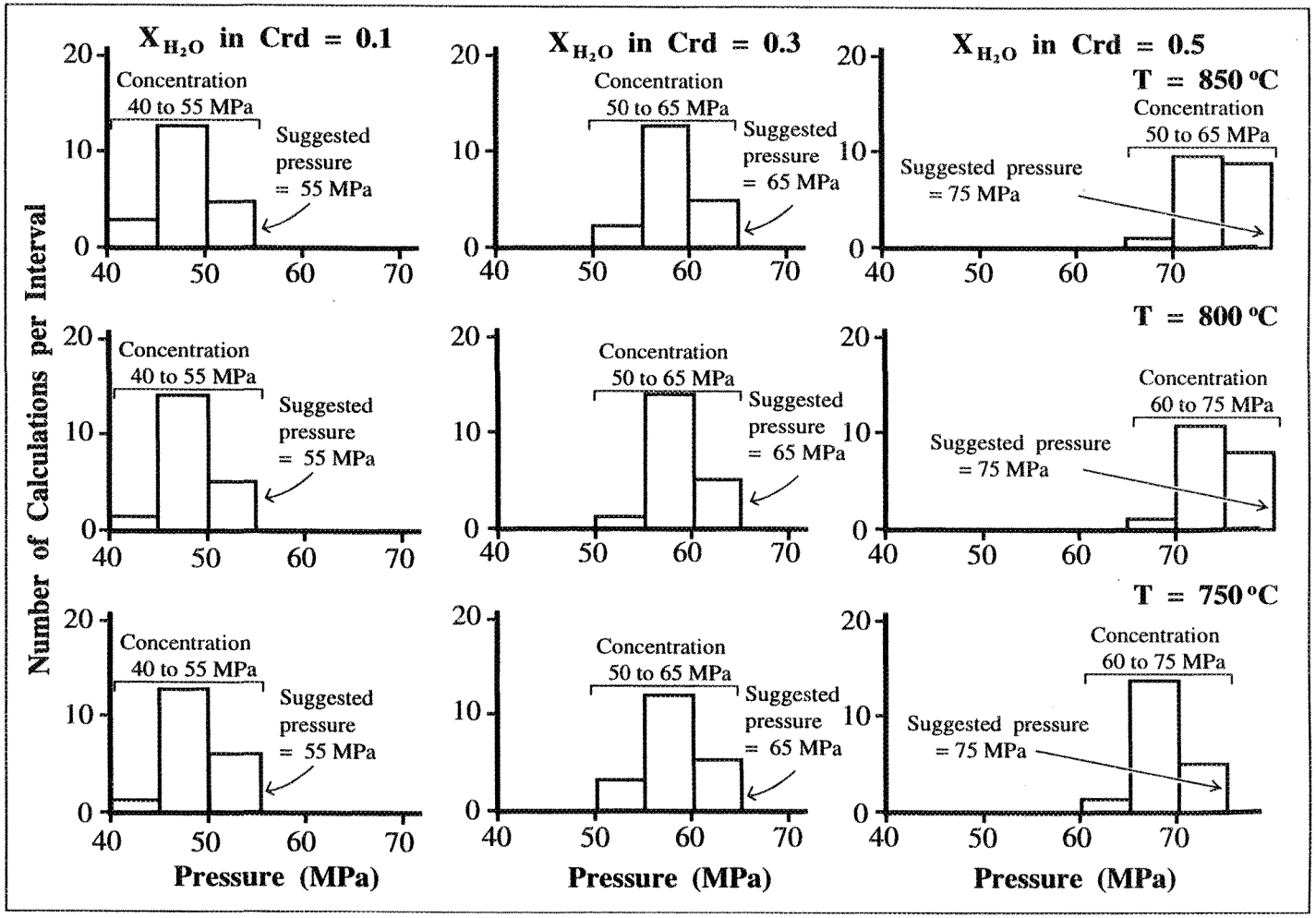

Figure 5-X: Histogram of results from cordierite-garnet barometer for sample 1659 (Garnet 1659-4). From Figures 3-VI and 3-VII, the moles of water in the melt was limited to < 0.4, implying a low water content in the Crd (likely near 0.3). These histograms demonstrate that the water content in Crd has a stronger influence on this barometer than does temperature. The suggested pressures were taken from the shoulder of the concentrations due to the effects of retrograde cation exchange. It is difficult to determine an exact point on the P-T trajectory represented by this data, however, it is suggested that the trajectory passed between 55 and 65 MPa between 750 and 850 °C.

unrealistically high, thus, the cordierite paired with this garnet must have formed during another reaction. The cordierite paired with garnet 1659-4 occur with sillimanite, and their calculated pressures are realistic, thus these pressures probably represent an approximate position on the P-T-t trajectory. An exact position is difficult to plot because the exact temperature at which the P-T-t trajectory crossed this reaction curve is unknown, however, it is likely that the conditions were near the 53 to 63 MPa at 800°C.

5.10 Summary

5.10a The Prograde Path and Isothermal Decompression

The peak temperature of 950°C was recorded by the medium-sized, inclusion-free, garnet-biotite pairs from outcrops located within both the Bondy Gneiss Complex and the Nominingue-Chénéville Deformation Zone. The garnet-biotite pairs were the only applicable thermometer observed in the NCDZ. The orthopyroxene-garnet pairs within the BGC also resulted in a peak temperature of 950°C. Due to this high peak temperature, slow cooling rates and the resultant retrograde cation exchange, the garnet zoning profiles do not contribute meaningful information to the prograde P-T trajectory.

The retrograde cation exchange created difficulties for determining the peak pressure. However, structural evidence within the NCDZ, and garnet zoning profiles within the BGC, both suggest an episode of isothermal decompression following the peak temperature. Thus, the peak pressure for both the BGC and the NCDZ, was likely near 105 MPa, obtained from the GASP barometer at 950°C. The garnet-aluminosilicate-sillimanite-plagioclase assemblage was the only suitable barometer observed in the NCDZ.

The spinel-garnet pairs from the BGC gave a pressure of 84 MPa at 950°C. The location of the spinel inclusions, on the garnet zoning profile, suggests that this reaction occurred towards the end of the isothermal decompression, thus this pressure of 84 MPa provides a lower pressure limit for the isothermal decompression. It is likely, that during this

episode of extension, the BGC was uplifted, which along with the comparative competency of the BGC focused the following episode of deformation and plutonism into the less competent NCDZ. Thus, it was after this isothermal decompression, that the P-T-t trajectories for the BGC and NCDZ diverged.

5.10b The Retrograde Path

5.10b.i The Bondy Gneiss Complex

The garnet + sillimanite = spinel + quartz reaction curve was crossed twice, once to produce and a second time to consume spinel + quartz. Therefore, during the retrograde path, after isothermal decompression, the BGC likely crossed this reaction curve between 64 MPa at 850°C and 52 MPa at 800°C. The assemblage cordierite-garnet-sillimanite-quartz is retrograde in some cases. The retrograde path for the BGC likely passed through a point near 53 to 63 MPa at 800°C with a X_{H2O} of 0.3 (Figure 5-XI).

5.10b.ii Nominingue-Chénéville Deformation Zone

The assemblages garnet + sillimanite = spinel + quartz and cordierite + garnet + sillimanite + quartz were not observed in the thin sections from the NCDZ. It is possible that the deformation and the syntectonic intrusions along the NCDZ would have destroyed these assemblages. Thus, the only evidence for the retrograde conditions within the NCDZ, are those preserved in the assemblages, as discussed in chapter 3 (Figure 5-XII).

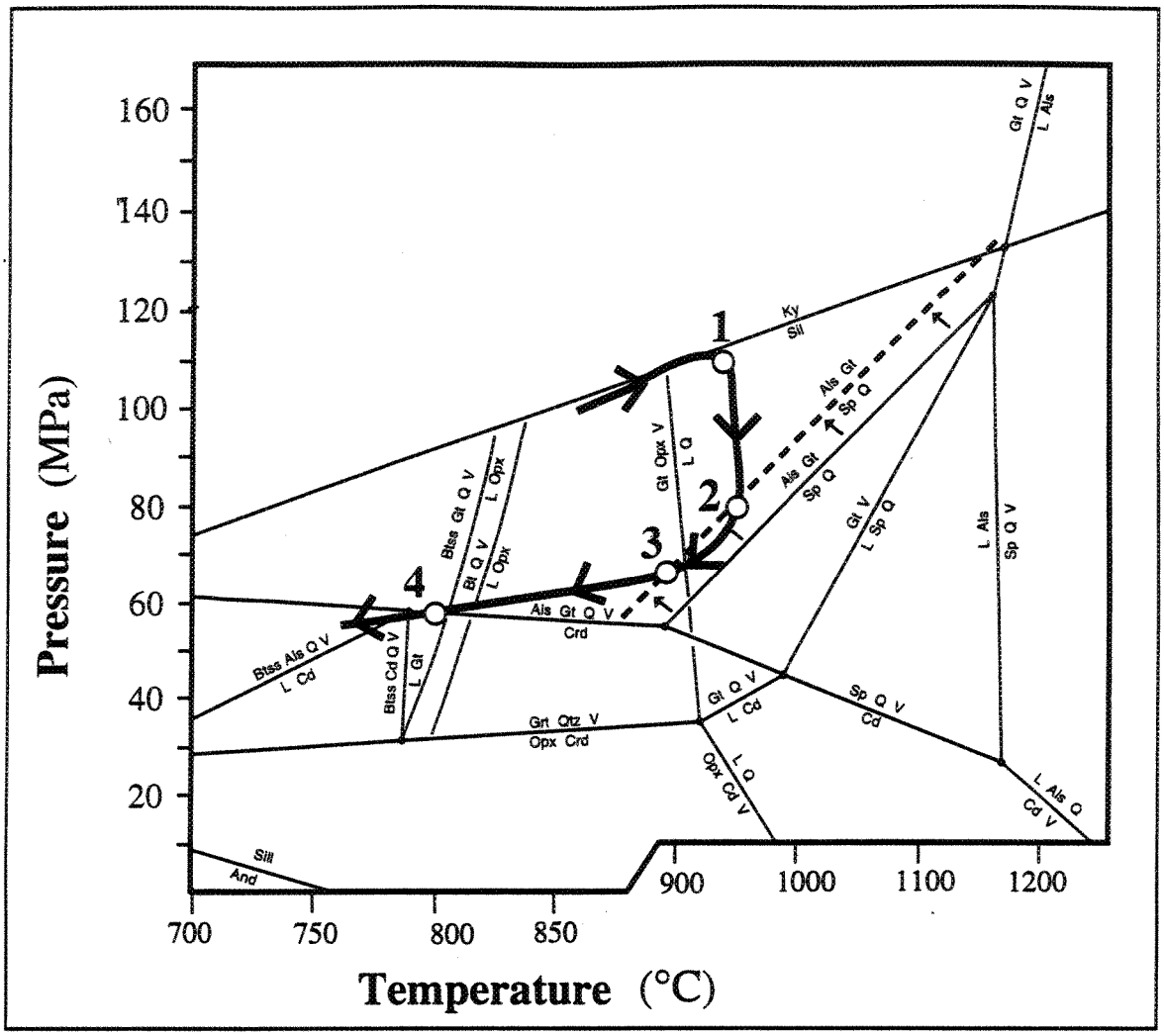

Figure 5-XI: P-T trajectory for BGC, inferred from the geothermobarometers. The P_{max} of 105 MPa (1) was calculated from the GASP barometer. The T_{max} of 950°C (1, 2) was calculated from the Bt-Grt thermometer. Isothermal decompression (2) was predicted due to the Grs profiles. The retrograde position (3) was calculated from the Spl-Grt barometer, and (4) was calculated from the Crd-Grt barometer. Isothermal decompression would not have been predicted with the use of the assemblages alone (Figure 3-VIII). The retrograde portions of the P-T trajectory were also placed lower when considering solely the assemblages (Figure 3-VIII). The petrogenetic grid is simplified after Figure 3-III.

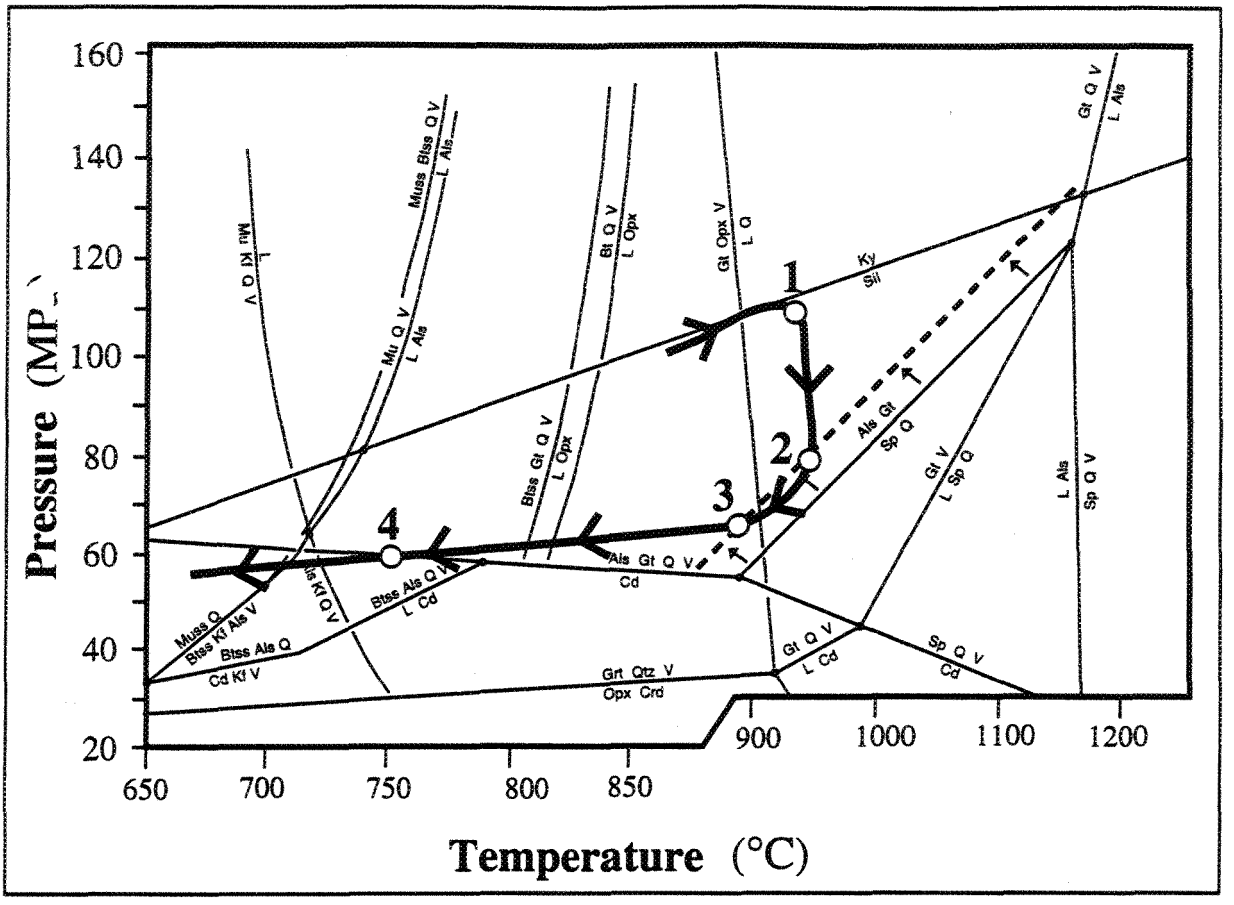

FIGURE 5-XII: P-T path for NCDZ, implied from geothermobarometry. The prograde conditions were approximately the same for the whole study area, therefore the P_{max} of 105 MPa (GASP) and the T_{max} of 950°C (Bt-Grt) are similar to the BGC (Figure 5-IV). The structural evidence for extension (2) was confirmed by the Grs profiles in the BGC. Neither Spl nor Crd was observed in the NCDZ, which limits the geothermobarometers available for determining positions along the retrograde path. However the assemblages limited position (4) in Figure 3-IX, which places this position of the retrograde path almost 10 MPa above the similar portion in the BGC (Figure 5-IV). The petrogenetic grid is simplified from Figure 3-III.

CHAPTER 6

GEOCHRONOLOGY

6.1 Introduction

This chapter presents the results of a co-operative project with van Breemen and Corriveau of the Geological Survey of Canada. The authors of the individual dates are identified in the Tables and the written work.

The purpose of these geochronological studies is twofold, first to calculate an age for peak metamorphic temperature and secondly to calculate the cooling and uplift rates. The T_{max} age, and the respective cooling rates will add information to the P-T-t trajectories. The cooling and uplift rates will provide important insight into the geological processes experienced in the Central Metasedimentary Belt of Québec. The cooling rates are also important in evaluating the results from geothermobarometric studies particularly in determining the likely extent of retrograde cation exchange (Chapters 4 and 5).

The concept of a closure temperature is herein introduced. Different minerals have different closure temperatures (Table 1-I), which permits the calculation of cooling and uplift rates when these mineral apparent ages and the corresponding pressures are determined. The U-Pb ages measured for monazite and zircon (Table 6-I) were used to estimate the age of peak metamorphic temperature because their closure temperatures are closest to the peak metamorphic temperature of 950°C (Chapter 5). The calculated cooling and uplift rates (Table 6-II) were calculated separately for the Bondy Gneiss Complex and the Nomininguе-Chénéville Deformation Zone. The results from this study were then used to develop a

Table 6-I: Results From U-Pb Analyses of Zircon, Monazite, Titanite, and Rutile

Sample	Area	Altitude (feet)	Rock	Mineral	Age (Ma)
1529	BGC	1250	Tonalitic Gneiss	Zircon-A	1177.1+2.9
vB-GSC				Zircon-B	1181.3+2.5
				Zircon-C	1178.9+1.5
1654	BGC	1200	Magnesian Gneiss	Zircon-A	1190.6+7.7
vB-GSC				Zircon-B	1195.7+2.4
				Zircon-C	1188.8+7.5
2688	BGC	900	Orthogneiss	Zircon-A	1214.9+1.1
vB-GSC				Zircon-B	1213.7+1.2
				Zircon-C	1181.6+1.1
				Zircon-D	1181.6+1.1
3565A	BGC	1250	Tonalite	Zircon-A	1259.7+1.5
vB-GSC				Zircon-B	1251.2+2.9
				Zircon-C	1305.2+1.9
3302	BGC	950	Magnesian Gneiss	Zircon-A	1699.8+1.2
Boggs				Zircon-B	1448.2+3.7
				Monazite-A	1164.6+3.0
				Monazite-B	1187.6+1.4
				Monazite-C	1184.0+1.7
				Monazite-D	1181.5+2.0
2401D	BGC	1200	Magnesian Gneiss	Monazite-A	1176.4+1.7
vB-GSC				Monazite-B	1175.0+2.6
				Monazite-C	1174.2+2.4
				Monazite-D	1177.6+2.2
2688	BGC	900	Orthogneiss	Monazite-A	1166.0+2.4
vB-GSC				Monazite-B	1167.1+2.8
1655D	BGC	1150	Lamprophyre dyke	Titanite-A	1068.9+25.6
vB-GSC				Titanite-B	1071.8+59.8
				Titanite-C	1036.4+89.0

Table 6-I: Results From U-Pb Analyses - continued

2378	BGC	1100	Marble	Titanite-A	1134.1+12
vB-GSC				Titanite-B	1132.6+15
3302	BGC	950	Metapelite	Rutile-A	962.3+3.7
Boggs				Rutile-B	974.3+5.4
				Rutile-C	987.4+7.7
3565A	BGC	1250	Pegmatite	Zircon-A	1163.7+2.5
vB-GSC				Zircon-B	1161.0+1.3
				Zircon-C	1159.5+1.3
1512D	BGC	1250	Metapelite?	Monazite-A	1173.4+1.4
vB-GSC				Monazite-B	1173.5+1.3
				Monazite-C	1173.5+1.3
1512C	BGC	1250	Calcsilicate	Titanite-A	1165.2+3.6
vB-GSC				Titanite-B	1153.4+3.5
				Titanite-C	1161.6+3.2
3603B	BGC	900	Marble	Titanite-A	1157.3+2.6
vB-GSC				Titanite-B	1155.1+2.8
				Titanite-C	1156.3+2.6
3473	NCDZ	800	Pegmatite	Zircon-A	1661.1+1.1
vB-GSC				Zircon-B	1398.4+1.5
				Monazite-A	1154.8+1.1
				Monazite-B	1153.4+1.1
1280	NCDZ	900	Metapelite	Zircon-A	1592.8+1.1
Boggs				Zircon-B	1969.6+1.2
				Monazite-A	1165.3+1.2
				Monazite-B	1161.9+1.1
				Monazite-C	1162.4+1.3
				Monazite-D	1163.4+1.2
1587B	NCDZ	875	Marble	Titanite-A	1126.5+3.9
vB-GSC				Titanite-B	1127.6+4.6

Table 6-Ia: Results From ^{40}Ar-^{39}Ar Analyses of Biotite

Sample	Area		Rock Type	Mineral	Age (Ma)
1280	NCDZ		Metapelite	Biotite	956+8
Boggs					
2039	NCDZ		Metapelite	Biotite	1190+9
Boggs					
3302	BGC		Metapelite	Biotite	932+7
Boggs					
3832	SW		Metapelite	Biotite	1028+8
Boggs					

Note here that vB-GSC designates dates from van Breemen of the GSC in Ottawa, and that Boggs designates dates from the author analyzed at the GSC
Because of space limitations, the + sign should actually be +/-

Table 6-II: Calculated cooling and uplift rates

Table 6-IIa: Mineral Closure Temperatures, and Apparent Mineral Age Ranges

Mineral	Zircon	Monazite	Titanite	Rutile	Biotite
Closure T (C)	>900	700-750	500-670	420-380	300-350
Apparent Age					
Range (Ma)					
BGC	1177-1196	1165-1188	1069-1133	962-987	932
NCDZ		1155-1165	1127		956
SW Corner	1182-1188				1028

Table 6-IIb: Calculated Cooling Rates

Minerals	BGC	NCDZ
	(C/Ma)	(C/Ma)
Zrn-Mnz	5 to 25	9.5 to 14.7
Mnz-Ttn	7.8 to 0.3	1.2 to 10.9
Ttn-Hbl	1.2 to 2.0	1.8 to 3.1
Ttn-Rt	1.5 to 1.7	
Ttn-Bt		1.7
Hb-Rt	1.5 to 2.4	
Hb-Bt		1.6 to 2.3
Rt-Bt	0.8	

Note that the hornblende ages are from Hanes and Corriveau (1994)

Table 6-IIc: Calculated Uplift Rates

Geothermal Gradient	Uplift Rates (mm/year)
(C/km) 1 (extension)	105 MPa (peak pressure) to 85 MPa (end isothermic decompression) 1186 Ma (peak metamorphism) to 1167 Ma (start plutonism in NCDZ) initial uplift during extension between 5 (NCDZ) and 25 (BGC)
25-BGC 35-NCDZ (plutonism in NCDZ)	85 MPa to 55 MPa (approximate at 670 C) 1167 Ma to 1069 -1133 Ma (apparent ages for titanite) uplift between 0.01 and 0.1mm in BGC uplift between 0.02 and 0.06 in NCDZ
25-BGC 25-NCDZ	55 MPa to 45 MPa (at 500 C) 1069-1133 Ma to 1020-1050 (apparent ages for hornblende) uplift between 0.03 and 0.35 in BGC uplift between 0.03 and 0.09 in NCDZ

tectonochronological model for the Mont Laurier Region of the Central Metasedimentary Belt.

6.2 Closure Temperatures

6.2a Definition and Examples

The concept of closure temperature (T_C) was defined by Dodson (1973); as the temperature at the time corresponding to the mineral's apparent age. For example (Table 1-I) the T_C for zircons is estimated to be >900°C, the closure temperature for ^{39}Ar-^{40}Ar analyses of biotite is estimated at 350°C (Harrison et al. 1985).

6.2b Closure Temperatures and Geological Processes

It is possible to determine if a mineral age records information about the cooling history, or an event during prograde metamorphism by comparing these closure temperatures with the peak metamorphic temperatures evaluated by geothermometers (Mezger et al. 1993). For example, the cooling rate can be calculated by dividing the range in temperature between the peak metamorphic temperature and the closure temperature for a specific mineral analysis by the difference in time between peak metamorphism and the attainment of closure temperature of the mineral.

Copeland et al. (1988) suggested three methods for calculating uplift rates:

1. Using two identical minerals and obtaining the ratio of the difference in elevation and their mineral ages. This method is inapplicable here because the difference in elevations between individual samples in the Mont Laurier Region is not significant.
2. Dividing the ratio between two mineral ages from the same sample and the difference in their closure temperatures by an assumed geothermal gradient.

3. Divide a known uplift amount by the length of time during which uplift took place. For this method, depths can be obtained:

a. by dividing the mineral Tc by an assumed geothermal gradient (depth below surface of the earth at the time that the mineral achieved its T_C), or

b. from geobarometers.

6.3 Appropriate Minerals

Zircon, monazite, titanite, rutile, hornblende and biotite are the minerals analysed for the chronological portion of this study. The minerals appropriate for this geochronological study are described below with their morphology, and their source rock types.

6.3a U-Pb System

This system is very powerful because two isotopes of U decay to two isotopes of Pb, which makes it possible to obtain three ages ($^{207}Pb/^{235}U$, $^{206}Pb/^{238}U$, $^{207}Pb/^{206}Pb$; Faure 1986). These three ages provide an internal check on possible disturbances of the system after its last re-equilibration. An upper intercept (ideally the mineral crystallization age) and the lower intercept (disturbance or partial re-equilibration), can provide further information, when the data are plotted on a U-Pb concordia diagram (Mezger 1990).

6.3a.i Zircon

Zircon ($ZrSiO_4$) is the most commonly used mineral for U-Pb geochronology due to its high uranium content with negligible initial common lead, its robust and resilient nature, and its widespread occurrence in many rock types (Heaman and Parrish 1991). Igneous zircon crystals can have a variety of colours and morphologies (Pupin 1980). A doubly-terminated prism dominated by the {100} face with a 3:1 length to width ratio is the most common zircon morphology. Frequently, the mineral separate colour is related to the uranium content and age of the zircons, for example, Proterozoic and younger zircons are typically colourless, and Archean zircons are commonly brown (>500 ppm U) or pink (50-300 ppm U; Heaman and Parrish 1991). The pre-Grenvillian zircons, from outcrop 3302

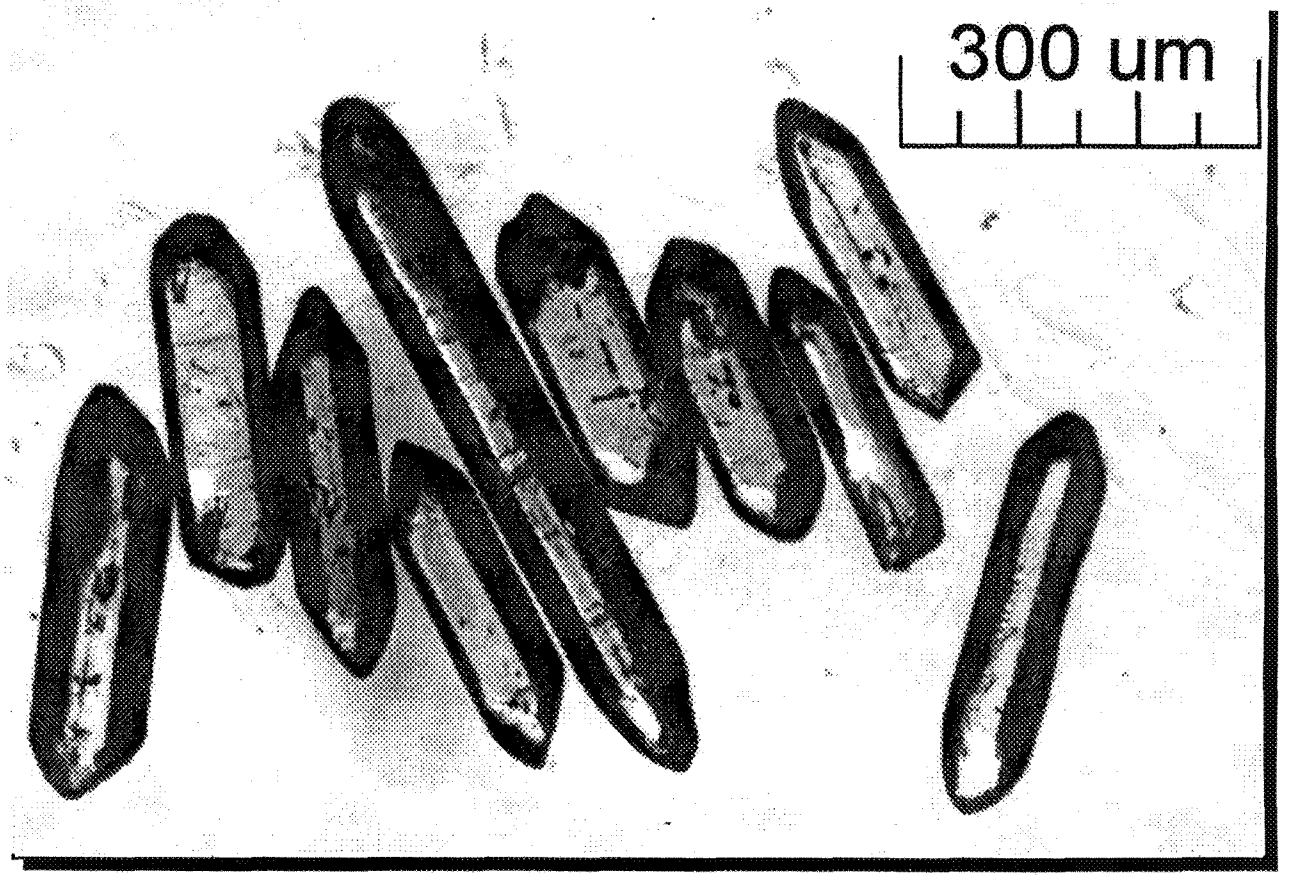

Figure 6-I: Zircon crystals from outcrop 3302. These colourless crystals have the prismatic habit suggestive of an igneous origin. These crystals were not analyzed as their habit is not suggestive of a metamorphic origin.

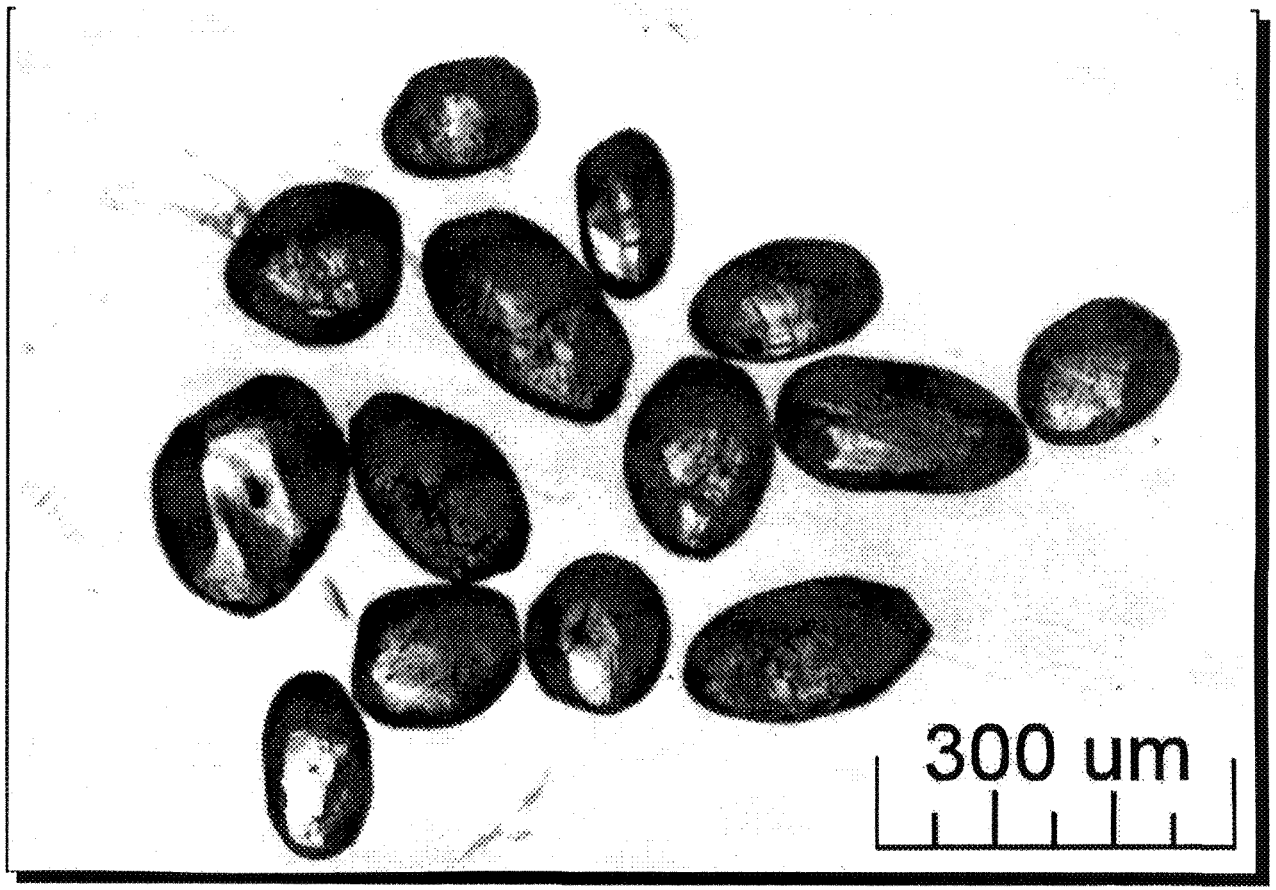

Figure 6-II: Zircon crystals from outcrop 1280. These crystals are clear to pale brown and have the multi-faceted spherical habit suggestive of a metamorphic origin.

were colourless doubly-terminated prisms (Figure 6-I), whereas those from outcrop 1280 were multi-faceted spheres (Figure 6-II). The uranium content ranged between 247 and 332 ppm. The Grenvillian age zircons from outcrop 3832, were colourless multi-faceted spheres, similar in morphology to the zircons from outcrop 1280 (Figure 6-III), with a uranium content between 559 and 746 ppm (TABLE 6-I).

The common tetragonal form, high birefringence, high refractive indices and straight extinction of zircons are fairly characteristic. Rutile and cassiterite, which may be mistaken for zircon, are typically reddish brown in thin section or grains, and have higher birefringences and refractive indices (Deer et al. 1966).

In the early days of U-Pb geochronology, there were many problems caused by the Pb-loss in zircons. These have been mostly overcome by the use of Krogh's (1982) air abrasion technique and the careful selection of crystals without turbidity, inclusions and fractures (Heaman and Parrish 1991). A transition to a metamict state can occur when the crystals accumulate between 10^{15} to 10^{16} alpha-decay events per milligram (Chakoumakos et al. 1987), which can cause a 5% volume expansion. This expansion in U-rich bands can lead to fracturing of the crystallographic structure, which renders the crystal sensitive to fluid penetration, alteration and Pb-loss (Krogh and Davis 1974). Extreme U-concentrations usually occur in the outer margin of zircon grains, which are removed by the abrasion process, removing the resultant discordance (Heaman and Parrish 1991).

The Pb-loss behaviour of zircon is a paradox. At high temperatures (>750°C), zircon has an extremely high retentivity for Pb, if there is little structural damage or accumulated radiation. However, zircons that have retained significant radiation damage may experience large amounts of Pb-loss caused by minor geological disturbances such as abundant fluid interactions or weathering (Heaman and Parrish 1991). The uranium content of the zircons

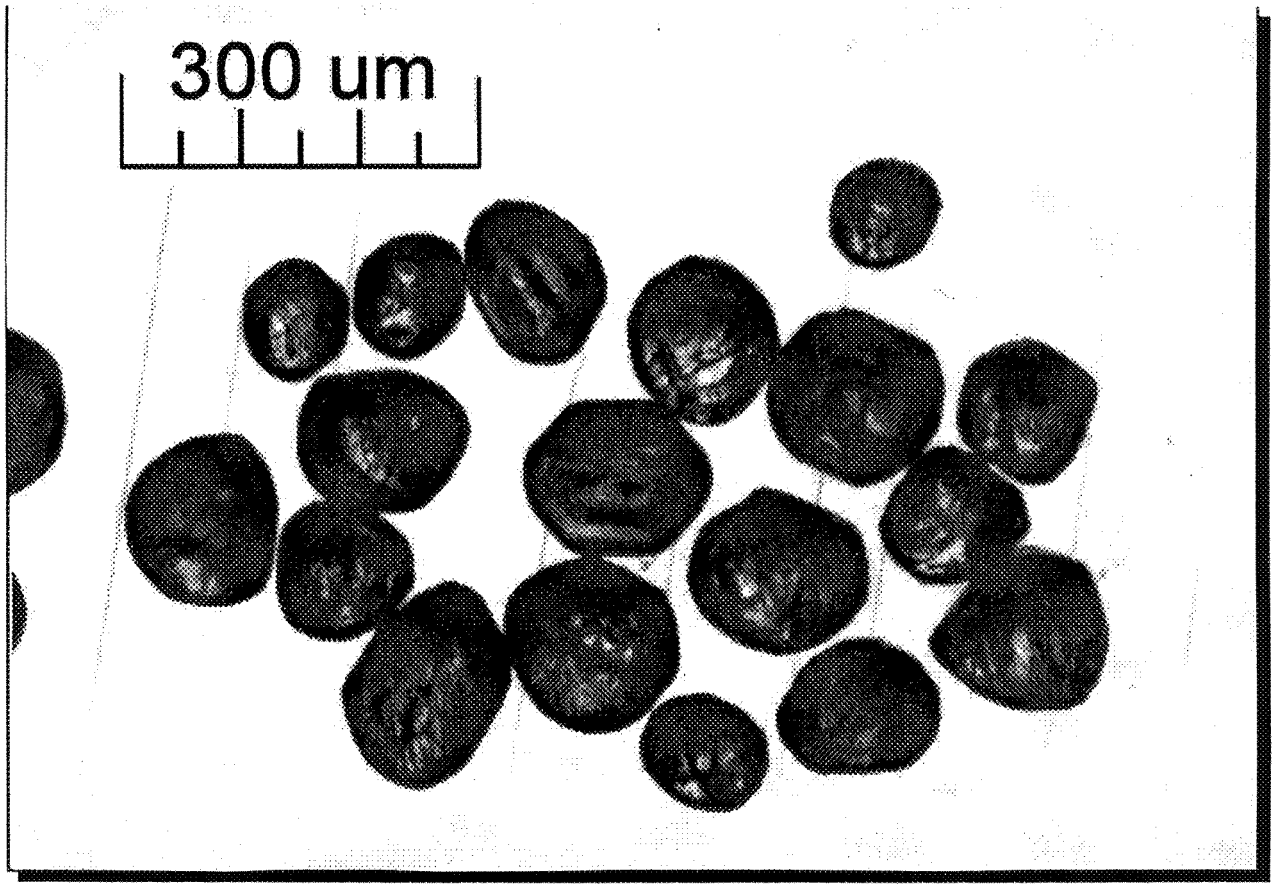

Figure 6-III: Zircon crystals from outcrop 3832. These crystals are clear to pale brown and have the multi-faceted habit suggestive of a metamorphic origin.

from this study were not very high, <800 ppm, and are thus not likely to have experienced very much Pb-loss because the radiation damage would not have been great.

The closure temperature for zircon is considered to be >900°C, and generally the zircon U-Pb systematics are considered to be the most difficult to completely reset even by granulite grade partial melting and metamorphism (Pidgeon and Aftalion 1978; Schenk 1980; Kröner et al. 1987a, 1987b; Mezger 1990). Metamorphism in the continental crust would likely only reset very small zircons. The memory of previous isotopic composition in zircons would only be erased if the zircons were completely destroyed and reprecipitated (Mezger 1990). Thus U-Pb analyses of metamorphically-produced zircons in this study (3832) can provide an approximate age at which peak metamorphic temperatures were reached. They can also, if combined with other mineral ages, and if pressure determinations are available, provide an upper limit from which to calculate both cooling and uplift rates (Mezger 1990).

6.3a.ii Monazite

Monazite ((Ce, La, Th)PO_4) occurs as an accessory mineral in a variety of igneous rocks, especially in granitic pegmatites and S-type granitoids. The S-type granitoid monazites are useful because they are igneous whereas the granitoids which are derived from the partial melting of continental crust usually contain ubiquitous inherited zircon (Heaman and Parrish 1991). The relationship between deformed granitic pegmatites, U-Pb monazite ages, and their host shear zones may be used to date stages of deformation (e.g., the Nominingue-Chénéville Deformation Zone). Monazite contains high levels of uranium (samples from this study contain 282-13,730 ppm), up to 60,000 ppm Th (Köppel 1974) and negligible (<1 ppm) common Pb; but is rarely metamict, possibly due to the ease with which monazite crystals anneal. Only a few grains of monazite are needed for a precise analysis due to its high uranium content. This is an important feature when examining migmatite leucosomes where only a few grams of material may be available, from which to

obtain monazites. Monazite inheritance is not as common a problem as zircon inheritance (Heaman and Parrish 1991).

Mineral separates of monazite are typically light straw yellow in colour, round, and multi-faceted (Figure 6-IV) in form, and have a high magnetic susceptibility, due to the abundance of light rare earth elements (Heaman and Parrish 1991). Staurolite is more strongly pleochroic, olivine and epidote have a larger 2V, zircon is uniaxial with higher refractive indices and titanite has a higher birefringence (Deer et al. 1966).

U-Pb dating of monazite has two potential problems. Many young (<200 Ma) monazites are reversely discordant, with the analyses plotting above the concordia curve (Schärer 1984; Schärer et al. 1986; Parrish 1990). This is due to the presence of excess ^{206}Pb, formed by the intermediate daughter product ^{230}Th, in the ^{238}U decay chain, during the crystallization of Th-rich minerals. The proportion of initial excess ^{206}Pb to radiogenic ^{206}Pb produced by the decay of ^{238}U is very minor or negligible in monazites older than about 200 Ma (e.g., this study), therefore a correction for this excess ^{206}Pb is not needed (Heaman and Parrish 1991).

The second concern for the U-Pb dating of monazite is that monazite contains high concentration of Th, and the amount of ^{208}Pb in an analysis may be so large as to cause difficulties in the resolution of the peaks at masses 208 and 207. The maintenance of a good vacuum (<2 x 10-7 torr) during the analyses and the careful monitoring of the tail of the ^{208}Pb peak may permit the mass spectrometer operator to make a first-order correction for this effect (Heaman and Parrish 1991).

The U-Pb systematics in monazite ($CePO_4$) are not disturbed by contact metamorphism at temperatures of ca. 650°C, are partially disturbed by anatexis at ca. 700°C (Parrish 1988; Copeland et al. 1988), and only completely reset by regional metamorphism

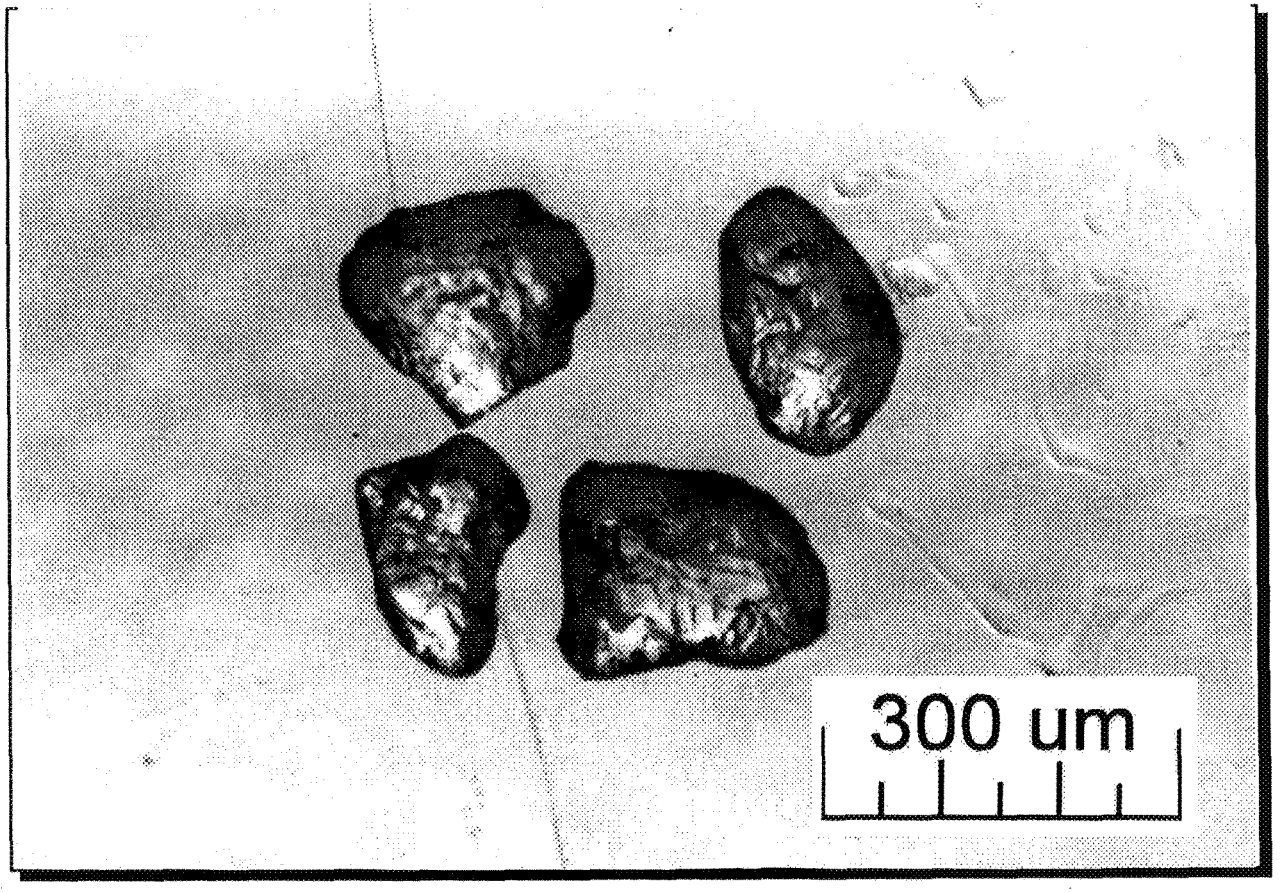

Figure 6-IV: Monazite crystals from outcrop 1280. These crystals are pale to light straw yellow in colour.

reaching 740°C (Mezger et al. 1991). Köppel and Grünenfelder (1975) proposed a T_c above 550°C, which contrasts with the suggestion of 550°C by Wagner et al. (1977), but is supported by the proposed closure temperature of 725 ± 25°C (Parrish 1990). The maximum temperature in the Mont Laurier Region is 950°C, therefore monazite ages would record cooling ages through 725 ± 25°C.

6.3a.iii Titanite

Titanite ($CaTi[SiO_4](O, OH, F)$), is an accessory mineral in many igneous rocks, it is the dominant titanium-bearing mineral in many intermediate and felsic plutonic rocks. In metamorphic rocks, it occurs mostly in impure skarns, marbles, and calc-silicates, and frequently in gneisses and schists rich in ferromagnesian minerals. The calcium may be replaced partially by barium, strontium, thorium or the rare earths. Tin, Nb and Ta may also partially replace the Ti group. The iron content likely influences the colour of titanites, with the green and yellow varieties being low in iron while the black or brown (this study) varieties having 1% or more Fe_2O_3. Orange hues appear to be due to rare earth content, however, this is often dominated by the iron coloration. The sphenoidal or rhombic cross-section of titanite is distinctive. The extreme dispersion, and birefringence distinguish titanite from monazite (Deer et al. 1966).

The analyses of titanites give concordant U-Pb dates in many terranes, however, some titanite populations result in discordant patterns similar to those observed in zircons (Tucker et al. 1987), where the titanites appear to record two ages (Mezger 1990). This discordancy may also be due to a second episode of titanite growth with new material surrounding older cores (Mezger 1990), or to a short period of thermal disturbance (Tucker 1988). It is necessary to evaluate the Th/U/Pb ratios, their concentrations, and the location of these analyses within the titanite grains (rim vs. core) to determine the cause of the

discordancy. The highest temperature during the period of disturbance, or new growth of the rim material, is also important (Mezger 1990).

Typical igneous and metamorphic titanites with a long dimension of less than 1 mm are considered to have a closure temperature between 500 and 550°C (Mattinson 1978; Gascoyne 1986; Cliff and Cohen 1980). A closure temperature of 670°C for titanites with a long dimension of 30 mm, typical of some marbles and pegmatites, at a cooling rate of 2°C/Ma was predicted by Mezger et al. (1992). Thus, the U-Pb analyses of titanites of different sizes, can reveal information about the cooling rates through 500 to 670°C (Mezger 1990).

One problem with the U-Pb dating of titanites is that they may contain negligible amounts of uranium (<5 ppm), much of which may be located within tiny U-rich mineral inclusions. This is of particular concern with the medium to dark brown titanite crystals, of this study, where it was difficult to select crystals devoid of visible inclusions (Heaman and Parrish 1991).

In this study, the peak metamorphic temperature was 950°C, thus the titanite ages likely record cooling through 670°C (these titanite crystals were picked from marbles and calc-silicates and have long axes close to 30 mm). The titanites in the NCDZ probably record evidence of a thermal disturbance, due to the deformation and syntectonic plutonism experienced in this zone after peak metamorphic conditions. A comparison of the NCDZ titanite and the BGC titanite U-Pb ages can determine the effect of this deformation and plutonism on the cooling rates in the study area.

6.3a.iv Rutile

Rutile (TiO_2) is widely distributed as minute grains in many igneous rocks, especially plutonic rocks, and as an accessory mineral in many metamorphic rocks, particularly in amphibolites and eclogites and metamorphosed limestones. As larger crystals, it is limited to

granitic pegmatites, aplite and quartz veins. It is fairly common as long hair-like needle inclusions in quartz, and as intergrowths with ilmenite and occasionally with biotite (Deer et al. 1966). Mineral separates are dark red-brown.

In thin section, the very high relief, extreme birefringence and deep red-brown colour are diagnostic. Baddeleyite has a lower birefringence and is less strongly coloured. Cassiterite has a poorer prismatic cleavage, and a lower birefringence and specific gravity (Deer et al. 1966).

The U-Pb systematics have been analysed for only a few rutiles from metamorphic rocks (Mezger 1990), with typically concordant or only slightly discordant results (Schärer et al. 1986; Mezger et al. 1989b). The U-Pb rutile ages are equivalent or slightly younger than the $^{40}Ar/^{39}Ar$ ages obtained from metamorphic amphiboles and younger than those determined for titanite ages, therefore the closure temperature is considered to be about 420°C for 0.2 to 0.4 mm grains (Mezger et al. 1989b). Therefore, the U-Pb rutile ages can add information to the cooling curves for the ranges near 420°C.

6.3b. K-Ar, and 40Ar/39Ar System

Potassium is the eighth most abundant element in the earth's crust, and is therefore present in most common igneous and metamorphic minerals (such as feldspars, micas and amphiboles). Thus the K-Ar method is applicable to many geochronological problems. The decay of the parent ^{40}K to the daughter ^{40}Ar has a half-life of 1250 Ma, which makes this method applicable to ages from the formation of the solar system to as young as a few thousand years (Hanes 1991).

Meaningful ages can often be interpreted from samples with very complex $^{40}Ar/^{39}Ar$ spectra from which the conventional K-Ar data would be meaningless. However, there is no simple method for interpreting $^{40}Ar/^{39}Ar$ age spectra because an individual age spectrum involves a combination of the geological history of the sample and the experimental step-

heating procedure used to obtain the date (Hanes 1991). Turner (1968) demonstrated how a partial argon-loss during a thermal disturbance can form disturbed spectra with diffusive-loss profiles, which can produce useful geochronological data. The Turner model can be modified to interpret more than one episode of gas loss since formation (Harrison 1983). It is possible to obtain a spectrum with the general characteristics of a diffusive-loss profile because of an episodic thermal event if the mineral cools slowly enough through its closure-temperature range (Dodson 1973; 1986; Harrison and McDougall 1982).

In granulite-grade metamorphic terranes, such as the Central Metasedimentary Belt of Quebec, the final cooling will be from temperatures above the argon closure temperature of all the K-bearing minerals. Thus the $^{40}Ar/^{39}Ar$ analyses of hornblende and biotite can provide information concerning the cooling rates from peak metamorphism (e.g., Cosca et al. 1991). This system can also be useful for estimating the age, temperature and duration of discrete thermal events, such as the timing of fault movements (Hanes 1991).

One problem with the $^{40}Ar/^{39}Ar$ system is that the heating of rocks may release ^{40}Ar that may be incorporated as excess-argon by minerals during cooling (Makobo et al. 1991). This contamination by excess argon, or the partial loss of argon since the mineral's original closure, can result in a meaningless $^{40}Ar/^{39}Ar$ date (Hanes 1991).

6.3b.i Hornblende

Hornblende $((Na,K)_{0-1}Ca_2(Mg, Fe^{+2}, Fe^{+3}, Al)_5(Si_{6-7}\ Al_{2-1}\ O_{22})(OH, F)_2)$ is the most widely dated mineral using the $^{40}Ar/^{39}Ar$ method. Among the major rock forming minerals, hornblende has the highest closure temperature (typically ca. 500°C, but very variable; Harrison 1981) for the $^{40}Ar/^{39}Ar$ system.

The composition of the hornblende and the cooling rate may affect the closure temperature. However, a direct correlation between the Fe/Mg ratio and the T_c has not yet been established. The composition has an effect on the alteration and exsolution of

hornblende during cooling (Robinson et al. 1982), which reduces the effective grain size of the hornblende, which in turn leads to a substantially lower T_c (Harrison and Fitzgerald 1986; Onstott and Peacock 1987). A second problem with hornblende is that it frequently contains intergrown biotite (e.g., this study) which may have younger cooling $^{40}Ar/^{39}Ar$ ages. During the step-heating analysis, the biotite will degas first, generating an apparent age spectrum that may resemble a diffusive-loss profile even if the hornblende has, in reality, a uniform distribution of ^{40}Ar (e.g., Berger 1975). Thus, it is important to determine the composition and structural state of the hornblende used for geochronology (e.g., Onstott and Peacock 1987).

Hornblende may also contain extraneous argon which can yield old ages of no geological significance. With the $^{40}Ar/^{39}Ar$ technique and step-wise degassing it is possible to note the presence of extraneous Ar and to make the required corrections (e.g., Harrison and McDougall 1980).

6.3b.ii Biotite

Biotite ($K_2(Mg, Fe^{+2})_{6-4}(Fe^{+3}, Al, Ti)_{0-2}(Si_{6-5}\ Al_{2-3}\ O_{20})(OH, F)_4$) can yield precise $^{40}Ar/^{39}Ar$ ages, however, it is prone to the incorporation of extraneous argon (e.g., Phillips and Onstott 1988). The closure temperature for most biotites is near 300°C (Purdy and Jäger 1976; Dodson and McClelland-Brown 1985), and can increase with the Mg/Fe ratio (Harrison et al. 1985) to as high as 450°C for phlogopite (Dodson 1979). The effective diffusion radius for biotite is between 0.15 and 0.2 mm, (Harrison et al. 1985) flakes larger than this would yield the same ages independent of grain size. This agrees with the K-Ar and Rb-Sr systematic studies of biotite flakes with a radius of 0.8 mm that discovered a significant decrease in ages from core to rim (Hart 1964).

Biotite may break down structurally during the step-heating stages, so that the gas is not evolved by simple volume diffusion (Foland 1983; Harrison et al. 1985; Gaber et al.

1988), which may allow spatial $^{40}Ar/^{39}Ar$ to be lost by homogenisation causing false plateau spectra. Thus, age spectra obtained from biotite analysis should be approached with caution (Hanes 1991). Biotite may also yield a disturbed spectrum with low dates at the low- and mid-temperatures of gas release, possibly due to the biotite behaving as a two reservoir system with each reservoir having a characteristic argon retentivity (York and Lopez-Martinez 1986). The younger than expected dates are interpreted to have resulted from the partial argon loss from the reservoirs, thus, it should be possible to extract significant ages from the spectra, however, care must be taken with such an approach (e.g., Gaber et al. 1988; Lo and Onstott 1989). Biotite is also particularly susceptible to excess-argon uptake, as was experienced in this study for samples 1280 and 3832, and in general throughout the Grenville Province from Ontario (Cosca et al. 1991) to Labrador (Dallmeyer and Rivers 1983).

The closure temperature for biotite in this field area was proposed to be 350°C for the NCDZ and 400°C for the BGC, due to the variation in magnesium content of biotite between the two regions. A careful comparison of the $^{40}Ar/^{39}Ar$ biotite ages with the U-Pb rutile, titanite, monazite and zircon ages can determine if the biotite analyses suffered from excess argon (the resultant ages would be anomalously high, i.e. older than the minerals with higher closure temperatures). When the plateaus are well-formed, and the $^{40}Ar/^{39}Ar$ biotite ages are younger than the other mineral ages, these biotite ages would represent cooling through 350°C.

6.4 Sample selection and preparation

Obtaining a date for peak metamorphic conditions is essential in reconstructing the P-T-t trajectories. After a careful petrographic examination, samples 1280, 3302 and 3832 (Figure 6-V) were chosen due to the presence of zircons.

U-Pb anâlyses of monazites, having a lower T_c than zircon, provide constraints on cooling and uplift rates. Thus two of these samples were chosen for monazite analysis:

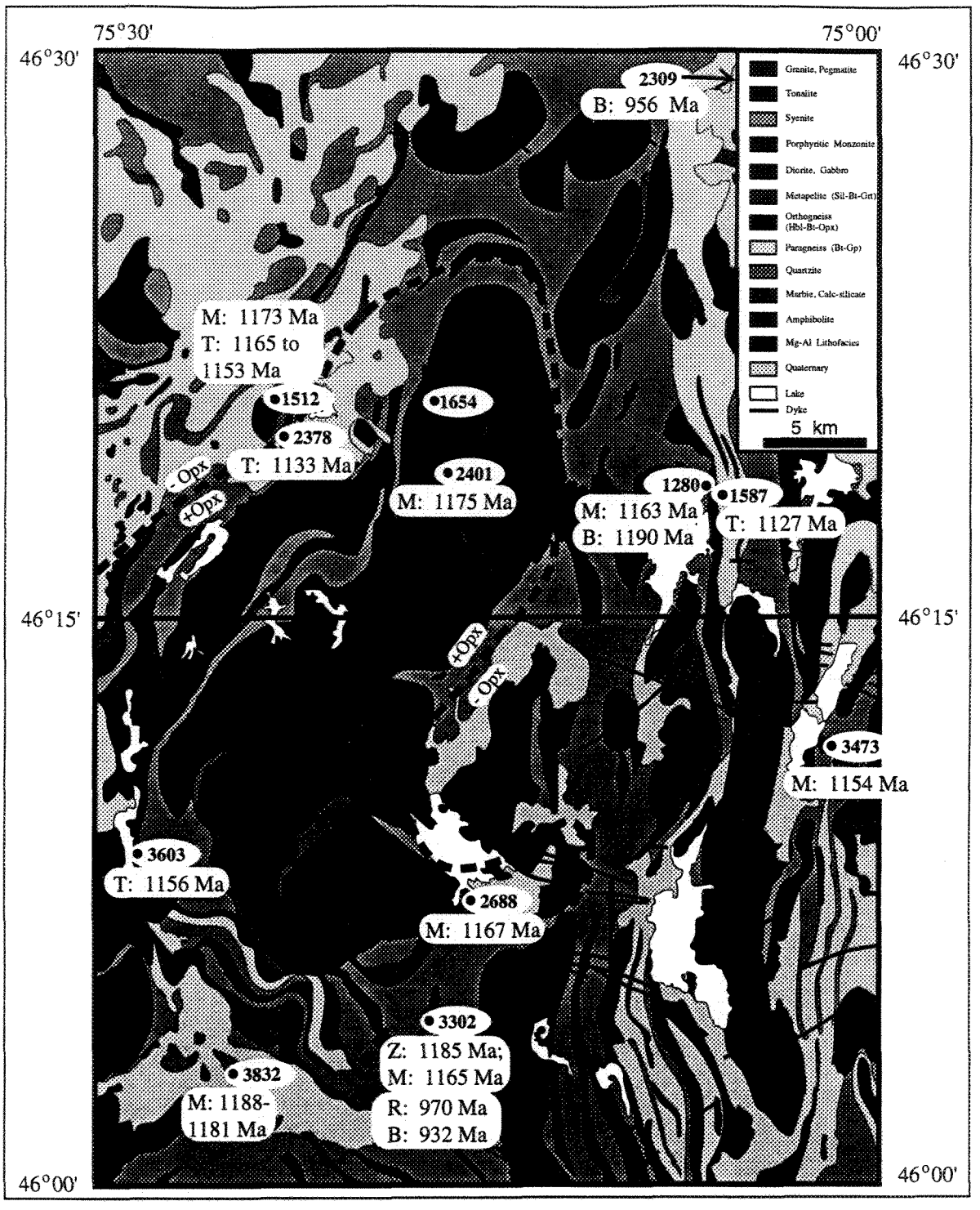

Figure 6-V: Geological map of field area with outcrops from which mineral ages were obtained. M-monazite; Z-zircon; T-titanite; R-rutile; B-biotite (simplified after Figure 2-I; after Corriveau et al. 1994).

3302, and 3832 (Figure 6-V). Because these samples contain both metamorphic zircons and monazites, it would be possible to calculate cooling and uplift rates over the interval 725°C to 950°C (the calculated peak temperatures from the geothermobarometers for the field area). Note that zircons will record the peak temperature age, even if the garnets are re-equilibrated, thus the peak temperature for the area must be used, not the peak temperature for the individual outcrops.

The four monazite samples (1512d, 2401D, 2688 and 3473) were analysed by van Breemen of the Geological Survey of Canada. He also examined six further samples of marbles and calc-silicates for titanites: 849, 925A, 1512c, 1587, 2378 and 3603 (Figure 6-V). Sample 1512c is from the same outcrop as a monazite sample, thus providing the opportunity for a comparison with the monazite data and the possible calculation of a cooling rate over the temperature range of 750°C to 670°C (Table 6-I).

Sample 3302 contains rutile provides further limits on the cooling rate. Samples 1280, 2039, 3302 and 3832 (Figure 6-V) also contain biotite from which ^{40}Ar-^{39}Ar ages were determined. Thus the dates for rutile and biotite provide a lower limit for the calculation of cooling rates down to temperatures as low as 350°C. It should be noted that ages from minerals with lower closure temperatures in high-grade domains with multiple metamorphic episodes, may represent resetting ages. The $^{40}Ar/^{39}Ar$ analysis of biotite is particularly susceptible to resetting, and may contain excess argon (Dallmeyer and Rivers 1983).

The samples for U-Pb zircon, monazite, rutile and titanite age determinations were prepared using the analytical techniques of Parrish et al. (1987; 1991). The zircon fractions for this study were air abraded to minimise the effects of peripheral lead loss (Krogh 1982). The results are contained in Table 6-I.

6.5 Peak Metamorphic Age

As discussed previously in Chapter 5, it is likely that the Bondy Gneiss Complex and the Nominingue-Chénéville Deformation Zone experienced similar prograde histories. Thus, the age for peak metamorphic conditions should be similar between the two regions. As demonstrated in Chapters 3 and 5, the P-T-t trajectory morphologies are clockwise, therefore, the peak metamorphic pressures would be achieved before the ages obtained from the U-Pb analysis of zircons and monazites which would provide an age for peak metamorphic temperature. Because the maximum temperature is so high (950°C), the zircon and monazite ages would provide a lower limit age for peak metamorphic temperatures.

6.5a Zircon U-Pb Analyses

The zircon separates from the metapelite samples 3302 and 1280 contained acicular zircons typical of igneous origin (Figure 6-I) and metamorphic zircons possibly of detrital origin (Figure 6-II). The two discordant zircon separates from 3302 yielded a Proterozoic lower intercept of 1233 ± 5 Ma and an Archean upper intercept of 2581 Ma (Figure 6-VI). The two discordant separates from sample 1280 also yielded a Proterozoic lower intercept of 1388 ± 5 Ma (Figure 6-VII). The third set of separates from sample 3832 had the spherical multi-faceted habit, suggestive of a metamorphic origin (Figure 6-III). The U-Pb ratios for these zircons define a Proterozoic upper intercept of 1186 ± 4 Ma.

The 50 to 200 Ma difference in U-Pb ages between sample 3832 and two other metapelitic zircon separates together with the morphology of the zircons suggests that these zircons either recrystallized or grew during peak metamorphism. The peak metamorphic temperature of 950°C (Fe-Mg exchange biotite-garnet and garnet-orthopyroxene geothermometers in Chapter 5) is only 50°C above the Tc of >900°C for zircons which further suggests that these zircons either grew or recrystallized at 1186 ± 4 Ma. This suggests an age of ≥ 1186 ± 4 Ma for peak metamorphic temperatures.

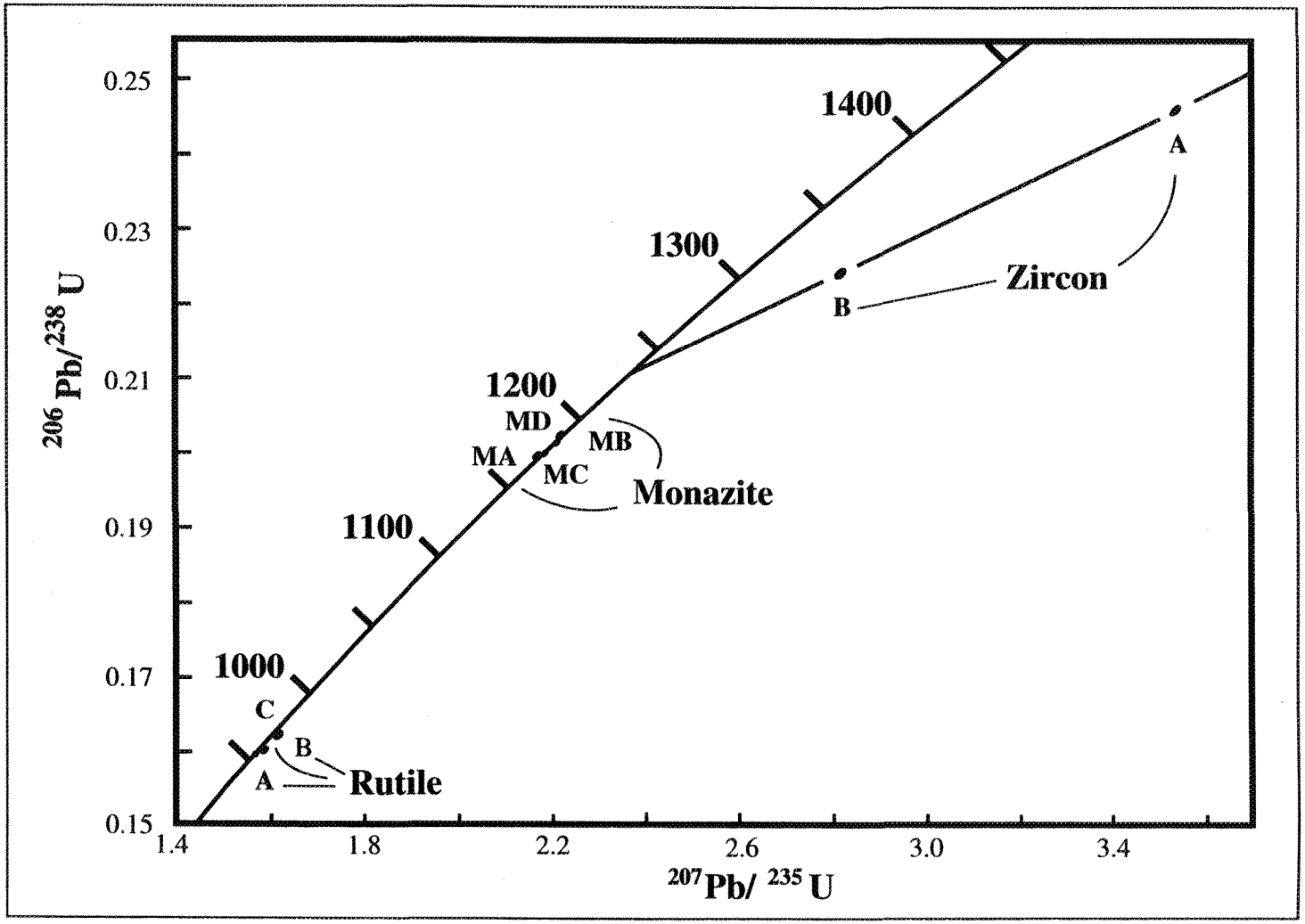

Figure 6-VI: Concordia plot for rutile, monazite and zircon from outcrop 3302. The lower intercept of the zircon data gives a Proterozoic age of 1233 ± 5 Ma, the upper intercept (not visible on this scale) gives an Archean age of 2581 Ma. Both these ages are pre-Grenvillian. Both the monazite and rutile ages are much younger than both these zircon ages, and the age of 1186 Ma for the peak metamorphic temperatures. Therefore, these mineral ages represent cooling through 725 ± 25 °C (closure temperature for monazite) and 380°C (closure temperature for rutile).

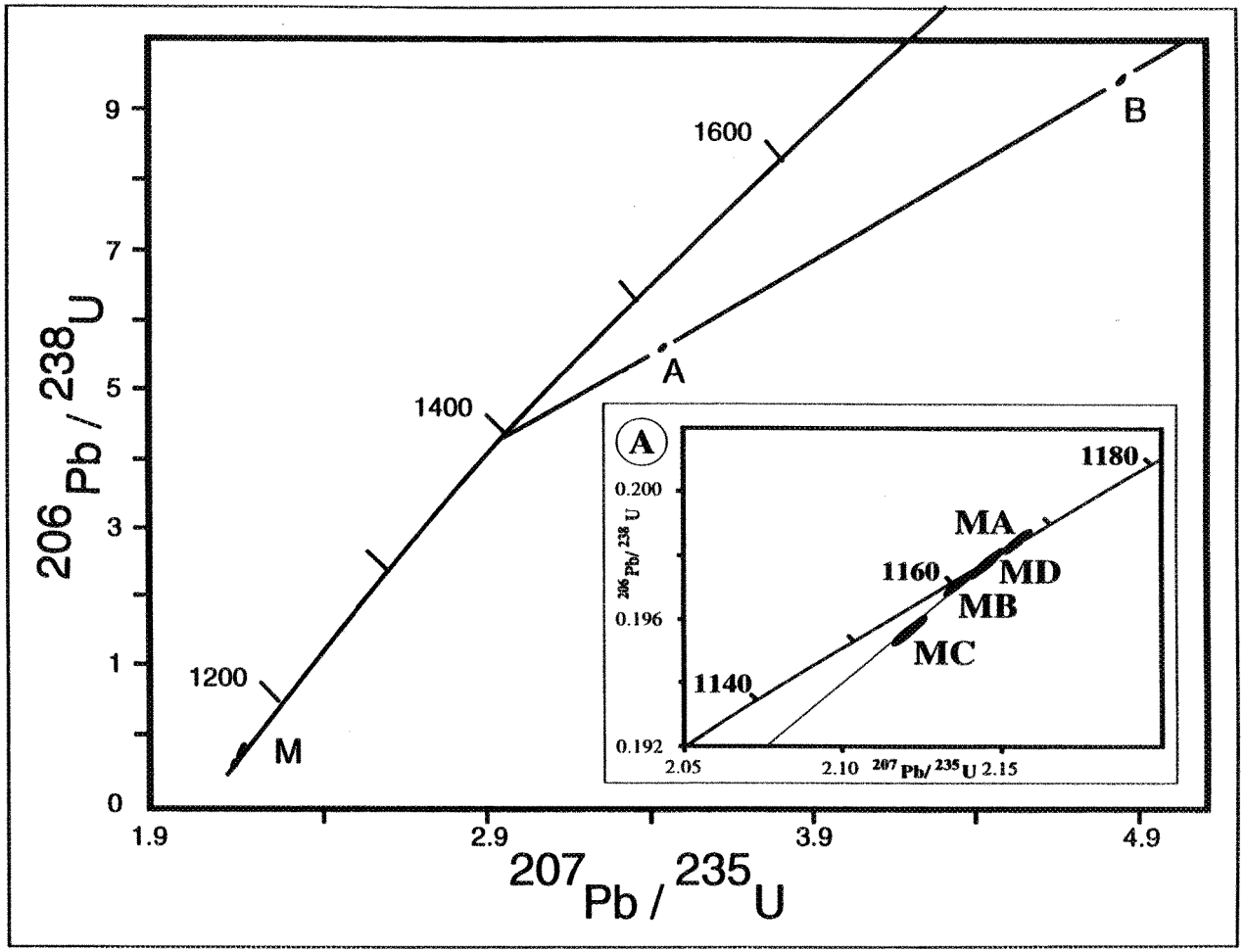

FIGURE 6-VII: Concordia plot for monazites and zircons from sample 1280 (NCDZ). The two discordant zircons yielded a Proterozoic lower intercept of 1388 ± 5 Ma. The inset 'A' contains a blow-up of the concordia for the four monazite analyses which define an upper intercept age of 1164 Ma. This monazite age is 21 Ma less than the inferred metamorphic age, which suggests an initial cooling rate of 8.7 °C/Ma for the temperature range between 950 and 725 ± 25°C.

Sample 3832 is from the southwestern corner of the field area (Figure 6-V), and located some 3 km southwest of the Bondy Gneiss Complex. Outcrop 3832 is strongly foliated, migmatized and folded. The garnets from this outcrop only record temperatures of 650°C (Ferry and Spear 1978; garnet-biotite Fe-Mg exchange thermometer), 300°C below the maximum metamorphic temperature, due to retrograde cation exchange. Partial melting, granulite metamorphism and retrograde cation exchange would not have affected the U-Pb ages of the zircon due to the extreme difficulty involved with completely resetting the U-Pb systematics (Pidgeon and Aftalion 1978; Schenk 1980; Kröner et al. 1987a 1987b). A zircon must be completely destroyed and reprecipitated in order to erase memory of its previous isotopic composition (Mezger 1990). However, at higher grades of metamorphism, such as this part of the Grenville Province experienced, new zircon overgrowths may result in discordant ages (Kröner et al. 1987a), which would explain the discordant nature of the Concordia plot for the zircons from sample 3302 (Figure 6-VI). As discussed in Chapter 5, it is likely that the entire field area experienced similar prograde conditions. Thus, it is proposed that $\geq 1186 \pm 4$ Ma is the age for peak metamorphic temperatures throughout the field area.

Note here that the detrital zircon U-Pb ages that are older than the proposed $\geq 1186 \pm 4$ Ma for peak metamorphic conditions do not limit the peak metamorphic temperatures to a point below the closure temperature for zircon; because of the extreme difficulty involved in completely resetting the U-Pb systematics of zircons (Pidgeon and Aftalion 1978; Schenk 1980; Kröner et al. 1987a; 1987b). In fact the peak metamorphic temperature of 950°C and the age of ≥1186 Ma for the metamorphic zircons suggest that the closure temperature for these zircons was ~950°C. The age of 1186 Ma for peak metamorphic temperatures appears to be a commonly supported age, such as for initial movement along the CMBBZ (McEachern and van Breemen 1993). Therefore, it is likely that peak metamorphic

temperatures occurred at approximately 1186 Ma, suggesting that the closure temperature for the U-Pb systematics in zircon would be near the peak temperature of 950°C.

6.5b. Monazite U-Pb Analyses

Four individual analyses of monazites from sample 3302 resulted in an U-Pb upper intercept of 1185 ± 3 Ma. If the error values are considered, this represents a period of 8 Ma over which the temperatures cooled from 950 down to 750°C, which results in an initial cooling rate of 25°C/Ma. An initially rapid cooling rate was predicted due to the isothermic decompression following peak metamorphic conditions. Thus, this monazite age supports the >1186 Ma age for peak metamorphic temperatures, inferring that the monazite crystals crystallised just after the peak metamorphic conditions as the temperatures cooled past 725 ± 25°C.

6.6 Cooling Rates

The Bondy Gneiss Complex was not penetrated by the retrograde deformational events that affected the NCDZ, neither does it contain the syntectonically emplaced monzonite-diorite complexes of the NCDZ. Thus, these two areas probably did not follow the same retrograde cooling paths (Corriveau et al. 1995; Chapters 2, 3, 4, 5). Table 6-II contains the closure temperatures, a summary of the results from the mineral U-Pb and ^{40}Ar-^{39}Ar analyses, and the calculated cooling/uplift rates for the BGC and the NCDZ.

As noted by van der Pluijm et al. (1994), much critical information is obscured when the times of peak metamorphism and the T-t paths are plotted together on the same plot. Thus, a more revealing approach is to separate the information from individual domains, then to compare the domain histories which establishes any differences of timing of separation, linkage of domains and displacements (van der Pluijm et al. 1994).

6.6a Bondy Gneiss Complex

6.6ai Monazite (950°C to 725 ± 25°C)

The monazite ages for samples within the Bondy Gneiss Complex range from 1166.0 ± 2.4 Ma for sample 2688 to the discordant upper intercept of 1186 ± 4 Ma for sample 3302 (Figure 6-VIII). Three U-Pb ages of 1173.4 ± 1.4 Ma were determined for monazites from sample 1512D; sample 2401D has four U-Pb monazite ages between 1174.2 ± 2.4 Ma and 1177.6 ± 2.2 Ma (Table 6-I).

Cooling rates from the proposed peak metamorphic temperature of 950°C at ~1186 Ma down to the closure temperature for monazite range between 25 and 5°C/Ma (Table 6-II). The higher portions of this range are higher than the 10°C/Ma that Mezger et al. (1993) proposed for the Frontenac Terrane in Ontario from the data of Marcantonio et al. (1990) and van Breemen and Davidson (1990).

6.6aii Titanite (725 ±25°C to 670°C)

U-Pb determinations for titanites from two marbles and one calc-silicate of the Bondy Gneiss Complex yielded ages of 1132.6 ±15 to 1134.1 ± 12 Ma (2378), 1153.4 ± 3.5 to 1165.2 ± 3.6 Ma (1512C), and 1155.1 ± 2.8 to 1157.3 ±2.6 Ma (3603B; Table 6-I). The cooling rates are between 7.8 and 0.3°C/Ma for the temperature range of 725 ± 25°C (closure temperature for monazite) and 670°C (closure temperature for rutile).

These cooling rates are lower than those for the temperature range between the proposed peak temperature of 950°C and the closure temperature for monazite (725 ± 25°C). These cooling rates are near the 10°C/Ma proposed by Mezger et al. (1993) for the Frontenac Terrane in Ontario.

6.6aiii Hornblende (670°C to 500°C)

Hanes and Corriveau (1994) obtained $^{40}Ar/^{39}Ar$ analyses of hornblendes from the Loranger pluton indicating an age of 1050 Ma, and from 1020 Ma the Kensington pluton.

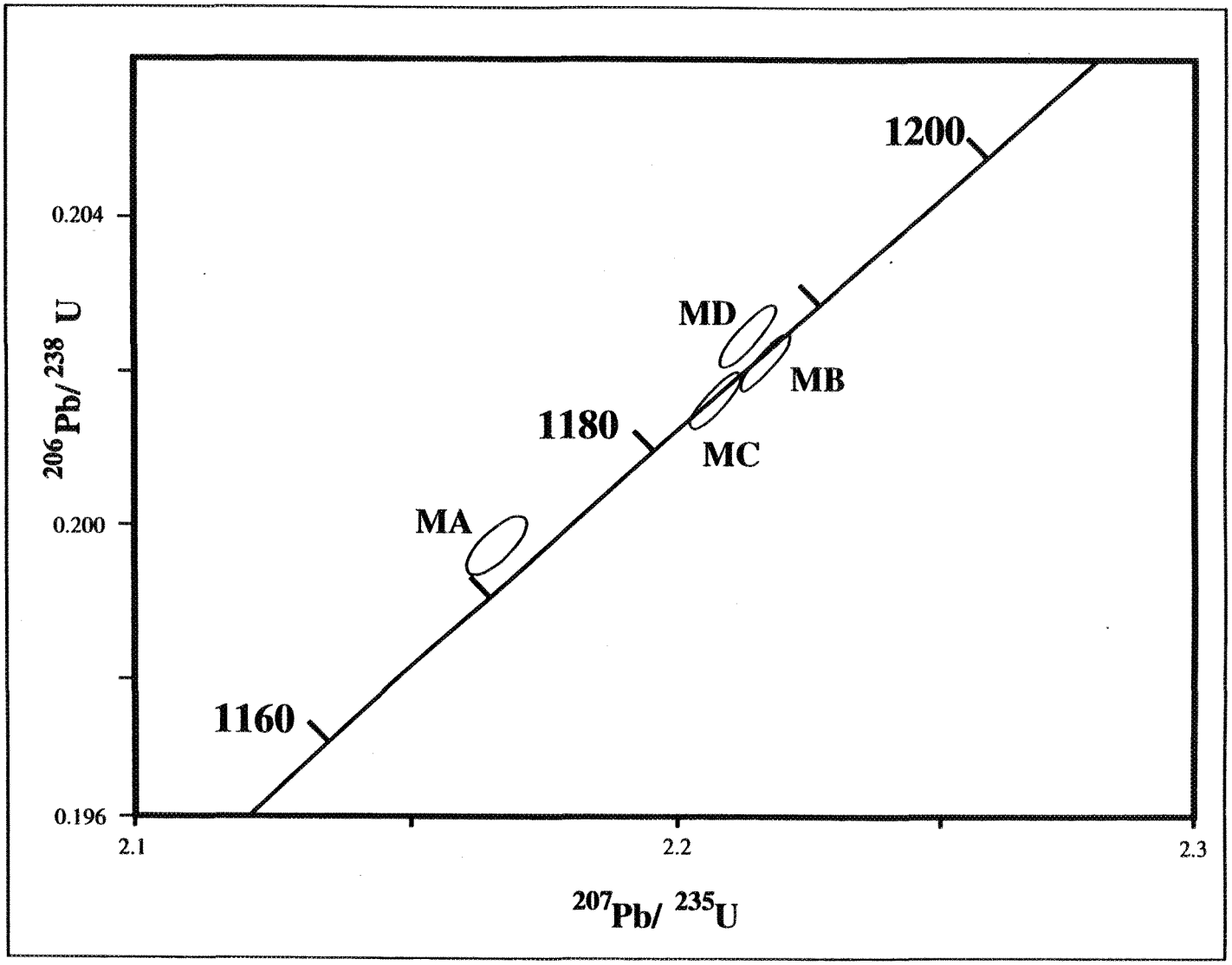

Figure 6-VIII: Concordia plot for monazites of sample 3302. These four monazite analyses define an upper intercept of 1185 ± 3 Ma. If the error values are taken into account, an initial cooling rate of 25°C/Ma was calculated from 950°C (the peak metamorphic temperature) through 725 ± 25 °C (the closure temperature for monazite).

These two plutons are located within the western portion of the Mont Laurier Region, therefore, this range of 1050 to 1020 Ma may be used to calculate cooling rates through 500°C. Using the above range of U-Pb titanite dates, cooling rates between 2.0 and 1.2°C/Ma were calculated over the temperature range 670 to 500°C. This cooling rate is within the 1-4°C/Ma range suggested by Cosca et al. (1991) for cooling below 500°C in the Grenville Province.

6.6aiv Rutile (725 ± 25°C to 380°C)

The rutile grains from sample 3302 (Figure 6-IX) are between 0.015 and 0.030 cm which implies a closure temperature of 380°C. The U-Pb analyses of these rutiles gives one age of 970 Ma, which represents a difference of 215 Ma from the U-Pb monazite age from the same sample. Thus, a range of cooling rates from 1.5 to 1.7°C/Ma over the temperature range of 725 ±25°C to 380°C was calculated. This cooling rate is significantly lower than that of the higher temperature ranges; however, it is within the 1-4°C/Ma range suggested by Cosca et al. (1991) for cooling between 500 and 150°C.

From the 1050 to 1020 Ma ^{40}Ar-^{39}Ar cooling ages of Hanes and Corriveau's (1994) a cooling rate of between 1.5 and 2.4C/Ma through 500°C was calculated using this 970 Ma rutile date. These values include the above range calculated for cooling from the monazite closure temperature through to the rutile cooling temperature. Thus, once past 725 ± 25°C (the closure temperature for monazite), the Bondy Gneiss Complex appears to have reached a constant cooling rate.

6.6av Biotite (380 to 350°C)

The Ar-Ar analysis of the biotite separate from sample 3302 resulted in an age of 932 Ma, that agrees with the U-Pb rutile age, both of which are significantly less than the U-Pb monazite age of 1185 Ma. This implies that this biotite preserved a cooling age. For this

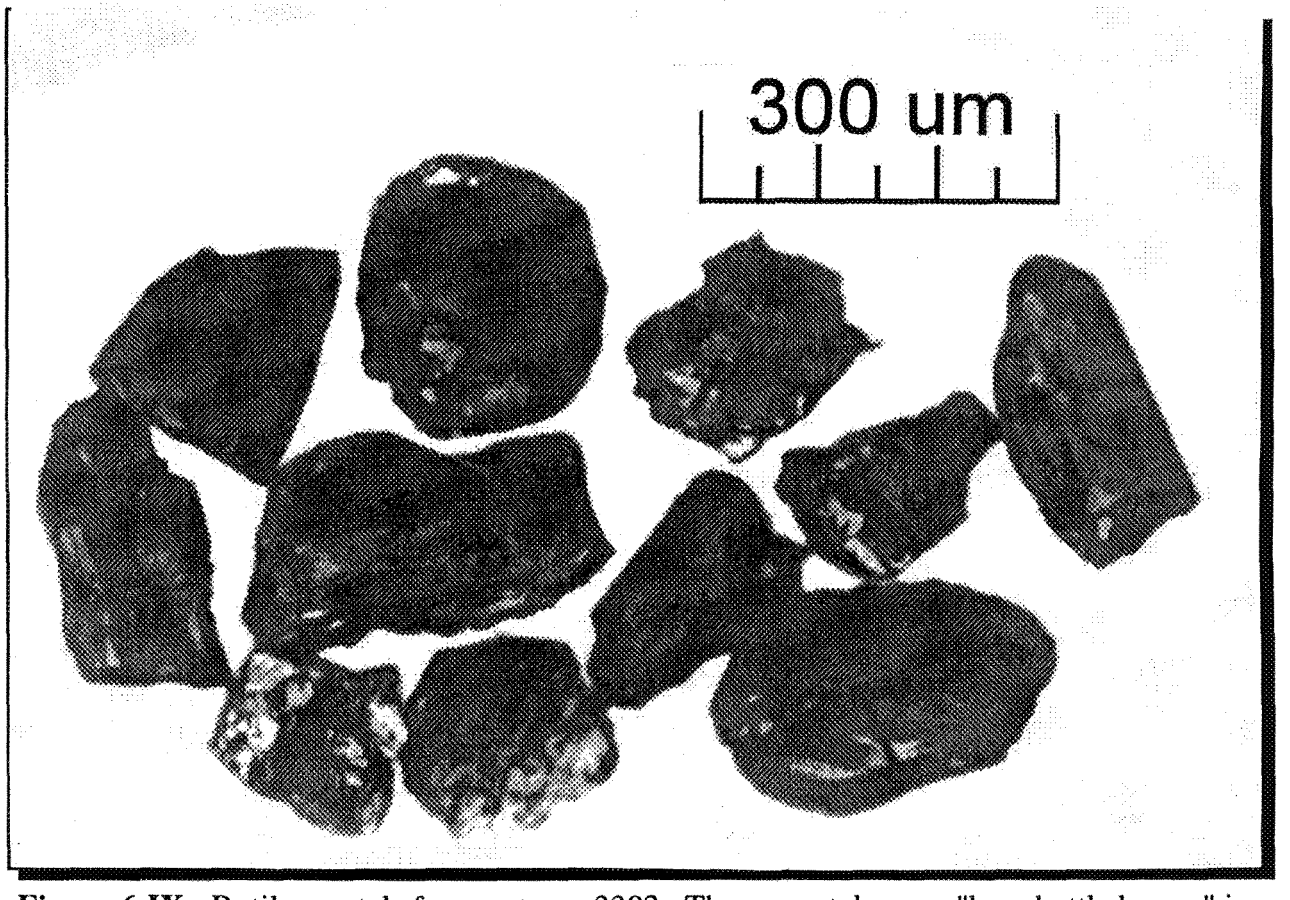

Figure 6-IX: Rutile crystals from outcrop 3302. These crystals were "beer bottle brown" in hand specimen, and pale reddish-brown in separated crystals (as above).

outcrop, the cooling rate from 380 to 350°C is 0.8°C/Ma which is below the 1 to 4°C/Ma range suggested by Cosca et al. (1991) for the Grenville.

6.6b Nominingue-Chénéville Deformation Zone

In comparison with the BGC, the NCDZ has undergone a complicated cooling history from the metamorphic peak involving both deformation (>1165 to 1156 Ma) and syntectonic plutonism (1167 to 1164 Ma; van Breemen and Corriveau 1995; Corriveau et al. in press). Thus, it is probable that the U-Pb systematics of monazite and titanite would record some evidence of the plutonic activity, not solely the uplift cooling history.

6.6bi Monazite (950 to 725 ± 25°C)

The four individual monazites from sample 1280 yielded U-Pb data that are discordant with an upper intercept of 1163.7 Ma (Figure 6-VII). This upper intercept value is 23 Ma younger than the inferred peak metamorphic age of 1186 ± 4 Ma, suggesting that these monazites have recorded an age during cooling from peak metamorphism. A range of 9.5 to 11.7 °C/Ma is implied for the cooling from the metamorphic peak temperature of 950°C down to the closure temperature of monazite (725 ±25°C). Note that this outcrop is not near the monzonite-diorite complexes, these monazite ages would therefore not represent a crystallization age.

These values for the cooling rates are lower than those of the BGC over the same temperature range, however, they are still near the value of 10°C/Ma proposed by Mezger et al. (1993) for the Frontenac Terrane of Ontario where detailed work has been completed.

6.6bii Titanite (725 ± 25°C to 670°C)

The U-Pb upper intercept of 1130 Ma for titanites from sample 1587 (Table 6-I) results in a cooling rate of 1.2 to 10.9 °C/Ma from the closure temperature of monazite down to the closure temperature of titanite. This range of cooling rates extends down to lower

The emplacement of the 1167 to 1164 Ma monzonite-diorite plutons into the NCDZ (van Breemen and Corriveau 1995; Corriveau et al. in press) thus appears to have influenced the cooling rates in the NCDZ from 725 ± 25°C (the closure temperature of monazite) to 670°C (the closure temperature of titanite). By 725 ± 25°C, the cooling rates in the BGC had slowed to a consistent rate through until 350°C (the closure temperature of biotite); whereas the NCDZ cooling rates did not reach a consistent rate until 670°C.

6.7 Uplift Rates

Using the second and third methods of Copeland et al. (1988), an uplift rate of between 5 and 25 mm per year was calculated for the initial episode of isothermic decompression in both the BGC and the NCDZ (Table 6-II). The 25 mm per year is likely the rate experienced by the BGC as it was uplifted with respect to the NCDZ. These values were obtained assuming a geothermal gradient of 1°C/km (due to isothermal decompression conditions), peak metamorphic conditions slightly before 1186 Ma, isothermal decompression from 105 MPa to 85 MPa at 950°C, and that the 1167 Ma syntectonic plutonism was channelled into the less competent NCDZ.

After the initial episode of isothermal decompression, the tectonic histories of the BGC and the NCDZ diverged due to the deformation (>1167 to 1156 Ma) and syntectonic plutonism (1167 to 1164 Ma; van Breemen and Corriveau 1995; Corriveau et al. in press) in the NCDZ. Assuming a geothermal gradient of 25°C/km (Cosca et al. 1992; and Culshaw et al. 1994), the uplift rates in the BGC ranged from 1.00 to 0.01 mm per year (from 950°C, the peak metamorphic temperature down to 670°C, the T_c for titanite) down to 0.03 mm per year (from 380°C, the T_c for rutile, down to 350°C, the T_c for biotite). Using a geothermal gradient of 35°C/km (to account for the plutonism), the uplift rates in the NCDZ ranged from 0.58 to 0.2 mm per year down to 0.03 mm per year, over the same temperature intervals. Thus, the uplift rates within the BGC were more rapid than in the NCDZ during the

extension. However, the uplift rates throughout the Mont Laurier Region study area were very similar towards the final stages of the cooling history (below ~600°C).

6.9 Summary

6.9a Nominingue-Chénéville Deformation Zone Versus Bondy Gneiss Complex

The graphs of apparent ages versus the mineral closure temperatures for the Nominingue-Chénéville Deformation Zone and the Bondy Gneiss Complex are contained in Figures 6-X and 6-XI. The NCDZ and the BGC graphs are similar between the zircon and monazite interval, suggesting that the NCDZ and the BGC experienced similar cooling conditions immediately after the peak temperatures were attained, with a cooling rate between 5 and 25°C/Ma, and an uplift rate between 2.3 and 0.6 mm per year. This initial cooling corresponds to extension (>1165 to 1156 Ma; van Breemen and Corriveau 1995; Corriveau et al. in press) in the NCDZ and isothermic decompression in the BGC.

The syntectonic plutonism (1167 to 1164 Ma; van Breemen and Corriveau 1995; Corriveau et al. in press) in the NCDZ is reflected in the cooling curves, since the titanite from the NCDZ is displaced to lower ages (i.e., slower cooling) relative to the BGC titanites. The heat from the magma injected into the NCDZ slowed the cooling process. The rate of uplift in the NCDZ also slowed with respect to the BGC.

Cooling past the closure temperature of titanite was similar between the NCDZ and the BGC. This is expected if there were no further influx of heat into the NCDZ, or into the BGC, which allowed the rocks to cool at a consistent rate from 670°C (the T_c of titanite) down to 350°C (the T_c of biotite). The uplift rates for the BGC and the NCDZ were similar at this stage, 0.03 mm per year for the BGC and 0.07 mm per year for the NCDZ.

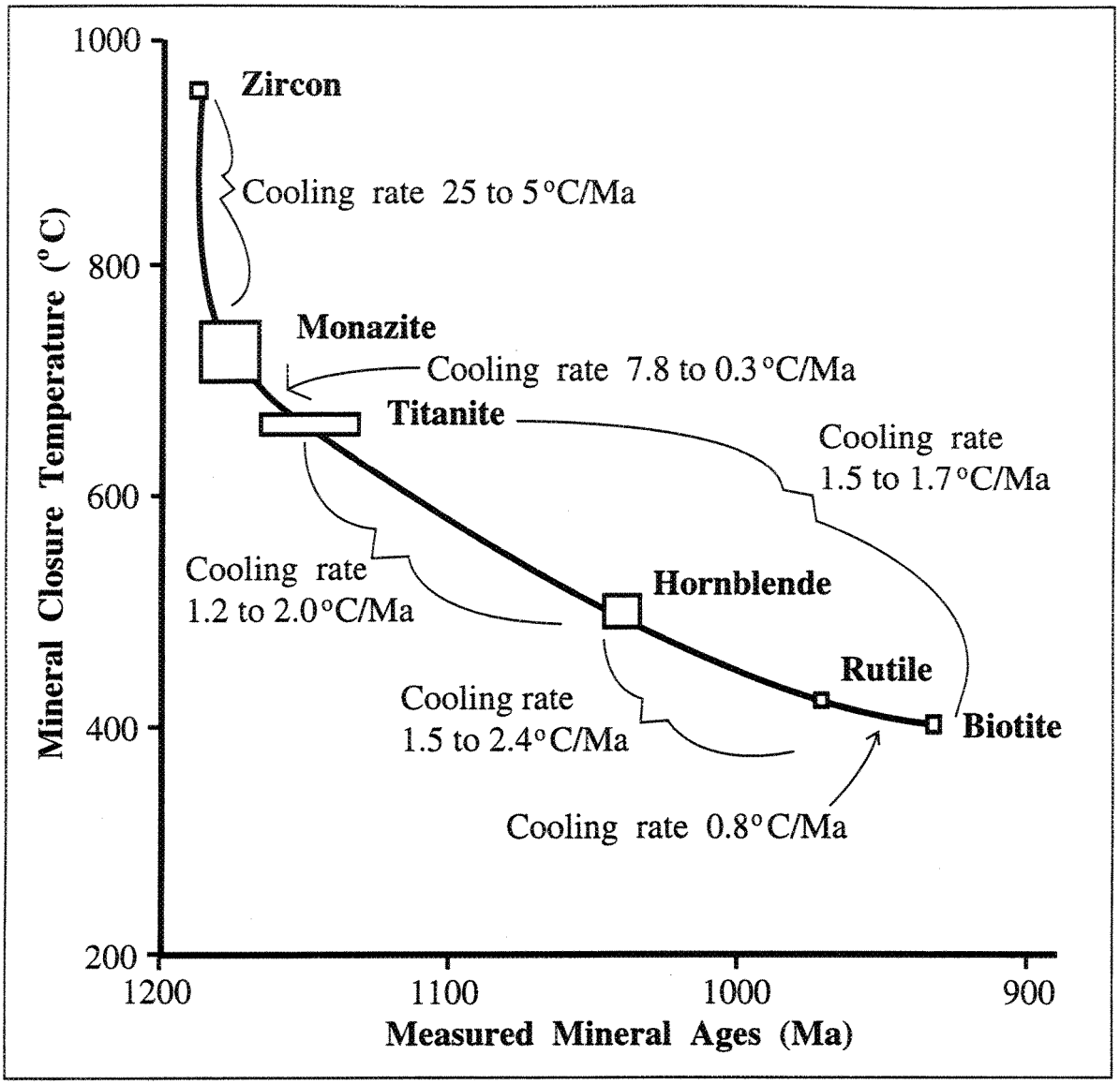

Figure 6-X: Cooling curve for the Bondy Gneiss Complex. The BGC did not have as complicated of a cooling history as did the NCDZ (Figure 6-XI). The BGCwas uplifted quickly just after peak metamorphism, after which it cooled gradually.

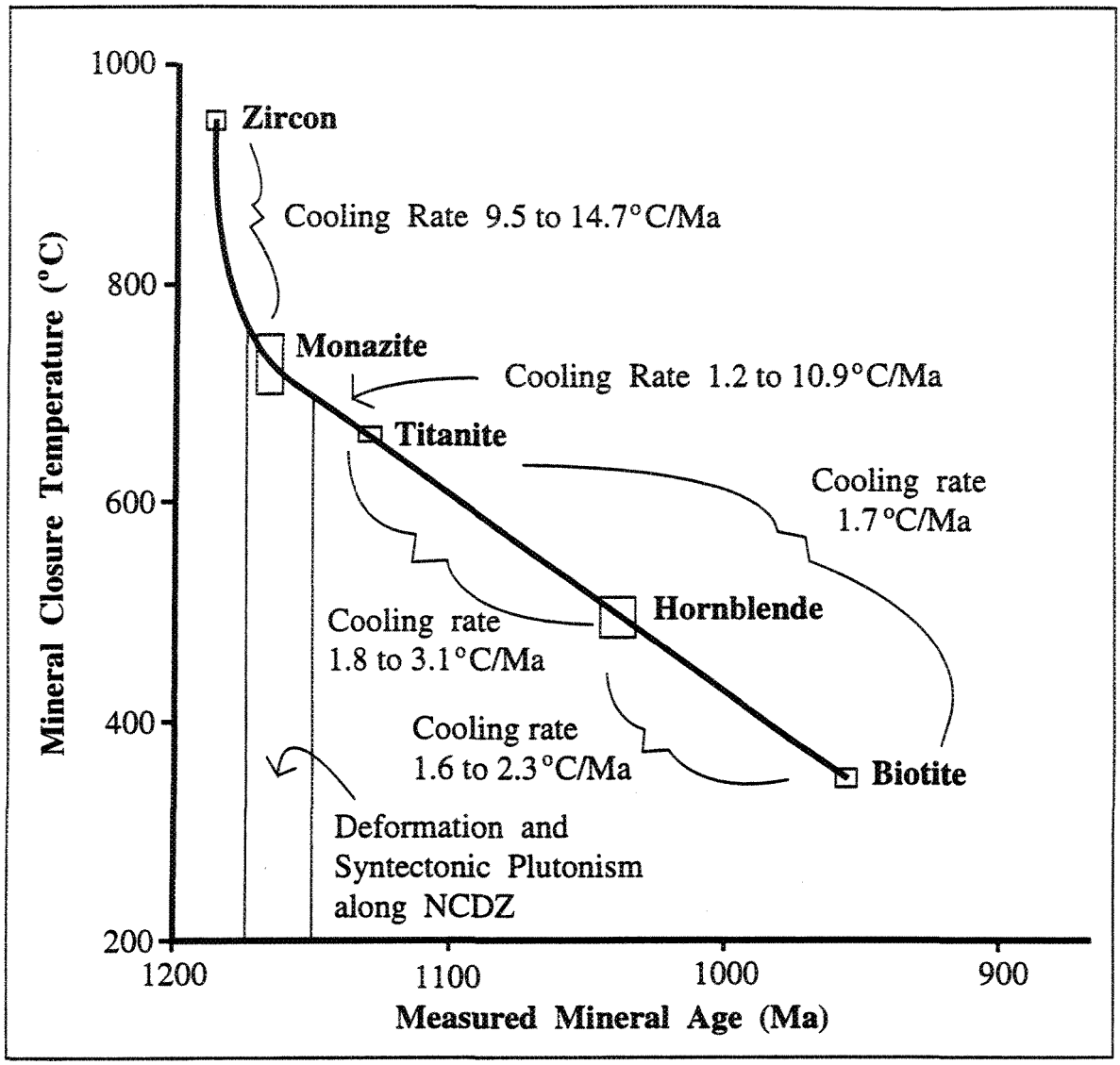

Figure 6-XI: Cooling curve for the Nominingue-Cheneville Deformation Zone. The syntectonic plutonism along the NCDZ did not affect the cooling rates until after the monazite closure temperature. Between the closure temperatures for monazite and titanite, the cooling rate slowed in comparison with the BGC (Figure 6-VIII). After the titanite closure temperature, the cooling rates were once again similar between the two tectonostratigraphic domaines.

6.9b Regional Significance

Past geochronological studies of the Grenville Province are summarised in Figures 6-XI, 6-XII. The proposed value of ≥1186 ± 4 Ma for the age of peak metamorphic temperatures for the CMB of Quebec is 10 to 45 Ma older than the values proposed for the Frontenac terrain (1175-1150 Ma) and the Adirondack Lowlands (1170-1130 Ma) of the CMB in Ontario and New York (Mezger et al. 1993). The values obtained by Mezger et al. (1993) were from U-Pb analyses of monazites. It is very possible that these monazite dates actually record cooling from peak metamorphic temperatures, and that the proposed ≥1186 ± 4 Ma actually corresponds with the peak metamorphism for these regions. It is also possible that peak metamorphism did in fact occur 10 to 15 Ma earlier in the northeastern portions of the CMB, especially since the 1170 Ma plutons in the field area are not migmatized (Corriveau 1990; Corriveau et al. 1994; Corriveau et al. 1995).

The ≥1186 ± 4 Ma age for peak metamorphic temperatures correlates with the initial stages of deformation along the Central Metasedimentary Belt Boundary Zone (U-Pb zircon age from a pegmatite; McEachern and van Breemen 1993). Hanmer and McEachern (1992) and McEachern and van Breemen (1993) proposed that the initial stages of deformation of the CMBBZ were caused by the collision between the Elzevir terrane and Laurentia as the marginal basin between the two was closed. The deposition of the Flinton Group, which was derived from the plutons in the Frontenac Terrane (Sager-Kinsman and Parrish 1993); and the emplacement of A-type monzonite, syenite and granites in the Frontenac Terrane (Davidson 1995) was also associated with this collision.

The collision resulted in the development of an overthickened crust in the interior of the Grenville Province and allowed the metamorphic conditions within the Mont Laurier Region to reach as high as 950°C and 105 MPa (Chapter 5). The overthickening of the Grenville crust led to orogenic collapse, and following peak metamorphic conditions,

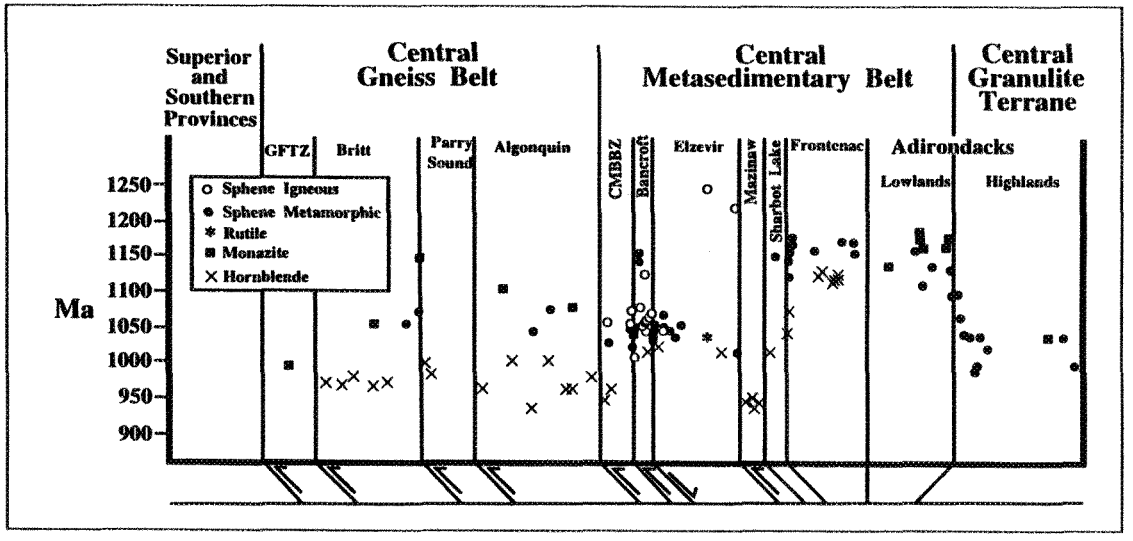

FIGURE 6-XII: Distribution of mineral ages versus distance from shear zones. A cross-section from NW to SE through the Grenville Province of Ontario and the Adirondacks is represented by the horizontal axis. The 40Ar/39Ar hornblende ages from Culshaw et al. (1991) and Cosca et al. (1991, 1992). The U-Pb ages from Mezger et al. (1993).

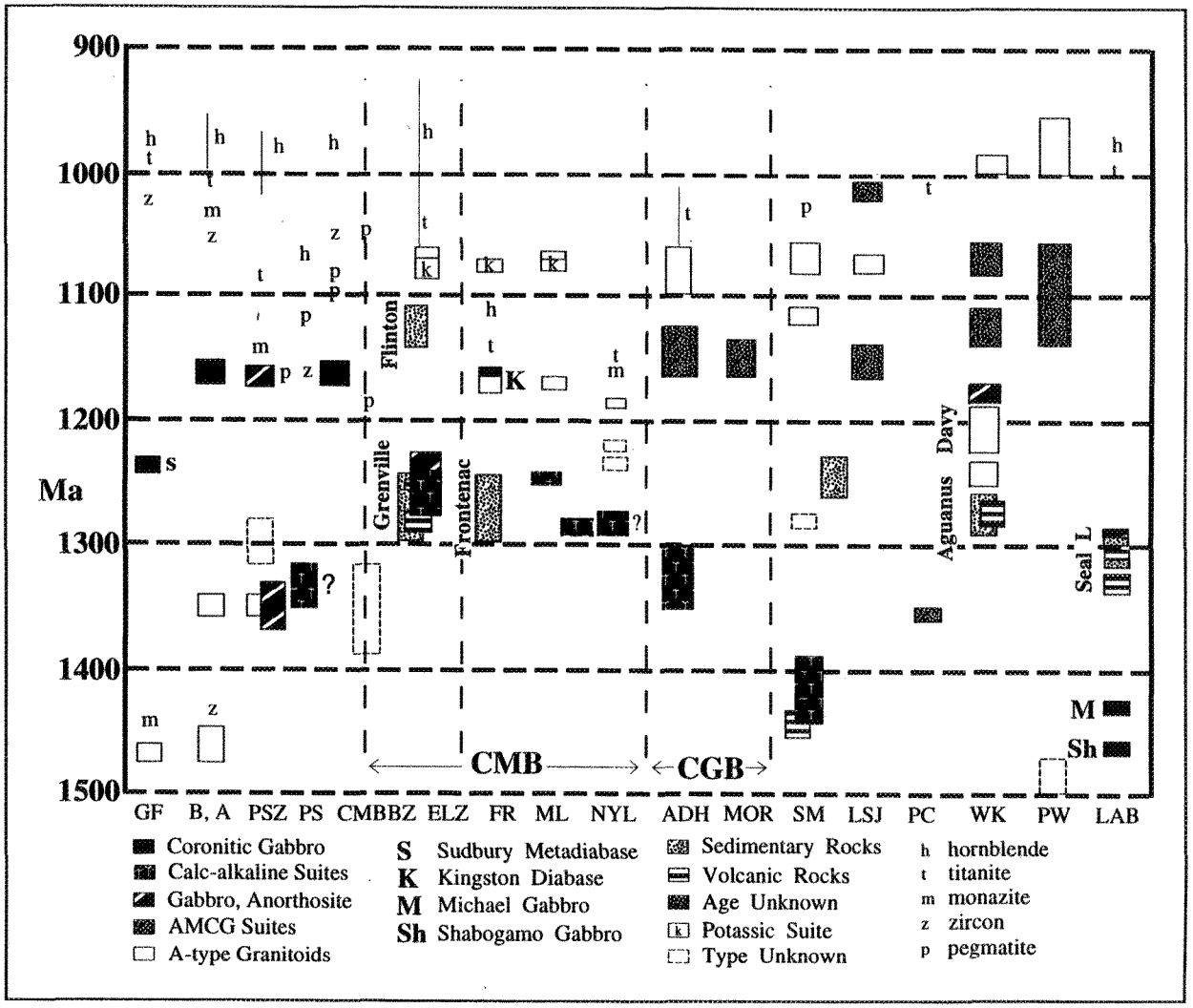

Figure 6-XIII: Distribution of post-1.5 Ga plutonic rocks within Grenville Province. The columns are oriented from southwest to northeast, abbreviations are in Annex C. Metamorphic ages (z, m) and cooling ages (t, h) are U-Pb ages, except hornblende which is 40Ar/39Ar. Syn-deformation pegmatite zircons are shown by 'p' (after Davidson 1995).

extension occurred in the NCDZ, accompanied by isothermal decompression in the BGC. Structural evidence of extension, following the original compressional event, have been observed in the Britt Domain, CGB (Culshaw et al. 1994); in the Bancroft Domain, CMB (van der Pluijm and Carlson 1989; Carlson et al. 1990); and in the Otter Lake Region, CMB (Madore and Sawyer 1991).

6.9c Closure Temperature for Zircon

The ≥1186 ± 4 Ma U-Pb zircon age appears to be geologically significant due to the 1190 Ma age for displacement along the CMBBZ, and similar ages for deposition of the Flinton Group sediments eroded from the Frontenac Terrane plutons. Thus, as proposed above, this date is likely close to peak metamorphic temperatures. Peak metamorphic temperatures in the Mont Laurier Region were measured at 950°C. Mezger (1990) proposed that the closure temperature for zircons is >900°C. Here, due to the link with peak metamorphic temperatures, it is proposed that the closure temperature was ≥950°C.

Chapter 7

SUMMARY AND CONCLUSIONS

7.1 Purpose and Outline

This chapter summarises the results, observations, data, and importance of this study. The local geology is examined first, with a comparison between the Nominingue-Chénéville Deformation Zone and the Bondy Gneiss Complex. The P-T-t trajectories and a lithotectonic model for the field area are then presented.

The characteristics of the local geology are then compared with the rest of the Grenville Province and the Grenville Orogeny. Finally, the tectonics from the field area of the Central Metasedimentary Belt are compared with those of the Kohistan Arc in the Himalayas. To facilitate such a comparison, the general characteristics of the Kohistan Arc are first introduced. The characteristics of these granulites are then compared with the proposed "general granulite" of Bohlen (1987).

7.2 Regional Significance

The Bondy Gneiss Complex dominates the central portion of the field area. The north-south oriented Nominingue-Chénéville Deformation Zone cuts through the eastern third of the field area. Figure 7-1 outlines the local tectonic history in cartoon form. The BGC and the NCDZ reached peak metamorphic conditions of 950°C at 105 MPa together at ~1186 Ma following the initial stages of collision between the Elzevir Terrane and Laurentia. During this event, the Central Metasedimentary Belt was thrust northwestwards over the Central Gneiss Belt along the Central Metasedimentary Belt Boundary Zone (Corriveau et al. in press; Sharma et al. 1993a; 1993b; 1994; 1995). Sediments from the erosion of the

Stage I: Pre 1186 Ma, Collision between Laurentia and Elzevir

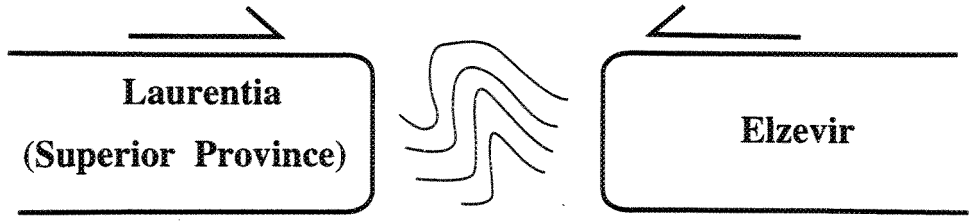

Stage II: Circa 1186 Ma, overthickened crust develops as series of nappes thrust over one another towards the north-northwest. This overthickened crust provides the conditions necessary to develop 950°C and 105 MPa peak metamorphic conditions in the study area. Behind the orogenic front, extensional shears develop as the nappe stack build-up becomes too much for the rheological conditions to support.

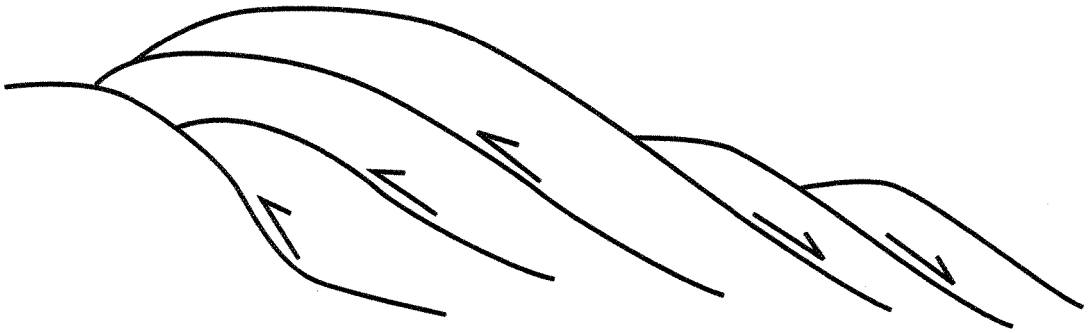

Stage III: Bondy Gneiss Complex thrust upwards with respect to the NCDZ. Extension (>1167 to 1156 Ma) along with the emplacement of monzonite-diorite complexes (1167 to 1164 Ma) occurs along the NCDZ

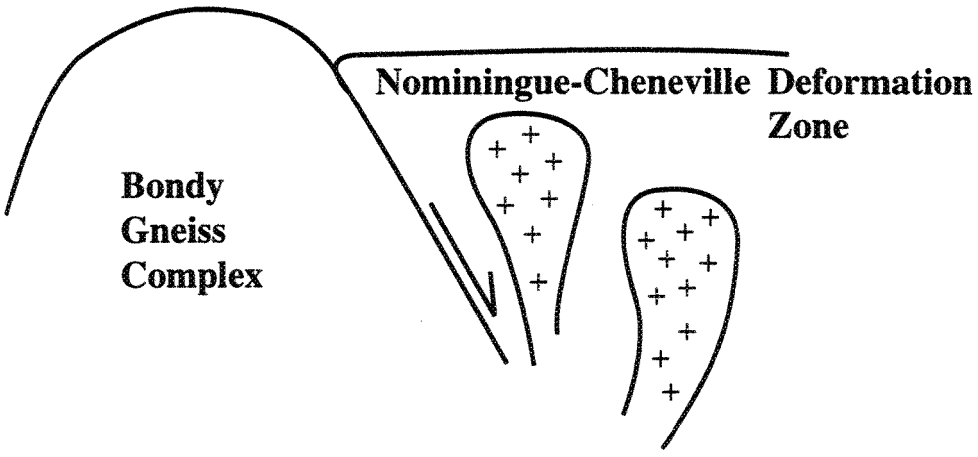

Figure 7-I: Model to explain the development of the metamorphic characteristics in the Mont Laurier Region of the CMB in Quebec. Deformation and plutonic dates from van Breemen and Corriveau (1995); Corriveau et al. (in press).

Frontenac plutons were deposited as the Flinton Group (Sager-Kinsman and Parrish 1993). Davidson (1995) proposed that this period represented an episode of crustal thickening by the emplacement of large gabbro-anorthosite massifs of mantle origin accompanied by high-grade metamorphism, and low-angle, thrust-sense ductile deformation directed to the north-northwest. Crustal thickening would be necessary in the Mont Laurier Region, in order to obtain the conditions necessary to create the very high metamorphic temperatures of 950°C (Harley and Hensen 1990).

The BGC was thrust upwards with respect to the NCDZ, initiating an episode of isothermic decompression from ~105 MPa at 950°C down to 85 MPa at 950°C, accompanied with extension in the NCDZ. Evidence for episodes of extension have been observed throughout much of the Grenville Province from the Britt Domain of the CGB (Culshaw et al. 1994), the Bancroft Shear Zone of the CMB (Carlson et al. 1990) to the Otter Lake Region of the Mont Laurier 'Area' (Madore and Sawyer 1991). Most of these extensional periods are younger than the one in this field area. However, Madore and Sawyer (1991) observed evidence for extension from peak metamorphism through much of the history of the Otter Lake region.

Harley and Hensen (1990) mentioned that rapid exhumation, with 1-2 mm per year uplift rates, of an overthickened crust is one model that would produce an isothermic decompression. This seems likely in the Mont Laurier Region as the isothermic decompression uplift rates were between 0.6 and 2.3 mm per year, which includes the range proposed by Harley and Hensen (1990).

As the BGC cooled, it behaved as a rigid body which focused deformation into the NCDZ. Elongate monzonite-diorite complexes were emplaced into the NCDZ while it was active (1165-1155 Ma; Corriveau et al. 1994; 1995). This episode of plutonism affected the

cooling pattern of the NCDZ, by slowing down the cooling rates with respect to the BGC. Below 600°C, both the NCDZ and the BGC cooled slowly, with cooling rates <10°C/Ma.

This plutonism synchronous with deformation correlates with many other tectonic activities throughout the Grenville. Deformation along the Carthage-Colton Mylonite Zone occurred at 1160 Ma (McLelland et al. 1988). Shortening occurred along the cryptic thrusts proposed by Hildebrand and Easton (1995) in the Frontenac terrane. The AMCG suite of anorthosites and granites intruded between 1160 and 1101 Ma into much of the central and eastern portions of the Grenville Province. Metamorphism in the Parry Sound Domain of the CGB was dated at between 1160 and 1120 Ma (Jamieson et al. 1992), corresponding to movement of the Parry Sound Domain over the Britt Domain (U-Pb zircon age from pegmatite; van Breemen et al. 1986).

7.3 Retrograde Cation Exchange

Using numerical modelling, Florence and Spear (1991) examined P-T calculations, on burial/uplift trajectories that reached peak temperatures of 585 to 635°C, and noted that where diffusion modified the garnet compositional profiles, there was modest to appreciable curvature in the inferred P-T paths. The actual peak temperature conditions, garnet crystal size and the heating/cooling rate affect the magnitude of these distortions caused by volume diffusion. In this study, the peak temperature is high (950°C), and the cooling rate slow (<10°C/Ma below 600°C) and lasted for an extended period of time (45 Ma). This would imply that the effects of volume diffusion in this region would be significant.

The garnet compositional profiles (Chapter 4) and the graphs of calculated temperatures versus garnet size (Chapter 5) demonstrate the influence of retrograde volume diffusion on the garnets. Only the largest garnets with inclusion-free cores preserve the actual peak temperatures suggested by the mineral assemblages and textures (Chapter 3). In this study, garnets under 3.5 mm^2 in size were compositionally homogenised. If only these

garnets were to be considered for geothermometers, the peak temperatures would have been underestimated by up to 550°C!

Resetting by these high-peak metamorphic temperatures created many difficulties with the construction of the P-T trajectories. The garnet zoning profiles no longer preserved geologically meaningful data, other than in the cores of the largest inclusion-free garnets. Much of the prograde information for the P-T trajectories was destroyed by these high temperatures. Therefore, great care must be exercised when building P-T trajectories in high-grade terranes as shown previously by Frost and Chacko (1989), Harley (1989), Spear (1991; 1992), Spear and Florence (1992), and Holdaway and Mukhopadhyay (1993)

7.4 The Grenville Orogen

A continental plate reconstruction at ~0.8 Ga (Figure 2-VI) places portions of Antarctica, Madagascar, eastern India and Australia as continuations of the Grenville Province of the Canadian Shield. This includes Dronning Maud Land, Antarctica; Eastern Ghats granulite belt, India; the Albany-Fraser Belt and the Musgrave Block of Australia (Dalziel 1991; Hoffman 1991; Moores 1991; Young 1992; Davidson 1995).

7.4ai Araku, Eastern Ghats, India

The Eastern Ghats granulite belt of eastern India (Figure 2-VI), consists of several types of para- and orthogneisses intruded by alkaline and anorthosite rocks (Naqvi and Rogers 1987). In the Araku region, the principle rock types are leptynite (garnet-quartz-perthite-plagioclase gneiss), calc-granulite (scapolite-wollastonite-garnet-clinopyroxene-calcite gneiss), mafic-granulite (orthopyroxene-clinopyroxene-plagioclase-quartz gneiss), orthopyroxene granulite (orthopyroxene-plagioclase-perthite-quartz-garnet gneiss), and khandalite (garnet-quartz-perthite-sillimanite gneiss; Dasgupta et al. 1990). The Mont Laurier Region contains assemblages similar to the leptynite, orthopyroxene granulite and khandalite (Chapter 3).

The orthopyroxene granulite and the leptynite contain spinel-bearing lenses with two distinct mineral assemblages:

i) spinel-garnet-quartz-sillimanite-perthite-biotite-magnetite-ilmenite,

ii) spinel-quartz-cordierite-orthopyroxene-sillimanite-perthite-biotite (Sengupta et al. 1991a). The first assemblage resembles one described by Stüwe and Powell (1989) from Larsemann Hills, East Antarctica. Ellis (1980) and Harley (1985) described an assemblage similar to the second from East Antarctica.

The spinel-bearing assemblage from the Mont Laurier Region of the CMB, is similar to the first one described by Sengupta et al. (1991a). In both, spinel is rimmed by sillimanite and garnet, but is not in contact with quartz (Chapter 3, Sengupta et al. 1991a). The chemical analyses of gahnite-spinel-hercynite contents are also similar between the two regions (Chapter 4, Figure 4-VI).

Both the Mont Laurier Region, and the Eastern Ghats have peak metamorphic temperatures of 950°C (Chapter 5, Sengupta et al. 1991a). However, the Mont Laurier Region, has peak pressures up to 105 MPa (Chapter 5), whereas the peak pressures for the Eastern Ghats are only 85 MPa (Sengupta et al. 1991a).

7.4aii Highland Series, Sri Lanka

Sri Lanka is an island located to the south-east of India (Figure 2-VI). The granulitic facies Highland Series occurs in the central part of the island. It is composed of metasediments (marbles, calc-silicates, metapelites and quartzites) and granitic to basic meta-igneous rocks (Schümacher et al. 1990). High-grade metamorphism there occurred at 1100 Ma (ion microprobe on single zircons from a quartzite and a garnet-biotite gneiss from the northern Highland Series and a garnet-biotite gneiss from the southwestern Highland Series), with later events occurring between 1000 and 500 Ma (Kröner et al. 1987a; 1987b).

Analyses of garnet porphyroblasts in pyroxene granulites resulted in pressures between 73 and 90 MPa (orthopyroxene-garnet-plagioclase-quartz) from the central and south-east parts of the Highland Series with a continuous decrease in pressure to approximately 35 MPa towards the west. The calculated temperatures for these areas show a similar distribution, with 760 to 840°C (orthopyroxene-garnet) in the central and south-east portions of the Highland Series, and a decrease to about 600°C towards the west (Schümacher et al. 1990). Temperatures up to 760 - 900°C were obtained from the porphyroblasts of garnet and clinopyroxene. These temperatures are almost as high as the peak metamorphic temperatures of 950°C calculated for the Mont Laurier Region (Chapter 5). However, the retrograde paths are very different between the Mont Laurier Region (initially isothermal decompression; Chapter 5) and the Highland Series (initially almost isobaric cooling; Schümacher et al. 1990).

7.4b Dronning Maud Land, Antarctica

Dronning Maud Land is located at approximately 3°E, 71°S on the East Antarctic Shield (Figure 2-VI). The Jutulstraument-Pencksøkket Rift Zone, a major large-scale structural feature, splits the western Proterozoic Platform from the eastern Fimbulheimen, a younger east-west trending linear mountain belt. Igneous and high-grade metamorphic rocks of the middle to deep continental crust are exposed in the Fimbulheimen (Bucher-Nurminen and Ohta 1993).

Two metamorphic events affected these rocks, the first reached granulitic conditions (90 to 110 MPa, 850°C), the second re-equilibrated the rocks to 60 to 70 MPa and 650°C. Rb-Sr whole-rock ages of 1173 to 1050 Ma from Sverdrupfjella (Wolmarans and Kent 1982) were correlated with the granulitic facies event (Bucher-Nurminen and Ohta 1993). The same sequence of metamorphic events, with an upper amphibolite facies assemblage overprinting an earlier granulite facies assemblage, was reported from the Sør-Rondanefjella

(Shiraishi et al. 1991) and the Wohlthatmassivet (Sengupta 1991b) to the east of the Gjelsvikfjella and Mühlig-Hofmannfjella. The Nominingue-Chénéville Deformation Zone demonstrates this same sequence of events, with the peak condition granulite facies minerals being overprinted by the effects of the (1167-1164 Ma) syntectonic emplacement of the monzonite-diorite complexes (van Breemen and Corriveau 1995; Corriveau et al., in press).

Peak metamorphic temperatures within the Mont Laurier Region occurred at ≥1186 Ma (Chapter 6), quite close in time to the 1173-1050 Ma Rb-Sr whole-rock ages suggested for the granulite facies conditions within Dronning Maud Land (Bucher-Nurminen and Ohta 1993). The retrograde portion of the proposed P-T trajectories for the Mont Laurier Region (Chapters 4, 5) are similar to the proposed P-T trajectory of Bucher-Nurminen and Ohta (1993) for Dronning Maud Land. The analysed spinel-gahnite-hercynite content of the spinels are also very similar between the Mont Laurier Region (Chapter 4), and Dronning Maud Land (Figure 4-VI).

7.4c Musgrave Block, Australia

The association and nature of metamorphism and magmatism during the Grenvillian time span, imposed on pre-Grenvillian, Proterozoic crystalline crust (mafic and felsic gneisses) comprise the main similarities between the Musgrave Block and the Grenville Province. In this sense, the Musgrave Block correlates with the Central Belt of the Grenville Province (Davidson 1995). The Giles Complex, a mantle-derived anorthosite and gabbro, was emplaced into the mid-crust during a short pulse of plutonism at ~1.08 Ga, corresponding to relatively low pressure metamorphism (Clarke et al. 1993). The Tollu volcanics, A-type and mafic volcanic rocks, may have been contemporaneous with the Giles Complex (Sun and Sheraton 1992; Sun et al. 1995).

Granitoid rocks, of a similar age, are present in the southeastern part of the Grenville Province, however, there is no coeval volcanism or sedimentation preserved. This was a

time of high-grade metamorphism and ductile deformation throughout much of the Grenville (Davidson 1995), but not in the CMB (Corriveau 1990). In the Mont Laurier Region of Quebec, there is a coeval episode of potassic plutonism, the 1090-1075 Ma Kensington-Skootamata K-rich alkaline suite, and the 1.08 Ga Rivard Breccia (Corriveau 1990; Corriveau et al. 1995; Corriveau and Gorton 1993).

7.4d Madagascar

Precambrian terrains occupy two thirds of Madagascar. It has been suggested (Caen-Vachette 1979) that the Bongolava-Ranotsara lineament separates two chronologically distinct domains. Granulite facies rocks outcrop over the majority of southern Madagascar. North of the Bongolava-Ranotsara lineament, up to 800 km long N-S oriented granulite belts are coincident with mafic-ultramafic belts. Three episodes of metamorphism have been identified, 2.6 Ga (whole-rock Rb-Sr isochron, Vachette and Hottin 1970) fusion of older continental crust, a Kibaran episode poorly defined at 1103 + 31 Ma (errorchron, Vachette and Hottin 1975), and the Pan-African megacycle at 500 to 740 Ma (Rb-Sr model ages on mostly biotite, Delbos 1965; Vachette and Hottin 1974; 1975).

The magmatic Andriamena and Maevatanana formations form two short belts to the north of the Bongolava-Ranotsara lineament that were emplaced under upper amphibolite to intermediate granulite grade conditions (T = 650 °C, P = 55 MPa; Nicollet 1990). Orthopyroxene-sillimanite granulites, orthoamphibole-cordierite granulites and ironstones could represent ancient hydrothermally altered volcanics (Spear and Schümacher 1982), or they could be residues after a high degree of partial fusion (40 to 50% melting; Nicollet 1990). The garnet-orthopyroxene thermometer of Harley and Green (1982) provides temperatures of approximately 1000°C at 60 MPa (similar to the 950°C of the Mont Laurier Region; Nicollet 1988). The assemblages orthopyroxene-sillimanite and orthoamphibole-cordierite are not present in the Mont Laurier Region, however, the protolith for the bronzite-

cordierite-kornerupine gneiss of the Bondy Gneiss Complex, which may be equivalent, is proposed to be the result of hydrothermal alteration of volcanic rocks (Corriveau et al. 1995).

7.5 The Himalayas

The Grenville Province is thought to be the root of an ancient mountain chain with possible tectonic similarities with the Mesozoic-Cenozoic Himalayas (Dewey and Burke 1973; Baer 1976; Davidson et al. 1982; Windley 1986; Hanmer 1988; van der Pluijm and Carlson 1989). The Central Metasedimentary Belt of the Grenville, and the Kohistan Belt of the Himalayas, are both considered to be island-arc successions (Tahirkheli and Jan 1979; Bard et al. 1980; Bard 1983; Coward et al. 1986) with Andean-type batholiths. Zones of lineated refoliated porphyroclastic gneisses and major thrust stacks, border both arc-batholith belts (Windley 1986). The northwestwards thrusting within the Central Gneiss Belt developed due to post-collisional deformation of the CGB margin during the continued northwestward movement of the CMB arc-batholith over the continental CGB. Windley (1986) proposed that the resultant geometry, caused by this continuing deformation of the interior of the Grenville Orogeny, was similar to the internal geometry of the Himalayas (Figures 7-II, 7-III).

7.5a The Kohistan Arc Complex Versus the Central Metasedimentary Belt

The Kohistan terrane represents an intra-oceanic island arc which formed during the Cretaceous due to northward subduction of the Neotethyan lithosphere and became sandwiched between the Indian and Karakoram (Asian) plates (Figure 7-IV). At least 85 Ma ago, the Kohistan Arc collided with the Karakoram plate to the north, and then at ~55 Ma with the Indian plate to the south (Petterson and Windley 1985; Treloar et al. 1988). The Kohistan arc has continued to override the Indian plate since the original collision, which developed a wide range of thrust stacks in the upper levels of the plate while imbricating cover and basement sequences at middle and lower crustal levels (Coward and Butler 1985;

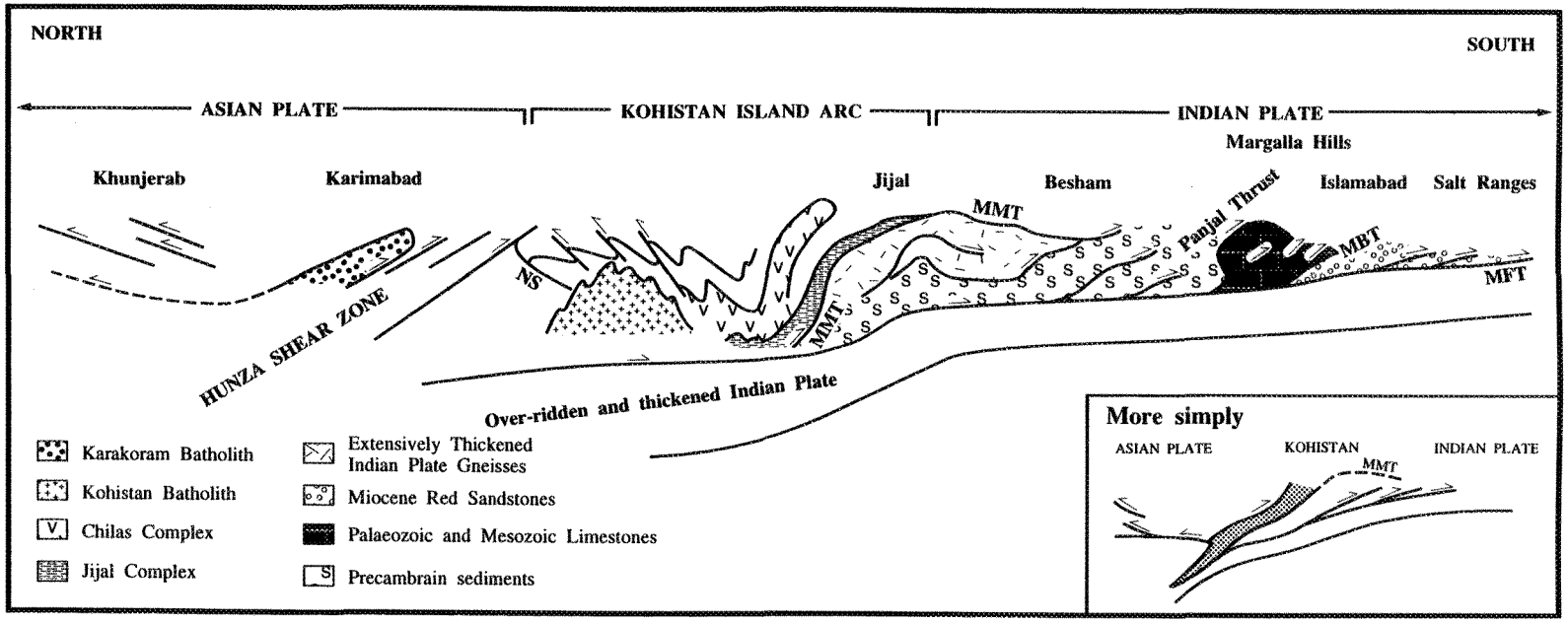

FIGURE 7-II: Schematic cross-section through the Himalayan Orogeny from the Salt Ranges on the Indian Plate to Kunjerab on the Asian Plate (after Treloar et al. 1989d). The general geometry of this cross-section is similar to that of the Grenville (Figure 7-III).

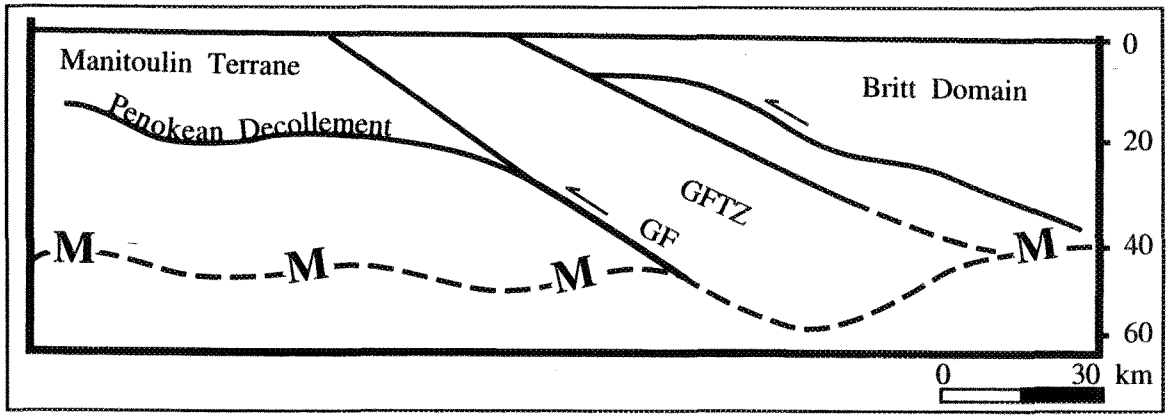

A: GLIMPCE seismic profile (Davidson 1990), across the Grenville Front in Georgian Bay, Ontario (modified after Green et al. 1988; 1989).

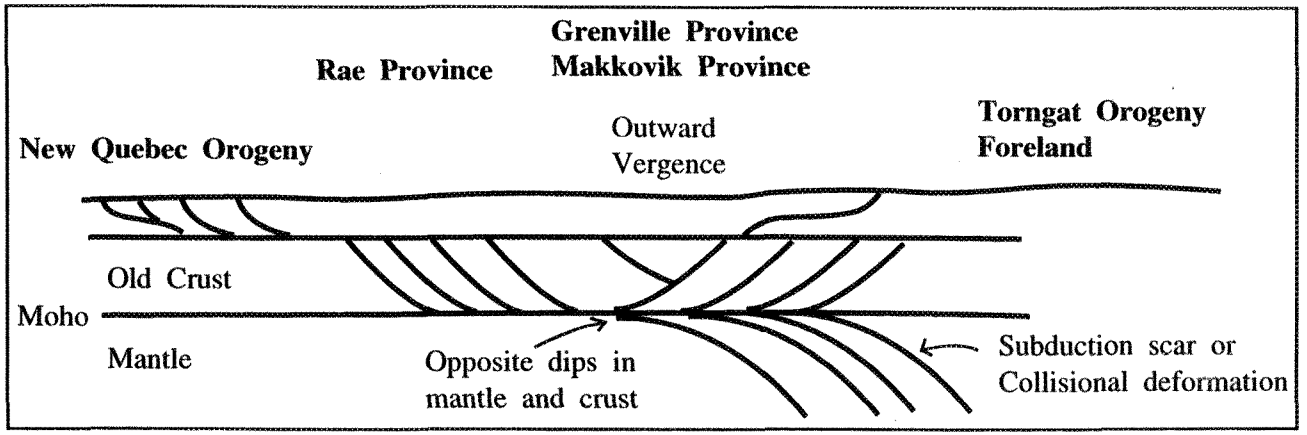

B: ESCOOT seismic profile (after Hall et al. 1995) across the Grenville Province in northern Labrador.

Figure 7-III: Cross-sections across the Grenville Province from seismic profiles. "A" demonstrates the northwest transport of the Grenville province over the neighbouring provinces. "B" demonstrates the converging tectonics experienced in the Grenville Province. This general geometry is similar to that of the Himalayas (Figure 7-II).

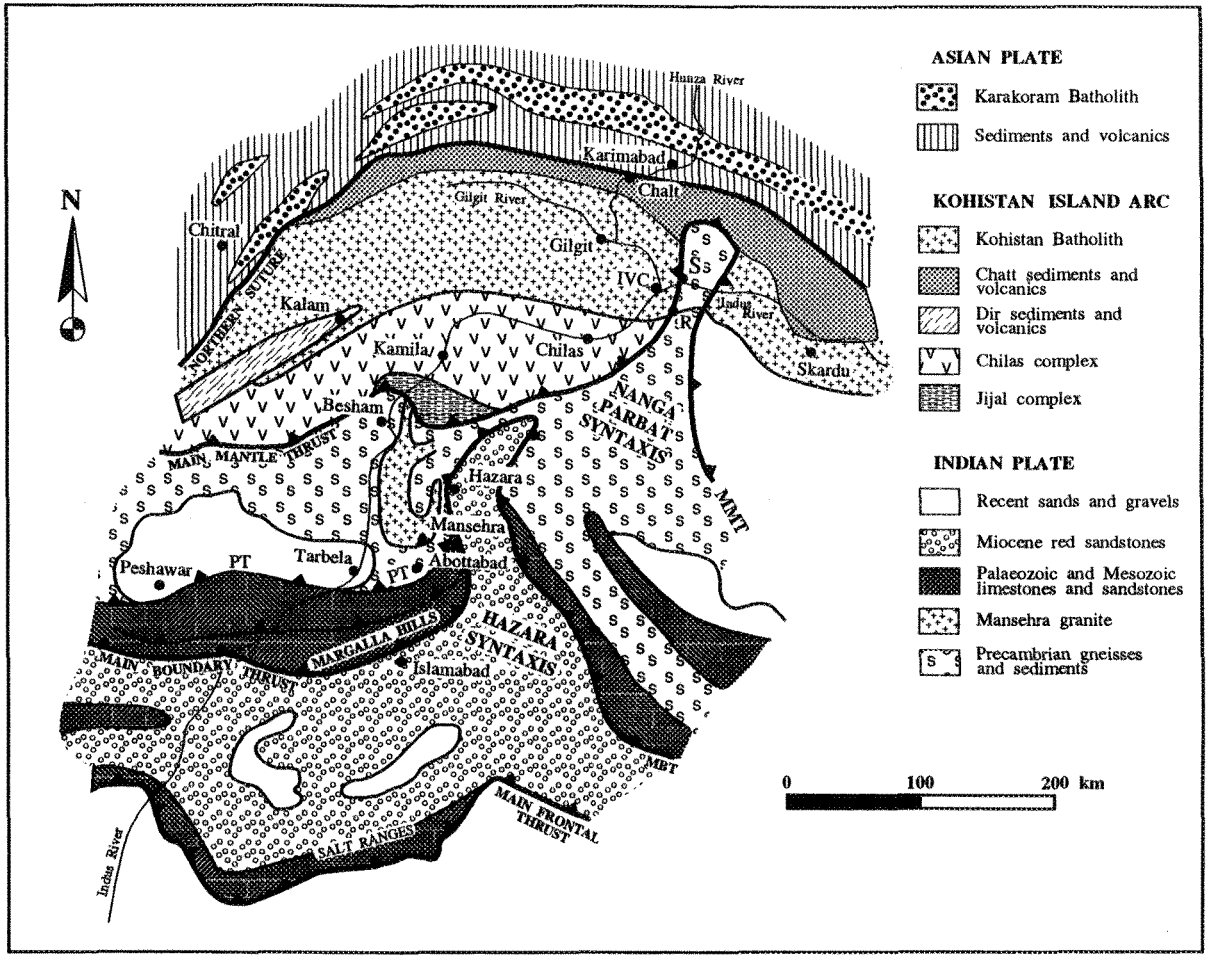

FIGURE 7-IV: Geological map of Himalayas (North Pakistan) showing the location of the Kohistan Island Arc, with its separation from the Indian Plate to the south by the Main Mantle Thrust, and from the Asian Plate to the north by the Northern Suture. The MMT bends northward around the Nanga Parbat syntaxis. R = Raikot, and S = Sassie, between which is the Raikot-Sassi fault zone. IVC = Indus-Valley Confluence; PT = Panjal Thrust (after Treloar et al. 1989).

Treloar et al. 1989b). Metamorphism occurred during the early stages of deformation, afterwards the continuing deformation formed a series of crustal-scale nappes. These nappes were internally imbricated during stacking, which caused higher-grade rocks to overlie lower grade rocks (Treloar et al. 1989a; 1989c). The Central Metasedimentary Belt and the Central Gneiss Belt of the Grenville Province are both composed of several domains and terranes, which have been proposed to represent crustal scale nappe structures overriding one another, with a general thrust direction to the N-NW (Davidson et al. 1982; Culshaw et al. 1994; Jamieson et al. 1995). These nappe structures in the Grenville Province are now exposed, possibly analagous to the tectonic structures existing today below the Himalayas.

During the Himalayan collision, the Kohistan Arc was turned on end and tilted to the north; uplift and erosion have since revealed a complete cross-section from the lower to upper crust. The lower crust is represented by the mafic to ultramafic Chilas and Jijal Complexes (Figure 7-IV); calc-alkaline plutons and the southern amphibolite belt constitute the middle crust. The upper crust consists of shallow-level granitic, sedimentary and volcanic rocks which occupy the northern portion of the arc complex. The best sedimentary and volcanic structures are preserved in the north, where the metamorphic grade is the lowest (Jan and Karim 1995). Due to the complexities of the Grenville Province structures and high-grade metamorphic events, it is impossible to determine the exact geometry of the Central Metasedimentary Belt with respect to its original orientation. However, the nappe-like geometry of the terranes within the CMB, combined with erosion and uplift, have brought various crustal levels to the surface (Indares and Martignole 1990a).

In the central portion of the Himalayas, India and Nepal, the junction of the main Asian and Indian plates is the relatively simple Indus Suture (Gansser 1980). In northern Pakistan, the Kohistan complex divides the two plates, bounded to the south by the 'Southern Suture' or 'Main Mantle Thrust', and bounded to the north by the 'Northern

suture' or 'Main Karakorum thrust' (Bard et al. 1980; Coward et al. 1982). The Northern Suture has been described as a tectonic melange, consisting of imbricated lenses of Kohistan sediments and volcanics mixed with mafic to ultramafic rocks of unknown origin and conglomerates and turbiditic sandstones of the adjacent Asian plate (Coward et al. 1986). No true ophiolitic sequences or high-pressure metamorphic rocks have been observed. The ocean represented by this suture zone may only have been a minor back-arc basin to the Kohistan arc (Coward et al. 1987).

The initial collision of the Elzevir terrane with Laurentia first occurred along the CMBBZ at approximately 1190 Ma (McEachern and van Breemen 1993). The geometry along this boundary is not as complex as the 'Northern Suture' of the Kohistan Arc. In Ontario, the CMBBZ is a relatively simple linear structure, however, in Quebec, further north towards the Cabonga Reservoir Terrane, the CMBBZ/Cayamant Shear Zone does become more complex (Figure 2-X; Sharma et al. 1993a; 1993b; 1994).

The Kohistan arc moved, not by simple collision in the Yasin-Skardu section, but by sinistral strike-slip movement against the Asian plate in the west. The frontal and lateral ramp portions of thrust profiles are analogous to the relationship represented within the Northern Suture. Over 2000 km of shortening occurred north of the Northern Suture since the initial collision. Northern Kohistan, Hindu Kush and the Pamirs must have absorbed much of this shortening by strike-slip and/or thrust fault tectonics (Coward et al. 1987).

Zircon and apatite U-Pb ages and $^{40}Ar/^{39}Ar$ biotite ages decrease towards the east in the northern Kohistan Arc. This pattern was proposed by Treloar et al. (1989b) to have resulted from increased amounts of recent uplift and unroofing toward the Nanga Parbat syntaxis. Approximate cooling rates from 500°C down through 300°C range from 6.5 to 4.9°C/Ma (calculated from Treloar et al. 1989b data). The rate of uplift near the syntaxis has increased over the last 20 Ma to about 5.5 mm a year. Coward et al. (1987) suggested that

the Nanga Parbat and Hazara syntaxes developed due to the interference of thrust transport directions between the western Himalayan and the Kohistan systems.

The calculated cooling rates and uplift rates from the Mont Laurier Region are lower than those of the Himalayas. Most ancient mountain belts experienced slower cooling rates, and uplift rates than the more recent younger mountain belts such as the Himalayas. The form of the CMBBZ around the Cabonga Reservoir Terrane (Figure 1-V) resembles the general form of the two syntaxes of the Kohistan Arc Complex (Figure 7-IV).

Much of central and northern Kohistan is formed by the Kohistan batholith (Coward et al. 1986), large granite, tonalite and diorite intrusives, which contain large xenoliths of foliated volcanics. The rocks of the Kohistan arc are largely composed of two groups, an early phase of mafic to intermediate magmatism which produced the volcanics and volcanoclastic sediments and a later phase of more acid calc-alkaline intrusives (Coward et al. 1987).

Whether or not the Central Metasedimentary Belt is an island arc has been the subject of much debate (see McEachern and van Breemen 1993; Corriveau 1990). This subject is still undetermined. It was not one of the original objectives of this study to determine whether or not this study area is part of an island arc. The proposed presence of volcanics which were later altered hydrothermally (Corriveau et al. 1995) and then metamorphosed could be indicative of an island arc origin. However, with both the hydrothermal alteration and subsequent granulite facies metamorphism, it would be difficult to determine the origin of these proposed volcanics.

7.6 The General Granulite?

Observations in classic high-grade terranes such as southern India (Newton et al. 1980b, Hansen et al. 1984) and the Adirondacks (Bohlen 1987) have recently been used to seek and identify somewhat generalised unified models (Harley and Hensen 1990). Some

studies have emphasised a perceived uniformity in granulite P-T-t trajectories and P-T conditions (Newton and Perkins 1982; Bohlen 1987), creating models in terms of one particular tectonic setting such as a magmatic arc. However, diversity, particularly of P-T conditions and P-T-t path configurations, but also of tectonic settings, lithologies and age structures, was emphasised by Harley (1989) as an important feature of granulite terranes.

The characteristics of a large number of granulites are contained in Figure 7-V (Harley 1989). Bohlen's (1987) general P-T conditions of 75 ± 10 MPa and 800 ± 50°C includes almost 50% of the worldwide granulites, however, many occurrences (i.e. Mont Laurier Region) do not fit into this box. There are significant low pressure granulite terranes (≤50 MPa), possibly associated with magmatism, and high pressure granulite terranes (≥90 MPa, i.e. Mont Laurier Region), which overlap with the P-T conditions determined for crustal xenoliths from basaltic volcanics (Griffin and O'Reilly 1986). There is also a third group of granulites that do not fit in the "box" of Bohlen (1987), very high temperature (VHT) granulites with peak temperatures as high as 900 to 1000°C (i.e. Mont Laurier Region; Harley and Hensen 1990).

Granulite P-T-t trajectories also exhibit a wide variety of morphologies, which can define the type of magmatic or tectonic settings under which the metamorphism occurred (England and Thompson 1986; Bohlen 1987; Ellis 1987; Sandiford and Powell 1986a; 1986b; Harley 1989). One end-member is the isothermal decompression (ITD, i.e. Mont Laurier Region) which suggests that peak metamorphism occurred due to an overthickened crust. An overthickened crust was suggested by Indares and Martignole (1990a) in their transect across the Central Metasedimentary Belt. Such a thickened crust is one explanation for the VHT conditions in this study of the Mont Laurier Region. An overthickened crust is also accepted for the Himalayas (Figure 7-III). Decompression intervals of 20 to 40 MPa are

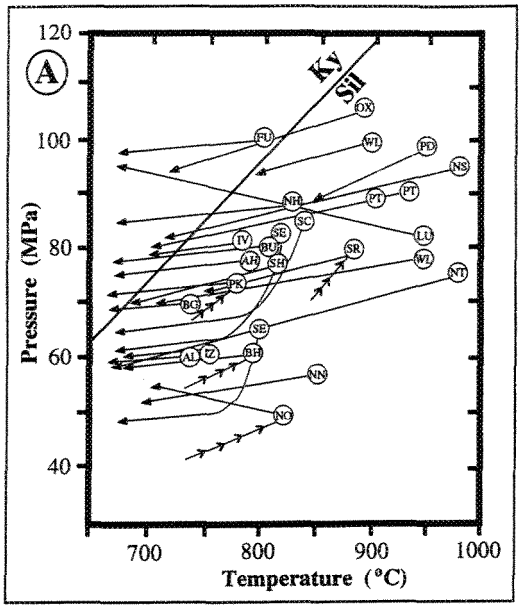

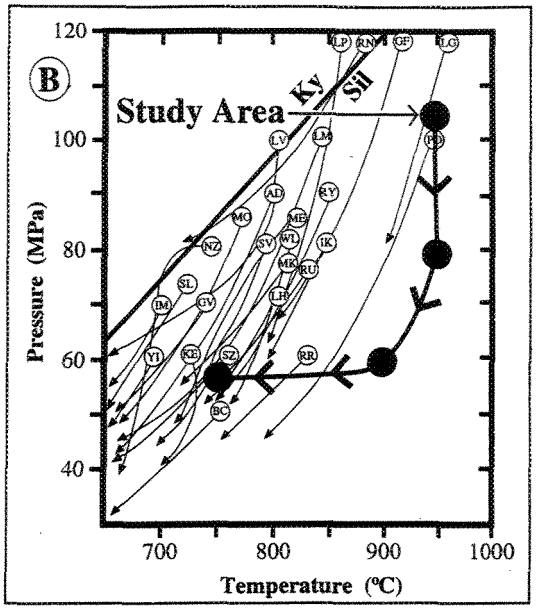

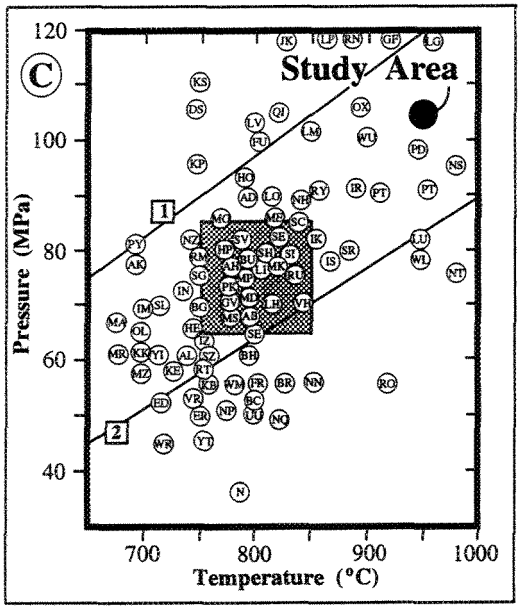

FIGURE 7-V: Peak metamorphic conditions, and the corresponding P-T trajectories for several granulites. "A" contains examples of isobaric cooling, "B" examples of isothermic decompression, and "C" the peak metamorphic conditions. For simplicity, typical pressure uncertainties of ± 0.5 to 10 MPa, and typical temperature uncertainties of ± 30 to 60°C are not shown. Abbreviations are explained in Annex C. The P-T trajectory from this study initially ressembles the cases in "B". The peak metamorphic conditions place this study in the very high temperature, medium pressure granulites, well outside of the 'best-fit' average granulite box of Bohlen (1987) in "C" (after Harley 1989).

usually preserved during ITD-type conditions (i.e., Mont Laurier Region, Harley and Hensen 1990).

The second extreme is isobaric cooling (IBC), which indicates that peak conditions were achieved in crust of almost 'normal' thickness (e.g., Ellis 1980; Bohlen 1987). IBC conditions typically involve a decrease in pressure (5-20 MPa) with low dP/dt gradients of 3 to 5 MPa per 100°C.

A combination of extreme initial temperatures, basal heat flux and crustal heat productivity are required in order to generate high temperature decompression paths (e.g., Mont Laurier Region) when considering simple collision models where erosion terminates crustal heating (Harley 1988; 1989; Stüwe and Powell 1989). These ITD paths could be generated with moderately rapid (1-2 mm/year) uplift rates (i.e., Mont Laurier Region), and exposure of overthickened crust in a collisional-extensional model (Harley 1989) where rapid exhumation and magmatic accretion during late-collision may be important (Harley and Hensen 1990). This second model requires a rather short timescale (<20 Ma) in comparison with the simple collisional models (20 - 60 Ma). Such a model involving collision-extension is proposed for this study of the Mont Laurier Region where peak metamorphic temperatures occurred at ~1186 Ma, extension was finished by 1164 Ma (van Breemen and Corriveau 1995), and the uplift rates were only as high as 2.3 mm/year.

7.7 Return to the Grenville, Concluding Remarks

As demonstrated by Harley (1989), it is unrealistic to propose one model or one set of metamorphic conditions from one granulite terrane to a worldwide model. In fact, if the "general granulite box" were considered, the granulites from this study would not be included. However, as proposed by Hoffman (1991), Moores (1991), Davidson (1995), portions of Antarctica, Madagascar, eastern India and Australia were all linked to the Grenville Province at approximately 0.8 Ga (Figure 2-VI). As summarised in this chapter,

there are similarities in P-T conditions, P-T-t trajectories, lithologies, chemistry, chronology and tectonics, between the Mont Laurier Region of the Grenville Province and these other regions. This suggests that during the Grenville Orogeny, very high temperature conditions were achieved, overthickened crust formed, and extension occurred after the original compressional event of the collision. These conditions are not pervasive throughout the entire Grenville Province, however, they are suggested in the studies of Araku, Eastern Ghats, India (Sengupta et al. 1991a), the Highland Series, Sri Lanka (Schümacher et al. 1990), and in Madagascar (Nicollet 1988; 1990).

Many authors have proposed similarities between the tectonics of the Himalayas to that of the Grenville (Dewey and Burke 1973; Baer 1976; Davidson et al. 1982; Windley 1986; Hanmer 1988; van der Pluijm and Carlson 1989). As one of the previous sections demonstrated, there are similarities between the Kohistan Island Arc Complex and the Central Metasedimentary Belt. The overall geometry is very similar. The Kohistan and possibly the CMB are both Island Arc Complexes, sandwiched between two continents in a multiple-stage collision. Both mountain belts produced an overthickened crust that induced isothermal decompression conditions. In conclusion, the general characteristics of the Grenville do resemble the Himalayas.

Therefore, an in depth comprehension of the Himalayas may assist in understanding the processes that existed in the eroded matter above the exposed rocks in today's Grenville. Conversely, a similar understanding of Grenville tectonics may lead to a greater knowledge of the processes occurring today, beneath the surface of the Himalayas.

As this study demonstrated (Chapter 4, 5), retrograde cation exchange is an important factor when studying these high-grade terranes. This process severely affects the geothermobarometers, underestimating temperatures up to 550°C. A new method of retrieving accurate geologically significant temperatures from garnets that have been subjected

to retrograde cation exchange has been used in this study with success (plotting thermometer results versus garnet size for the various samples and lithotectonic units). This method may be applicable to other studies in granulite grade terranes.

Of equal importance is the proposed closure temperature of 950°C for the U-Pb systematics for zircons (Chapter 6). This value may aid in the study of geological processes in these other high-grade terranes.

REFERENCES

Anovitz, L. M. 1991. Al zoning in pyroxene and plagioclase: Window on late prograde to early retrograde P-T paths in granulite terranes. American Mineralogist, **76**: 1328-1343.

----, and Essene, E. J. 1990. Thermobarometry and pressure-temperature paths in the Grenville Province of Ontario. Journal of Petrology, **31:** 197-241.

Arima, M., and Gower, C. F. 1990. Osumilite-bearing granulites in the eastern Grenville Province, eastern Labrador, Canada: Mineral parageneses and metamorphic conditions. Journal of Petrology, **32**: 29-61.

Ashworth, J. R. (ed.), 1985. Migmatites. Blackie, Glasgow and London. 302 pp.

Ayres, L. D., Lumbers, S. B., Milne, V. G., and Robertson, D. W. 1971. Ontario geological map 2197. Scale 1:1,013,760.

Baer, A. J. 1976. The Grenville Province in Helikian times: a possible model of evolution. Royal Society of London Philosophical Transactions, **280**: 499-515.

Baragar, W. R. A. 1977. Volcanism of the stable crust. *In* Volcanic regimes in Canada. *Edited by* W. R. A. Baragar, L. C. Colemen, and J. M. Hall. Geological Association of Canada, Special Paper **16**: 377-405.

Bard, J. P. 1983. Metamorphism of an obducted island arc: example of the Kohistan sequence (Pakistan) in the Himalayan collided range. Earth and Planetary Science Letters, **65**: 133-144.

----, Maluski, H., Matte, Ph., and Proust, F. 1980. The Kohistan sequence: crust and mantle of an obducted island arc. Special Issue Geological Bulletin, University of Peshawar, **13**: 87-93.

Bell, K., and Blenkinsop, J. 1980. Whole rock Rb/Sr studies in the Grenville Province of southeastern Ontario and western Quebec--a summary report. *In* Current Research, Part C. Geological Survey of Canada, Paper 80-1C, 152-154.

Berger, G. W. 1975. $^{40}Ar/^{39}Ar$ step heating of thermally overprinted biotite, hornblende and potassium feldspar from Eldora, Colorado. Earth and Planetary Science Letters, **26**: 387-408.

Berman, R. G. 1990. Mixing properties of Ca-Mg-Fe-Mn garnets. American Mineralogist, **75**: 328-344.

Bhattacharya, A. 1986. Some geobarometers involving cordierite in the FeO-Al_2O_3-SiO_2 (H_2O) system: refinements, thermodynamic calibration, and applicability in granulite facies rocks. Contributions to Mineralogy and Petrology, **94**: 387-394.

----, Krishnakumar, K. R., Raith, M., and Sen, S. K. 1991. An improved set of a-X parameters for Fe-Mg-Ca garnets and refinements of the orthopyroxene-garnet thermometer and the orthopyroxene-garnet-plagioclase-quartz barometer. Journal of Petrology, **32**: 629-656.

----, and Sen, S. K. 1985. Energetics of hydration of cordierite and water barometry in cordierite granulites. Contributions to Mineralogy and Petrology, **89**: 370-378.

Bohlen, S. R. 1987. Pressure-temperature-time paths and a tectonic model for the evolution of granulites. Journal of Geology, **95**: 617-632.

----, Boettcher, A. L., Wall, V. J., and Clemens, J. D. 1983. Stability of phlogopite-quartz and sanidine-quartz: A model for melting in the lower crust. Contributions to Mineralogy and Petrology, **83**: 270-277.

----, and Essene, E. J. 1980. Evaluation of coexisting garnet-biotite, garnet-clinopyroxene, and other Mg-Fe exchange thermometers in Adirondack granulites. Geological Society of America Bulletin, **91**: 685-719.

Boyd, F. R., and England, J. L. 1961. Melting of silicates at high pressures. Carnegie Institution of Washington Year Book, **60**: 113-125.

Brady, J. B., and McCallister, R. H. 1983. Diffusion data for clinopyroxenes from homogenization and self-diffusion experiments. American Mineralogist, **68**: 95-105.

Brock, B. S., and Moore, J. M. 1983. Chronology, chemistry, and tectonics of igneous rocks in terranes of the Grenville Province, Canada. Geological Society of America Abstracts with Programs, **15**: 533.

Brodie, K. H., and Rutter, E. H. 1985. On the relationship between deformation and metamorphism, with special reference to the behaviour of basic rocks. *In* Metamorphic Reactions. Advances in Physical Geochemistry, **4**. *Edited by* A. B. Thompson, and D.C. Rubie. Springer, New York, pp. 138-179.

Brown, M., and Earle, M. M. 1983. Cordierite-bearing schists and gneisses from Timor, eastern Indonesia: P-T conditions of metamorphism and tectonic implications. Journal of Metamorphic Geology, **1**: 183-203.

Bucher-Nurminen, K., and Ohta, Y. 1993. Granulites and garnet-cordierite gneisses from Dronning Maud Land, Antarctica. Journal of Metamorphic Geology, **11**: 691-703.

Caen-Vachette, M. 1979. Le Precambrien de Madagascar. Radiochronometrie par isochrones Rb/Sr sur roches totales. Revues Geologie Dynamique et Geologie physique, **21**: 331-338.

Carlson, K. A., van der Pluijm, B. A., and Hanmer, S. 1990. Marble mylonites of the Bancroft shear zone: evidence for crustal extension in the Canadian Grenville. Geological Society of America Bulletin, **102**: 174-181.

Carswell, D. A., and Harley, S. L. 1990. Mineral thermometry and barometry. *In* Eclogite Facies Rocks. *Edited by* D. A. Carswell. Blackie, Glasgow, pp. 83-110.

Carmichael, D. M., Moore, J. M. Jr., and Skippen, G. B. 1978. Isograds around the Hastings metamorphic "low". *In* Toronto '78 Field Trip Guidebook. *Edited by* A. L. Currie, and W. O. Mackasey. Geological Association of Canada, Waterloo, Ontario, 325-346.

Carrington, D. P., and Harley, S. L. 1995. The stability of osumilite in metapelitic granulites. Journal of Metamorphic Geology, **13**: 613-625.

Chakoumakos, B. C., Murakami, T., Lumpkin, G. R., and Ewing, R. C. 1987. Alpha-decay-induced fracturing in zircon: the transition from the crystalline to the metamict state. Science, **236**: 1556-1559.

Chipera, S. J., and Perkins, D. 1988. Evaluation of biotite-garnet geothermometers: application to the English River subprovince, Ontario. Contributions to Mineralogy and Petrology, **98**: 40-48.

Clarke, G. L. 1988. Structural constraints on the Proterozoic reworking of Archaean crust in the Rayner Complex, MacRobertson and Kemp Land Coast, East Antarctica. Precambrian Research, **40**: 137-156.

----, Stewart, A., and Glikson, A. 1993. High-pressure granulite to eclogite-facies metamorphism in the western Musgrave Block, central Australia. Australian Geological Survey Organisation, Research Newsletter, **18**: 6-7.

Clemens, J. D. 1984. Water contents of silicic to intermediate magmas. Lithos, **17**: 273-287.

---- 1995. Phlogopite stability in the silica-saturated portion of the system $KAlO_2$-MgO-SiO_2-H_2O: New data and a reappraisal of phase relations to 1.5 GPa. American Mineralogist, **80**: 982-997.

----, and Mawer, C. K. 1992. Granitic magma transport by fracture propagation. Tectonophysics, **204**: 339-360.

Cliff, R. A., and Cohen, A. 1980. Uranium-lead isotope systematics in a regionally metamorphosed tonalite from the Eastern Alps. Earth and Planetary Science Letters, **50:** 211-218.

Copeland, P., Parrish, R. R., and Harrison, T. M. 1988. Identification of inherited radiogenic Pb in monazite and its implication for the U-Pb system. Nature, **333**: 700-763.

Corfu, F., and Easton, R. M. 1995. U-Pb geochronology of the Mazinaw terrane, an imbricate segment of the Central Metasedimentary Belt, Grenville Province, Ontario. Canadian Journal of Earth Sciences, **32**: 959-976.

Corriveau, L. 1990. Proterozic subduction and terrane amalgamation in the southwestern Grenville province, Canada: evidence from ultrapotassic to shoshonitic plutonism. Geology, **18:** 614-617.

----, and Gorton, M. P. 1993. Coexisting K-rich alkaline and shoshonitic magmatism of arc affinities in the Proterozoic: a reassessment of syenitic stocks in the southwestern Grenville province. Contributions to Mineralogy and Petrology, **113**: 262-279.

---- and Jourdain, V. 1992. Terrane characterisation in the Central Metasedimentary Belt of the southern Grenville Orogen, Lac Nominingue map area, Quebec. *In* Current Research, Part C. Geological Survey of Canada Paper, **92-1C**: pp. 81-90.

---- and Leblanc, D. 1995. Sequential nesting of magmas in marble, SW Grenville Province, Quebec: from fracture propagation to diapirism. Tectonophysics, **246**: 183-200.

---- Morin, D., and Madore, L. 1994. Géologie et cibles d'exploration de la partie centre est de la ceinture métasédimentaire du Québec, Province de Grenville. *In* Current Research, Part C. Geological Survey of Canada, Paper **94-C**: pp. 355-365.

---- Morin, D., van Breemen, O., Rivard, B., Tremblay, P., Boggs, K. J. E. and Deschenes, G. 1995. Magmatic and hydrothermal activity in the Central Metasedimentary Belt of Quebec; tectonic and metallogenic implications. Friends of Grenville Field trip.

----, van Breemen, O., and Boggs, K. 1996. The Bondy gneiss complex and its cupriferous hydrothermal system: implications for exploration of volcanic-related massive sulphide deposits in the Grenville province, SW Quebec. Geological Association of Canada, Mineralogical Association of Canada, Program and Abstracts, in press.

Cosca, M. A., Essene, E. J., Kunk, M. J., and Sutter, J. F. 1992. Differential unroofing within the Central Metasedimentary Belt of the Grenville Orogen: constraints from $^{40}Ar/^{39}Ar$ thermochronology. Contributions to Mineralogy and Petrology, **110**: 211-225.

---- Essene, E. J., Mezger, K., van der Pluijm, B. A., 1995. Constraints on the duration of tectonic processes: protracted extension and deep-crustal rotation in the Grenville orogen. Geology, **23**: 361-364.

----, Sutter, J. F., and Essene, E. J. 1991. Late metamorphic cooling and inferred uplift/erosion history of the Grenville Orogen, Ontario: Constraints from ^{40}Ar-^{39}Ar thermochronology. Tectonics, **10**: 959-977.

Coward, M. P., and Butler, R. W. H. 1985. Thrust tectonics and the deep structure of Pakistan Himalayas. Geology, **13**: 417-420.

----, Butler, R. W. H., Asif Khan, M., and Knipe, R. J. 1987. The tectonic history of Kohistan and its implications for Himalayan structure. Journal of the Geological Society, London, **144**: 377-391.

----, Jan, M. Q., Rex, D., Tarney, J., Thirlwall, M., and Windley, B. F. 1982. Geotectonic framework of the Himalayas of North Pakistan. Journal of the Geological Society, London, **139**: 299-308.

----, Windley, B. F., Broughton, R., Luff, I. W., Petterson, M., Pudsey, C., Rex, D., and Asif Khan, M. 1986. Collision tectonics in the NW Himalayas. *In* Collision Tectonics. *Edited by* M. P. Coward and A. C. Ries. Special Publication of the Geological Society, London, **19**: 203-219.

Culshaw, N. G., Davidson, A., and Nadeau, L. 1983. Structural subdivisions of the Grenville Province in the Parry Sound-Algonquin region, Ontario. *In* Current Research, Part B. Geological Survey of Canada, Paper **79-1B**: 155-163.

----, Ketchum, J. W. F., Wodicka, N., and Wallace, P. 1994. Deep crustal ductile extension following thrusting in the southwestern Grenville Province, Ontario. Canadian Journal of Earth Sciences, **31**: 160-175.

----, Reynolds, P. H., Check, G. 1991. A ^{40}Ar-^{39}Ar study of post-tectonic cooling in the Britt domain of the Grenville Province, Ontario. Earth and Planetary Science Letters, **105**: 405-415.

Currie, K. L. 1971. The reaction 3 cordierite = 2 garnet + 4 sillimanite + 5 quartz as geological thermometer in the Opinicon Lake region, Ontario. Contributions to Mineralogy and Petrology, **33**: 215-226.

Dahl, P. S. 1980. The thermal-compositional dependence of Fe^{2+} - Mg^{2+} distribution between coexisting garnet and pyroxene: applications to geothermometry. American Mineralogist, **65**: 852-866.

Dallmeyer, R. D., and Rivers, T. 1983. Recognition of extraneous argon components through incremental-release ^{40}Ar-^{39}Ar analysis of biotite and hornblende across the Grenvillian metamorphic gradient in southwestern Labrador. Geochmica et Cosmochimica Acta, **47**: 413-428.

Dalziel, I. W. D. 1991. Pacific margins of Laurentia and East Antarctica-Australia as a conjugate rift pair: Evidence and implications for an Eocambrian supercontinent. Geology, **19**: 598-601.

Dasgupta, S., Sengupta, P., Fukuoka, M., and Bhattacharya, P. K. 1990. Mafic granulites from Eastern Ghats, India: further evidence for extremely high-temperature crustal metamorphism. Journal of Geology, **99**: 124-133.

Davidson, A. 1984. Identification of ductile shear zones in the southwestern Grenville Province of the Canadian shield. *In* Precambrian Tectonics Illustrated. *Edited by* A. Kroner, and R. Greiling. E. Schweizerbart'sche Verlagsbuchhandlung, Stuttgart, pp. 263-279.

---- 1986. New interpretations in the southwestern Grenville Province. *In* The Grenville Province. *Edited by* J.M. Moore, A. Davidson, and A.J. Baer. Geological Association of Canada, Special Paper **31**: pp. 61-74.

---- 1990. Summary of new developments in Grenville Front geology, Ontario. Geological Society of America, Abstracts with Programs, **22**: p. 11.

---- 1995. A review of the Grenville orogen in its North American type area. AGSO Journal of Australian Geology and Geophysics, **16**: 3-24.

----, Culshaw, N. G., and Nadeau, L. 1982. A tectonometamorphic framework for part of the Grenville Province, Parry Sound region, Ontario. Geological Survey of Canada Paper **82-1A**: 175-190.

Davis, D. W., and Barlett, J. R. 1988. Geochronology of the Belmont Lake Metavolcanic Complex and implications for crustal development in the Central Metasedimentary Belt, Grenville Province, Ontario. Canadian Journal of Earth Science, **25**: 1751-1759.

Deer, W. A., Howie, R. A., and Zussman, J. 1966. An Introduction to the Rock-Forming Minerals. Longman Scientific and Technical, New York, 528 pp.

Delbos, L. 1965. Sur l'age de quelques mineralisations de Madagascar. Bull. B.R.G.M., 1, 80-89.

Dewey, J. F., and Burke, K. C. A. 1973. Tibetan, Variscan and Precambriam basement reactivation: products of continental collision. Journal of Geology, **81**: 683-692.

Dietvorst, E. J. L. 1980. Biotite breakdown and the formation of gahnite in metapelitic rocks from Kemiö, Southwest Finland. Contributions to Mineralogy and Petrology, **75**: 327-337.

Dimroth, E. 1966. Deformation in the Grenville Province between Gatineau and Petite nation rivers, Quebec. Neues Jahrbuch fur Mineralogie Abhandlungie, **105**: 93-109.

Dodson, M. H. 1973. Closure temperatures in cooling geochronological and petrological systems. Contributions to Mineralogy and Petrology, **40**: 259-274.

---- 1979. Theory of cooling ages. *In* Isotope Geology, *Edited by* E. Jäger and J.C. Hunziker. Springer-Verlag, Berlin, pp. 194-202.

---- 1986. Closure profiles in cooling systems. Materials Science Forum, **7**: 145-153.

----, and McClelland-Brown, E. 1985. Isotopic and paleomagnetic evidence for rates of cooling, uplift and erosion. *In* The Chronology of the Geological Record, *Edited by* N.J., Snelling, Memoirs of the Geological Society of London, **10**: 315-325.

Easton, R. M. 1986. Geochronology of the Grenville Province. *In* The Grenville Province. *Edited by* J.M. Moore, A. Davidson, and A.J. Baer. Geological Association of Canada, Special Paper **31**: pp. 127-173.

---- 1988. Regional mapping and stratigraphic studies, Grenville Province with some notes on mineralization environments. Ontario Geological Survey Miscellaneous Paper, **141**: 300-308.

---- 1992. Geology of Ontario: Ontario Geological Survey, **4**: 714-904.

---- and Bartlett, J. R. 1984. Precambrian geology of the Howland area, Haliburton, Peterborough and Victoria Counties. Ontario Geological Survey Preliminary Map P 2699, Geological Series.

---- and Davidson, A., 1994. Terranes, domains and lithotectonic assemblages within the Grenville Province. Geoscience Canada, **21**: 30-34.

---- and Ford, F. D. 1990. Geology of the Mazinaw Lake area (31C/14); Ontario Geological Survey, Open File Map 167, scale 1:50,000.

---- and ---- 1991. Geology of the Mazinaw area. Ontario Geological Survey, Miscellaneous Paper **157**: 95-106.

Ebadi, A., and Johannes, W. 1991. Beginning of melting and composition of first melts in the system Qz-Ab-Or-H_2O-CO_2. Contributions to Mineralogy and Petrology, **106**: 286-295.

Edwards, R. L., and Essene, E. J. 1988. Pressure, temperature and C-O-H fluid fugacities across the amphibolite-granulite transition, northwest Adirondack Mountains, New York. Journal of Petrology, **29**: 39-72.

Ellis, D. J. 1980. Osumilite-sapphirine-quartz granulites from Enderby Land, Antarctica: P-T conditions of metamorphism, implications for garnet-cordierite equilbiria and the evolution of the deep crust. Contributions to Mineralogy and Petrology, **74**: 201-210.

Ellis, D. J. 1986. Garnet-liquid Fe^{2+} - Mg equilibria and implications for the beginning of melting in the crust and subduction zones. American Journal of Science, **286**: 765-791.

---- 1987. Origin and evolution of granulites in normal and thickened crusts. Geology, **15**: 167-170.

England, P. C., and Richardson, S. W. 1977. The influence of erosion upon the mineral facies of rocks from different metamorphic environments. Journal of the Geological Society of London, **134**: 61-74.

----, and Thompson, A. B. 1986. Some thermal and tectonic models for crustal melting in continental collision zones. *In* Collisional Tectonics. *Edited by* M.P. Coward, and A.C. Ries. Geological Society of London, Special Publication **19**: 83-94.

Faure, G. 1986. Principles of Isotope Geology, 2nd ed., J. Wiley and Sons, New York. 589 pp.

Ferry, J. M. 1980. A comparative study of geothermometers and geobarometers in pelitic schists from south-central Maine. American Mineralogist **65**: 720-732.

----, and Spear, F. S. 1978. Experimental calibration of the partitioning of Fe and Mg between biotite and garnet. Contributions to Mineralogy and Petrology, **66**: 113-117.

Fitzsimons, I. C. W., and Harley, S. L. 1994. The influence of retrograde cation exchange on granulite P-T estimates and a convergence technique for the recovery of peak metamorphic conditions. Journal of Petrology, **35**: 543-576.

Florence, F. P., Darling, R. S., and Orrell, S. E. 1995. Moderate pressure metamorphism and anatexis due to anorthosite intrusion, western Adirondack Highlands, New York. Contributions to Mineralogy and Petrology, **121**: 424-436.

----, and Spear, F. S. 1991. Effects of diffusional modification of garnet growth zoning on P-T path calculations. Contributions to Mineralogy and Petrology, **107**: 487-500.

Foland, K. A. 1983. $^{40}Ar/^{39}Ar$ incremental heating plateaus for biotites with excess argon. Isotope Geoscience, **1**: 3-21.

Forsyth, D. A., Moore, J. M., Abinett, D., and Halpenny, J. 1988. Geological interpretation of regional geophysics for the Central Metasedimentary Belt. Proceedings, Grenville Workshop, Gananoque, Ontario, p. 10.

----, Thomas, M. D., Real, D., Abinett, D., Broome, J., and Halpenny, J. 1992. Geophysical investigations of the Central Metasedimentary Belt, Grenville Province: Québec to northern New York State. *In* Proceedings of the 7th International Conference on Basement Tectonics: Kingston, Ontario, Basement Tectonic Group Special Publication . *Edited by* R. Mason.

Freer, R., Carpenter, M. A., Long, J. V. P., and Reed, S. J. B. 1982. "Null result" diffusion experiments with diopside: Implications for pyroxene equilibria. Earth and Planetary Science Letters, **58**: 285-292.

Frost, B. R., and Chacko, T. 1989. The granulite uncertainty principle: limitations on thermobarometry in granulites. Journal of Geology, **97**: 435-450.

Gaber, L. J., Foland, K. A., and Corbato, C. E. 1988. On the significance of argon release from biotite and amphibole during $^{40}Ar/^{39}Ar$ vacuum heating. Geochimica et Cosmochimica Acta, **52**: 2457-2465.

Ganguly, J. 1979. Garnet and clinopyroxene solid solutions, and geothermometry based on Fe-Mg distribution coefficient. Geochimica et Cosmochimica Acta, **43**: 101-129.

----, and Chakraborty, S. 1990. Characterisation of metamorphism by Fe-Mg exchange reactions and Sm-Nd geochronology involving garnet: Diffusion kinetic analysis. Geological Society of America Abstracts with Programs, **22**: A72.

----, and Saxena, S. K. 1985. Mixing properties of aluminosilicate garnets: constraints from natural and experimental data, and applications to geothermometry. American Mineralogist, **69**: 88-97.

Gannser, A. 1980. The diversion between Himalaya and Karakorum. Geological Bulletin of the University of Peshawar, Pakistan, **13**: 9-22.

Gascoyne, M. 1986. Evidence for the stability of potential nuclear waste host, sphene, over geological time, from uranium-lead ages and uranium series disequilibrium measurements. Applied Geochemistry, **1**: 199-210.

Gasparik, T. 1984. Experimental study of subsolidus phase relations and mixing properties of pyroxene in the system $CaO-Al_2O_3-SiO_2$. Geochimica et Cosmochimica Acta, **48**: 2537-2545.

Geraghty, E. P., Isachsen, Y. W., and Wright, S. F. 1980. Extent and character of the Carthage-Colton mylonite zone, northwest Adirondacks, New York. Nuclear Regulatory Commission NUREG/CR-1865, 93 p.

Gill, J. E. 1948. Mountain building in Canada. 18th International Geological Congress, pt. XIII, 97-104.

Goldman, D. S., and Albee, A. L. 1977. Correlation of Mg/Fe partitioning between garnet and biotite with O^{18}/O^{16} partitioning between quartz and magnetite. American Journal of Science, **277**: 750-767.

Goldsmith, J. R. 1980. The melting and breakdown reactions of anorthite at high pressures and temperatures. American Mineralogist, **65**: 272-284.

Gower, C. F. 1985. Correlations between the Grenville Province and Sveconorwegian orogenic belt----implications for Proterozoic evolution of the southern margins of the Canadian and Baltic shields. *In* The Deep Proterozoic crust in the North Atlantic Provinces. *Edited by* A. C. Tobi, and J. L. R. Touret. NATO ASI Series, serial C, **158**: 827-830.

---- 1990. Mid-Proterozoic evolution of the eastern Grenville Province, Canada. Geologiska Föriningens i Stockholm Förhandlingar, **112**: 127-139.

Green, A. G., Cannon, W. F., Milkereit, B., Hutchinson, D. R., Davidson, A., Behrendt, J. C., Spencer, C., Lee, M. W., Morel-a-l'Huissier, P., and Agena, W. F. 1989. A "Glimpce" of the deep crust beneath the Great Lakes. In Properties and Processes of Earth's Lower Crust, American Geophysical Union, Monograph **51**: 65-80.

----, Milkereit, B., Davidson, A., Spencer, C., Hutchinson, D. R., Cannon, W. F., Lee, M. W., Agena, W. F., Behrendt, J. C., and Hinze, W. J. 1988. Crustal structure of the Grenville Front and adjacent terranes. Geology, **16**: 788-792.

Griffin, W. L., and O'Reilly, S. Y. 1986. The lower crust in eastern Australia: xenolith evidence. *In* The Nature of the Lower Continental Crust. *Edited by* J. B. Dawson, D. A. Carswell, H. Hall, and K. H. Wedepohl. Geological Society of London, Special Publication, **24**: 363-374.

Hall, J., Wardle, R. J., Gower, C. F., Kerr, A., Coflin, K., Keen, C. E., and Carroll, P. 1995. Proterozoic orogens of the northeastern Canadian Shield: new information from the Lithoprobe ECSOOT crustal reflection seismic survey. Canadian Journal of Earth Sciences, **32**: 1119-1131.

Hames, W. E., and Menard, T. 1993. Fluid-assisted modification of garnet composition along rims, cracks, and mineral inclusion boundaries in samples of amphibolite facies schists. American Mineralogist, **78**: 338-344.

Hand, M., Scrimgeour, E., Powell, R., Stuwe, K., and Wilson, C. J. L. 1994. Metapelitic granulites from Jetty Peninsula, east Antarctica: formation during a single event or by polymetamorphism? Journal of Metamorphic Geology, **12**: 557-573.

Hanes, J. A. 1991. K-Ar and $^{40}Ar/^{39}Ar$ geochronology: Methods and applications. *In* Mineralogical Association of Canada Short Course Handbook on Applications of Radiogenic Isotope Systems to Problems in Geology. *Edited by* L. Heaman, and J.N. Ludden, pp. 27-28.

----, and Corriveau, L. 1994. Late-stage cooling history of the Central Metasedimentary Belt of Quebec in the southwestern Grenville Province from ^{40}Ar-^{39}Ar dating of 1083-1076 Ma K-rich alkaline plutons. Geological Association of Canada, Mineralogical Association of Canada, Program with Abstracts, **19**: A46.

Hanmer, S. 1988. Ductile thrusting at mid-crustal level, south-western Grenville Province. Canadian Journal of Earth Sciences, **25**: 1049-1059.

----, and Ciesielski, A. 1984. A structural reconnaissance of the northwestern boundary of the Central Metasedimentary Belt, Grenville Province, Ontario and Québec. *In* Current Research, Part B. Geological Survey of Canada, Paper **84-1B**: 121-131.

----, and McEachern, S. 1992. Kinematical and rheological evolution of a crustal-scale ductile thrust zone, Central Metasedimentary Belt, Grenville orogen, Ontario. Canadian Journal of Earth Sciences, **29**: 1779-1790.

----, Thivierge, R. H., and Henderson, J. R. 1985. Anatomy of a ductile thrust zone: part of the northwest boundary of the Central Metasedimentary Belt, Grenville Province, Ontario. *In* Current Research, Part B. Geological Survey of Canada, Paper **85-1B**: pp. 1-5.

Hansen, E. C., Newton, R. C., and Janardhan, A. S. 1984. Fluid inclusions in rocks from the amphibolite-facies gneiss to charnockite progression in southern Karnataka, India: direct evidence concerning the fluids of granulite metamorphism. Journal of Metamorphic Geology, **2**: 249-264.

Hanson, G. N., Catanzaro, E. J., and Anderson, D. H. 1971. U-Pb ages for sphene in a contact metamorphic zone. Earth and Planetary Science Letters, **12**: 231-237.

----, and Gast, P. W. 1967. Kinetic studies in contact metamorphic zones. Geochimica et Cosmochimica Acta, **31**: 1119-1153.

Hariya, Y., and Kennedy, G. C. 1968. Equilibrium study of anorthite under high pressure and high temperature. American Journal of Science, **266**: 193-203.

Harley, S. L. 1984a. An experimental study of the partitioning of Fe and Mg between garnet and orthopyroxene. Contributions to Mineralogy and Petrology, **86**: 359-373.

---- 1984b. The solubility of alumina in orthopyroxene coexisting with garnet in FeO-MgO-Al_2O_3-SiO_2 and CaO-FeO-MgO-Al_2O_3-SiO_2. Journal of Petrology, **25**: 665-696.

---- 1985. Paragenetic and mineral--chemical relationships in orthoamphibole-bearing gneisses from Enderby Land, East Antarctica: a record of Proterozoic uplift. Journal of Metamorphic Geology, **3**: 179-200.

---- 1988. Proterozoic granulites from the Rauer Group, East Antarctica. I. Decompressional pressure-temperature paths deduced from mafic and felsic gneisses. Journal of Petrology, **29**: 1059-1095.

---- 1989. The origins of granulites: a metamorphic perspective. Geological Magazine, **126**: 215-247.

----, and Green, D. H. 1982. Garnet-orthopyroxene barometry for granulites and peridotites. Nature, **300**: 697-701.

----, and Hensen, B. J. 1990. Archaean and Proterozoic high-grade terranes of East Antarctica (40-80°C): a case study of diversity in granulite facies metamorphism. *In* High-Temperature Metamorphism and Crustal Anatexis. *Edited by* J.R. Ashworth, and M. Brown. The Mineralogical Society Series, **2**: 320-370.

Harris, N. B. W. 1981. The application of spinel bearing metapelites to P/T determinations: an example for South India. Contributions to Mineralogy and Petrology, **76**: 229-233.

Harrison, T. M. 1981. Diffusion of ^{40}Ar in hornblende. Contributions to Mineralogy and Petrology, **78**: 324-331.

---- 1983. Some observations on the interpretation of $^{40}Ar/^{39}Ar$ age spectra. Isotope Geoscience, **1**: 319-338.

----, Duncon, I., McDougall, I. 1985. Diffusion of ^{40}Ar in biotite: temperature, pressure and compositional effects. Geochimica et Cosmochimica Acta, **49**: 2461-2468.

----,and Fitzgerald, J. D. 1986. Exsolution in hornblende and its consequences for $^{40}Ar/^{39}Ar$ age spectra and closure temperature. Geochimica et Cosmochimica Acta, **50**: 247-253.

----, and McDougall, I. 1980. Investigations of an intrusive contact, northwest Nelson, New Zealand, II. Diffusion of radiogenic and excess ^{40}Ar in hornblende revealed by ^{40}Ar-^{39}Ar age spectrum results. Geochimica et Cosmochimica Acta, **44**: 2005-2020.

----, and McDougall, I. 1982. The thermal significance of potassium feldspar K-Ar ages inferred from $^{40}Ar/^{39}Ar$ age spectrum results. Geochimica et Cosmochimica Acta, **46**: 811-1820.

Hart, S. R. 1964. The petrology and isotopic mineral age relations of a contact zone in the Front Range, Colorado. Journal of Geology, **72**: 493-525.

Hays, J. F. 1967. Lime-alumina-silica. Carnegie Institution of Washington Year Book, **65**: 234-239.

Heaman, L. M., McNutt, R. H., and Krogh, T. E. 1986. Geological significance of U/Pb and Rb/Sr ages for two pre-tectonic granites from the Central Metasedimentary Belt, Ontario. *In* The Grenville Province. *Edited by* J.M. Moore, A. Davidson, and A.J. Baer. Geological Association of Canada Special Paper, **31**: 209-221.

Heaman, L., and Parrish, R. 1991. U-Pb Geochronology of accessory minerals. *In* Mineralogical Association of Canada Short Course Handbook on Applications of Radiogenic Isotope Systems to Problems in Geology. *Edited by* L. Heaman, and J.N. Ludden, pp. 59-102.

Hensen, B. J. 1977. Cordierite-garnet bearing assemblages as geothermometers and barometers in granulite facies terranes. Tectonophysics, **43**: 73-88.

----, and Green, D. H. 1971. Experimental study of the stability of cordierite and garnet in pelitic compositions. I. Compositions with excess aluminosilicate. Contributions to Mineralogy and Petrology, **33**: 309-330.

----, and ---- 1972. Experimental study of the stability of cordierite and garnet in pelitic compositions at high pressures and temperatures. Contributions to Mineralogy and Petrology, **35**: 331-354.

----, and ---- 1973. Experimental study of the stability of cordierite and garnet at high pressures and temperatures. III. Synthesis of experimental data and geological applications. Contributions to Mineralogy and Petrology, **38**: 151-166.

Hildebrand, R. S., and Easton, R. M., 1995. An 1161 Ma suture in the Frontenac terrane, Ontario segment of the Grenville Orogen. Geology, **23**: 917-920.

Hodges, K. V., and McKenna, L.W. 1987. Realistic propagation of uncertainties in geologic thermobarometry. American Mineralogist, **72**: 671-680.

Hoffman, P. F. 1989. Precambriam geology and tectonic history of North America. *In* The Geology of North America--An Overview, Geological Society of America, Decade of North American Geology, **A**: 447-512.

---- 1991. Did the break-out of Laurentia turn Gondwana inside-out? Science, **252**: 1409-1412.

Holdaway, M. J., and Lee, S. M. 1977. Fe-Mg cordierite stability in high grade pelitic rocks based on experimental, theoretical and natural observations. Contributions to Mineralogy and Petrology, **63**: 175-198.

----, and Mukhopadhyay, B. 1993. Geothermobarometry in pelitic schists: A rapidly evolving field. American Mineralogist, **78**: 681-693.

Hutcheson, I., Froese, E., and Gordon, T. M. 1974. The assemblage quartz-sillimanite-garnet - cordierite as an indicator of metamorphic conditions in the Daly Bay Complex, N.W.T. Contributions to Mineralogy and Petrology, **44**: 29-34.

Indares, A., and Martignole, J. 1985. Biotite-garnet geothermometry in granulite facies: the influence of Ti and Al in biotite. American Mineralogist, **70**: 272-278.

---- and ---- 1990a. Metamorphic constraints on the tectonic evolution of the allochthonous monocyclic belt of the Grenville Province, western Quebec. Canadian Journal of Earth Sciences, **27**: 371-386.

---- and ---- 1990b. Metamorphic constraints on the evolution of the gneisses from the parautochthonous and allochthonous polycyclic belts, Grenville Province, western Québec. Canadian Journal of Earth Sciences, **27**: 357-370.

Jäger, E., Niggli, E., Weiss, E. 1967. Rb-Sr Altersbestimmungen an Blimmern der Zentralalpen. Beiträge zur Geologischen Karte der Schwiz, Neue Folge, 134. Lieferung.

Jamieson, R. A., Culshaw, N. G., and Corrigan, D. 1995. North-west propagation of the Grenville orogen: Grenvillian structure and metamorphism near Key Harbour, Georgian Bay, Ontario, Canada. Journal of Metamorphic Geology, **13**: 185-207.

----, Culshaw, N. G., Wodicka, N., Corrigan, D., and Ketchum, J. W. F. 1992. Timing and tectonic setting of Grenvillian metamorphism---constraints from a transect along Georgian Bay, Ontario. Journal of Metamorphic Geology, **10**: 321-332.

Jan, M. Q., and Karim, A. 1995. Coronas and high-P veins in metagabbros of the Kohistan island arc, northern Pakistan: evidence for crustal thickening during cooling. Journal of Metamorphic Geology, **13**: 357-366.

Johannes, W., and Gupta, L. N. 1982. Origins and evolution of a migmatite. Contributions to Mineralogy and Petrology, **79**: 114-123.

Jones, K. A., and Brown, M., 1990. High-temperature 'clockwise' P-T paths and melting in the development of regional migmatites: an example from southern Brittany, France. Journal of Metamorphic Geology, **8**: 551-578.

Köppel, V. M. 1974. Isotopic U-Pb ages of monazites and zircon from the crust-mantle transition and adjacent units of the Ivrea and Ceneri zones (Southern Alps, Italy). Contributions to Mineralogy and Petrology, **43**: 55-70.

----, and Grünenfelder, M. 1975. Concordant U-Pb ages of monazite and xenotime from the Central Alps and the timing of the high-temperature Alpine metamorphism - a preliminary report. Schweizer Mineral Petrogr Mitt, **55**: 129-132.

Koziol, A. M., and Newton, R. C. 1988. Redetermination of the anorthite breakdown reaction and improvement of the plagioclase-garnet-Al_2SiO_5-quartz geobarometer. American Mineralogist, **73**: 216-223.

Kretz, R. 1959. Chemical study of garnet, biotite, and hornblende from gneisses of southwestern Quebec, with emphasis on distribution of elements in coexisting minerals. Journal of Geology, **67**: 371-403.

----- 1964. Analysis of equilibrium in garnet-biotite-sillimanite gneisses from Quebec. Journal of Petrology, **5**: 1-20.

---- 1977. Fort Coulonge - Otter Lake - Kazabazua area. Pontiac - Temiscamingue and Gatineau electoral districts. Ministère des Richesses Naturelles, Exploration Géologique, Québec (Qué.), Open File Report DPV-154.

---- 1978. Distribution of Mg, Fe^{2+} and Mn in some calcic pyroxene-hornblende-biotite-garnet gneisses and amphibolites from the Grenville Province. Journal of Geology, **86**: 599-619.

---- 1980. Occurrence, mineral chemistry, and metamorphism of Precambrian carbonate rocks in a portion of the Grenville Province. Journal of Petrology, **21**: 573-620.

----, Jones, P., and Hartree, R. 1989. Grenville metagabbro complexes of the Otter Lake area, Quebec. Canadian Journal of Earth Sciences, **26**: 215-230.

Krogh, T. E. 1982. Improved accuracy of U-Pb zircon ages by the creation of more concordant systems using an air abrasion technique. Geochimica et Cosmochimica Acta, **46**: 637-649.

----, and Davis, G. L. 1974. Alteration in zircons with discordant U-Pb ages. Carnegie Institute of Washington Yearbook, **73**: 560-567.

Kröner, A., Stern, R. J., Dawoud, A. S., Compston, W., and Reischmann, T. 1987a. The Pan-African continental margin in northeastern Africa: evidence from a geochronological study of granulites at Saboloka, Sudan. Earth and Planetary Science Letters, **85**: 91-104.

-----, Williams, I. S., Baur, N., Vintage, P. W., and Perera, L. R. L. 1987b. Zircon ion microprobe dating of high-grade rocks in Sri Lanka. Journal of Geology, **95**: 775-791.

Lal, R. K. 1993. Internally consistent recalibrations of mineral equilibria for geothermobarometry involving garnet-orthopyroxene-plagioclase-quartz assemblages and their application to the South Indian granulites. Journal of Metamorphic Geology, **11**: 855-866.

Lamb, W. M. 1993. Retrograde deformation within the Carthage-Colton Zone as recorded by fluid inclusions and feldspar compositions: tectonic implications for the southern Grenville Province. Contributions to Mineralogy and Petrology, **114**: 379-394.

Lasaga, A. C. 1983. Geospeedometry: an extension of geothermometry. *In* Kinetics and Equilibrium in Mineral Reactions. *Edited by* S. K. Saxena. Springer-Verlag, New York, pp. 81-114.

Laurin, A. F. 1960. Région de Turquetil-Émard, district électoral de Pontiac. Ministère des Mines du Québec, rapport préliminaire 424.

---- 1961. Dieskau-Loubias area. Ministère des Richesses naturelles du Québec, rapport préliminaire 452.

Le Breton, N., and Thompson, A. B. 1988. Fluid-absent (dehydration) melting of biotite in metapelites in the early stages of crustal anatexis. Contributions to Mineralogy and Petrology, **99**: 226-237.

Lee, H. T., and Ganguly, J. 1988. Equilibrium compositions of coexisting garnet and orthopyroxene: experimental determinations in the system FeO-MgO-Al_2O_3-SiO_2 and applications. Journal of Petrology, **29**: 93-113.

Lévesque, J., and Sharma, K. 1990. Corridors de déformation au contact de la limite ouest du Bassin de Mont-Laurier. Four posters presented at the Information Seminar, Ministère de l'Énergie et des Ressources du Québec, Québec City.

Lister, J. R., and Kerr, R. C. 1991. Fluid-mechanical models of crack propagation and their application to magma transport in dykes. Journal of Geophysical Research, **96B6**: 10049-10077.

Lonker, S. W. 1980. Conditions of metamorphism in high-grade pelitic gneisses from the Frontenac Axis, Ontario, Canada. Canadian Journal of Earth Sciences, **17**: 1666-1686.

---- 1981. The P-T-X relations of the cordierite-granet-sillimanite-quartz equilibrium. American Journal of Science, **281**: 1056-1090.

Lo, C. H., and Onstott, T. C. 1989. ^{39}Ar recoil artifacts in chloritized biotite. Geochimica et Cosmochimica Acta, **53**: 2697-2711.

Lumbers, S. B., Heaman, L. M., Vertolli, V. M., and Wu, T. -W. 1990. Nature and timing of Middle Proterozoic magmatism in the Central Metasedimentary Belt, Grenville Province, Ontario. *In* Mid-Proterozoic Laurentia-Baltica. *Edited by* C. F. Gower, T. Rivers and B. Ryan. Geological Association of Canada Special Paper.

Madore, L, and Sawyer, E. W. 1991. Extensional phenomena in the Grenville Province of Quebec. GACMAC Abstracts with Program, **16**: A79.

----, Sharma, K. N. M., and Giguère, E. 1993a. Synthèse géologique et structurale de la région de Fort-Coulonge, secteur sud-ouest du Grenville au Québec. Rapport d'activité 93. Ministère de l'Énergie et des Ressources du Québec, DV 93-02, 17-19.

----, Sharma, K. N. M., and Giguère, E. 1993b. Synthèse géologique et structurale de la région de Fort-Coulonge. Posters presented at the Information Seminar, Ministère de l'Énergie et des Ressources du Québec, Québec City.

----, Sharma, K. N. M., Barrette, P., and Boudreault, S. 1994. Synthèse géologique de la région du lac Pythonga, évidence de nappes de charriage dans le Grenville de l'Outaouai. Posters presented at the Information Seminar, Ministère de l'Énergie et des Ressources du Québec, Québec City. Program with abstracts. Ministère de l'Énergie et des Ressources du Québec, DV 94-09, 54.

Makobo, M. A. H., McDougall, I., Zeitler, P. K. and FitzGerald, J. D. 1991. Discordant $^{40}Ar/^{39}Ar$ ages from the Musgrave Ranges, central Australia: implications for the significance

of hornblende $^{40}Ar/^{39}Ar$ spectra. Chemical Geology (Isotope Geoscience Section), **86**: 139-160.

Marcantonio, F., McNutt, R. H., Dickin, A. P., and Heaman, L. M. 1990. Isotopic evidence for the crustal evolution of the Frontenac Arch in the Grenville Province of Ontario, Canada. Chemical Geology, **83**: 297-314.

Martignole, J., Machado, N., and Indares, A. 1994. The Wakeham Terrane: a Mesoproterozoic terrestrial rift in the eastern part of the Grenville Province. Precambrian Research, **68**: 291-306.

---- and Pouget, P. 1993. Contrasting zoning profiles in high-grade garnets: evidence for the allochthonous nature of a Grenville province terrane. Earth and Planetary Science Letters, **120**: 77-185.

----, and Sisi, S.-C. 1981. Cordierite-garnet-H_2O equilibrium: a geological thermometer, barometer and water fugacity indicator. Contributions to Mineralogy and Petrology, **77**: 38-46.

Mattinson, J. M. 1978. Age, origin and thermal histories of some plutonic rocks from the Salinian Block of California. Contributions to Mineralogy and Petrology, **67**: 233-245.

McEachern, S. J., and van Breemen, O. 1993. Age of deformation within the Central Metasedimentary Belt boundary thrust zone, southwest Grenville Orogen: Constraints on the collision of the Mid-Proterozoic Elzevir terrane. Canadian Journal of Earth Sciences, **30**: 1155-1165.

McLelland, J. M., Chiarenzelli, J., Whitney, P., and Isachsen, Y. 1988. U-Pb zircon geochronology of the Adirondack Mountains and implications for their tectonic evolution. Geology, **16**: 920-924.

Mezger, K. 1990. Geochronology in Granulites. *In* Granulites and Crustal Evolution. *Edited by* D. Vielzeuf and Ph. Vidal. Kluwer Academic Publishers, Netherlands, pp. 451-470.

----, Bohlen, S. R., and Hanson, G. N. 1988. U-Pb garnet, monazite and rutile ages: Implications for the duration of high-grade metamorphism and cooling histories, Adirondack Mts., NY. Geological Society of America Abstracts with Programs: **A100**.

----, Essene, E. J., van der Pluijm, B. A., and Halliday, A. N. 1993. U-Pb geochronology of the Grenville Orogen of Ontario and New York: constraints on ancient crustal tectonics. Contributions to Mineralogy and Petrology, **114**: 13-26.

----, Hanson, G. N., and Bohlen, S. R. 1989a. U-Pb systematics of garnet: dating the growth of garnet in the Late Archean Pikwitonei granulite domain at Cauchon and Natawahunan Lakes, Manitoba, Canada. Contributions to Mineralogy and Petrology, **101**: 136-148.

----, ----, and ---- 1989b. High-precision U-Pb ages of metamorphic rutile: application to the cooling history of high-grade terranes. Earth and Planetary Science Letters, **96**: 106-118.

----, Rawnsley, C. M., Bohlen, S. R., and Hanson, G. N. 1991. U-Pb garnet, sphene, monazite, and rutile ages: implications for the duration of high-grade metamorphism and cooling histories, Adirondack Mts., New York. Journal of Geology, **99**: 415-428.

----, van der Pluijm, B. A., Essene, E. J., and Halliday, A. N., 1992. The Carthage-Colton Mylonite Zone (Adirondack Mountains, New York): The site of a cryptic suture in the Grenville Orogen? The Journal of Geology, **100**: 630-638.

Miyamoto, M., and Takeda, H. 1977. Evaluation of a crust model of eucrites from the width of exsolved pyroxenes. Geochmical Journal, **11**: 161-169.

Moecher, D. P., Essene, E. J., and Anovitz, L. M. 1988. Calculation and application of clinopyroxene-plagioclase-quartz geobarometers. Contributions to Mineralogy and Petrology, **100**: 92-106.

Moore, J. M. Jr. 1982. Stratigraphy and tectonics of the Grenville Orogen in eastern Ontario. 1982 Grenville Workshop, Rideau ferry, Abstracts, p. 7.

---- 1986. Introduction: The 'Grenville problem' then and now. In The Grenville Province. Edited by J.M. Moore, A. Davidson, and A.J. Baer. Geological Association of Canada Special Paper **31**: 1-11.

----, and Thompson, P. H. 1980. The Flinton Group: a late Precambrian metasedimentary succession in the Grenville Province of eastern Ontario. Canadian Journal of Earth Sciences, **17**: 1685-1707.

Moores, E. M. 1991. Southwest U.S.-East Antarctic (SWEAT) connection: A hypothesis. Geology, **29**: 425-428.

Mukhopadhyay, B., and Holdaway, M. J. 1994. Cordierite-garnet-sillimanite-quartz equilibrium: I. New experimental calibration in the system FeO-Al_2O_3-SiO_2-H_2O and certain P-T-X_{H2O} relations. Contributions to Mineralogy and Petrology, **116**: 462-472.

Nadeau, L., and Hanmer, S. 1992. Deep crustal break-back stacking and slow exhumation of the continental footwall beneath a thrusted marginal basin, Grenville orogen, Canada. Tectonophysics, **210**: 215-233.

Naqvi, S. M., and Rogers, J. J. W. 1987. Precambrian Geology of India. Oxford University Press, Oxford, 223 pp.

Newton, R. C., and Perkins, D. III. 1982. Thermodynamic calibration of geobarometers based on the assemblages garnet-plagioclase-orthopyroxene-(clinopyroxene)-quartz. American Mineralogist, **67**: 203-222.

----, Smith, J. V., and Windley, B. F. 1980. Carbonic metamorphism, granulites, and crustal growth. Nature, **288**: 45-50.

----, and Wood, B. J. 1979. Thermodynamics of water in cordierite and petrologic consequences of cordierite as a hydrous phase. Contributions to Mineralogy and Petrology, **68**: 391-405.

Nichols, G. T., Berry, R. F., and Green, D. H. 1992. Internally consistent gahnitic spinel-cordierite-garnet equilibria in the FMASHZn system: geothermobarometry and applications. Contributions to Mineralogy and Petrology, **111**: 362-377.

Nicollet, C. 1988. Métabasites granulitiques, anorthosites et roches associées de la croûte inférieure. Exemples pris à Madagascar et dans le Massif Central francais. Arguments en faveur d'un métamorphisme associé à l'extension lithosphérique. These d'Etat, Clermont - Ferrand.

---- 1990. Crustal evolution of the granulites of Madagascar. *In* Granulites and Crustal Evolution. *Edited by* D. Vielzeuf and Ph. Vidal. NATO ASI Series, Series C: Mathematical and Physical Sciences, **311**: 291-310.

O'Hara, M. J. 1977. Thermal history of excavation of Archaean gneisses from the base of the continental crust. Journal of the Geological Society of London, **134**: 185-200.

----- Yarwood, G. 1978. High pressure-temperature point on an Archaean geotherm, implied magma genesis by crustal anatexis, and consequences for garnet-pyroxene thermometry and barometry. Philosophical Transactions of the Royal Society of London, **A288**: 441-456.

Olsen, S. N. 1983. A quantitative approach to local mass balance in migmatites. *In* Migmatites, Melting and Metamorphism. *Edited by* M. P. Atherton, and C. D. Gribble. Shiva, Nantwich, pp. 201-233.

Onstott, T. C., and Peacock, M. W. 1987. Argon retentivity of hornblendes: A field experiment in a slowly cooled metamorphic terrane. Geochimica et Cosmochimica Acta, **51**: 2891-2903.

Otton, J. K. 1978. Région des lacs Bouchette et Landron. Ministère des Richesses naturelles du Québec, rapport géologique, 181.

Parrish, R. 1988. U-Pb systematics of monazite and a preliminary estimate of its closure temperature based on natural examples. Geological Association of Canada, Program with Abstracts, **13**: A94.

---- 1990. U-Pb dating of monazite and its application to geological problems. Canadian Journal of Earth Sciences, **27**: 1431-1450.

----, Roddick, J. C., Loveridge, W. D., and Sullivan, R. W. 1987. Uranium-lead analytical techniques at the geochronology laboratory, Geological Survey of Canada. *In* Radiogenic age and isotopic studies: report 1. Geological Survey of Canada, Paper **88-2**: 3-7.

----, Bellerive, D., and Sullivan, R. W. 1991. U-Pb chemical procedures for titanite and allanite in the Geochronology Laboratory, Geological Survey of Canada. *In* Radiogenic age and isotopic studies: report 1. Geological Survey of Canada, Paper **91-2**: 187-190.

Patiño Douce, A. E., and Johnston, A. D. 1991. Phase equilibria and melt productivity in the pelitic system: Implications for the origin of peraluminous granitoids and aluminous granulites. Contributions to Mineralogy and Petrology, **107**: 202-218.

-------, and Rice, J. M. 1993. Octahedral excess mixing properties in biotite: A working model with applications to geobarometry and geothermometry. American Mineralogist, **78**: 113-131.

Perchuk, L. L., and Lavrent'eva, I. V. 1983. Experimental investigation of exchange equilibria in the system cordierite-garnet-biotite. *In* Kinetics and equilibrium in mineral reactions. *Edited by* S. K. Saxena. Springer-Verlag, New York, pp. 199-239.

Perkins, D., Essene, E. J., and Marcotty, L. A. 1982. Thermometry and barometry of some amphibolite-granulite facies rocks from the Otter Lake area, southern Quebec. Canadian Journal of Earth Sciences, **19**: 1759-1774.

Petterson, M. G., and Windley, B. F. 1985. Rb-Sr dating of the Kohistan arc-batholith in the Trans-Himalaya of N Pakistan, and its tectonic implications. Earth and Planetary Science Letters, **74**: 45-57.

Philipps, D., and Onstott, T. C. 1988. Argon zoning in mantle phlogopite. Geology, **16**: 542-546.

Pidgeon, R. T., and Aftalion, M. 1978. Cogenetic and inherited zircon U-Pb systems in granites: Paleozoic granites of Scotland and England. *In* Crustal evolution of Northwestern Britain and Adjacent Regions. *Edited by* R. D. Bowes, and B. E. Leake, Geological Journal Special Issue, **10**: 183-220.

Pupin, J. P. 1980. Zircon and granite petrology. Contributions to Mineralogy and Petrology, **73**: 207-220.

Purdy, J. W., and Jäger, E. 1976. K-Ar ages on rock-forming minerals from the Central Alps. Memoirs, Institute of Geology and Mineralogy, University of Padova, **30**: 1-31.

Puziewicz, J., and Johannes, W. 1990. Experimental study of a biotite-bearing granitic system under water-saturated and water-undersaturated conditions. Contributions to Mineralogy and Petrology, **104**: 397-406.

Rankin, D. W., et al. 1993. Proterozoic rocks east and southeast of the Grenville front. *In* Precambrian: Conterminous U.S. Geological Society of America, The geology of North America C-2. *Edited by* J. C., Jr. Reed, M. E. Bickford, R. S. Houston, P. K. Link, D. W. Rankin, P. K. Sims and W. R. Van Schmus, pp. 335-461.

Reitmeijer, F. J. M. 1983. Inter-diffusion coefficients parallel to the c-axis in iron-rich clinopyroxenes calculated from microstructures. Contributions to Mineralogy and Petrology, **83**: 169-176.

Reynolds, P. H., Culshaw, N. G., Jamieson, R. A., Grant, S. L., and MeKenzie, K. J., 1995. $^{40}Ar/^{39}Ar$ traverse - Grenville Front Tectonic Zone to Britt Domain, Grenville Province, Ontario, Canada. Journal of Metamorphic Geology, **13**: 209-221.

Richardson, S. W. 1968. Staurolite stability in a part of the system Fe-Al-Si-O-H. Journal of Petrology, **9**: 467-488.

Rivers, T., Martignole, J., Gower, C. F., and Davidson, A. 1989. New tectonic divisions of the Grenville Province, southeast Canadian Shield. Tectonics, **8**: 63-84.

Robinson, P., Spear, F. S., Schümacher, J. C., Laird, J., Klein, C., Evans, B. W., and Doolan, B. L. 1982. Phase relations of metamorphic amphiboles: natural occurrence and theory. *In* Amphiboles: Petrology and Experimental Phase Relations. *Edited by* D. R. Veblen, and P. H. Ribbe. Mineralogical Society of America, Reviews in Mineralogy, **9B**: 1-227.

Ruiz, J., Patchett, P. J. and Ortega-Gutierrez, F. 1988. Proterozoic and Phaneorzoic basement terranes of Mexico from Nd isotopic studies. Geological Society of America Bulletin, **100**: 274-281.

Sager-Kinsman, E. A., and Parrish, R. R. 1993. Geochronology of detrital zircons from the Elzevir and Frontenac terranes, Central Metasedimentary Belt, Grenville Province, Ontario. Canadian Journal of Earth Sciences, **30**: 465-473.

Sandiford, M. A. 1985a. The metamorphic evolution of granulites at Fyfe Hills: implications for Archaean crustal thickness in Enderby Land, Antarctica. Journal of Metamorphic Geology, **3**: 155-178.

---- 1985b. The origin of retrograde shear zones in the Napier Complex: implications for the tectonic evolution of Enderby Land, Antarctica. Journal of Structural Geology, **7**: 477-488.

----, and Powell, R. 1986a. Pyroxene exsolution in granulites from Fyfe Hills, Enderby Land, Antarctica: evidence for 1000°C metamorphic temperatures in Archean continental crust. American Mineralogist, **71**: 946-954.

----, and ---- 1986b. Deep crustal metamorphism during continental extension: modern and ancient examples. Earth and Planetary Science Letters, **79**: 151-158.

----, and Wilson, C. J. L. 1984. The structural evolution of the Fyfe Hills - Khmara Bay region, Enderby Land, East Antarctica. Australian Journal of Earth Sciences, **31**: 403-426.

Schärer, U. 1984. The effect of initial ^{230}Th disequilibrium on young U-Pb ages: the Makalu case, Himalaya. Earth and Planetary Science Letters, **67**: 191-204.

----, Xu, R. -H., and Allègre, C. J. 1986. U-Th-Pb systematics and ages of Himalayan leucogranites, South Tibet. Earth and Planetary Science Letters, **77**: 35-48.

Schenk, F. 1980. U-Pb and Rb-Sr radiometric dates and their correlation with metamorphic events in the granulite facies basement of the Serre, southern Calabria (Italy). Contributions to Mineralogy and Petrology, **73**: 23-38.

Schmid, R., Cressey, G., and Wood, B. J. 1978. Experimental determination of univariant equilibria using divariant solid-solution assemblages. American Mineralogist, **63**: 511-515.

Schümacher, R., Schenk, V., Raase, P., and Vitanage, P. W. 1990. Granulite facies metamorphism of metabasic and intermediate rocks in the Highland Series of Sri Lanka. *In*

High-temperature Metamorphism and Crustal Anatexis. *Edited by* J. R. Ashworth. The Mineralogical Society Series, **2**: 235-271.

Selverstone, J., and Chamberlain, C. P. 1990. Apparent isobaric cooling paths from granulites: two counter examples from British Columbia and New Hampshire. Geology, **18**: 307-310.

Sen, S. K., and Bhattacharya, A. 1984. An orthopyroxene-garnet thermometer and its application to the Madras charnockites. Contributions to Mineralogy and Petrology, **88**: 64-71.

Sengupta, P., Karmakar, S., Dasgupta, S. and Fukuoka, M. 1991. Petrology of spinel granulites from Araku, Eastern Ghats, India, and a petrogenetic grid for sapphirine-free rocks in the system FMAS. Journal of Metamorphic Geology, **9**: 451-459.

Sharma, K. N. M., Hocq, M., Lévesque, J., and Rive, M. 1993a. Région de Grand-Remous - Maniwaki - Danford Lake. Excursion des amis du Grenville au Québec. Observations structurales et importance économique. Ministère des ressources naturelles du Québec, MB 93-50.

---- Morasse, C., and Singhroy, V. 1993b. Structural Interpretation of the Baskatong area from SAR images. Oral presentation and posters. Radar Data Development Program, Workshop, Ganonoque, Ontario, 1993. Canada Centre for Remote Sensing, Ottawa.

---- Lévesque, J., and Singhroy, V. H. 1994. Geology, structure and economic importance of the Fort-Coulonge area, Outaouais. Poster presentation. Toronto-94, Annual General Meeting and Trade Exhibition of the Canadian Institute of Mining and Metallurgy, Toronto.

---- Singhroy, V. H., and Lévesque, J. 1995. Discussion: A two-stage emplacement for the Cabonga allochthon (central part of the Grenville Province): evidence for orthogonal and oblique collision during the Grenville orogeny. Canadian Journal of Earth Sciences, **32**: 1474-1478.

Sheraton, J. W., Black, L. P., and McCulloch, M. T. 1984. Regional geochemical and isotopic characteristics of high-grade metamorphic of the Prydz Bay area: the extent of Proterozoic reworking of Archaean continental crust in east Antarctica. Precambrian Research, **26**: 169-198.

Shiraishi, K., Asami, M., Ishizuka, H., Kojima, H., Koijma, S., Osanai, Y., Sakiyama, T., Takahashi, Y., Yamazaki, M., and Yoshikura, S. 1991. Geology and metamorphism of the Sør Rondane Mountains, East Antarctica. *In* Geological Evolution of Antarctica. *Edited by* M. R. A. Thompson, J. A Crame, and J. W. Thompson. Cambridge University Press, Cambridge, pp. 77-82.

Silver, L. T., and Lumbers, S. B. 1966. Geochronologic studies in the Bancroft-Madoc area of the Grenville Province, Ontario. Geological Society of America Abstracts and Programs, **87**: 156.

Spear, F. 1991. On the interpretation of peak metamorphic temperatures in the light of garnet diffusion during cooling. Journal of Metamorphic Geology, **9**: 379-388.

------ 1992. Thermobarometry and P-T paths from granulite-facies rocks: an introduction. Precambrian Research, **55**: 201-207.

------ Florence, F. P. 1992. Thermobarometry in granulites: pitfalls and new approaches. Precambrian Research, **55**: 209-241.

----, and Schümacher, J.C. 1982. Origin of cordierite-anthopyllite rocks. *In* Amphiboles: petrology and experimental phase relations. *Edited by* D. R.., and P. H.. Ribbe. Reviews in Mineralogy, **9B**: 160-163.

Spry, P. G., and Scott, S. D. 1986a. Zincian spinel and staurolite as guides to ore in the Appalachians and Scandinavian Caledonides. Canadian Mineralogist, **24**: 147-163.

---- 1986b. The stability of zincian spinels in sulfide systems and their potential as exploration guides for metamorphosed massive sulfide deposits. Economic Geology, **81**: 1446-1463.

Stoddard, E. F. 1979. Zinc-rich hercynite in high-grade metamorphic rocks: a product of the dehydration of staurolite. American Mineralogist, **64**: 736-741.

St-Onge, M. R. 1987. Zoned poikiloblastic garnets: P-T paths and syn-metamorphic uplift through 30 km of structural depth, Wopmay Orogen, Canada. Journal of Petrology, **28**: 1-21.

Stuwe, K., and Powell, R. 1989. Low pressure granulite facies metamorphism in the Larsemann Hills area, East Antarctica: petrology and tectonic implications for the evolution of the Prydz Bay area. Journal of Metamorphic Geology, **7**: 465-483.

Sun, S., Gray, C. M., Sheraton, J. W., Glikson, A. Y., and Stewart, A. J., in press. Zircon U-Pb chronology and neodymium isotope study of tectonothermal and crust-forming events in the Tomkinson Ranges, western Musgrave Block, Central Australia. AGSO Journal of Australian Geology and Geophysics.

Sun, S., and Sheraton, J. 1992. Zircon U/Pb chronology, tectono-thermal and crust-forming ages in the Tomkinson Ranges, Musgrave Block, Central Australia. AGSO Research Newsletter, 17: 9-11.

Tahirkheli, R. A. K., and Jan, M. Q. 1979. Geology of Kohistan, Karakorum Himalaya, northern Pakistan. Special Issue of the Geological Bulletin of the University of Peshawar, Pakistan, **11**: 1-30.

Thompson, J. B. 1957. The graphical analysis of mineral assemblages in pelitic schists. American Mineralogist, **42**: 842-858.

Thompson, A. B. 1976a. Mineral reactions in pelitic rocks: I. Prediction of P-T-X (Fe-Mg) phase relations. American Journal of Science, **276**: 401-424.

---- 1976b. Mineral reactions in pelitic rocks: II. Calculation of some P-T-X(Fe-Mg) phase relations. American Journal of Science, **276**: 425-454.

---- 1982. Dehydration melting of pelitic rocks and the generation of H_2O-undersaturated granitic liquids. American Journal of Science, **282**: 1567-1595.

----, and Tracy, R. J. 1979. Model systems for anatexis of pelitic rocks. II. Facies series melting and reactions in the system CaO-$KAlO_2$-$NaAlO_2$-Al_2O_3-SiO_2-H_2O. Contributions to Mineralogy and Petrology, **70**: 429-438.

Treloar, P. J., Broughton, R. D., Williams, M. P., Coward, M. P., and Windley, B. F. 1989a. Deformation, metamorphism and imbrication of the Indian Plate south of the Main Mantle Thrust, North Pakistan. Journal of Metamorphic Geology, **7**: 111-125.

----, Coward, M. P., Williams, M. P., and Khan, M. A. 1989b. Basement-cover imbrication south of the Main Mantle thrust, North Pakistan. Special Publication of the Geological Society of America, **232**: in press.

----, Williams, M. P., and Coward, M. P. 1989c. Metamorphism and crustal stacking in the North Indian plate, North Pakistan. Tectonophysics, **165**: in press.

----, Rex, D. C., Guise, P. G., Coward, M. P., Searle, M. P., Windley, B. F., Petterson, M. G., Jan, M. Q., and Luff, I. W. 1989d. K-Ar and Ar-Ar geochronology of the Himalayan collision in NW Pakistan: Constraints on the timing of suturing, deformation, metamorphism and uplift. Tectonics, **8**: 881-909.

Tuccillo, M. E., Essene, E. J., and van der Pluijm, B. A. 1990. Growth and retrograde zoning in garnets from high-grade metapelites: Implications for pressure-temperature paths. Geology, **18**: 839-842.

---- Mezger, K., Essene, E. J., and van der Pluijm, B. A. 1992. Thermobarometry, geochronology and the interpretation of P-T-t data in the Britt Domain, Ontario Grenville Orogen, Canada. Journal of Petrology, **33**: 1225-1259.

Tucker, R. D. 1988. Contrasting crustal segments in the central Norwegian Caledonides: Evidence from U-Pb dating of accessory minerals. Geological Association of Canada Program with Abstracts, **13**: A127.

----, Raheim, A., Krogh, T. E., and Corfu, F. 1987. Uranium-lead zircon and titanite ages from the northern portion of the Western Gneiss Region, south-central Norway. Earth and Planetary Science Letters, **81**: 203-211.

Turner, G. 1968. The distribution of potassium and argon in chondrites. *In* Origin and distribution of the Elements. *Edited by* L. H. Ahrens. Pergamon, London, pp. 387-398.

Vachette, M., and Hottin, G. 1970. Âges au strontium des granites d'Antongil et de l'Androna (Nord-Est et Centre-Nord de Madagascar). C.R. Seminar de Geologie, Madagascar, 73-76.

---- and ---- 1974. Ages de 682 et de 527 Ma dans le massif granitique de Carion (Centre de Madagascar). C.R.Academie des Sciences, Paris, **278**: 1669-1671.

---- and ---- 1975. Ages de 726 million d'années déterminés au strontium ajusté par isochrone sur roches totales des granite d'Ankaramena (Centre Sud de Madagascar). C.R.Academie des Sciences, Paris, **281**: 1975-1977.

----, and Corriveau, L. 1995. Evolution of the Central Metasedimentary Belt in Quebec, Grenville orogen: U-Pb geochronology. Precambriam '95-International Conference on Tectonics and Metallogeny of Early/Mid Precambrian Orogenic Belts, Program and Abstracts, p. 137.

van Breemen, O. and Davidson, A. 1990. U-Pb zircon and baddeleyite ages from the Central Gneiss Belt, Ontario. Geological Survey of Canada Paper **89-2**: 85-92.

----, Davidson, A., Loveridge, W. D., and Sullivan, R. W. 1986. U-Pb zircon geochronology of Grenville tectonites, granulites, and igneous precursors, Parry Sound, Ontario. Geological Association of Canada Special Paper, **31**: 191-207.

----, and Hanmer, S. K. 1986. Zircon morphology and U/Pb geochronology in active shear zones: studies on syntectonic intrusions along the northwest boundary of the Central Metasedimentary Belt, Grenville Province, Ontario. *In* Current Research, Part B. Geological Survey of Canada, Paper **86-1B**: 775-784.

van der Pluijm, B. A., and Carlson, K. A. 1989. Extension in the Central Metasedimentary Belt of the Ontario Grenville: timing and tectonic significance. Geology, **17**: 161-164.

----, Mezger, K., Cosca, M. A., and Essene, E. J. 1994. Determining the significance of high-grade shear zones by using temperature-time paths, with examples from the Grenville Orogen. Geology, **22**: 743-746.

Vielzeuf, D. 1980. The spinel-quartz association in high grade xenoliths from Tallante (Spain) and their potential use in geothermometry. Contributions to Mineralogy and Petrology, **82**: 301-311.

----, and Holloway, J. R. 1988. Experimental determination of the fluid-absent melting relations in the pelitic system. Contributions to Mineralogy and Petrology, **98**: 257-276.

----, and Montel, J. M. 1994. Partial melting of metagreywackes. Part I: Fluid-absent experiments and phase relationships. Contributions to Mineralogy and Petrology, **117**: 375-393.

Wagner, G. A., Reimer, G. M., and Jäger, E. 1977. Cooling ages derived by apatite fission track, mica Rb-Sr and K-Ar dating: the uplift and cooling history of the Central Alps. Geological Memoires of the Petrological University, Padova, **30**: 1-28.

Waters, D. J. and Moore, J. M. 1985. Kornerupine in Mg-Al-O rich gneisses from Namaqualand, South Africa: mineralogy and evidence for late-metamorphic fluid activity. Contributions to Mineralogy and Petrology, **91**: 169-182.

Watson, E. B., Harrison, T. M., Ryerson, F. M. 1985. Diffusion of Sm, Sr and Pb in fluorapatite. Geochimica et Cosmochimica Acta, **49**: 1813-1823.

Weisbrod, A. 1973a. Refinements of the equilibrium conditions of the reaction Fe-cordierite = almandine + sillimanite + quartz + (H_2O). Carnegie Institute of Washington Yearbook, **72**: 518-521.

---- 1973b. Cordierite-garnet equilibrium in the system Fe-Mn-Al-Si-O. Carnegie Institute of Washington Yearbook, **72**: 515-518.

Wilson, M. E. 1918. The subprovincial limitations of pre-Cambrian nomenclature in the St. Lawrence basin. Journal of Geology, **26**: 325-333.

----- 1925. The Grenville pre-Cambrian subprovince. Journal of Geology, **33**: 389-407.

-----, 1939. The Canadian Shield. In Geologie der Erde: Geology of North America, Volume 1. *Edited by* R. Ruedemann, and R. Balk. Verlag von Gebruder Borntraeger, Berlin, pp. 232-311.

Windley, B. F. 1986. Comparative tectonics of the western Grenville and the western Himalaya. *In* The Grenville Province. *Edited by* J. M. Moore, A. Davidson, and A. J. Baer. Geological Association of Canada Special Paper, **31**: 341-348.

----- 1989. Anorogenic magmatism and the Grenvillian orogeny. Canadian Journal of Earth Sciences, **26**: 479-289.

----- 1993. Proterozoic anorogenic magmatism and its orogenic connections. Journal of the Geological Society of London, **150**: 39-50.

Wodicka, N. 1994. Middle Proterozoic evolution of the Parry Sound domain, southwestern Grenville orogen, Ontario: Structural, metamorphic, U/Pb and $^{40}Ar/^{39}Ar$ constraints. Unpublished PhD Thesis, Dalhousie University, Halifax, Nova Scotia.

Wolmarans, L. G., and Kent, K. E. 1982. Geological investigations in western Dronning Maud Land, Antarctica--a synthesis. South African Journal of Antarctic Research, supplement 2.

Wood, B. J. 1974. The solubility of alumina in orthopyroxene coexisting with garnet. Contributions to Mineralogy and Petrology, **46**: 1-15.

Woussen, G., Roy, D. W., Dimroth, R. E., and Chown, E. H. 1986. Mid-Proterozoic extensional tectonics in the core zone of the Grenville Province. Geological Association of Canada Special Paper, **31**: 297-311.

Wynne-Edwards, H. R. 1972. The Grenville Province. Geological Association of Canada Special Paper, **11**: 263-334.

York, D., and Lopez-Martinez, M. 1986. The two-faced mica. Geophysical Research Letters, **13**: 973-975.

Young, G. M. 1992. Late Proterozoic stratigraphy and the Canada-Australia connection. Geology, **20**: 215-218.

APPENDEX A

THIN SECTION DESCRIPTIONS

1280-2: Migmatitic Metapelite Grt-Bt-Pl-Qtz
Bt-Pl-Qtz-Ilm-Kfs-Ap

-Grt - 2% - 1.0mm x 1.0mm to 2.5mm x 1.5mm, embayed borders, fractured, broken apart, filled with inclusions of Bt and Qtz throughout core to rim, rimmed partially by quartz-plagioclase-biotite
-Bt - 30% - small flakes about 0.1mm, poorly developed, matrix
-Qtz - 53% - graphic intergrowth with Pl, quartz rods in oval pods up to 5mm x 2cm
-Pl - 10% - graphic intergrowth with quartz (<1%; approximately 0.1mm round blebs)
-Ilm - 3% - not in contact with Grt, small rods 0.1mm x 1.0mm
-Kfs - 1% - perthitic
-Ap - 1%
-Ser - <1% - minor alteration of Pl

-Bt-Ilm bend around Grt, likely Grt growth pre-Bt-Ilm
-Bt-Ilm also bend around felsic pods
-felsic pods are discontinuous undulose leucosomes ranging in size from 2mm x 2mm to 7mm x 25mm

1475-A1: Migmatitic Metapelite -Grt-Bt-Hbl-Pl-Ilm-Qtz-Ap

-Grt - 30% - 1mm x 1mm to 3.0cm x 0.7cm, embayed borders, fractured, filled with inclusions of Qtz, Ilm, Bt, Pl, Ap throughout, poikiloblastic, ameboidal
-Bt - 2% - intergrown pseudo-symplectically with Hbl
-Hbl - 2% - symplectic with Bt-Qtz; alteration from Bt
-Ilm - 2%
-Ap - 1%
-Qtz - 55% - undulating extinction
-Pl - 8%
-Ser - <1%

1475-A3: Migmatitic Metapelite Grt-Opx-Hbl-Bt-Ap-Pl-Ilm-Qtz
(leucosome)

-Grt - 10% - 1mm x 1mm to 2mm x 4mm, embayed borders, fractured, inclusions of Qtz, Ilm, Bt, ameboidal, associated with Opx, Hbl, Bt, Ap, Qtz, Pl
-Opx - 5% - altering to Hbl, Bt, Ilm
-Hbl - 2% - alteration of Opx along cleavages
-Bt - 3% - same as Hbl

-Ap - 1%
-Qtz - 30% - undulating extinction
-Kfs - 1% - perthitic
-Pl - 45%
-Ilm - 3% - same as Bt, Hbl
-OPq - 1% - needles, rods, globules, one rod which surrounds Ap
-Ser - <1%

1475B1: Migmatitic Metapelite Grt-Bt-Hbl-Qtz-Pl-Ilm

-Grt-15%, more or less rounded, embayed contacts frequently partially rimmed with Ilm-Bt, filled with inclusions (more or less in spheres around the core) of Ilm-Qtz-Bt
-Bt-2%, symplectic with Qtz, defines foliation
-Hbl-1%
-Qtz-28%, grain boundary migration
-Pl-30%, slight sericitization
-Ilm-5%, defines foliation
-Kfs-<1%, perthitic, 0.1mm isolated rounded blobs, <1%
-Ser<<1%

1475B2 (L): -similar to previous thin section; however, layers alternate concentrations of Ilm (ranging from 1% to 5%)

1512: Migmatitic Metapelite Grt-Bt-Sil-Qtz-Opq-Pl

-Grt - 6% - snowball (inclusions Qtz, Bt, Sil, Opq); rims of inclusions, Sil parallel to old rim, porphyroclast now approximately triangular because consumed by reaction
-Bt- 6% - more or less long axis parallel to foliation; pressure shadows on Grt
-Sil - 6% - cross-section and blades, more or less long axis parallel to foliation; pressure shadows on Grt
-Qtz - 80% - grain size reduction, undulating extinction, rods
-Opq (Ilm?) - 2% - interstitial, mostly associated with Sil and Bt
-Pl - <1% - in pressure shadows on Grt
-Ser-<<1%
-poorly developed compositional zoning
-reaction Grt to Sil + Bt + Qtz + Pl

1512 (L): Migmatitic Metapelite Grt-Bt-Sil-Qtz-Opq-Pl

-Grt - 3% - 1mm x 1mm to 4mm x 4mm; ameboidal; embayed borders; filled with concentric rings of inclusions of Sil-Bt-Qtz-Opq
-Bt - 3%
-Sil - 5% - up to 2mm long
-Qtz - 82% - rods with grain boundary migration and grain size reduction
-Pl - 5 % - porphyroclasts up to 3mm x 5mm
-Opq - 2% - acicular

1654A1 (L): Kornerupine-tourmaline-orthopyroxene bearing quartzo-feldspathic gneiss

Krn-Tur-Opx-Qtz-Pl

-Krn- 5% - closely associated with Tur-Opx-Qtz; contains inclusions of Tur-Qtz; columnar with long axis parallel to long axis of thin section
-Tur - 2% - short axis in thin section; perpendicular to Krn and Opx
-Opx - 10% - parallel to Krn; intergrown with Krn
-Qtz - 42%
-Pl - 45%
-Bt - 1% - very poorly formed laths

1654C1 (L): Krn-Tur-Opx-Crd bearing quartzo-feldspathic gneiss
Krn-Tur-Opx-Crd-Opq-Qtz-Pl

-Krn - 1% - closely associated with Tur-Opx
-Tur - 30% - long axis perpendicular to Krn-Opx
-Opx - 10% - closely associated with Tur-Krn
-Crd - 5% - concentrated in one layer, thinly dispersed throughout rest of thin section
-Opq - 2% - interstitial
-Qtz - 8%
-Pl - 25%

1654C2 (L): Krn-Tur-Opx-Crd bearing quartzo-feldspathic gneiss
Krn-Opx-Tur-Bt-Opq-Qtz-Pl
Ttn-Bt-Crd-Opx-Zrn-Pl-Qtz-Kfs

POD
-Krn - 25%
-Opx -15%
-Tur - 5%
-Bt - 1%
-Opq- 2%
-Qtz - 47%
-Pl - 5%
-more or less same as other pods (1654C1)

MATRIX
-Ttn - 1% - finely disseminated; <1mm
-Bt - 3% - concentrated in discontinuous layers 1-3mm thick, 5 to 60mm long
-Crd - 5% - grains mostly 1-3mm; subidiomorphic
-Opx - 5% - concentrated in discontinuous layers 1-5mm thick, 10mm to 40mm long
-Zrn - <1% - in Crd
-Pl - 45% - graphitic with Qtz; <1% 0.1-0.3 x 0.1mm U-shapes, rounded blobs, twisted tubes
-Qtz - 36% - graphitic with Pl
-Kfs - 5% - perthitic; <1%; <0.05mm isolated oval-shaped tubes

-at boundary between pod and matrix layer of Opx-rich; very undulose irregular boundary; matrix is very inhomogenous with changing concentrations of Opx and Bt

1654D: Krn-Tur-Opx-Crd bearing quartzo-feldspathic gneiss
Krn-Opx-Tur-Qtz-Crd-Pl-Phl-Opq

-Krn - 20% - inclusions of Tur, Qtz, poorly formed blades
-Opx - 10% - inclusions Qtz, Opq, subidiomorphic, pleochroic grey-red brown
-Tur - 10% - cross-sections, oriented perpendicular to Krn and Opx; pleochroic yellow-brown-green-brown
-Qtz -15% - grain size reduction, mosaic, undulating extinction
-Crd - 3% - pleochroic yellow halos around zircons, sector twins
-Pl - 38%
-Phl - 2% - associated with Opx as alteration product; poorly formed
-Opq - 2% - disseminated, interstitial
-Zrn - <1% - in Crd

1654D2: Krn-Tur-Opx bearing quartzo-feldspathic gneiss
Krn-Qtz-Tur-Opx-Opq-Phl

-Krn - 45% - more or less bladed up to 7.0 x 20.0mm; central masses with inclusions Qtz and Tur
-Opx - 1% - idiomorphic
-Qtz - 40% - mosaic, undulating extinction
-Tur - 10% - inclusions in Krn, mostly blebs, zoned yellow green; pleochroic; oriented perpendicular to Krn and Opx
-Opq - 3% - interstitial
-Phl - 1% - poorly formed
-Sil - <1% - fibrolite

1654E3: Krn bearing quartzo-feldspathic gneiss
Pl-Kfs-Qtz-Phl-Sil/Krn?

-Pl-Kfs - 90% - perthitic, approximately 30% of Kfs, 0.3 x 0.1mm rounded tubes intertwined as a net, oriented parallel to twins, exsolution destroyed twinning
-Qtz - 5% - mosaic, undulating extinction
-Phl - 5% - blades, alteration of Sil/Krn
-Sil/Krn - <1% - alteration to Phl; very tiny, impossible to identify

1654F2: Tur-Opx-Crd bearing quartzo-feldspathic gneiss
Crd-Opx-Tur-Pl-Qtz-Opq

-Crd - <1%
-Opq - <1% - interstitial
-Opx - 20% - some within TM complexes (not inclusions)
-Tur - 40% - fine grained complexes, zoned
-Pl - 35%
-Qtz - 25% - partial mosaic, undulating extinction, grain boundary migration

1654F2: Krn-Tur-Opx bearing quartzo-feldspathic gneiss
Krn-Tur-Opx-Qtz-Opq-Phl

-Krn - 40% - inclusions Tur, Opq, Qtz, Opx; well-formed blades (up to 6mm x 12mm)
-Tur - 10% - complexes zoned cross-sections (6mm x 6mm of 0.5mm x 0.5mm)
-Opq - <1% - interstitial 0.1mm to 1.0mm
-Qtz - 47% - good grains, some grain boundary migration, grain size reduction

-Opx - 3% - inclusions Krn; also included in Krn at one boundary

1654H (L): Opx bearing quartzo-feldspathic gneiss
Opx-Bt-Ttn-Pl-Qtz

-Opx - 5%
-Bt - 3%
-Ttn - 1%
-Pl - 60% - graphic intergrowth with Qtz; <0.05 mm isolated rounded blobs at edges of grains
-Qtz - 30% - graphic intergrowth with Pl

1654I3: Cordierite bearing quartzo-feldspathic gneiss
Crd-Zrn; Qtz-Phl-Crd-Sil

-Crd - 14%
-Zrn - <1% - inclusions in Crd
-Phl - <1%
-Qtz - 85% - semi-mosaic; grain size reduction
-Opq - 1% - interstitial blebs approximately 0.1mm
-Sil - <1% - fibrolitic, complex with Phl and Opq

1654K (L): Tur bearing quartzo-feldspathic gneiss
Tur-Qtz-Sil

-Tur - 45% - intergrown with Qtz; one large crystal that goes into extinction as one unit
-Qtz - 55% - mosaic
-Sil - 1% - fibrolitic
-Kfs - surrounds intergrowth; slightly sericitic
-Ser <1%

1654L: Opx bearing quartzo-feldspathic gneiss
Phl-Pl; Opx-Phl-Pl

-Phl - 15% - lepidoblastic
-Opx - 15%
-Pl - 70%
-minerals concentrated in zones, Opx with minor Pl-Phl; Pl; Pl-Phl

1659H1: Migmatized Metapelite Opx- Grt-Crd-Sil
Crd-Bt-Sil-Grt; Crd-Zrn

-Opx - 40% - cleavage altering to Bt; crack altering to Sil; embayments and irregular boundaries filled with Crd
-Grt - 2% - average 3mm; irregular; inclusions Qtz-Opq; cracks and embayments filled with Crd-Sil-Bt
-Crd - 15% - unaltered; sector twins; 2mm x 2mm to 5mm x 9mm
-Sil - 2% - fibrolite along cracks and grain boundaries
-Bt - 1% - along cleavage Opx; in between Crd grains associated with Gt
-Zrn - <1% - in Crd with pleochroic yellow haloes

-Qtz - 40% - grain size reduction

-Opx separated by moat Crd-Qtz from Grt-rich zone

1659H2: Migmatized Metapelite Grt-Opx; Crd-Zrn
Opx-Grt-Crd-Sil
Crd-Bt-Sil-Grt

-Opx - 15% - crystal poikiloblastic with Qtz inclusions; one large Grt inclusion; boundaries embayed with Qtz-Crd-Sil-Opq
-Grt - 10%
-Crd - 10%
-Sil - 2%
-Bt - 5% - define foliation; some symplectite with Qtz at Opx boundary
-Opq - 3% - interstitial; associated with Bt
-Zrn - <1% - in Crd
-Qtz - 60% - more or less mosaic; grain size reduction

2039A: Metapelite Grt-Bt-Pl-Qtz-Ms-Ap

-Grt - 2% - 1-4mm rounded, inclusion Qtz, Bt
-Bt - 30% - more or less long axis parallel foliation
-Pl - 7% - fine grained
-Qtz - 60% - fine grained
-Ms - 1% - concentrated in one layer
-Opq - <1% - associated with Bt
-Ap <1%

2039B: Metapelite Hbl-Ap-Bt-Qtz; Grt-Bt-Qtz-Pl-Opq

-Hbl - 5% - not associated with Grt; sub to idioblastic
-Grt - 5% - 1-7mm rounded, inclusions Qtz, Bt
-Bt - 40% - more or less parallel to foliation
-Pl - 15% - grains 0.1mm to 0.3mm
-Qtz - 33% - grains 0.1mm to 0.3mm
-Opq - 2%
-Ap - <1% - some interstitial; some acicular 0.3mm length

2373: Metapelite Grt-Sil-Bt-Pl-Opq

-Grt - 15% - replaced by Sil + Bt + Pl + pq, inclusions Sil, Bt
-Sil - 15% - 2 generations; one bladed (define foliation), second fibrolite associated with Grt + Bt
-Bt - 10% - parallel foliation; pressure shadows on Grt
-Qtz - 60% - fine grained
-Opq - 5% - mostly interstitial; <1% acicular

-possibly three generations of Sil; one as inclusions in Grt which are not parallel to foliation; second as first generation in foliation and pressure shadows; third as fibrolitic growth on Sil in foliation and pressure shadows

2401U/2401G3: Migmatized Metapelite Grt-Bt-Qtz-Pl-Opx

-Opq - 10% - some as inclusions Grt, some interstitially with Sil, Bt
-Grt - 25% - 2x2mm to 15 x 20mm, inclusions of Opq,Bt,Qtz, rounded; embayed; one large Grt (14mm x 16mm) has core large inclusions Opq-Bt-Spl-Pl, and rim of smaller inclusions Spl-Pl
-Bt-30% - symplectic with Qtz, defines foliation
-Qtz - 5% - undulating extinction, mosaic, graphic intergrowth with Pl; 5% of grains, 0.2 x 0.5mm rounded ameboidal blobs
-Pl - 30% - some envelopes Spl in matrix, graphic intergrowth with Qtz
-Kfs - <1% - perthitic; 5% of grains, mostly 0.1 x 0.05 angular rods more or less parallel to twin lamellae, <1% 0.05 x 0.4mm lamellae parallel to twin lamellae
-Opx - <1% - inclusion trails of Bt; alteration to Bt

-2401G3 is very similar to 2401U; except that 2401G3 is very perthitic

2401D1: Migmatized Metapelite Opx-Grt-Bt-Pl-Qtz

-Opx - 5% - from 4x4mm to 7x15mm, inclusion trails of Bt; embayed with Pl; cracked, surrounded by moat of Pl
-Grt - 25% - 3x3mm to 8x10mm; inclusions Bt-Qtz-Opq; more or less round, cracked, broken, embayed with Pl-Bt
-Bt - 15% - defines foliation
-Pl - 50% - partial moats (0.1 - 0.5 x 5 - 10mm undulating rounded) around Opx and Grt
-Qtz - 5% - undulating extinction, mosaic
-Opq - <1% - interstitial, inclusions GT (<2mm)

-reaction Opx + Grt goes to Bt + Pl

2401D2: Migmatized Metapelite Grt-Bt-Kfs-Sil-Ap-Pl-Qtz-Bt-Qtz; Grt-Sil-Spl-Pl Grt-Pl

MELANOSOME (50%) Grt-Bt-Kfs-Sil-Ap-Pl-Qtz; Grt-Sil-Spl-Pl
-Grt - 50% - up to 9mm x 10mm; more or less rounded; offset inclusion free cores with inclusion-rich rim Spl-Bt-Qtz-Pl-Kfs; embayed cracked boundaries
-Bt - 30%
-Kfs - <1%
-Sil - <1%
-Spl - <1% - never in contact with Qtz, inclusion in Grt, Sil
-Ap - <1%
-Pl - 5% - minor graphitic intergrowth with Qtz
-Qtz - 15% - minor graphitic intergrowth with Pl

LEUCOSOME (50%) PIN-Bt-Pl-Qtz; Grt-Pl
-Grt - <1% - tiny (1mm x 1mm) surrounded by moat Pl
-PIN - 10% - greenish alteration, most likely of Crd
-Pl - 30%
-Bt - 2%

-Qtz - 58% - undulous extinction, partially mosaic
-Kfs? - <1%

-boundary between two domains is undulose, irregular, and poorly defined in thin section other than by change from presence of large Grt to no large Grt

2401D2 Migmatized Metapelite Bt-Grt-Opq
Bt-Qtz-Opq
Qtz-Bt-Opq

MELANOSOME A (15%) Bt-Grt-Opq
-Bt - 40%
-Grt - 60% - 9mm x 6mm; rounded; inclusions Bt-Qtz-Pl-Kfs-Opq
-Opq - <1%

MELANOSOME B (35%) Bt-Qtz-Opq
-Bt - 90%
-Qtz - 10%
-Opq - <1%

QUARTZ VEIN (50%) Qtz-Bt-Opq
-Opq - 2%
-Bt - 5%
-Qtz 93%

-irregular undulating boundary between three domains; domains more or less parallel to each other and foliation

2401E/2401F2: Migmatized Metapelite Grt-Bt-Qtz-Pl-Kfs
Grt-Bt-Pl-Spl-Sil

-Grt - 50% - up to 16mm x 18mm
-Bt - 15%
-Kfs - 5% - perthitic; 10% of grains, 0.01 x 0.05 mm isolated annular spots oriented parallel to ex-twin lamellae, where perthitic, twin lamellae obliterated; where twinning preserved, 10% of twin lamellae are bent
-Spl - <1%
-Qtz - 20%
-Pl - 15%
-Sil - <1% - acicular randomnly oriented inclusions in Grt

2401F2: Migmatized Metapelite Opx-Grt-Bt-Opq-Pl-Qtz
Spl-Opx-Grt-Bt-Opq
Pl-Ser

MELANOSOME
-Opx - 25% - subidioblastic, pleochroic green-pink
-Grt - 15% - more or less rounded
-Bt - 30%
-Opq - 10% - interstitial up to 1mm x 3mm

-Pl - 15% - 80% of Pl as partial moats (1-6mm x 10->15mm rounded, ameboidal) around Grt and Opx
-Qtz - 5%
-Ser - <1%
-Spl <1% - included in Grt, Opx and Pl

-Grt and Opx included within one another; Opx with Bt along cleavages; Grt with Bt in embayments

2401F3: Migmatized Metapelite Grt-Opx-Opq-Qtz-Bt

-Grt - 10%
-Opx - 5%
-Opq - 5%
-Qtz - 60%
-Bt - 20%

-grain of Grt and Opx closely intergrown within Pl moat

2401G1: Migmatized Metapelite Opx-Bt-Qtz-Pl-Kfs-Opq
Grt-Bt-Qtz-Pl-Opx-Opq
Pl-Kfs-Ser

Opx-rich (55%)
-Opx - 15% - 3mm rounded
-Opq - 5% - interstitial up to 3mm
-Bt - 35%
-Qtz - 15% - mosaic, grain size reduced
-Pl - 25% - mostly as porphyroclasts between 1mm and 4mm x 6mm
-Ser - <1%
-Kfs - 5% - perthitic; <1%, 0.1 mm rounded isolated blobs

Grt-rich (45%)
-Grt - 50%
-Bt - 25%
-Qtz - 8%
-Pl - 12%
-Opq - 5%
-Opx - <1%

-boundary between two domains is defined by presence of GT; and a reduction in the percentage of BT; boundary is irregular and undulating

2401G2: Migmatized Metapelite Grt-Bt-Qtz-Pl-Opq-Kfs

-Grt - 30% - rounded, inclusions Bt-Opq-Qtz-Kfs
-Opq - 10% - half concentrated in pressure shadows, partly interstitial and parallel to foliation
-Bt - 45% - defines foliation
-Qtz - 5% - approximately 0.5mm
-Pl - 10% - up to 2mm

-Kfs - 5% - perthitic; 10% of grains, 6% 0.1 x 0.5-2.0mm twisted tubes parallel to twin lamellae; 2% 0.2mm rounded isolated blobs perpendicular to first set of tubes; 2% 0.2mm rounded isolated blobs crosscut twinning (separate grains from first two sets of perthitic intergrowths)

2672: Metapelite Grt-Sil-Bt-Opq-Pl-Qtz

-Grt - 35% - inclusions Qtz + Bt + Opq + Sil; collar of Opq
-Sil - 10% - blades approx parallel foliation
-Bt - 2% - poorly formed
-Opq - 5% - interstitial
-Pl - 3%
-PIN? - <1%
-Qtz - 45%
-Ser - <1%

2672: Metapelite Grt-Sil-Bt-Opq-Pl

-Grt - 65%
-Sil <1% - fibrolite, few blades
-Bt - 10% - very red, alteration of Opq
-Opq - 8% - interstitial
-Pl - 12% - alteration
-Ms - <1%
-Fe staining - 5%

2759: Coronitic Metagabbro Opx-Hbl; Hbl + Pl; Pl

-Opx - 8% -interior of coronas
-Hbl - 12% -symplectic ring around Opx with Pl and Opq
-Opq - 5%
-Pl - 75% - well-formed laths in matrix

NB: symplectic Opq-Opx interior Opx

2770: Quartzite Grt-Sil-Bt-Qtz-Pl-Opq

-Grt - 2% - 2x2mm to 7x8mm, fractured, pieces, somewhat rounded
-Sil - <1% - minor, some bent aournd Grt; some forms clots on plagioclase porphyroblasts
-Bt - 5% - defines foliation
-Qtz - 70% - grain reduced rods, parallel foliation
-Pl - 20% - altered to Ser; parallel to foliation; fish-shaped porphyroblasts up to 1x5mm
-Ser - 3%
-Opq- <1% - interstitial, acicular, up to 1mm long
-Tur - <1%

2995: Quartzite Qtz-Ms-Bt-Opq

-Bt - 5% - Parallel foliation
-Ms - 5% - parallel foliation

-Qtz - 90% - recrystallized around Opq-Bt-Ms
-Opq - <1%

3028 (L): Migmatized Metapelite Qtz-Bt-Grt-Opq
Grt-Bt-Sil-Qtz-Ttn-Pl-Opq

LEUCOSOME (50%)
-Qtz - 90% - mosaic
-Bt- 3% - interstitial and associated with Grt
-Grt - 5% - 1mm; inclusions Qtz-Bt-Opq; more or less rounded
-Opq - 2% - interstitial and associated with Grt

MELANOSOME (50%)
-Grt - 35% - up to 5mm x 10mm; inclusions Sil-Qtz-Opq; some fish-shaped; broken; embayments filled with Pl-Bt-Sil
-Bt - 15% - parallel to foliation
-Sil 25%
-Opq - 4%
-Qtz - 10%
-Ttn - 1%
-Pl - 5%

-leucosomes parallel foliation; undulating continuous layers between 3 and 14mm thick; melanosomes surrounded with 1mm thick Bt lamina which defines boundary between leucosome and melanosome

3045/3045A1/A2: Metapelite Grt-Bt-Hbl-Pl-Qtz

-Grt - 5% - 1x1mm to 8x9mm; poorly formed, embayed, broken, inclusions Qtz
-Bt - 25% - defines foliation
-Ap - <1%
-Hbl - <1%
-Qtz - 40% - fine grain, few rods parallel foliation; graphic intergrowth with Pl
-Pl - 25% - fine grain, from melt; graphic intergrowth with Qtz
-Kfs - 5%

3302: Migmatized Metapelite Grt-Pl-Qtz-Bt-Kfs-Opq
Pl-Kfs-Opq

LEUCOSOME
-Grt - 5% - ameboidal generally <3mm
-Pl - 40% - sericitized; graphitic with Qtz
-Qtz - 40% - mosaic
-Bt - 5% - more or less laths
-Kfs - 5% - sericitized; perthitic; 3% of grains, 0.01 x 0.2mm fine angular lines parallel to twin lamellae
-Ser - 5%

3302A: Migmatized Metapelite Grt-Bt-Qtz
Grt-Bt-Qtz-Sil-Opq-Pl

Pl-Ser

LEUCOSOME
-Grt - 5% - round 4mm x 4mm; inclusions Bt-Qtz
-Bt - 5% - disseminated, interstitial
-Qtz - 90% - mosaic

MELANOSOME
-Kfs - 5%
-Grt- 10% - mostly 3-4mm, round, broken, inclusions Opq
-Bt - 25%
-Qtz - 30% - grain size reduced
-Sil - 38% - 2 generations, first coarse, second fibrolitic growth on first; fibrolite grows along Kfs boundaries; overgrows Kfs in spots
-Opq - 2% - blebs (1mm) interstitial
-Pl - 5%
-Ser - <1%

-Grt has forms symplectic boundaries with Bt-Pl-Qtz-Kfs in melanosome

3333A (L): Migmatized Metapelite Bt-Grt-Qtz-Pl-Sil-Opq

-Bt- 35% - mostly long axis parallel to foliation
-Qtz - 15%
-Pl - 30% - porphyroblasts 3mm; winged
-Grt - 1% - reacting out to Sil-Bt-Pl; inclusions SIL; embayments full Sil-Bt-Pl
-Sil - 18% - 2 generations; one reacting out; second replacing at Grt; inclusions in Qtz-Pl
-Opq - 1% - blebs associated with Bt; interstitial; acicular (Ilm) parallel with foliation

-leucosomes approximately 15%; discontinuous 1-3mm thick anastomosing pods of Qtz-Pl

3333A: Migmatized Metapelite Bt-Grt-Sil-Opq-Kfs-Qtz

-Bt - 30% - parallel foliation - not well formed
-Grt - 10% - Sil + Bt + Qtz inclusions, Sil lined up at angle to foliation; winged; pressure shadows consist of perthitic Kfs-Sil-Bt
-Sil - 10% - parallel foliation
-Opq - 3% - parallel foliation; needles (likely Ilm)
-Kfs - <1% - porphyroblasts; 5% inclusions of biotite and quartz
-Qtz - 42% - rods parallel foliation

3354: Metapelite Grt-Bt-Opq-Pl-Qtz

-Grt - 30% - 2x2mm to 8x15mm; big inclusion free core, rim with inclusions Bt-Pl-Qtz-Opq; ameboidal embayed; reaction to Bt + Pl + Ser
-Bt - 10% - associated with Grt
-Opq - 3% - blebs associated with Bt + Grt
-Pl - 35% - sericitized
-Qtz - 20% - undulating extinction, more or less mosaic
-Ser - 2%

3364-2: Migmatized Metapelite Qtz-Bt-Opq-Sil-Kfs

-Qtz - 75% - fine grained, minor rods; grain size reduced; minor mosaic
-Bt - 10% - parallel foliation
-Opq - 5% - some associated with Bt, parallel foliation, interstitial; needles (Ilm)
-Pl- <1%
-Kfs - 8% - porphyroblasts, perthitic; 4% range from 0.01mm rounded blobs to <0.01 x 0.3mm lines parallel to ex-twin lamellae; twinning mostly obliterated
-Sil - 2% - parallel foliation, wrap around Kfs pblasts; also inclusions in edges Kfs porphyroblasts; and in pressure shadows of Kfs

-leucosomes discontinuous undulous pods from 1mm x 15mm to 5mm x 15mm; approximately 5%

3600: Migmatized Garnetite Grt-Bt-Opq-Pl-Qtz

-Grt - 35% - embayed, ameboidal, inclusions Qtz + Opq + Bt
-Bt - 2% - associated with Grt
-Opq - 5% - between Pl, in and rim Grt; acicular (Ilm)
-Pl - 45% - alteration?; graphic
-Qtz - 13% - grain size reduction; undulating, mosaic, graphic

-undulous leucosome 3-6mm wide crosscuts thin section

3603B: CALC-SILICATE Scp-Di-Ttn-Opq-Qtz

-Scp - 80% - grown around some Ttn
-Di - 5% - rounded, approximately 1mm
-Ttn - 2%
-Opq - 2%
-Qtz - 1% - porphyroclasts

3603B: CALC-SILICATE

-similar to above; 80% Qtz; 1 Grt porphyroclast - Qtz + Scp inclusions

3604: Migmatized Metapelite Grt-Bt-Sil-Qtz-Pl-Opq

-Grt - 10% - mostly 1x1mm to 3x3mm with one 9x11mm, ameboidal, embayed, inclusions Bt-Opq-Qtz
-Bt - 5% - symplectic with Qtz on rims of Grt, aggregates with Opq-small Grt-Sil
-Sil - 10% - 2 generations; 1 well-formed, 2 fibrolite (cross cut Grt, Qtz, Pl; rim Grt, Sil)
-Qtz - 40%
-Pl -30%
-Opq - 5% - interstitial; 1mm blobs

reaction Grt going to Sil + Bt + Pl

3634: Migmatized Metapelite Grt-Bt-Sil-Qtz-Pl-Opq

-Grt - 15% - poikiloblastic, embayed
-Bt - 5%
-Pl - 25% - 10% as porphyroblasts up to 7mm x 7mm
-Qtz - 40% - grain size reduction
-Sil - 10% - 2 generations - dominated well-formed, 2 fibrolite along pseudo shear zones, rim Grt-Sil
-Opq - 5%
-Kfs <1%

similar to 3604, less fibrolite

3634-1: Migmatized Metapelite Kfs-Pl-Qtz-Bt-Opq

-Kfs - 1% - porphyroblasts grew during melt reactions; inclusions Bt-Qtz-Opq
-Pl - 4% - some porphyroblasts, some fine grain in matrix
-Qtz - 5% - fine grain
-Bt - 35% - parallel to foliation
-Opq - 5% - parallel to foliation, bend around feldspar porphyroblasts; acicular (Ilm); interstitial

compositional zoning (varying % Bt and felsics); first step of anatexis

3694 (L): Migmatized Metapelite Grt-Bt-Sil-Pl-Qtz-Opq-Kfs

-Grt - 15% - fractures, rounded, inclusions Qtz-Bt-Pl; poikiloblastic; rimmed with 0.5 to 1mm Bt; surrounded by moats of Pl
-Bt - 32% - rim Grt; matrix between Pl grains and along Pl twin plains
-Kfs - 1%
-Pl - 40% - matrix 1-3mm; Bt alteration along grain boundaries and twin plains; moats around Grt-Bt
-Qtz - 5%
-Sil - 1%
-Opq - 3% - with BT; rim GT
-Tur - 3% - pleochroic brown-brown/green;

3705: Metapelite Bt-Ms-Qtz-Pl
Bt-Sil-Qtz-Pl

-Bt - 30% -
-MS - 20% - parallel foliation
-Sil - 25% - Sil occurs as inclusions in Ms (before Sil?), parallel foliation
-Qtz - 20%
-Pl - 3%
-Opq - 2%

3712: CALC-SILICATE Qtz-Scp-Di-Ttn-Grt-Opq

3777: Migmatized Metapelite Crd-Pl-Kfs-Grt-Qtz
Hbl-Qtz-Pl-Opq-Ser-Kfs

MELANOSOME (25%)
-Crd - 5%
-Pl - 35% - forms large (6mm x 8mm) porphyroblast
-Kfs - <1%
-Grt - 40% - rounded; embayed; up to 7mm x 8mm
-Qtz - 25% - undulose extinction

LEUCOSOME (75%)
-Hbl - 5%
-Qtz - 10% - rods whose long axis parallels foliation; undulose extinction; grain size reduction
-Pl - 15%
-Opq - 15% - acicular (ILM)
-Ser - 60% - alteration of Hbl and Pl
-Kfs - <1%

-slightly undulating boundary between leucosome and melanosome
-boundary crosscuts old foliation; defined by orientation of QZ rods and BT

3777F: Migmatized Metapelite Grt-Bt-Qtz-Pl-Ser-Opq

MELANOSOME
-Grt - 5%
-Bt - 10% - random orientation
-Qtz - 40% - graphic intergrowth with Pl
-Pl - 35% - graphic intergrowth with Qtz
-Ser - <1% - alteration of Pl

3794 (L): Migmatized Metapelite Grt-Bt-Sil-Ilm-Qtz
Qtz-Grt-Ttn-Bt-Crd-Sil

-Qtz - 80% - mosaic
-Grt - 6% - tiny, eroded by Bt-Sil-Qtz-Ilm; define first foliation; also in leucosome (poikiloblastic with inclusions Qtz-Bt-Ttn
-Bt - 10% - 1-3mm long; define first foliation
-Sil - 3% - fibrolite on Grt
-Ilm - 1% - 1-3mm long, define first foliation; associated with Bt
-Ttn - 1% - only leucosomes
-Opq - <1% - interstitial

-leucosomes of Grt-Qtz defines second foliation which crosscuts first foliation
-tiny Grt-Bt-Sil-Ilm-Qtz define first foliation

3804: Migmatized Garnetite Grt-Bt-Qtz-Opq-Pl

-Grt - 60% - poikiloblastic; inclusions dominately Opq, trails and collars, minor Qtz + Bt
-Bt - 15% - matrix
-Qtz - 7% - matrix, grain size reduction; graphic intergrowth with Pl
-Opq - 10% - inclusions and rims Grt, crosscut Bt; acicular (Ilm)

-Pl - 8% - matrix, graphic intergrowth with Qtz
-Kfs - <1%

3829: Migmatite Sil-Bt-Pl-Qtz

-Sil - 40% - well-formed
-Bt- 20% - interstitial
-Pl - 30% - fine grained
-Opq - 3% - very fine grained
-Qtz - 8%

3832: Migmatized Metapelite Grt-Bt-Krn-Qtz-Pl-Kfs-Opq

-Grt - 25% - 1mm to 15mm x 20mm
-Bt - 10% - more or less interstitial, rim Grt, symplectic with Pl-Opq-Krn
-Krn - 10% - cross-section up to 4mm, pleochroic blue-green to brown
-Qtz - 15% - mosaic; graphic intergrowth with Pl; 40% of grains, 20% 0.1mm rounded isolated blobs; 20% 0.1 x 0.3 mm twisted intergrown tubes
-Pl - 30% - graphic intergrowth with Qtz
-Opq - 5% - blebs up to 2mm in Grt; interstitial in matrix; sulphides
-Kfs - 5% - perthitic; 5% 0.05 x 0.2 thin lines oriented with long axis more or less parallel to twin lamellae

-compositionally zoned; Krn-rich with Bt-Opq-Grt; large Grt with Opq inclusions and Bt rim; Qtz-Pl leucosome with minor Opq-Grt-Bt
-boundaries between all three are irregular and undulose

3832: Migmatized Metapelite Qtz-Pl-Opq-Bt-Grt

LEUCOSOME (70%)
-Qtz - 50% - graphic with Pl; same form as above
-Pl - 45% - graphic with Qtz
-Opq - 2% - interstitial; sulphides
-Bt - 3%
-Grt - 5% - 1-2mm; inclusions Qtz; rimmed with Opq;

MELANOSOME (30%)
-Grt - 20% - up to 6mm x 10mm; inclusions Opq-Qtz
-Bt - 15% - interstitial
-Qtz - 55% - grain size reduction
-Pl - 5%
-Opq - 5% - interstitial; sulphides

-slightly undulating boundary between leucosome and melanosome

3869 (L): Migmatized Metapelite Bt-Kfs-Qtz-Sil-Tur

-Bt - 45% - defines foliation
-Kfs - 30% - perthitic; <<1% 0.1 to 0.5 mm rounded isolated blobs porphyroblasts up to 10mm x 15mm throughout

-Qtz - 13% - some rods with grain size reduction
-Sil - 2% - along 1-3mm shear zones; cuts foliation
-Tur - <1% - throughout; <0.7mm; also as inclusions in Kfs porphyroblasts
-Opq - 3% - disseminated
-Ap - <1% - included in Kfs porphyroblasts

-leucosomes discontinuous ranging from wispy stretched quartz rods <1mm thick to Kfs-rich porphyroblasts up to 10mm x 15mm; parallel to foliation

4012: Migmatized Metapelite Grt-Bt-Qtz-Pl-Cal-Opq
Qtz-Pl-Tur-Bt-Opq
Pl-Ser

-Grt - 10% - embayed with Qtz - Bt; rounded, broken, inclusions Qtz-Bt-Opq; up to 6mm x 6mm
-Bt - 25% - form pressure shadows on Grt
-Qtz - 35% - crystal growth around Bt; grain size reduction; boundary migration
-Pl - 25% - alteration to Ser, crystal growth around Bt
-Tur - 1% - in leucosome
-Ser - 4% - alteration of Pl
-Opq - 4% - interstitial throughout
-Cal - <1% - interstitial between Grt-Bt-Pl in melanosome

-one small Qtz vein crosscuts pressure shadow and Grt
-80% melanosome; 20% leucosome
-boundary between two defined by compositional change; irregular and undulating

4012: Migmatized Metapelite Qtz-Pl-Kfs-Bt-Ser-Cal-Opq
Grt-Bt-Qtz-Pl-Opq

LEUCOSOME (55%)
-Qtz - 20% - mosaic; grain size reduction
-Pl - 65% - alteration to Ser
-Kfs - 5% - perthitic; 40% of grains, 0.01 mm isolated angular blobs more-or-less parallel to twin lamellae; alteration to Ser
-Bt - 5%
-Opq - 1% - interstitial
-Ser - 5 % - alteration of Pl and Kfs
-Cal - <1% - interstitial

MELANOSOME (45%)
-Grt - 10% - broken, rounded, inclusions Opq-Qtz; pressure shadows of Opq-Bt-Qtz; Bt bends around
-Bt - 20% - defines foliation
-Qtz - 40% - ribbons, grain size reduction
-Pl - 25% - porphyroblasts (1mm to 5mm x 5mm; some rounded; some fish-shaped); alteration to Ser
-Opq - 5% - interstitial
-Ser - <1%

-boundaries between leucosomes and melanosomes is undulatory; layers range in thickness from 1mm to over 1cm

4012 (L): Migmatized Metapelite

-similar in composition to above
-snowball Grt 40mm x 25mm; inclusions Qtz; embayed boundaries
-leucosome along one side of mosaic Qtz with Kfs (from melt) along boundary with melanosome

4044: Migmatized Metapelite Grt-Bt-Qtz-Opq-Pl

-Grt - 20% - embayed with symplectic Qtz-Bt; generally Grt has symplectic border with Qtz-Bt; surrounded by QZ-PG;
-Bt - 30% - symp with Qtz in matrix and rim of Grt
-Qtz - 30% - very fine grain, reduced grain size, mosaic; graphic intergrowth with Qtz; 20 % of grains, 15% as 0.01 x 0.2 mm twisted intertwined tubes; 5% as 0.01 rounded blobs throughout grains
-Opq - 5% - inclusions in Grt, throughout matrix; radiating acicular habit (Ilm)
-Pl - 15% -graphic intergrowth with Qtz; grain size reduction; grain boundary migration
-Kfs - 5% - perthitic; 15% of grains, 14% 0.01 x 0.05 fine angular blobs parallel to twin lamellae, 1% as 0.1 mm rounded isolated blobs; grain size reduction; grain boundary migration
-Cal - <1% - interstitial; <0.1mm; alteration between Bt-Pl; around border Grt with rusty stain
-Ap - <1%
-Ser - <<1%

-Pl moats around Grt suggestive of compositional zoning

4209: Migmatized Metapelite Grt-Bt-Qtz-Pl-Opq

-Grt - 5% - porpyroblasts ±rounded, inclusions Qtz-Bt; broken
-Bt - 50% - parallel foliation, mostly wraps around porphyroblasts; minor inclusions in Grt
-Qtz - 30% - some rods with grain size reduction up to 1mm wide; leucosomes (5%)
-Pl - 5% - porphyroblasts up to 2mm x 5mm
-Opq - 10% - blades parallel foliation; wrap around porpyroblasts; up to 5mm long
-Kfs - <1% - porphyroblasts from melt (inclusions Bt-Qtz); perthitic; <1% 0.1 to 0.2mm rounded isolated blobs

-distinct undulose boundary between leucosomes and melanosomes; leucosomes are discontinuous mostly parallel to foliation, ranging in thickness from 1mm to 4mm and length from 10mm to 40mm

4220: Migmatized Metapelite Qtz-Pl-Kfs-Bt-Grt-Opq-Ap
Grt-Bt-Qtz-Pl-Ap-Zrn-Opq

LEUCOSOME (45%)

-Qtz - 60% - rods grain size reduced; graphic intergrowth with Pl, <1% 0.01 x 0.1 mm twisted intergrown tubes
-Pl - 20% - porphyroblasts up to 3mm from melt; inclusions Bt; undulatory extinction; graphic intergrowth with Qtz
-Kfs - 5% - porphyroblasts up to 3mm; from melt; inclusions Bt; undulatory extinction
-Bt - 5% - interstitial
-Grt - 10% - up to 2mm; broken; inclusions Qtz
-Opq - <1% - interstitial
-Ap - <1%

MELANOSOME (55%)
-Grt - 10% - up to 4mm
-Bt - 30% - define foliation
-Qtz - 45% - fine grained (<0.1mm)
-Pl - 8% - porphyroblasts up to 1mm
-Opq - 5% - interstitial blobs up to 2mm long
-Ap - 1% - mostly < 0.1mm; two grains 1mm
-Zrn - 1%

-boundaries between leucosomes and melanosomes are undulose and indistinct; leucosomes vary in thickness from 4mm to 8mm and are continuous on the thin section scale

4475A/B: Migmatized Metapelite Grt-Bt-Qtz-Kfs-Opq-Sil

-Grt - 10% - irregular shape; broken; up to 9mm x 10mm; inclusion Qtz-Opq-Bt-Spl; ameboidal
-Bt - 15% - parallel to foliation
-Qtz - 62% - ribbons between Bt; parallel to foliation; grain size reduction
-Kfs - 5% - perthitic; 50% of grains, 0.1 x 0.5 mm rods intertwined, more or less parallel to ex-twin lamellae; obliterated twin lamellae
-Opq - 5% - interstitial irregular
-Sil - 3% - fibrolite and 1mm cross-sections

4475D2/D3: Migmatized Metapelite Grt-Sil-Bt-Opq
Grt-Crd-Bt-Sil-Qtz-Pl

LEUCOSOME
-Grt - 15% - irregular; up to 2mm x 3mm; inclusions Qtz
-Crd - 2%
-Bt - 5% - between Qtz grains
-Sil - 15% - between Qtz grains
-Qtz - 60% - grain size reduction
-Pl - 3%

MELANOSOME
-Grt - 25% - up to 12mm x 15mm; 5% Opq inclusion lines; more or less round with irregular boundaries
-Sil - 5% - up to 3mm cross-section; mostly fibrolite
-Bt - 60
-Opq - 10% - forms lines of inclusions

-boundary undulatory; defined by concentration of Bt in melanosome

APPENDEX B

MELT REACTIONS

1. Evidence for Reactions Producing Melt

1.a. Migmatization

Many outcrops within this field area contain leucosomes which provide evidence for processes which produced a melt. The following thin sections contain evidence for migmatization that range from the compositional zoning of samples 2401G2, 3634-1, 3832 through the discontinuous leucosomes of samples 1280-2, 3364-2, 3869 and the felsic moats around garnets of samples 3694, 2401F2, 4012 to the continuous leucosomes greater than 1cm thick of samples 3028A, 3302A, 3777.

1280-2

-discontinuous fish-shaped leucosomes that range from 2x2mm to 7x25mm
-Pl-Qtz-Kfs-Grt(<1%)-Opq(<1%)-Bt(<1%))

2401D2

->cm scale continuous leucosomes with undulatory boundaries, more or less parallel to foliation
-Pl-Qtz-Bt(5%)-Opq(<1%)

2401G1

-compositional zonation with Opx-rich layers and Grt-rich layers

3028

-undulating continuous leucosomes 3-14mm thick, parallel with foliation
-melanosomes rimmed with 1mm thick biotite
-Qtz-Grt(2%)-Opq(1%)-Sil(<1%)

3302A

-undulating continuous leucosomes >cm scale; parallel to foliation
-Qtz-Grt(2%)-Opq(1%)-Bt(1%)-Pl

3364-2

-discontinuous leucosome pods 1x15mm to 5x20mm
-Kfs-Qtz-Pl-Opq(1%)-Bt(2%)-Sil(<1%)

3600

-continuous leucosomes 3-6mm thick
-Qtz-Kfs-Pl-Opq(2%)-Grt(<1%)

3634-1

-compositional zonation defined by variation in modal% Bt

3694

-garnet rimmed with biotite surrounded by plagioclase moats up to 1cm wide
-Pl-Kfs-Qtz-Bt(2%)-Tur(2%)-Opq(<1%)

3794

-1cm thick continuous leucosome of Grt-Qtz defines second foliation which crosscuts first foliation
-Qtz-Grt(20%)-Crd(<1%)-Bt(3%)-Ttn(<1%)-Opq(<1%)-Sil(<1%)

3777

->1cm thick continuous leucosome, undulatory boundary which crosscuts first foliation
-Pl-Qtz-Opq(<1%)-Bt(<1%)

3832

-compositional zonation in melansome with Krn-rich layers and Grt-rich layers
-continuous leucosomes >1cm thick with undulating boundaries
-Qtz-Pl-Opq(2%)-Bt(3%)-Grt(5%)

3869

-discontinuous leucosomes from wispy quartz ribbons <1mm thick to KF-rich porphyroblasts up to 10x15mm; parallel to foliation
-Kfs-Qtz-Bt(5%)-Opq(<1%)-Tur(1%)-Cal(<1%)

4012

-discontinuous leucosomes 1x1mm to continuous 5mm x >10cm; parallel to foliation
-Qtz-Pl-Kfs-Bt(5%)-Opq(<1%)-Ser(<1%)-Tur(1%)

4044

-plagioclase-rich leucosomes forms moats surrounding garnets 1-5mm wide; leucosomes also continuous with undulating boundaries 3-6mm wide
-Qtz-Pl-Bt(1%)-Ilm(3%)-Grt(1%)

4209

-discontinuous leucosomes 1-4mm thick, 10-40mm long with undulose boundaries; parallel to foliation
-Qtz-Pl-Bt(2%)-Grt(1%)-Opq(1%)

4220

-continuous leucosomes with undulose boundaries; 4-8mm thick
-Qtz-Pl-Kfs-Bt(5%)-Grt(10%)-Opq(<1%)

4475D2/D3

-continuous >1cm thick, undulatory boundaries
-Grt(15%)-Crd(2%)-Bt(5%)-Sil(15%)-Qtz-Pl

1.b. Feldspars

Generally in most conditions, feldspars form more or less equant grains with regular boundaries. However where reactions that produce melts occur, the residual feldspars form irregular grains with embayed boundaries and inclusions of the minerals that reacted out to produce the melt.

The following thin sections contain evidence of feldspars having grown from a melt. This evidence ranges from the feldspars occurring in leucosomes which likely grew from a melt (samples 4475A, 1475A3) to the K-feldspar with embayed boundaries and inclusions of biotite (samples 1280-2, 3364-2, 3832). Also, samples 2401F2, 3694, 3777 contain plagioclase-quartz-K-feldspar moats around garnets which likely formed from a melt produced by the biotite reacting out leaving garnet as the solid restite.

1280-2:

-Kfs - some occurs as porphyroblasts (2-4mm) with inclusions of Bt-Opq and embayed boundaries
-other occurs as border around edges of Qtz porphyroblasts
-suggests that Bt reacted out to form melt from which Kfs crystallized

1475A3:

-Kfs - small amounts present in leucosome (grains 1-2mm); suggests that Kfs crystallized from melt-producing reaction

1654E3:

-Kfs - minor in matrix (1-2mm), partial inclusions of Bt
-suggests that Bt reacted out to form melt from which Kfs crystallized

2401D2:

-Kfs - in matrix (1-2mm) with irregular embayed boundaries and inclusions of Bt
-suggests that Bt reacted out to form melt from which Kfs crystallized

2401E:

-Kfs - in matrix (1-2mm); similar to 2401D2

2401F2:

-Grt-Opx - intergrown; both have inclusions of each other; this suggests prograde reaction producing garnet and orthopyroxene. Garnet-orthopyroxene surrounded by moat of Pl; both alterring to Bt (Bt along cleavages of Opx; partial rims on Grt); suggests that Grt-Opx reacting out to Pl+Bt with Pl likely forming from a melt

2770:

-Sil - bends around Grt porphyroblasts; also forms clots, possibly after Pl (fish-shaped up to 1mm x 5mm); suggests Pl reacting out to produce Sil+melt

3302:

-Kfs - embayed boundaries; possibly formed during melt reaction; no inclusions (<1mm); graphitic and perthitic

3302A:

-Kfs - in matrix (<1mm) ; possibly from melt reaction; perthitic
-Grt - symplectic boundaries filled with Sil-Pl-Bt-Qtz-Kfs?; suggests Grt going to Sil+Bt+Pl+Qtz+melt (Kfs)
-fibrolite growing along Kfs boundaries; overgrowing Kfs; suggests Kfs reacting out to form Sil

3333A:

-Kfs - in matrix (1-2mm); embayed boundaries filled with Bt-Opq-Qtz
-acicular Sil included in Grt; equant crystals in matrix forming F which bends around Grt porphyroblasts---suggests two generations of Sil, the first which reacted out
-Sil-Bt-Pl-Qtz - fill in embayments of Grt----suggests reaction Grt going to Sil+Bt+Pl+Qtz+melt (Kfs)

3364-2:

-Kfs - forms porphyroblasts (1-3mm grains in fish-shaped leucosomes which are up to 4x8mm) with embayed boundaries and inclusions of Bt-Qtz-Pl-Opq
-suggests melting reaction of Bt-Qtz-Pl going to Kfs
-Sil-Bt define foliation and bend around porphyroblasts; suggests that this Sil pre-melting and not involved in reaction forming Kfs from melt
-other Sil inclusions in edges of Kfs and in the pressure shadows of Kfs suggesting that some Sil may have been involved in forming melt from which Kfs crystallized

3634-1:

-Pl - porphyroblasts (1x1mm to 7x7mm) formed from melt; embayed boundaries with inclusions of Bt-Opq-Qtz; suggests that here Bt-Qtz formed melt from which Pl crystallized (some K^+ may be in the Pl structure)

3694:

-Grt - rimmed with Bt, both surrounded by Pl moat (grains 1-4mm; leucosomes up to 1cm thick between garnets)
-Pl and Kfs both embayed with inclusions of Bt; suggests that Grt reacted to Bt+Pl; then Bt+Pl melted to form Pl + Kfs

3777:

-Kfs-Pl-Qtz - moat around Grt (1-4mm grains in leucosomes up to 1cm thick); embayed irregular boundaries with inclusions Bt-Opq-Qtz; suggesting formed from Grt-Bt reacting out

3832:

a)-Kfs - irregular porphyroblasts (1-3mm) in leucosomes with inclusions Bt-Qtz; suggests Bt-Qtz reacting out to form melt from which Kfs crystallized
-Pl also has inclusions of Bt; in leucosomes (1-5mm)
-fibrolite forming along cracks in Grt and over Bt; suggests that Grt-Bt reacting out to form Sil; possibly synchronous with production of melt to form Kfs

b)-Kfs - (1-2mm) in leucosomes with Krn; probably melt-related
-Bt with Kfs-Krn is symplectic with Bt-Qtz and possibly Kfs or Pl; suggesting Kfs-Krn producing reaction from Bt-Qtz (and likely Krn)
-Pl-Qtz - (1-4mm) in leucosomes with inclusions Krn-Bt; likely melt-related

3869:

-Kfs - porphyroblasts in leucosomes; embayed with inclusions of Bt-Qtz-Ap-Tur; also in matrix (0.1-0.5mm) with inclusions Bt and irregular boundaries
-Tur - porphyroblasts (up to 0.5mm) associated with leucosomes
-suggests that both Kfs and Tur formed from melt; Kfs from melt of Bt-Qtz

4012:

-Kfs and Pl (0.5 to 1.5mm) in matrix; irregular boundaries with inclusions of Bt; suggesting that both Kfs and Pl formed from a melt-producing reaction

4220:

-Kfs - in leucosomes (<1mm grains) with irregular boundaries and inclusions of Bt; suggesting Bt reacting out to produce melt from which Kfs formed

4475A2:

-Kfs - (up to 1mm) in leucosomes with inclusions of Qtz; suggesting KF formed from melt

2. Sillimanite - Fibrolite

Sample 3794 contains sillimanite which along with biotite defines the first foliation within this sample. The first foliation is crosscut by the leucosomes which define a second foliation. Clearly here, the sillimanite is primary, before the formation of the leucosomes from the reactions that produce a melt.

Several thin sections (2373, 2401E, 3028, 3302, 3333A, 3604, 3634, 4475A, 4475B, 4475D2, 4475D3) demonstrated evidence for two generations of sillimanite growth. In most cases, sillimanite formed equant cross-sections or blades with fibrolite growing upon these crystals. Sample 2373 possibly has three generations of sillimanite. The first being acicular inclusions in garnet, the second and third being blades with fibrolite in the pressure shadows of these garnets. It is very likely that the last generation of sillimanite grew from the melt produced from the above reactions. Sample 2401E has acicular sillimanite randomnly oriented inclusions within garnets. In the matrix, sillimanite occurs as equant grains up to 0.5mm x 5mm which are oriented parallel to the foliation. The difference in habit and orientation between the sillimanite in the garnets and the matrix suggests that these are from two different generations. Sample 3333A also contains acicular sillimanite included within garnets, and equant sillimanite crystals in the matrix which define the foliation and bend around garnet porphyroblasts.

Five thin sections (1654K, 1659H1, 1659H2, 3794, 3832) also contain fibrolite which forms at grain boundaries, or in the cracks-embayments-rims of garnet and orthopyroxene. This fibrolite is likely retrograde, possibly forming from the melt produced by the above reactions.

The sillimanite in sample 3869 crosscuts the foliation, suggesting that sillimanite formed post-foliation, possibly from the melt of the above reactions. In sample 2770, sillimanite in the matrix bends around garnet porphyroblasts, sillimanite also forms clots over plagioclase porphyroblasts. This suggests that plagioclase is reacting out to form sillimanite, quite likely involving a melt phase to move the calcium and sodium from the plagioclase.

3. Accessory Minerals

Apatite occurred in the leucosomes of samples 3869 and 4220. In samples 3869, apatite was included within Kfs porphyroblasts. In both cases, the melts must have contained minor phosphorus.

Tourmaline occurred in the leucosomes of sample 3869, 3333A, 3869 and 4012. Kornerupine occurred in the leucosomes of sample 3832. The presence of tourmaline and kornerupine implies that these melts must have contained minor boron.

APPENDEX C

LIST OF ABBREVIATIONS

Minerals (after Kretz, 1983)

Alm	Almandine
Ank	Ankerite
An	Anorthite
Ap	Apatite
Bt	Biotite
Cpx	Ca Clinopyroxene
Cal	Calcite
Crd	Cordierite
Dol	Dolomite
En	Enstatite
Fs	Ferrosilite
Grt	Garnet
Gr	Graphite
Brs	Grossularite
Hbl	Hornblende
Ilm	Ilmenite
Kfs	K-feldspar
Krn	Kornerupine
Ky	Kyanite
Mag	Magnetite
Mc	Microcline
Mnz	Monazite
Ms	Muscovite
Oam	Orthoampibole
Opx	Orthopyroxene
Phl	Phlogopite
Pl	Plagioclase
Py	Pyrite
Pl	Plagioclase
Py	Pyrite
Prp	Pyrope
Qtz	Quartz
Rds	Rhodocrosite
Rt	Rutile
Sa	Sanidine
Spr	Sapphirine
Sil	Sillimanite
Sps	Spessartine
Spl	Spinel
Ttn	Titanite
Tur	Tourmaline
Wo	Wollastonite
Zrn	Zircon

Others:

Als	Aluminosilicate
Ser	Sericite
Opq	Opaque

Grenville Terms:

A	Algonquin domain
ADH	Adirondack Highlands
AMP	Allochthonous Monocyclic Belt
APB	Allochthonous Polycycle Belt
B	Britt domain
BCS	Baie Comeau Segment

BGC	Bondy Gneiss Complex
BEMS	Bancroft-Elzevir-Mazinaw-Sharbot Lake Superterrane
BRT	Baskatong Reservoir Terrane
CCMZ	Carthage-Colton Mylonite Zone
CGB	Central Gneiss Belt
CGT	Central Granulite Terrane
CMB	Central Metasedimentary Belt
CMBBZ	Central Metasedimentary Belt Boundary Zone
CMB-Q	Central Metasedimentary Belt of Québec
CRT	Cabonga Reservoir Terrane
DRT	Dazois Reservoir Terrane
EGP	Eastern Grenville Province
ELZ	Elzevir terrane
FR	Frontenac terrane
GF	Grenville Front
GFTZ	Grenville Front Tectonic Zone
LAB	Grenville Front region in Labrador
LSJ	Lac St. Jean area
LSZ	Labelle Shear Zone
ML	Mont Laurier area
MBBZ	Monocyclic Belt Boundary Zone
MLT	Mont Laurier Terrane
MOR	Morin terrane
MT	Morin Terrane
NCDZ	Nominingue-Chénéville Deformation Zone
NYL	New York Lowlands
PB	Parautochthonous Polycyclic Belt
PC	Pentecôte
PS	Parry Sound domain
PSZ	Parry Sound thrust zone
PW	Pinware terrane
SM	Saint Maurice
WK	Wakeham terrane

Metamorphic Terms

Tc	Closure Temperature
Tmax	Peak Metamorphic Temperature
Pmax	Peak Metamorphic Pressure
P-T-t	Pressure-Temperature-time

Analytical Terms

bdl	below detection limit

Harley (1989) abbreviations

AB	Arendal, Norway
AD	Aldan shield
AH	Adirondack Highlands

AL	Adirondack Lowlands
AK	Akilia, Greenland
BC	British Columbia
BG	Bengal
BH	Broken Hill, Australia
BU	Buksefjorsen, Greenland
CA	Cariaba, Brazilo
DS	Doubtful Sound, NZ
ED	Ellesmere-Devon Island
ER	English River, Ontario
FR	Fraser Range
FU	Furua, Tanzania
GF	Gruf Complex, Alps
GV	Grenville
HE	Hebei, China
HO	Hoggar (NE)
HP	Hercynian Pyrenees
IK	Indian Khondalies, Tamil Nadu
IM	Iforas, Mali
IN	Inarjarvi, Finland
IS	Isortoq, Greenland
IR	Ivrea zone sapphirine
IZ	Ivrea zone, north
IV	Ivrea zone, south
JK	Jijal Complex, Kohistan
KB	Kabbal, India
KE	Kerala Khondalites
KK	Kapuskasing, Quetico
KP	Kapuskasing, Kapuskasing
KS	Kristiansund, Norway
LG	Longuparti, India
LI	Limpopo Belt
LM	Limpopo Belt
LP	Limpopo Belt
LV	Limpopo Marginal Zone
LH	Lutzow-Holm Bay
LO	Lofoten, Norway
LU	Labwor Hills, Uganda
MK	Maniwaki, Grenville
MD, MS	Madras
MP	Madras-Pallavaran
MA	Massachusetts
MO	Moldanubian
ME	Musgrave Block
MR	Minnesota River Valley
MZ	Molodezhnaya
NA	Nain Complex
NS	Napier Complex - Scott
NT	Napier Complex - Tula
NN	Napier Complex - Napier

NZ	Napier Complex - Shears
NQ	Namaqualand
NH	Nilgiri Hills
NP	Northampton Block, WA
OL	Otter Lake, Quebec
OX	Ox Mts, Ireland
PD	Paderu, India
PK	Pikwitonei, Manitoba
PT	Pikwitonei, Sipawesk
PY	Pennsylvania
QI	Quiznxi, China
RY	Rayner Complex
RU	Rauer Group, Antarctica
RR	Rauer Group, Antarctica
RN	Roan, Norway
RO	Rogaland, Norway
RM	Ruby Range, Montana
RT	Ruby Range, Montana
SC	Scourie Complex, Scotland
SE	Serre, Calabria
SH	Sri Lanka, Highlands
SL	Sri Lanka, Vijayan
SR	Strangways Range, Aruta Complex North
SG	Sargur Schists
SI	Sittampundi
SV	Sverdrupfjella, Antarctica
SZ	Sharyzhalgay, Baikal
UU	Uusimaa, Finland
VH	Vestold Hills, Antarctica
VR	Vredeport Dome
WL	Wilson Lake Ontario
WM	Windmill Island, Antarctica
WR	Wind River
YT	Yamato Mts, Antarctica
YI	Yilgarn shears